UNIVERSITY OF BIRMINGHAM

Towards Semi-Quantitative Mass Spectrometry Imaging of Drugs in Tissue

by

Sarah Didem Turker

Supervisor: Dr J. Wilkie

Nov 2020
School of Chemistry
University of Birmingham

Abstract

Mass spectrometry has recently become a popular approach for the determination of the spatial distribution of drugs in vivo and in vitro, which has given rise to the field of mass spectrum imaging (MSI). A major challenge in this field is to make analysis quantitative, which relies on the construction of accurate calibration curves using standards that accurately simulate the ion suppression found in biological tissues. Another challenge is to rapidly screen tissues without resort to the labour intensive sample preparation associated with mass spectrum imaging. I hypothesise that these points may be addressed potentially by the use of drug spiked tissue homogenates in mass spectral analysis, which may both serve to act as accurate calibration standards that simulate ion suppression in tissues as well as being very straightforward to prepare. Hence in this thesis I address these points using the following methodology. In chapter 2, new calibration standards based on drug spiked liver tissue homogenates are used to produce calibration curves for a range of drugs. In chapter 3, liquid extraction sampling analysis (LESA) is used in combination with the spiked homogenate approach to produce calibration curves for fenclozic acid and propanolol. In both cases we show that semi-quantititative or quantitative calibration curves can be produced using tissue homogenates, which could potentially allow routine quantitative analysis to be made possible. In chapter 4 we use homogenates from excised animal subjects to compare against radiolabelling techniques used in industry (QWBA and LSC). We find that MALDI MS can detect the drugs, and if not the drug, the metabolites of the drugs, and it could be a useful tool for rapidly screening

organs to ascertain which may merit further interrogation thus speeding up the process of drug discovery.

Index

Glossary

BBB	blood-brain barrier
CHCA	α-cyano-4-hydroxycinnamic acid
CID	collision induced dissociation
DCM	dichloromethane
DESI	desorption electrospray ionisation
DHB	2,5-dihydroxybenzoic acid
ESI	electrospray ionisation
FWHM	full width half maximum
IR	infrared
LESA	liquid extraction surface analysis
LMJ	liquid micro-junction
M	molecule
$[M+H]^+$	protonated molecule
MALDI	matrix-assisted laser desorption/ionisation
MS	mass spectrometry
MSI	mass spectrometry imaging
MS/MS	tandem mass spectrometry
m/z	mass-to-charge ratio
N_2	nitrogen
Nd:YAG	neodymium: yttrium-aluminum garnet
Nd:YVO_4	neodymium yttrium vanadium oxide
PC	phosphatidylcholine
Q	quadrupole

q	RF only quadrupole
QqTOF	quadrupole time-of-flight
QqQ	triple quadrupole
SA	sinapinic acid
SIMS	secondary ion mass spectrometry
TFA	trifluoroacetic acid
THAP	2’, 4’, 6’-trihydroxyacetophenone
THF	tetrahydrofuran
TOF	time-of-flight
UV	ultraviolet

Chapter 1: Introduction.

N.b. Parts of this chapter have been published by the author as ‘MALDI-MS of drugs: Profiling, imaging, and steps towards quantitative analysis’.[1]

[Appl. Spectroscopy Rev., **2016,** 1 - 27.]

1.1 Mass Spectrometry.

Mass spectrometry is the science of determining molecular or atomic mass by measuring the mass to charge ratio (*m/z*) of ions. [2], [3] To analyse the ions produced from a sample, a series of steps must be taken where atomic or molecular species are firstly manipulated to produce gaseous ions; these ions are then separated by their difference mass / charge ratios, and finally, the ions produced are detected. These processes are known as *ionisation*, *mass analysis* and *detection*. There is a range of techniques in existence to achieve each of the three stages of the process; a mass spectrometer may be thought of as a series of modular parts (which in theory can be interchanged) suitable for the required experimental conditions (Figure 1.1). The first step of any mass spectrometric analysis involves the production of gaseous ions – either positively charged *cations* or negatively charged *anions*. Initially a molecule is ionised to the *molecular ion* – that is, a charged version (M^+ or M^-) of the parent molecule (M). The molecular ions may then undergo *fragmentation* where the molecular ion falls apart into smaller species, either charged or radical species. Ions can then be introduced into a mass analyser where they are sorted according to their mass-to-charge ratio (*m/z*). Tandem mass spectrometry experiments (MS/MS) can be carried out in two ways. Spatial MS/MS subject ions to two or more analyses. In general this require two scanning mass spectrometers linked in sequence; in the first instrument an ion of a certain *m/z* is selected for analysis with the second spectrometer to analyse fragmentation patterns, with the ions transferred through space during the analysis steps.

Tandem mass spectrometry may also be carried out with temporal resolution, where time is used to separate ions. This is performed by trapping ions with analysis done over time in a single sample cell.

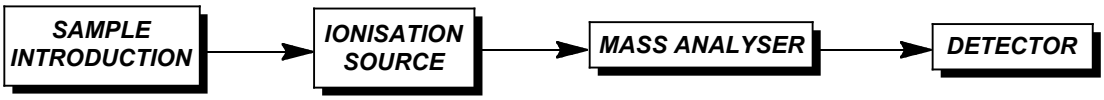

Figure 1.1: The modular nature of a mass spectrometer showing the four components universal to all systems. Sample is introduced into the ionisation source, ions are separated by their *m/z* values by the mass analyser, and are finally detected as an electric current at the detector.

1.2. Matrix-assisted laser desorption / ionisation (MALDI).

Matrix assisted laser desorption/ionisation (MALDI)[4-7] is a soft ionisation technique which can be used to produce ions from both small and large molecules. In MALDI, a solution of analyte is co-crystallised with a matrix molecule onto a sample plate. This is most frequently performed by using a solution containing both analyte and matrix and spotting it onto the plate, allowing the solvent to then evaporate, though the sample may also have the matrix spotted on top of it. This is known as 'dried droplet deposition'. Other popular matrix deposition techniques include airspray, inkjet printing and automated spray deposition . Often the matrix is in a molar excess of up to one thousand to ten thousand times greater compared with the analyte in the crystals. The plate is placed under vacuum

and the solid sample is irradiated with a pulsed laser beam, which leads to desorption and ionisation of the analyte (and matrix) molecules (Figure 1.2) which rises as a plume of ions from the target plate. These ions are then accelerated into the mass analyser by application of electric fields. Note this review generally deals with positive mode MALDI, i.e. the ionisation and detection of cationic species.

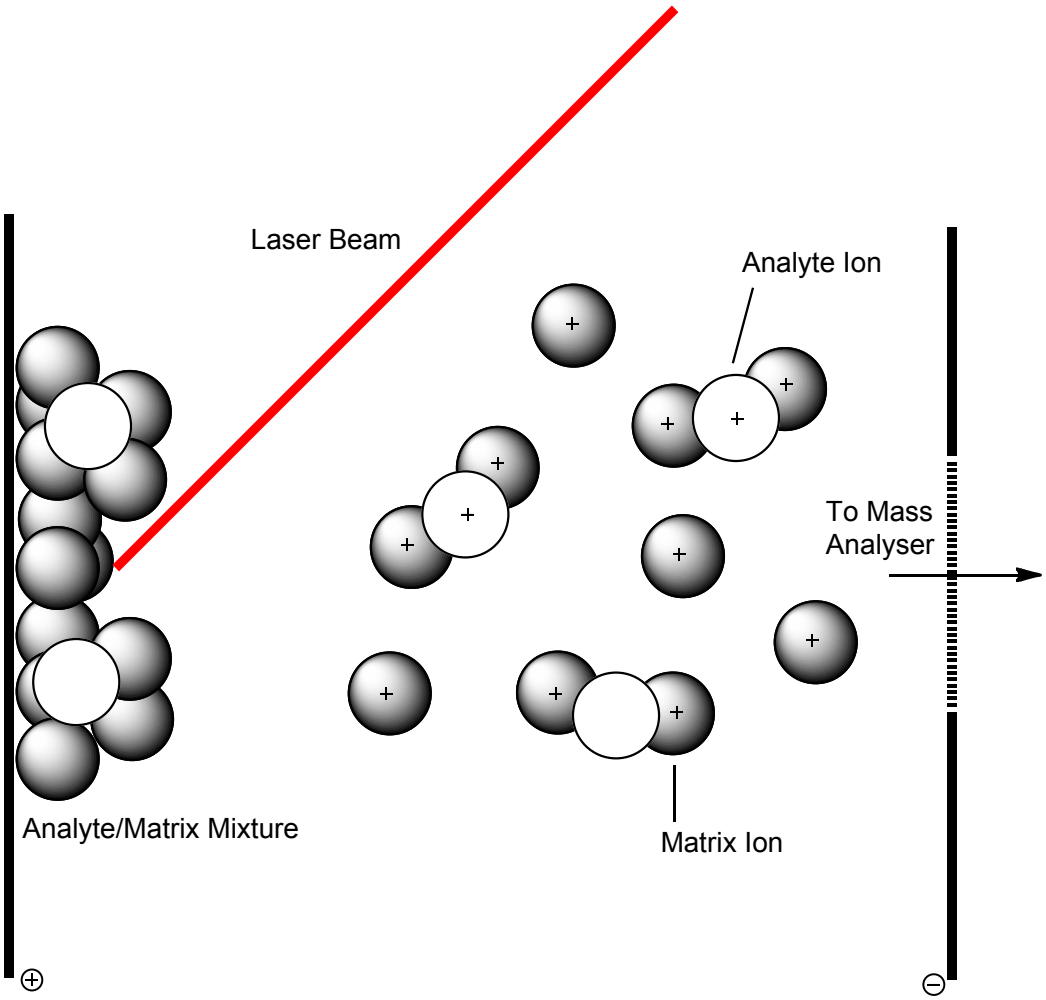

Figure 1.2: The ionisation process in a typical MALDI source. A solid state sample of analyte and matrix is irradiated with a laser of known wavelength, leading to localised heating of the sample and subsequent desorption and ionisation of the analyte and matrix as a rising ionic plume which is directed into the mass analyser. Ablation occurs at the site of irradiation.

1.3. MALDI Matrices

MALDI matrices have been crucial in the analysis of a range of ubiquitous biomolecular species such as peptides[8-11] oligonucleotides[12-20] drugs,[21-23] lipids,[24-30] proteins,[31, 32] and carbohydrates.[33, 34] The matrix material in MALDI is primarily used to protect the analyte molecules from the energy of the pulsed laser; typically the matrix molecule used has an absorption maximum (or close to the absorption maximum) that coincides with the laser wavelength in operation.[35] This protects the analyte from thermal degradation primarily, as photons are absorbed by the matrix and the energy gained by absorbance of the photons ($E = h\nu$) is transferred in a *controlled manner* to the analyte, circumventing thermal degradation and covalent bond breakage. Desirable properties of a matrix also include low molecular mass (particularly for high M_w measurements) so as not to interfere with the signals of larger M_w analytes; non-volatility at low pressures; the ability to solubilise a range of compounds of all polarities and chemical inertness.[3] The matrix must also not sublime under high vacuum for obvious reasons.

Crystals of the matrix should be of decent quality, and must able to effectively entrain the analyte into the matrix crystal as an impurity as it is growing i.e. the solubility of the analyte in the solid state matrix should be good. Thus, when the laser energy hits the sample, the analyte molecules can be ionised efficiently by the surrounding matrix molecules, as well as being protected from degradation by the laser as discussed. Crystallisation and crystal quality should, ideally be uniform across the sample. Thus good signal and good resolution can be obtained. Examples of the commonly

used matrices which show these features for analysis of a broad range of analytes include sinapinic acid (SA), alpha-cyano-4-hydroxycinnamic acid (CHCA), 2,4,6-trihydroxyacetophenone (THAP) and 2, 5-dihydroxybenzoic acid (DHB)[10, 36] and their chemical structures are shown in Scheme 1.1. Picolinic acid is also a useful matrix.[16] Para-nitroaniline has recently been reported as a useful matrix for imaging experiments on an intermediate pressure MALDI QqTOF system leading to equal or better ion counts and less fragmentation as-compared with CHCA.[37] All matrices have similar features: aromatic ring structures for absorption of photons in the UV region with acidic functional groups for proton transfer to analyte. Interestingly, natural carboxylic acids have recently emerged as being well-suited to MALDI mass spectroscopic analysis (including MALDI imaging), for example turmeric (1,7-bis-(4-hydroxy-3-methoxy-phenyl)-hepta-1,6-diene-3,5-dione *a.k.a.*curcumin) which is a natural product from the *Curcuma longa* plant,[38] mainly due to the conjugated pi systems, which allow wavelength tuning for sample protection, combined with numerous carboxylic acid groups for initial protonation of the samples for ionisation. The advantage to using natural matrix sources is that they can be produced in large scale from biomass.

Scheme 1.1: Matrices commonly used in routine MALDI-MS analyses including SA, CHCA, THAP and DHB. Curcumin has also been used as a natural product MALDI matrix, potentially being produced in large scale from biomass.

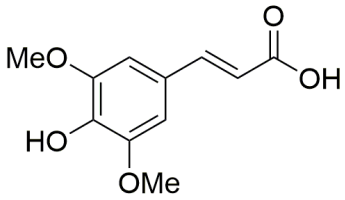

Sinapinic acid (SA)

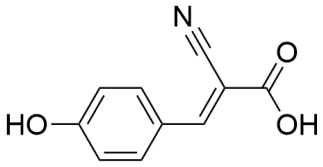

α-Cyano-4-hydroxycinnamic acid (CHCA)

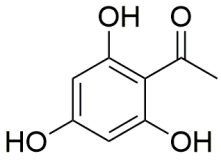

2,4,6-Trihydroxyacetophenone (THAP)

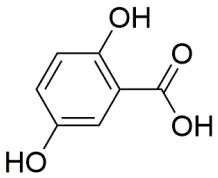

2,5-dihydroxybenzoic acid (DHB)

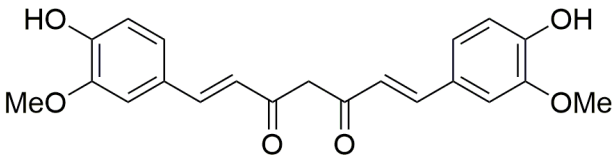

Curcumin

Due to the nature of the ionisation process in MALDI and due to the presence of the matrix, intact molecular ions are produced in general.[3] However, as the matrix is also involved in entraining the analyte into desorption, matrix *ions* are also observed in the mass spectrum, which must be taken into consideration when analysing small molecules in the same mass range as the matrix peaks. The relative molecular masses of SA (224.0 g mol^{-1}), CHCA (189.17 g mol^{-1}), DHB (154.12 g mol^{-1}) and THAP (168.15 g mol^{-1}) ensure that they have a low M_w cut-off and are thus useful

for the analysis of lipids, drugs and most metabolites relevant to the field of metabolomics, as well as larger proteins and other biomolecules. The introduction of the matrix as an intermediary between the laser pulse and the analyte, however, confers a number of advantages [3] The wavelength of the laser need not be tuned to the absorption spectrum of the analyte as the matrix performs this role. As the analyte need not absorb at a certain wavelength, a range of sample types may be ionised thus diversifying the use of the technique. Analytes are ionised with great efficiency and the sensitivity of the technique is greatly increased; this applies equally to large molecules such as proteins and biopolymers as it does to small, i.e. ionisation is independent of molecular mass (and thus the size of the molecule generally speaking) in theory. In practice a number of other considerations such as how voltile the material may be at large molecular weights may prevent an ionised molecule from desorbing at all e.g. mass spectra of large polymeric species is very challenging. To illustrate this latter point, it is possible to detect proteins of 300 kDa mass at femtomolar (10^{-15}) concentrations.[3]

There are a number of techniques that have been developed in order to deposit the matrix and analyte in such a way as to generate homogeneous crystal quality, something that is often helpful to achieve accurate and sensitive analysis[39] (although in certain cases it is not a pre-requisite[36]). Table 1.1 lists some of the techniques reported in literature, along with a brief physical description. All are purported to be superior in performance compared with standard dried droplet deposition.

Table 1.1: Novel deposition methods for analyte-matrix co-crystallisation.

Method	Description	References
Two-layer sample preparation (seeding, fast evaporative seeding)	Matrix solutions of varying concentrations are spotted, and solvents allowed to evaporate at various rates to form crystal seeds. Matrix and analyte co-spotted on top of grown matrix seeds. Improves crystal quality.	Dai *et al.*[40] Onnerfjord *et al.*[41] Vorm *et al.*[42]
Vacuum Sublimation	Matrix is sublimed onto the target plate under vacuum to produce high quality pure crystals.	Jaskolla *et al.*[43]
Tribological Homogenisation-Seeding	Matrix crystals are deposited as a first layer and are then physically crushed to form seeds for analyte – matrix deposition. Near homogeneity claimed.	Allwood *et al*.[44]
Automated Acoustic Deposition	Matrix deposited via acoustic ejector which avoid capillary use and thus blockages.	Aerni *et al.*[45]
Airbrush	The matrix is sprayed on top of the analyte as a fine mist. Can be also automated.	Yamada *et al.*[46]
Electrospray Deposition	In principle, similar to airbrush technique, but using an electrospray to produce extremely fine droplets which can produce homogeneous matrix-analyte crystals, decreasing spot to spot variability vs dried droplet deposition.	Hensel *et al.*[47]
Inkjet Printing	Use of modified inkjet printers to deposit matrix – analyte mixture on target plates with high precision via computer control.	Baluya *et al.*[48]
Automated Deposition	Robotic systems that can deposit matrix / analyte with high precision, often with drying capabilities included. e.g. Bruker ImagePrep system.	http://www.bruker.com/products/mass-spectrometry-and-separations/maldi-ms/imageprep/overview.html Marko-Varga *et al*.[158]

1.4. Laser Choice for MALDI

Lasers are used as part of the ionisation source in MALDI MS. Hence, there has been much research into optimisation of laser source in various analytical applications. Generally MALDI uses UV laser sources such as frequency-tripled or -quadrupled Nd:YAG lasers (1064 nm tripled to 355 nm or quadrupled to 266 nm),[6, 49] nitrogen lasers (337 nm)[50, 51] or more recently, high repetition (up to 20 kHz, but optimally 5 – 10 kHz) frequency tripled Nd:YVO_4 lasers (355 nm), the latter which allows rapid throughput of samples compared to low-repetition lasers e.g. N_2 lasers which run at 50 Hz.[52] The solid-state neodymium lasers generally have longer instrumental lifetimes compared to nitrogen lasers. However, N_2 lasers do generally offer more energy per pulse, and are generally inexpensive compared with solid state lasers. Hence there are advantages and disadvantages to both types of laser. Although the work in this thesis is primarily concerned with UV MALDI (herein simply referred to as MALDI), MALDI using infrared-emitting lasers (IR MALDI) is also possible.[53-55] Generally, the choice of laser will influence the choice of matrix used, as it is prudent to choose a matrix that has a maximum absorbance at the lasing wavelength or close thereto to avoid degradation of samples from direct laser irradiation.

The beam profile of the laser, which is incident on the sample, is extremely important for the generation of respectable ion yields.[50, 56]

The spatial distribution of incident photons,in the beam profile, and hence incident on the sample, is an important factor to consider (and indeed measure) in MALDI. This is because the ion yield, *Y*, is mathematically

related to the so-called incident fluence (flux, *H*) of photons falling on an area, by the power law $Y \propto H^m$ where *m* can be elucidated by taking the gradient of plots of log *Y* vs log *H.* Additionally there is a threshold, under which fluence should fall the ion yield vanishes to zero. To calculate the fluence falling on an area of sample, the shape and size of the laser beam must be known. Therefore the incident laser beam profile is an important parameter to measure in MALDI, Ideally an incident beam should be circular and without speckle or hot-spots (i.e. is uniform in shape and photon flux), to ensure uniformity of ionisation by ensuring constant fluence over an area. Generally the beam incident on a sample has a Gaussian profile. Use of fibres to deliver the laser to a sample can introduce speckle patterns through attenuation of the beam.[58]

A range of different physical techniques can be used to measure the beam profile.[57-59] The area of the beam as well as its position is crucial for the determination of the energy administered to the sample in a certain area i.e. the beam fluence in units J m^{-2}. Recently Steven *et al.* recently reported a comparative study of a fluorometric beam profiling technique *vs.* ablation of a film of CHCA with discrepancies observed in the calculated beam area between the two techniques, thus demonstrating the need for caution if calculating beam fluence using a single technique alone.[60]

1.5. Desorption-Ionisation

Desorption-ionisation of the solid analyte into the gas phase are the crucial steps in MALDI in order to generate gaseous-phase ions. This process is initiated by irradiation of the sample, which is held under vacuum, by the laser. A plume of ions is the result of the process. But, due to the rather empirical nature of early MALDI research hampered by a lack of consistent model, questions still remain over the true nature of the DI process, though a number of theories have been proposed. The lack of consistent theories to bolster the empirical observations , particularly with respect to ionisation and desorption processes in MALDI has led to challenges later on in research requiring more non-empirical, quantitative and semi quantitative approaches, particularly in imaging experiments where non-standard substrates such as biological tissue can influence yields of ionisation.

It is almost universally agreed that the desorption (or ablation) process begins with the absorption of photons by the matrix. This generates molecular excited singlet states which are depleted by vibrational relaxation which causes localised thermal heating in the sample. The energy is released comparatively slow compared to the absorption process. The slow release of energy via the matrix's excited state, which is dictated by the lifetime of the excited state, avoids thermal degradation of the sample. However, the localised heating is still enough that the molecules begin to separate by expansion until they desorb as a gas from the solid surface, and are entrained by the electromagnetic fields. The plume itself is often described as an adiabatic free jet. Laser fluence is critical to the nature of this process. High fluences tend to desorb more material at once as more

energy is supplied to the sample in one go, and the regime is described as 'ablative' i.e. removes substantial amounts of material from the surface, and often clusters are produced and are then are seen in the resulting mass spectrum due to the sheer amount of material removed from the surface. Lower laser fluences tend to give a more steady 'desorptive' regime, where a constant amount of material is removed steadily with negligible cluster formation. This model is often known as the thermal desorption model. An alternative to the latter model is the phase explosion model. In this model the matrix and analyte are superheated to a thermodynamically unstable state, where the rate of energy supplied to the sample far exceeds the ability to shed the energy by conventional melting / boiling. This is said to be rapidly followed by a phase explosion through 'spinodal decomposition' (i.e. rapid transition to the gas phase and ablation of the material over a wide area) which is followed by desorption. The physical processes involved in both models have been reviewed in great detail by Driesewerd,[61] (and references therein) who tends to reject the phase explosion model as most research on spinodal decomposition – the major route for desorption proposed in this model – was performed on homogeneous systems, whereas for MALDI, where co-crystals of matrix and analyte are analysed, this is obviously not the case. In all likelihood It is most probable that the desorption process occurs as a mixture of processes.

Regarding ionisation in MALDI, a consensus has emerged that a two-step framework is in operation, with a primary ionisation step followed by a secondary ionisation step. Primary ionisation is a hotly debated

subject, with many of the processes explained in detail in the excellent review by Knochenmuss, and the references contained within.[62] Primary ionisation mechanisms proposed include the cluster model by Karas (formerly known as the *lucky survivor* model) where clusters of ions are already pre-formed in the analyte-matrix co-crystal in the solid state, and only some make it through the plume into the mass analyser.[63, 64] This model is indeed plausible if one considers that certain molecules when mixed with acidic matrices may themselves become protonated *before* co-crystallisation i.e. $[M+H]^+$ can essentially be pre-formed. The energy pooling model[62, 65-67] suggests that an energy 'pool' is created in the bulk co-crystal after laser irradiation. Generation of two matrix excited singlet states (S_1) from the ground state (S_0) by absorption of a photon is followed by non-radiative energy transfer processes between a pair of proximal excited state matrix molecules (S_1, S_1) regenerating a ground state molecule (S_0) and an even higher-energy excited state molecule (S_n). Thus, energy can be pooled, and if sufficiently high-energy states can be reached, photoionisation of the matrix can occur instantaneously.

The secondary ionisation process, unlike the primary ionisation process is not perhaps the subject of as much debate. It is generally accepted that secondary ionisation i.e. of the analyte (M), occurs in the rising gas plume, which consists mostly of neutral matrix and analyte molecules can simply be described by bimolecular reactions and conventional thermodynamics e.g. [Matrix-H] + M → $[Matrix]^-$ + $[M+H]^+$.[62, 68, 69] Collision of analyte with matrix ions in the rising plume thus leads to

reactions such as proton transfer or electron transfer, generating ions within the plume. Proton transfer from the acidic matrix to analyte is a major source of the $[M+H]^+$ peaks observed in many MALDI mass spectra. The ability of a matrix molecule to protonate an analyte can be predicted from standard tables of ionization potentials.[62]

1.6. Atmospheric Pressure Ionisation Techniques

Traditional MALDI is a vacuum ionisation technique, and as such is impractical for some analysis. There are however a range of techniques that have been developed where ionisation proceeds under atmospheric conditions. However, this presents an interesting problem: whereas these techniques generate ions at atmospheric pressure, mass analysers are under ultrahigh vacuum. Therefore pumping systems have been developed which compartmentalise a series of chambers under sequentially increasing vacuum. This has therefore allowed the development of a range of techniques outlined herein.

Electrospray Ionisation (ES, ESI) is an atmospheric pressure ionisation technique that ionises molecules using an electric field.[70] Analyte molecules are passed as a liquid through a capillary with flow rates of around 1 – 10 μL min^{-1}. A potential difference of the order of kilovolts is generated between the capillary and an electrode resulting in electric fields of 10^6 V m^{-1}. Charge then builds up at the end of the capillary, which leads to nebulisation of the liquid and ionising the molecules in the process. Thus a spray of ions is generated. The potential difference required to generate

the electrospray is known as the 'onset voltage', and is different for various solvents. The shape of the droplet is known to change depending on the voltage applied. At the onset voltage a so-called Taylor cone is observed, and droplets are produced from the pressure produced by the growing charge at the tip, the force of which becomes greater than the surface tension. After the electrospray is generated, solvent is removed by passing the sprayed molecules through a stream of inert gas or alternatively, a heated region before introduction to the mass analyser. A schematic of a typical electrospray ionisation source is presented in Figure 1.3.

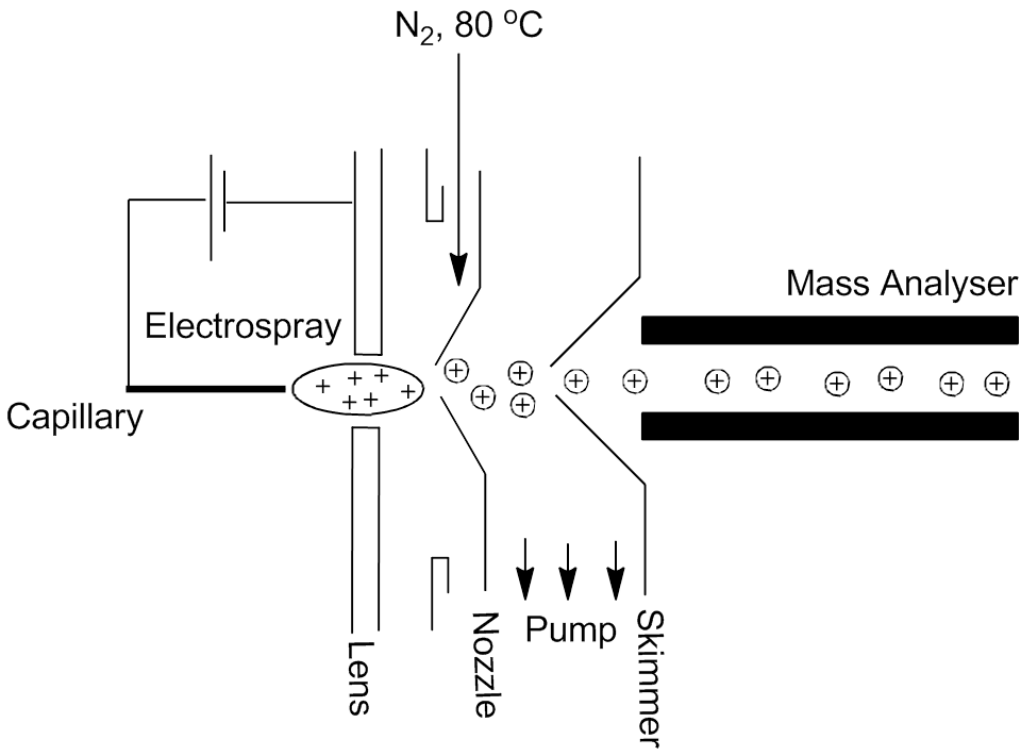

Figure 1.3.: Schematic of a typical electrospray ionisation source including capillary with potential difference applied, Taylor cone and focussing through a nozzle and skimmer with sequential pumping. A curtain of heated nitrogen gas is used to strip the solvent in the electrospray before introduction to the mass analyser(s).

Ionisation of large molecules using electrospray will generally produce multiply charged ions as all possible sites, producing spectra with a charge ladder. Proteins for instance produce this effect due to their large number of ionisable sites.[71] Although this may seem like a complicating factor, it can actually improve sensitivity by allowing the user to tune the *m/z* of the ion of interest to the most sensitive range of the mass analyzer that the source is coupled to. Electrospray of small molecules generally produces monocharged ions, as for MALDI, so it can be a useful ionisation technique for the analysis of drugs, metabolites and lipids also as well as for chemical characterisation of novel compounds that have *m/z* too large for techniques such as electron impact (EI) or fast atom bombardment (FAB).

Atmospheric pressure MALDI (AP-MALDI) has been developed to extend the MALDI technique to ambient pressure analyses.[72, 73] Laser irradiation of a sample target plate is performed exactly the same as vacuum MALDI, using the same matrices, for example CHCA. However, AP-MALDI is pneumatically assisted; the ions desorbed from the target plate are transferred orthogonally into an AP/vacuum interface by a stream of nitrogen gas. Therefore, ions generated at ambient pressure by MALDI are introduced into the mass spectrometer for analysis (Figure 1.4). AP MALDI is less sensitive than vacuum MALDI, and the sample amounts required can be higher. This is due to the fact that ions can be 'quenched' by collision with atmospheric species prior to being introduced into the mass

analyser. Thus, it is generally less sensitive and in the analysis of proteins in particular is limited to the ionisation of small proteins which even then form clusters rather than protonated molecules.

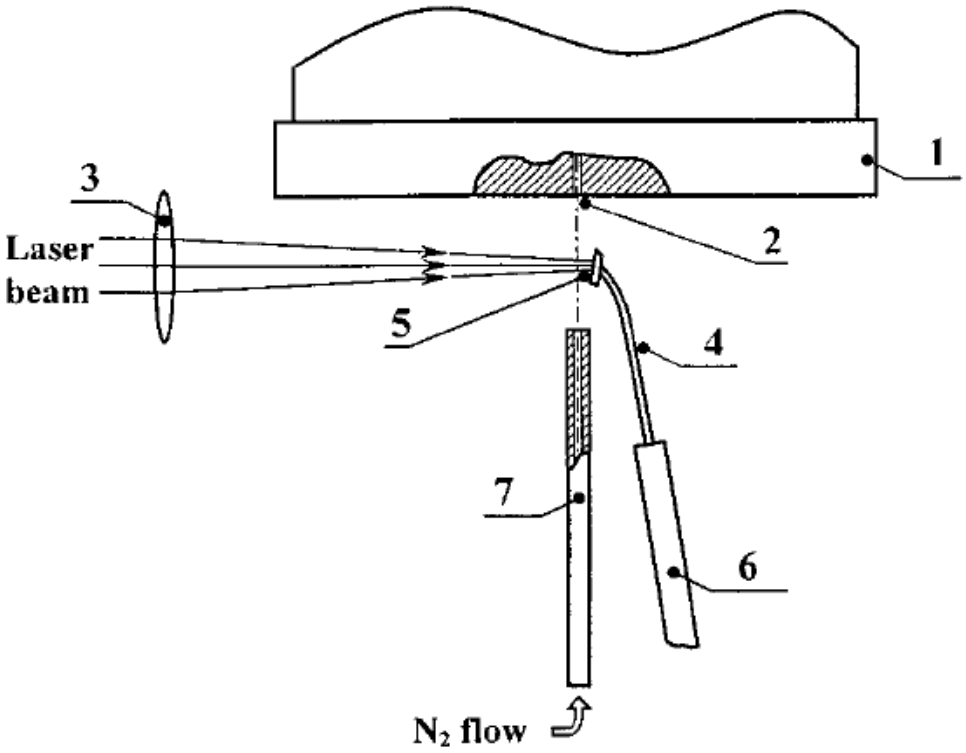

Figure 1.4: The physical principes of Atmospheric pressure matrix assisted laser desorption ionisation (AP-MALDI). 1, AP interface; 2, inlet nozzle to MS instrument; 3, quartz lens; 4, replaceable target tip ; 5, stainless steel MALDI target plate; 6, target holder; 7, stainless steel capillary gas nozzle. Reprinted with permission from Laiko *et al*.[72] Copyright 2000 American Chemical Society

1.7. Mass spectroscopic Imaging under Ambient Pressure using LESA coupled to mass spectrometry.

Liquid extraction surface analysis mass spectrometry imaging (LESA-MSI) is a relatively new and novel technique that can analyse surfaces by mass spectrometry. Contrary to traditional vacuum-based MS imaging techniques such as MALDI and secondary ion mass spectrometry (SIMS), it takes place under ambient temperatures and pressures. Other popular ionisation sources used for imaging under ambient conditions include (but are by no means limited to): probe electrospray ionisation (PESI)[74] desorption electrospray ionisation (DESI),[75, 76] laser-ablation electrospray ionisation (LA-ESI),[77] and nanoelectrospray desorption electrospray ionisation (nano-DESI).[78, 79] A review of the area is available[80], and so a discussion of LESA-MSI only is made herein.

The LESA sampling technique[81] involves two steps. In the first step, a micro liquid extraction termed as a 'liquid microjunction' (LMJ) is performed on the surface, using a microscale pipette containing either a polar organic solvent such as methanol or acetonitrile, or containing water. A small amount of solvent (μL to nL) is deposited on the surface. The analyte is then directly taken up into the solvent from the surface, and the solvent, now containing the analyte, sucked back into the microsyringe. The contents of the microsyringe are then introduced into a chip-based nano-electrospray ionization source for mass spectral or tandem mass spectral analysis. Dissolution rates of the analyte in the solvent used to produce the LMJ are crucial to this analysis technique; the faster the analyte dissolves, or is extracted by, the solvent used for the LMJ, the more analyte can be ionised and the better the signal shall be i.e. more ion counts. It is often therefore useful to study the solubility of an analyte before a solvent for

LESA is chosen. Further details on the practical use of LESA for analysis is given in the introduction of Chapter 3.

1.8 Mass Analysers used in this Thesis

After gaseous ions have been generated, they must be separated according to their mass to charge ratio (*m/z*). This can be achieved in a number of ways. Mass analysers are often graded according to a number of benchmarks:

- Mass limit – the upper *m/z* which the mass analyser can measure.
- Resolution – how well the mass analyser can resolve closely spaced peaks. This is usually defined as *m/z* / FWHM e.g. a peak at *m/z* 1000 with a FWHM of *m/z* 0.5 would have a resolution of 2000.
- Accuracy – how close the experimentally determined mass is to the theoretical mass. Usually measured in parts per million (ppm).

There are a number of mass analysers used in this thesis, as described forthwith.

1.8.1. Time-of-Flight Mass Analysers

Time-of-flight (TOF) mass analysers separate ions according to their velocity in an evacuated field free flight-tube.[82, 83] Ions are introduced into the flight tube after being accelerated through an electric field. A typical

setup is shown in Figure 1.5. The velocity (v) caused by acceleration of ions from the ion source is dependent on the mass of the ion as follows:

$$v = (2zeV_s / m)^{1/2}$$

Where z is the charge of the ion, e is the elementary charge, V_s is the accelerating potential, and m is the atomic mass of the ion. After this initial acceleration the ion is free to fly in the field free flight tube, in the direction of the detector at a constant velocity, v. The time taken to reach the detector for a flight tube of length L is:

$$t = L / v$$

And then by replacing v in the previous equation, one can obtain:

$$t^2 = m/z\ (L^2/2eV_s)$$

and if we consider that the terms in the parenthesis are an experimental constant associated with the spectrometer in question we simply obtain:

$$t^2 = k \bullet m/z$$

thus by measurement of t^2 we can directly calculate m/z.

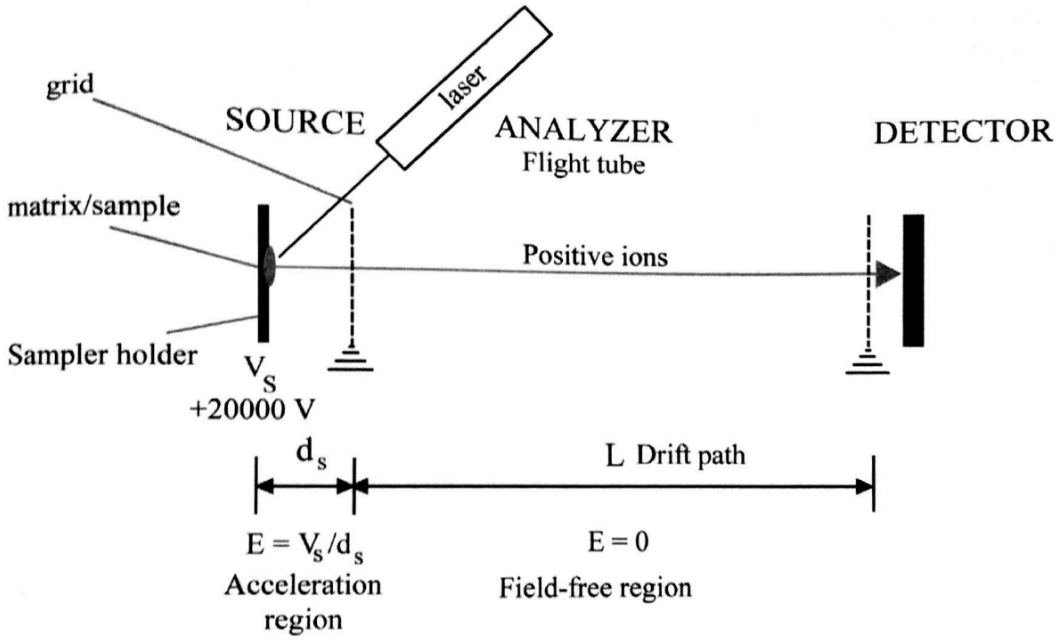

Figure 1.5: A MALDI instrument set up to accelerate and measure the *m/z* of positive ions by Time-of-Flight (TOF) mass analysis. After ions are generated in the source, they are accelerated by the voltage V_s. They then drift toward the detector in a field-free region of length *L* known as the flight tube. The initial velocity of the ions entering this field free region depends upon the mass of the ions. The ions can therefore be resolved by the time they take to reach the detector.

Ions with large masses enter the flight tube with lower velocities (as $E_k = (mv^2)/2$) than those with lower masses and the time taken to reach the detector for the larger ions is longer, and thus these will be calculated as having large *m/z*. However, as these measurements are arbitrary, calibration of the TOF with standards is essential for maintaining the accuracy of an instrument over its lifespan.

Technically there is no mass limit for TOF mass analysers, and they have an accuracy of 200 ppm and a resolution of 4000. With orthoganol ion source TOF mass analysers resolutions of up to tens of thousands is

possible due to the minimisation of the initial velocities of the ions in the flight tube, which reduces dispersion and subsequently improves mass resolution. A variant of the TOF mass analyser called the TOF-reflectron was introduced for improved resolution. The reflectron corrects inconsistencies in kinetic energy for ions with the same *m/z* value by the introduction of a curved flight path.[84] TOF reflectrons have improved resolution and accuracy (20 000, 10 ppm) at the expense of mass limit (*m/z* 10 000) compared with TOF mass analysers.

1.8.2. Quadrupole Mass Analysers

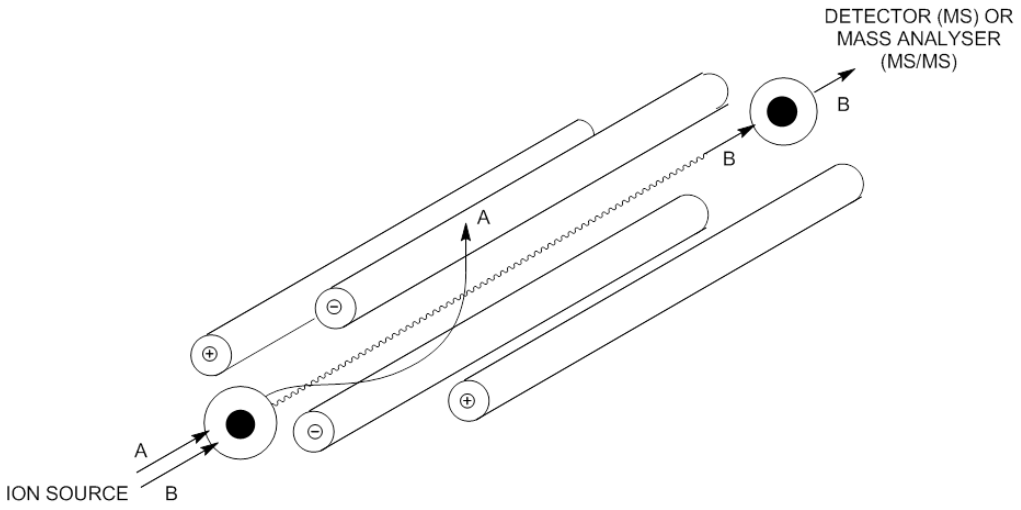

Figure 1.6: Quadrupole (Q) mass analyser showing the arrangement of four parallel rods with AC current applied at radio frequency. Two ions of differing *m/z* (A and B) are pictured entering the quadrupole with only B exiting (resonance condition) and A discharged upon the rods (non-resonant condition). Note in Q mode, a DC potential is applied over the four rods, whilst in RF only mode (q), the

DC potential is not superimposed. Note that the direction of ion motion is always defined as the *z* axis.

Quadrupole (Q or q) mass analysers[85] separate ions according to their *m/z* by the trajectory stability of the ions in an electric field.[86] The quadrupole consists of 4 parallel rods. There is a radiofrequency (RF) alternating current (AC) potential applied to the rods which give them either a negative or positive charge. A direct current (DC) potential can also be applied across the rods. A typical setup is shown in Figure 1.6. The quadrupolar electric field generated by the anodes (+ Φ) and cathodes (– Φ) that ions are subjected to is therefore a superposition of direct potential (U) and oscillating RF potential ($V \cos 2\pi\nu t$) and can be mathematically described as:

$$+\Phi = (U - V \cos 2\pi\nu t) \text{ and } -\Phi = -(U - V \cos 2\pi\nu t)$$

Where ν is RF frequency in Hz and *V* is the maximum amplitude of the RF voltage. In a typical quadrupole *U* can vary from 500 to 2000 V and *V* can vary from – 3000 to +3000 V.

Resolution is achieved in the quadrupole by variation of the ratio between *U* and *V*. By alteration of the AC:DC applied potential ratio, a certain *m/z* ratio can be selected as ions that are not stable in the electric field collide with the rods and discharge. Ions that are stable in the field pass through unadulterated. The mathematics of motion (and thus stability

with respect to hitting the rods) of the ion in the electric field describing this are beyond the scope of this thesis, but the result found is that by linear variation of *U* and *V*, the mass of an ion can be selected. The so-called Mathieu Diagram plots stability areas of ions in the quadrupole as a function of *U* vs. *V*. Hence by keeping the ratio of *U* and *V* constant, whilst increasing both linearly as a function of each other, masses can be selected based upon their stability (or instability) in the quadrupole. Mathieu stability diagrams summarise this relationship graphically (Figure 1.7).

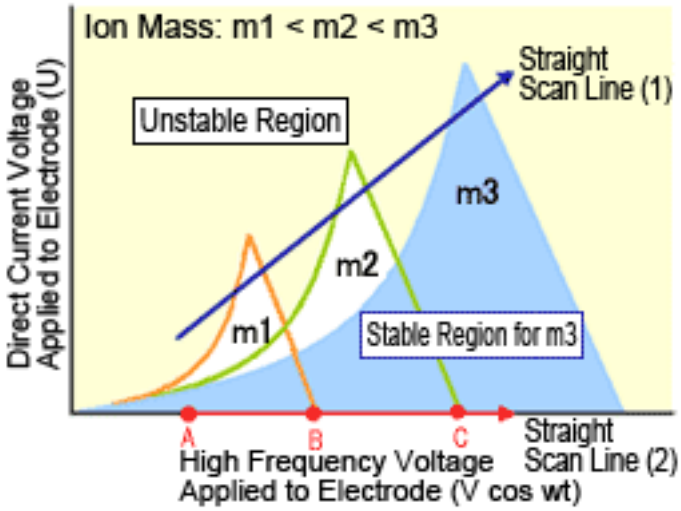

Figure 1.7: A Mathieu stability diagram as a function of *U* and *V* for ions with masses *m*1 < *m*2 < *m*3. Changing *U and V* whilst keeping the *U:V* ratio constant allows selection of ions successively. If *U* is zero i.e. no direct potential is applied then there is no resolution. In this case, ions will pass through the quadrupole if *V* is within their stability area.

A quadrupole that has both AC and DC potentials applied to it are denoted in the literature by a capital Q. Those that work in RF mode only i.e. with no mass selection, are denoted by a lower-case q. However, these

may be used as collision cells for MS/MS experiments. Combinations of q and Q mass analysers can be assembled sequentially for tandem mass spectrometry experiments (see later). Linear ion trap (LIT) mass analysers work in a similar manner to quadrupole mass analysers, though eject ions *via* resonance frequency destabilisation in an electric field.[87] The mass limit of quadrupole mass analysers is around *m/z* 4000, with accuracies typically of 100 ppm, and resolution of 2000.

1.8.3. Orbitrap® Mass Analyser

The orbitrap® mass analyser is an ion trap analyser that also acts as a detector for ions (Figure 1.8).[88] An electrode is placed within a hollow barrel, which also acts as an electrode. A DC potential difference in the range of kV is applied across the electrodes creates an electric field. Ions are introduced into the orbitrap® and orbit the inner electrode, held in position by a combination of centrifugal force and electrostatic attraction. The frequency at which the ions orbit the central electrode can be detected by their image current on the outer electrode. The mathematical expression by which the motion has been described is that of a simple harmonic oscillator or pendulum where the position of the ion in the *z* direction in time can be described by:

$$z(t) = z_0 \cos \omega t + (2E_z / k)^{1/2} \sin \omega t$$

where

$$\omega = (k \cdot z/m)^{1/2}$$

Hence from these equations it is possible to see that the *m/z* ratio is directly linked to the frequency of spiral oscillation within the orbitrap®; using Fourier transform, it is possible to change from the time domain to the frequency domain, all the ions can be detected instantaneously and a mass spectrum can be produced.

The mass limit of Orbitrap® mass analysers is around *m/z* 50 000, with accuracies typically of < 5 ppm and resolutions of around 100 000. Hence they are amongst the most accurate and high-resolution mass analysers available.

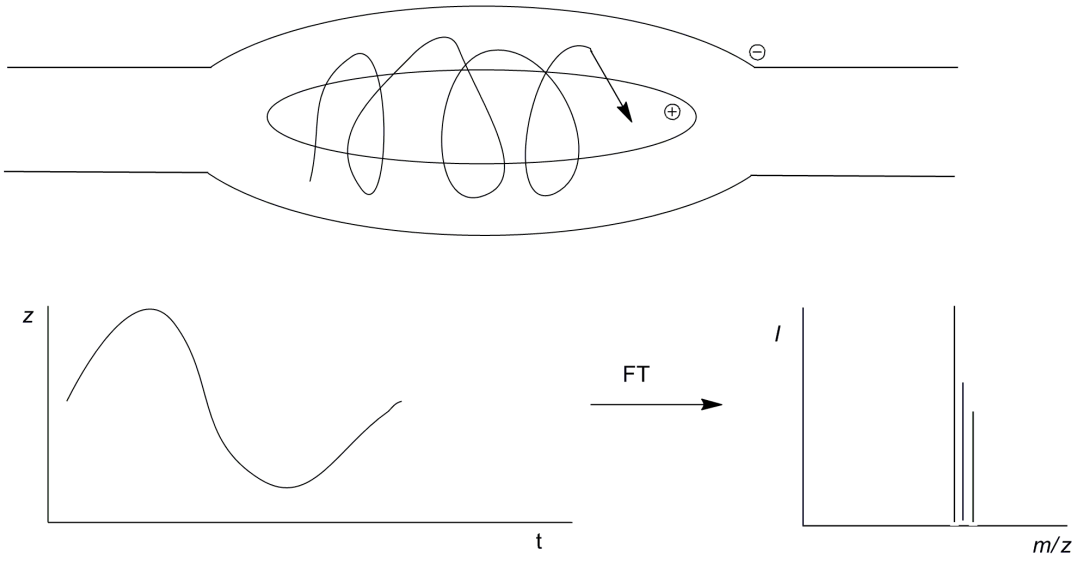

Figure 1.8: The principles behind the orbitrap® mass analyser. Ions orbit the central electrode, at a resonant frequency depending on their *m/z* in a spiral pattern. Detection is achieved by Fourier Transform (FT) of all the frequencies detected at once.

1.8.4 Other Mass Analysers

The previous section detailed the mass analysers used within this thesis. There are however, many other mass analysers used for mass spectral analysis.

Magnetic and electromagnetic mass analysers use perpendicular fields to deflect ions according to their mass to charge ratio thus creating spatial resolution in the flight paths taken and generating a mass spectrum from differences in path length. *Ion traps* such as the 3D Paul ion trap and 2D (LIT) ion traps utilise enclosed quadrupoles, that are equipped with electromagnetic focusing lenses that allow the reflection of ions within them thus trapping the ions inside the analyser.[87] Ions can be expelled from the trap by variation of these fields to select ions, much like the standard quadrupole, in order to obtain a mass spectrum. As a result, the mass limit of ion traps are similar to quadrupole mass analysers (ca, 5000 Da), but the resolution is slightly improved due to the cycling of the ions multiple times within the trap (Resolution of ca. 4000 compared to ca. 2000 for a standard quadrupole) . *Fourier Transform Ion Cyclotron Resonance (FTICR) mass analysers* inject ions into a cubic trap located in an high strength magnetic field (typically 3 - 24 T) which has an orthogonal trap voltage applied (typically 1 V). This leads to ion cyclotron motion around the pole of the magnetic field. Ions can be resolved into a mass spectrum by Fourier transform of the frequency-time domain spectrum by which they rotate in the cyclotron. Because of the large frequency range induced by the

cyclotron motion, the resolution of the measurement suprasses most MS analysers, including the Orbitrap® (resolutions of ca. 500,000 in FTICR MS compared to 100,000 for Orbitrap® MS), but takes a longer time to acquire spectra and can be affected adversely by ion-ion interactions in the cyclotron.[87] It should also be mentioned that Caprioli et al has coupled FTICR mass analysis to MALDI and has reported imaging of drugs such as olanzapine and imatnib in real tissues such as kidney, liver and diseased tissue such as glioma.[89] Because of the high resolution of the technique, accurate measurement of drug mass is possible, with final confirmation of the drug identity from an external quadrupole in an MS/MS experiment. However, the time of analysis of MALDI-FTICR imaging is typically very slow (4 pixels per min) compared to other MALDI imaging techniques such as MALDI-QTOF (30-50 pixels per min), and hence may not be suitable for routine screening applications, but rather for situations where images containing high resolution mass spectral information is needed.

1.9. Tandem Mass Spectrometry and the QSTAR XL Instrument

The sequential linking of two or more mass analysers can be used for performing tandem (MS/MS) experiments. Instruments with two or more mass analysers in sequence are known as *hybrid instruments.* It is these latter instruments that have revolutionised the study of small molecules in biological environments. Generally these are denoted by the combination of letters e.g. qQTOF would denote an instrument with three mass analysers - RF quadrupole, quadrupole and time-of-flight mass analysers –

linked in sequence. Alternatively, mass analysis may be performed through time, though we will not discuss these techniques in this introduction.

A number of MS/MS scan types are possible:

- *Product ion scan.* Requires a setup such as QqQ or QqTOF. The precursor ion is selected and then fragmented into product ions by collision-induced dissociation, which are scanned.

- *Precursor ion scan.* Requires two mass analysers e.g. QQ. A product ion is selected by the second mass analyser and the precursor ion is determined by scanning the first mass analyser.

- *Neutral loss scan.* Requires two mass analysers e.g. QQ. A mass difference is defined by the user and all the precursor / products are identified with the specified mass offset are identified by scanning both mass analysers simultaneously.

Collision-induced dissociation (CID) is often used to deliberately fragment molecules for MS/MS analysis. The most widely used method to accomplish this is by passing the ions through a collision cell, which contains an inert gas. In the process of CID, precursor ions collide with the immobile gas molecules in the collision cell, which in turn increases their internal energy. This process is known as collisional activation (CA) If this internal energy is greater than a certain threshold, the molecule can

fragment (or decompose). Collision cells are often RF-only quadrupoles, q, and these are usually placed in between two mass analysers. This setup allows the selection of precursor ion in the first mass analyser, CID in the RF-only quadrupole, and mass analysis of the product ions (fragmentation products) in the second mass analyser.

Tandem mass spectrometry is useful for a number of reasons:

- *Determination of structure.* Product ions can serve as a molecular 'fingerprint' for certain structural features within a molecule.
- *Selectivity.* For the same reason, molecular 'fingerprints' based on the product ion scans can be used to determine the presence of a molecular species within a mixture of other species.

Whilst these are common triple quadrupole methods, the majority of work in this thesis, an Applied Biosystems QSTAR XL quadrupole time-of-flight (QqTOF) mass spectrometer (Figure 1.9) is used, which is a hybrid instrument that incorporates quadrupolar mass analysers in tandem with a flight tube. Despite its Qq designation, the instrument actually incorporates 3 quadrupoles within it, designated q0, Q1 and q2. q0 is an RF only quadrupole that is used for collisional cooling of the ions from an ion source (in this case MALDI) to reduce the extent of fragmentation experienced and to fully focus the ions into Q1. Q1 is a full quadrupole that can be operated with DC current superimposed to select an ion of interest, as described in the quadrupole section. q2 is a RF only quadrupole that is used as a

collision cell. In MS/MS mode, Q1 is used to select the ion of choice and q2 to fragment it further to obtain a signature fragmentation for the precursor ion of interest, whose product ions are then resolved by the TOF mass analyser – a product ion scan. Collisional fragmentation requires the introduction of a stream of an inert gas, either nitrogen or preferably argon into the q2 collision cell.

The QqTOF arrangement prohibits precursor ion and neutral loss scanning (recall this requires two full Q), and in theory mass range is dictated by the quadrupoles only but balances it out with high sensitivity and resolution.

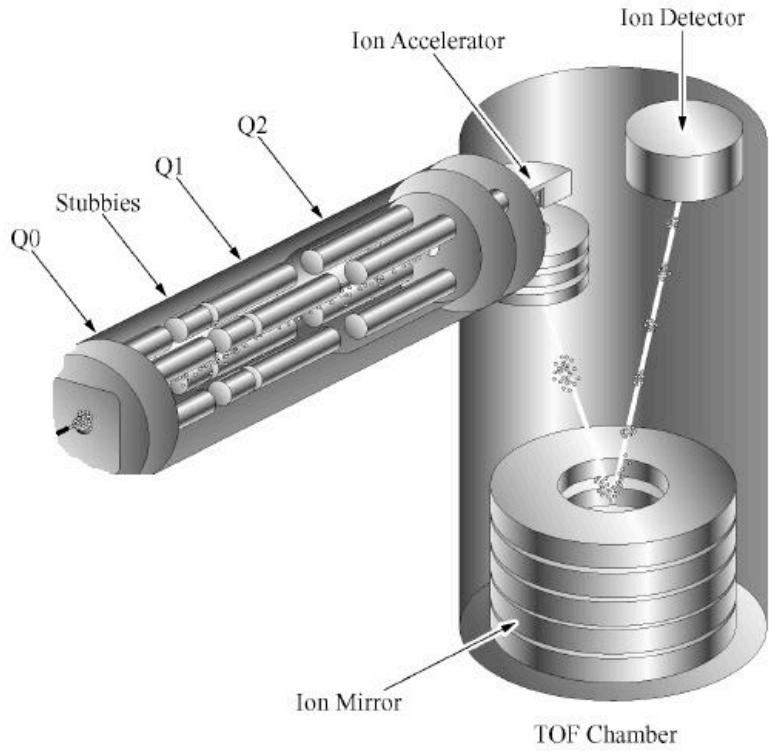

Figure 1.9: Schematic of the Applied Biosystems QSTAR XL hybrid QqTOF mass spectrometer used predominantly in this study (taken from Applied Biosystems

hardware overview). Q0 and Q2 are q RF-only quadrupoles with Q2 used as the collision cell. Q1 is used to select the ion of interest.

1.10 Analysis of Drug Molecules Using Mass Spectrometry

Generally, mass spectra generated using MALDI as the ionisation source are simple, being dominated by the single-charged mass ion. Due to this fundamental property of the technique, and the fact that an organic matrix protects the sample from the full laser energy (thus minimising fragmentation), it is suitable for the analysis of complex mixtures such as the distribution of a specific analyte in biological tissues and fluids. MALDI is also the least sensitive of the ionisation techniques to ion suppression,[3] which makes it a good candidate for studies on complex samples like human biofluids or biological tissues, where this can be problematic.

MALDI is suitable for the analysis of a range of molecules of all molecular weights including peptides[8-11] oligonucleotides[12-20] lipids,[24-30] proteins,[31, 32] and carbohydrates.[33, 34] This led to the realisation that it could be used for the analysis of drug molecules in samples,[21-23] and often in complex biological samples. There are, in general two types of analysis that can be performed using MALDI MS with drug molecules:

i) *Profiling;* where a sample is mounted onto a MALDI plate and matrix is applied in areas of interest on the samples, and the mass spectrometric analysis is performed on the area, collecting spectra where the matrix was applied. Instances of this could be checking for a drug in cross-sectioned tissue on an organ of

interest. The advantage to this technique is that it is extremely rapid and thus many samples can be analysed, the disadvantage is that the full distribution of the drug may only be estimated.

ii) *Imaging or MALDI MSI;*[90] where a sample is mounted onto a MALDI plate and matrix is applied across the whole sample. The laser is rastered across the sample and mass spectra collected in a serial manner, collecting a hyperspectral data cube of (*x,y*) position and *m/z*. Images are presented in 2-D form by choosing a single *m/z* and showing its distribution in (*x,y*). The advantage to this is that 2D images are thus constructed from *voxels* as they encode spectral intensity information, and thus contains *quantitative* data regarding the distribution of a drug across the whole sample. The disadvantage to using MALDI MSI is that it is often slower than profiling as many more mass spectra need to be collected, depending on the imaging resolution required i.e. at higher spectral resolutions and smaller voxels then more spectra have to be collected,[91] though continuous raster sampling using high repetition-rate lasers may speed up analysis.[92] MALDI MSI can be used to screen drug distributions across drug-dosed whole animal sections,[93] important for drug development, assessing pharmacodynamics and toxicodynamics.[94]

Both MALDI profiling and imaging share the important advantages that they are both one-step, label free analysis of molecules. It is especially powerful

when used on drug molecules from biological samples, as one can discern between the observation of the drug and its metabolites, which one cannot tell the difference with standard industry benchmark techniques such as autoradiography. Relative abundance of the drug may be realised, and steps toward quantitative analyses are being researched.[95-105] The final advantage of using mass spectrometry as an analysis technique is that all the ions from a certain area of interest can be collected at once when applying a TOF or FT mass analyser, giving unprecedented throughput. Herein, we outline how both profiling and imaging using MALDI MS has been used for the analysis of drugs in a range of different analytical samples.

1.11 MALDI MS profiling of drug molecules

Luider and co-workers[106] used MALDI-TOF MS to give qualitative and quantitative analysis of the anti-retroviral protease inhibitors lopinavir and ritonavir, used in the treatment of HIV. The result demonstrated the suitability of MALDI as the ionisation source for the analysis of small organic molecules; previously the technique had been generally applied to ionise large biomolecules. It was possible to detect and quantify clinically relevant levels of lopinavir using a clinical sample of monocytes extracted from blood.

Acetyl salicylic acid (aspirin) was detected and the conditions for detection optimised by Lacey *et al.* using a triple quadrupole MALDI-QqQ mass spectrometer.[107] The drug molecule was observed in the mass

spectrum generated, always as the sodium or potassium adduct; the protonated species was not observed. This led the authors to use a cationisation strategy to optimise the detection of the drug. Metal chloride salts (MCl, M = Li, Na, K, Rb, Cs) were co-evaporated onto the sample plate with the drug and 2,5-dihydroxybenzoic acid (DHB) as matrix (ratio: 2:6:1 aspirin : DHB : MCl). It was found that significantly better signals were obtained with the use of rubidium chloride and caesium chloride as the cationisation source compared to other metal chloride salts tested. Density functional theory calculations were then used to probe the mechanism and energetics of drug-metal adduct formation. The authors concluded that the energy available after plume formation would favour the formation of adducts with the heavier metal ions i.e Rb^+ and Cs^+ and increase the intensity of the signal generated, which was consistent with what had been observed experimentally.

Persike and Karas used a range of phenothiazines (10 in total, frequently used in the treatment of psychiatric diseases) as well as a group of mixed drug molecules, (again 10 in total including Loperamide and Procaine) in order to demonstrate the versatility of the MALDI technique for the quantitative determination of small pharmaceutical molecules.[108] α-Cyano-4-hydroxycinammic acid (CHCA) was used as the matrix, due to its high level of crystallinity which aids the ionisation of small molecules (<600 Da) such as those used in this study. To minimise the effects from poor crystallisation, the authors used a large number of laser shots per sample well. It was possible to quantify all ten of the phenothiazines

simultaneously with each drug at a concentration of 250 fmol μL^{-1}, generating a spectrum that could easily identify all 10 drugs separately from each other. Furthermore, any of the phenothiazine drugs could be used as an internal standard to determine the concentration of the other 9 drugs. The same results were also observed with the mixed drug cocktails. The authors, to demonstrate the potential of the technique for analysis of authentic biological samples, then used human plasma spiked with phenothiazine drugs. The spiked plasma samples were extracted with an organic solvent mixture (1:1 TBME/EtOAc) and co-crystallised with CHCA matrix. It was possible to detect, as well as quantify the amount of drug in all samples. The MALDI assay was found to be comparable, and in many cases superior, in its sensitivity compared to HPLC, fluorescence and colorimetric detection methods reported for the detection of phenothiazines in blood plasma samples.

The success of MALDI MS in drug analysis is probably best summarized in the sheer amount of low molecular weight pharmaceuticals that have been analysed. Over-the-counter drugs such as aspirin [107], dramamine and Sudafed [109], HIV inhibitors and retroviral drugs [106, 110, 111]; narcotic substances such as cocaine [112], performance-enhancing steroids [113], beta blockers such as Talinolol [114], Tamiflu [109], Viagra [115, 116] and the anti-cancer drug Pemetrexed [117] have all been detected successfully by MALDI. Chemical derivatisation of drugs may make increase ionization efficiency and hence improve the sensitivity of analyses; for example Flinders *et al* have used the reaction of hydrazine-based reagents such as

2,4-dinitrophenylhydrazine with carbonyl containing drugs such as fluticasone propionate to improve sensitivity by up to ca. ten fold. However, it must be noted that caution should be used when interpreting results from derivatised drug molecules. In practice, derivatisation of the drug molecules could potentially change the therapeutic properties and so the approach is of limited value unless derivatisation can be performed at the point of analysis and for that purpose only.

Profiling has been used to rapidly optimise the choice of matrix for MALDI experiments on authentic tissues. The ionisation of the anticancer drugs Afatnib, Erlotnib, Irinotecan and Perfenidone, for instance, has been assessed with a range of matrices including DHB and CHCA in ex vivo spotting experiments by Huber et al.[118] The authors demonstrated a relationship between the profiling experiments and results from MALDI MSI. Profiling of drugs ex vivo is therefore a useful predictive tool for gauging the performance of a matrix in combination with a drug prior to embarkation on more time-consuming in vivo experiments.

The detection of impurities from degradation by processes such as oxidation over time in active pharmaceutical ingredients is important to gauge the shelf life of nascent potential drug molecules. MALDI MS has been used successfully for the detection of Atorvastatin lactone, an oxidation product, in commercial statin Atorvastatin calcium tablets.[119] The use of the impurity in the sample allowed the relative quantification of the amount of Atorvastatin in the tablets, from the analysis of the signal intensity in the MALDI images, and thus potentially represents an important

step toward one-step drug semi-quantitative quality control procedures, circumventing the use of HPLC or GC after laboratory-scale liquid extraction. MALDI coupled to multivariate statistical analysis algorithms can be used to ensure drug product quality.[120]

1.12 MALDI imaging of drugs

MALDI-MS imaging (MALDI-MSI) seeks to produce two-dimensional images of (often biologically relevant) samples.[121-123] Preparation of samples[124] differs slightly in MALDI imaging experiments compared to standard MALDI-MS. Thin tissue samples[125] of low μm depth are prepared by cryosection, mounted on sample plates (usually stainless steel sheets or glass slides) and fixed, often with adhesive tape. Matrices are applied in imaging experiments, as listed in Table 1, using a number of techniques including acoustic matrix deposition,[45] dry and solvent-assisted blotting,[126] automated inkjet printing[48] and sublimation.[25] Air-spraying of the sample with matrix[127] rapidly leads to homogenously coated tissue samples at low cost and so is a fairly popular approach. Often, MALDI imaging experiments of drugs uses biological tissue samples,[128] which lead to unique challenges including suppression of ion counts, which leads to poor quality images, variability in ion counts across the tissue sample due to various tissue types and competition for ionisation from lipids and other ambient ions. *Thus, analysis of drugs by MALDI MS, and quantification in particular, is possibly the most challenging discipline of mass spectrometry currently being researched.*[1]

In a typical MALDI-MSI experiment (Figure 1.10), thousands of laser shots are taken in an ordered pattern across the mounted sample. Either the laser or the sample plate is rastered relative to the other.[129] Resolutions of 25–100 μm are attainable due to the highly collimated lasers used in the MALDI technique;[130] resolution of the images is dictated by the diameter of the laser beam and matrix crystal size; in general, MALDI imaging, in its current state cannot achieve diffraction limit images (ca. < 200 nm resolution) primarily due to the laser spots used being of the micrometer (10^{-6} m) order as well as the wavelengths of the lasers used.

As the images produced in MALDI are constructed from pixels containing intensity information (i.e. are technically voxels), this also has implications for resolution and sensitivity; larger pixels mean the generated images will be less-resolved, but the sensitivity per pixel is increased as more ions can be generated per unit area in the image. Smaller pixels give less sensitivity, yet the image will have greater resolution. The mass spectrometric data is acquired using a user-defined number of laser shots. Each division of the sample where MALDI has occurred will therefore be associated with a full mass spectrum for that area. Integrated signal intensities for each *m/z* ratio may then be reconstructed into images from the generated hyperspectral data cube (*x, y, m/z*); in theory, a separate image can be generated for any of the mass signals detected throughout the section, leading to the possibility of producing images that allow the spatial localisation of drugs and metabolites, all in one analysis step. Spot-to-spot voxel intensity is proportional to ion counts for a certain *m/z* in that area of the sample. The ion count intensity is dictated by the concentration

of the analyte in the sample in that region, but also from how efficiently it is ionised and relayed to the detector via whatever mass analysers are in place.

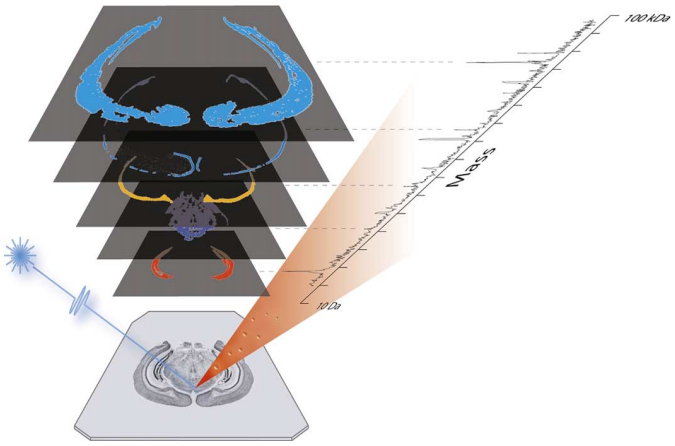

Figure 1.10: MALDI MS imaging of a thin tissue section from Rohner *et al*.[129].Reproduced with permission from Elsevier. A full MALDI MS spectrum is taken at each *xy* position in the sample, and images are constructed from pixels containing information regarding the intensity of an *m/z* of interest.

1.13 General Context of Thesis and Outstanding Research Questions

At the time this thesis was written (2016) the major challenges in taking MALDI MS imaging forward were associated with quantitation of drug molecules. This is challenging for many reasons which are mainly associated with ion suppression due to the complicated nature of biological specimens. For example, tissues contain a range of biological molecules that may interfere with the detection of a drug molecule by appearing at similar *m/z* and ionisation of the target drug may also be harder due to competing species and salts, both which may significantly reduce ionisation

yields. Another significant problem lies within extraction of drug molecules out of tissue sections –cells are generally aqueous, yet matrices are generally organic and non polar species. The ability to form solid solutions between matrix and analyte so that effective ionisation can occur is also more difficult, and so surface sampling needs to be improved. Finally, MALDI MS imaging of biological tissues is a slow technique requiring very careful preparation of samples which takes a long time. The improvement of capacity for screening is also currently an open research question in this field. The following literature review summarizes efforts to address these questions.

1.14 Literature Review: MALDI-MS of drugs: Profiling, imaging, and steps towards quantitative analysis

Caprioli and co workers identified MALDI as an ionisation source for imaging peptides and proteins in tissues in 1997.[131] Using a series of MALDI-TOF spectra obtained by rastering of the sample plate on which thin tissue sections which had been coated with matrix were mounted, it was possible to obtain *images* of proteins and peptides localised within tissues e.g. insulin in rat pancreas. This work was followed by a landmark paper in which direct profiling of proteins and peptides in cryo-sectioned tissue was achieved.[132] Over 100 peptide and protein signals in the 2000 – 30000 Da range were distinguishable including myoglobin and ubiquitin, with remarkable homology (>90%) between mass spectra taken in the same tissue types. The mass spectral profiles were also found to be highly similar in identical strains of mice yet different in multiple strains of mice as

would be expected for the proteomes of genetically similar/different animals. Reyzer *et al.* reported the extension of the MALDI-MSI technique to the direct analysis and imaging of drug molecules in tissue by MS/MS.[133] Using a hybrid MALDI-QqTOF (tandem MS/MS; quadrupole time-of flight) and standard MALDI-TOF instruments, it was possible to image administered anti-tumour drug candidates in tumours from rats. Comparison of the two instruments with each other demonstrated that the use of the tandem instrument was superior for imaging applications in eliminating spectral noise in the lower regions of the MS spectra caused by matrix ionisation and clustering. Specifically, the $[3M+Na]^+$ cluster-ion of the sinipinic acid matrix had the same *m/z* ratio as the protonated $[M+H]^+$ drug candidate ion in question, and signals were hard or impossible to resolve in MS mode. MS/MS mode – incorporating collision-induced dissociation (CID) - however allowed the detection of structure specific ions unique to the drug, which made detection simple. The use of tandem mass spectrometry, as demonstrated in the pioneering work by Troendle *et al.* on detection of paclitaxel in ovarian tumour sections,[134] is often crucial to the efficient detection of the drug and drug metabolites as the QQQ instrument can act to filter for exclusive detection of the desired ion in complex tissue samples.

Bunch *et al.* used MALDI-MSI to determine the depth of penetration of an anti-fungal drug, ketoconazole, into porcine epidermal tissue.[21] The drug was allowed to soak into the skin tissue, and cross sections of the tissue blotted onto plates which had been airsprayed with CHCA matrix. MALDI imaging of the ketoconazole penetration was presented. Through the construction of a calibration curve for the Na adduct of ketoconazole, it

was shown that as epidermal depth increased, the level of ketoconazole decreased, and it was not detected by ca. 1 mm skin tissue depth, and that in fact most of the drug must therefore be absorbed into the dermal skin layer. Clench and co-workers reported the imaging of the anti-cancer prodrug AQ4N (banoxatrone), and its bioreduced drug form AQ4 in human tumour xenografts. By imaging the distribution of adenosine triphosphate (ATP) in the tumour xenografts, it was demonstrated that the drug is only reduced in hypoxic regions of the tumour cells, as intended in its design [135]. Stoeckli and co-workers have used MALDI imaging to analyse the distribution of drugs and metabolites in whole animal sections. Imaging of whole sections is important in the pharmaceutical industry for determining the distribution of drug molecules *in vivo*. MALDI imaging offers a great advantage in determining distributions, as the drug molecule itself may be directly profiled with great assurance that it is the drug being imaged rather than any drug metabolites, although it still offers images of the latter too, simultaneously, for comparative purposes. Stoeckli *et al.* demonstrated that an undisclosed ^{14}C-labelled drug molecule gave similar distributions by MALDI compared to whole-body autoradioluminography in dosed mice.[136] In more recent work, Hopfgartner *et al.*, again using an undisclosed pharmaceutical compound, used MALDI imaging to determine the distribution in sectioned mice in a rapid and efficient manner, as well as its metabolites.[137] The time from obtaining the tissue section to the production of the final image-distribution map was 15 minutes, demonstrating the potential of MALDI imaging for future clinical applications e.g. rapid biopsy analysis. Likewise, Trim *et al.* imaged the distribution of the potent

chemotherapeutic drug vinblastine in whole rat sections using the standard MALDI MS/MS imaging experiment coupled with a further ion mobility separation (IMS) step to give greater specificity; IMS is able, in this case, to separate the signals arising from vinblastine from an isobaric (i.e. of same molecular mass) lipid.[138] The method was validated by comparison of the MALDI images to WBA of the distribution of ^{3}H-vinblastine and found to be in excellent agreement.

Hsieh *et al.* developed a mass spectrometric method for the determination of the anti-psychotic drug molecule clopazine in rat brain tissue.[22] The use of MALDI-QTOF in these experiments allowed the researchers to correlate autoradiography images of injected radioactive ^{3}H-clopazine with MALDI-MS/MS images of the same brain sections; the results demonstrated the excellent correspondence of the MALDI analysis with the traditional autoradiography approach. The drug molecule was found to be distributed fairly evenly across the brain tissue with the highest concentration of clopazine found in the lateral ventricle with both methods giving excellent agreement. Shanta *et al*. used MALDI MS imaging to detect donepezil in mouse brain liver and kidney tissues.[139] Marko-Varga *et al.* used MALDI MS as well as MS/MS to analyse ipratropium in human lung tissue.[140] Liu *et al.* analysed the time-dependent penetration of the anti-cancer drug irinotecan (Camptosar, Pfizer) into colon carcinoma spheroids using MALDI MS. As drug penetration into solid tumours is a crucial aspect of anticancer therapies, the study by Liu *et al*. is potentially important for the development of more effective cancer therapies.[141] Kuwayama *et al.* used MALDI MSI to image MDMA ('ecstasy') distribution in overdosed mice brain

liver and kidney tissues using an automated deposition technique for matrix application. It was observed that major sites of MDMA build up included the brain stem and kidney of the animals used in the study.[142] The distribution of the bioactive ellagitannin, strictinin, in green tea has been imaged by MALDI MSI of orally-dosed rat kidney sections.[143]

A study by Wang *et al*. detailed the use of MALDI TOF to separately detect cocaine and the nicotinic acetylcholine receptor antagonist chlorisondamine in the cryosectioned brains of rats after intracranial injection of the drug molecules.[112] Matrices were applied directly to the tissue sections post-cryosection. Further identification of the drugs was performed by tandem MS/MS experiments (MALDI-TOF-TOF) using the $(M+H)^+$ peaks for both drugs as the source for the second analysis to give a fingerprint unique to the drug molecule. The distribution of the cocaine peak (*m/z* 304.4) in the mass spectra of brain tissues of rats in terms of relative abundance (normalised to the cholesterol minus water base peak at *m/z* 396.6) in major cerebral structures such as the cortex (34.8%), hippocampus (53.6%) and hypothalamus (35.7%) was reported. Drexler and co-workers have also used MALDI coupled with sequential ion trap mass spectrometry to image the distribution of a pro-drug candidate from the laboratories of Bristol-Myers Squibb & Co. (USA).[144] Adult mice were given high dosages of the pro-drug BMS-X for two weeks before being euthanised and necropsied. Analysis of the mice organs by light microscopy during necropsy showed the presence of microcrystalline deposits in the mice spleen and lymph nodes; analysis of these cryosectioned organs by

MALDI imaging demonstrated that the microcrystalline material distributed in these organs was the active pharmaceutical (*m/z* 448). The latter result correlated with the light microscopy studies. To further confirm the result, MS/MS imaging of the drug was performed using a product ion (*m/z* 202) originating solely from the active drug molecule precursor ion.

Three-dimensional cell cultures have become a useful predictive tool for drug infiltration, especially with respect to the efficacy of drugs designed to penetrate solid tumours.[145] Three dimensional analysis of HCT116 colon carcinoma multicellular spheroids using MALDI MSI has been reported by Liu *et al*.[146] MALDI was used to image the penetration of the anti-cancer drug irinotecan in the 3D cell culture, as a function of time (Figure 1.11). Ten metabolites of irinotecan were also mapped. The method is high-throughput and requires the use of no animal subjects and hence a more cost-effective approach to mapping drug efficacy, especially with respect to the penetration and pharmacological fate of drugs for the treatment of solid tumours.

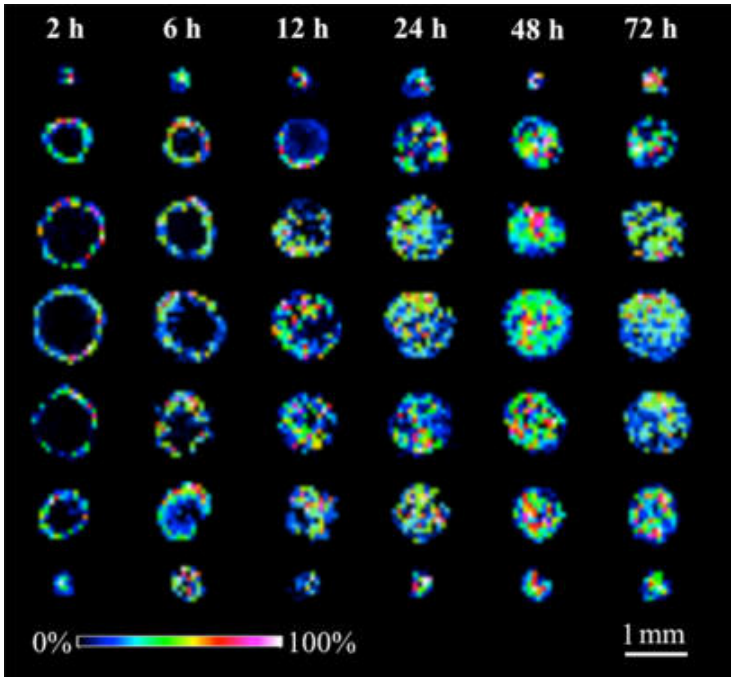

Figure 1.11: MALDI MSI of 3D cell cultures: penetration of Irinotecan into HCT116 colon carcinoma multicellular spheroids.[146] Reprinted with permission from Liu *et al*. *Anal. Chem.* 2013, 85, 6295. Copyright 2005 American Chemical Society.

The distribution in mice spleens of the terpene glycoside cucumarioside A_2-2, a immunomodulatory drug, by MALDI profiling and imaging has been reported as a function of time by Pislyagin *et al*.[147] Using MALDI MSI it was possible to demonstrate that cucumarioside A_2-2 was absorbed rapidly by the spleen, with a peak concentration 30 minutes post-injection, and with almost full excretion by 3 h. The drug was mainly detected in the tunica serosa of the spleen, which is a serous membrane consisting of two layers of mesolithium found on the outside of the organ, and whose primary function is to secrete serous fluid. The results were compared to radiospectroscopic distribution of ^{3}H-cucumarioside A_2-2 and found to give similar results, though the peak distribution of the drug was found to be at 15 mins using radiospectroscopy.

Experimental models for the study of drug distributions in tissue by MALDI MSI have been suggested by Vegvari *et al* (Figure 1.12).[148] The *concentration gradient model* (CGM) was developed by the immersion of A549 solid xenograft tumours into a lung cancer drug cocktail (tiotropium + erlotinib) for 2.5 h followed by sectioning. The drugs infiltrates into the tissue, as imaged by MALDI MSI. The *dispersion model* (DM) uses cryostat-sectioned tissues of the type that might be used in biopsies etc which are immersed in anticancer drug solutions for 1 h, either tiotropium, erlotinib or gefitnib. Analysis of the tissue sections by MS/MS allowed the unambiguous detection of the distribution of the drugs. Finally the *directed dosage model* (DDM) takes into account guided deposition of a drug to a certain tissue type i.e. targeted therapies to disease.[149] In this model, the drug is spotted onto various regions of a whole tissue sample and the response in MALDI MSI measured after washing to show any affinity for the drug for certain tissue types e.g. diseased vs. healthy tissue. The CGM model will be useful for the study of drugs that are required for the penetration of solid tumours, whilst the DM is extremely useful for studying the general distribution of drugs over a tissue cross section (i.e. the normal mode of MALDI MSI in general). The DDM could be extremely useful in future, where directed therapies and personalized medicines could become mainstream, and thus pre-clinical prediction of the drug in a patient biopsy could be useful for predicting drug efficacy prior to treatment.

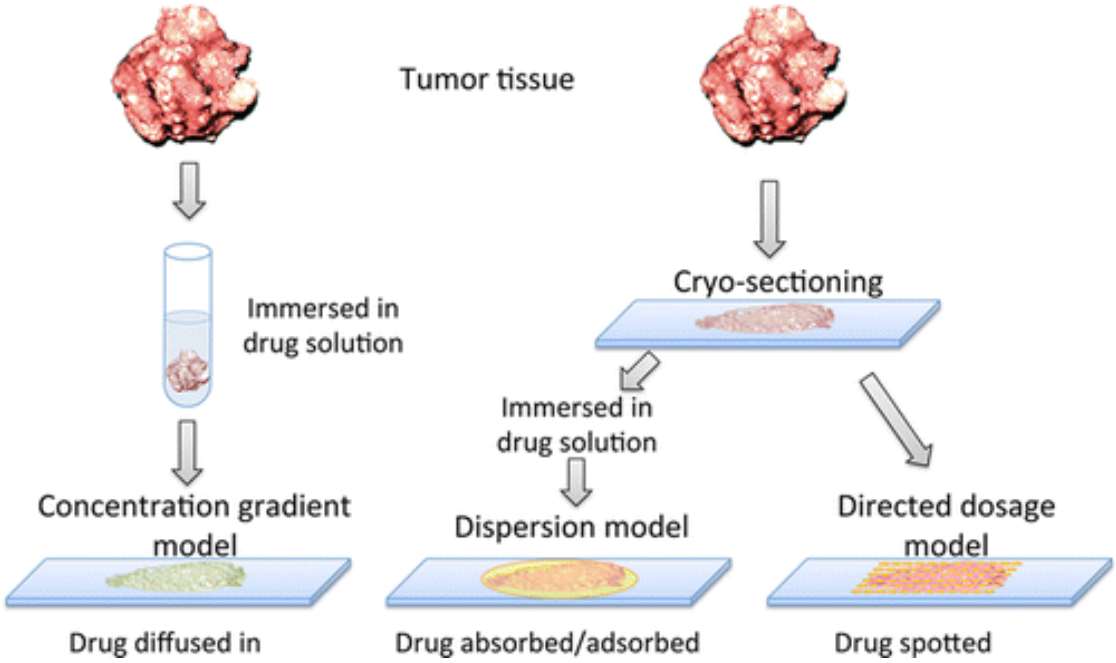

Figure 1.12: Model for drug distributions which are of use for various drugs that work in different ways including penetrative drugs (concentration gradient model), non-targeted drugs (dispersion model) and targeted drugs (directed dosage model).[148] Reprinted with permission from Vegvari *et al*. *J. Proteome Res*. 2013, 12, 5626. Copyright 2013 American Chemical Society.

Digital image analysis is a critical step in MALDI imaging. As a hyperspectral data cube is generated during any MALDI imaging experiment, hundreds of gigabytes and in many cases terabytes of raw data are generated. Obviously, there are fundamental limits on the analysis of such datasets due to their inherent dimensionality and thus the facile processing of data from MALDI imaging experiments has become a sub-field of research which has been reviewed by Jones *et al*.[150] Reduction of dimensionality has been achieved by Palmer *et al* by the use of random projections in combination with principal component analysis to reduce

dimensionality by up to 99%.[151] Schwartz *et al* validated this method for effectively de-noising clinical data sets.[152] Race *et al* used principal component analysis to reduce the dimensionality of MALDI imaging datasets to reduce their dimensionality prior to clustering and segmentation.[153] Full processing for an entire organ dataset of 44 GB was presented. A range of clustering workflows for unsupervised analysis of MSI data has been reviewed by Sarkari *et al*.[154]

Presentation of hyperspectral data recorded in MALDI imaging experiments has been addressed by Fonville *et al*. [155] using a single colour image to represent the data set. The colours generated are based on spectral charateristics at each pixel; pixels with similar MS profiles are displayed with the same RGB colour combinations. The colour coding approach is compatible with popular pre-processing algorithms (principal component analysis, t-distributed stochastic neighbour embedding and self-organising maps). Race *et al*. have developed a universal converter for different MALDI file formats, ensuring that users with older instruments are not excluded from the developing field.[156]

The quality of the digital image analysis in the MALDI MSI workflow has a significant effect on the resolution of the MALDI images produced. Histological staining of tissues is a traditional microscopic technique with high spatial resolution, as dyes are used that bind with high specificity to certain tissue types. The correlation of CD-31 immunohistogical blood vessel staining with the MALDI MSI technique has been described by Walch and co-workers,[157] investigating the distribution of the anticancer

drugs Afatnib, Erlotnib and Sorafenib in mice models bearing Ewing's sarcoma xenograft tumours. It was found by coupling the immunohistogical staining of the blood vessels in tumours that there is a direct correlation between the extent of tumour vascularisation with the intensity of the signals derived from mass spectrometry, and as a result, the distribution of the drugs was found to be heterogeneous across the tumours.

Ultra high-resolution mass spectrometry using MALDI MSI with an Orbitrap® mass analyser has been used by Jirasko et al. for the analysis of atorvastatin and its metabolites in rat liver tissues.[158] Sample preparation was optimised by variation of section thickness, steel vs glass MALDI plates and the screening of 13 matrices. Figure 1.13 summarises the results of the study, showing CHCA and DHB are the best matrices for maximizing ion counts in positive mode MALDI. DAN matrix performs well in both negative and positive mode detection. The advantage of using the Orbitrap® as the mass analyser becomes apparent when one considers that mass resolution can be reported to 4 decimal places, separating ions of very similar m/x (e.g. 500.1000 and 500.1050) and thus extremely accurate drug distributions can be compiled, in the confidence that there is most probably no interference in the signal from other ions.

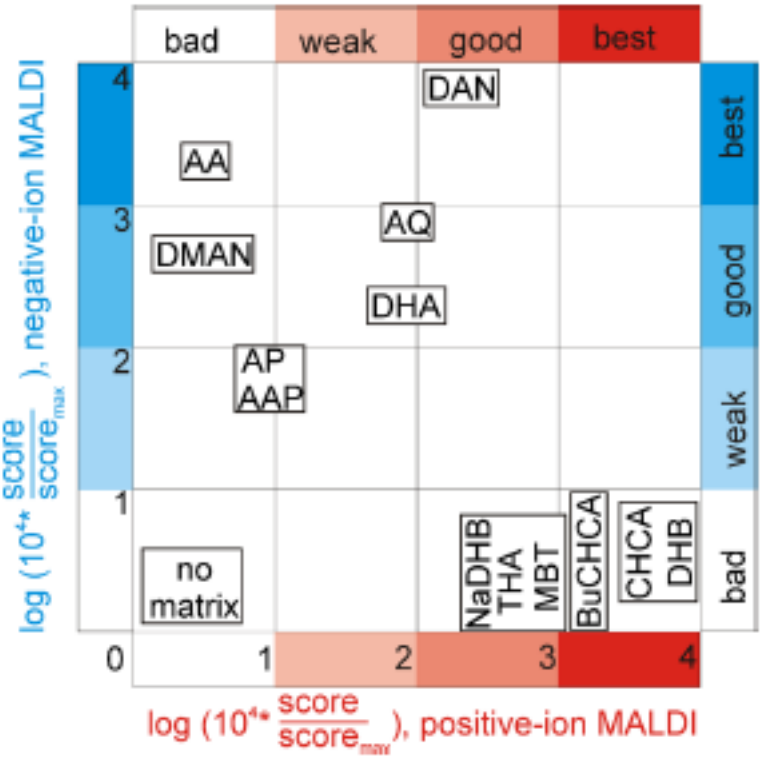

Figure 1.13: A map based on ion counts in negative and positive detection mode MALDI MSI of astorvastatin to give a figure of merit for 13 matrix molecules (and no matrix) from profiling-screening.[158] Reproduced with permission from Springer.

The forensic analysis of single hair samples is an important technique in criminology and pathology to detect the presence of drug and illicit substances or poisons in either a suspect, victim or even a cadaver.[159] Indeed, hair could be thought of as a matrix for the continual recording of drug use.[160] Current methods for testing hair involve chemical testing and are often laborious and time-consuming. Nakanishi *et al* have reported the quantitative imaging of nicotine in longitudinally-sliced hairs taken from long term smokers.[96] A ^{13}C-nicotine internal standard was used and a linear calibration curve (R^2 = 0.997) was presented in the range 1 – 50 ng mL^{-1} hair, with a limit of quantification as 1.6 ng mL^{-1} hair. However, this dynamic

range is not great for quantification, which often requires a greater dynamic range to be useful. Images of the hairs are reminiscent of barcodes in heavy smokers, whereas there is hardly any signal in a control group of non-smokers. Similarly, the analysis of ketamine, a horse tranquiliser often used as an illegal recreational drug, in single scalp hairs has been reported by Shen *et al*. using MALDI MSI with a FT-Ion Cyclotron Resonance (FT-ICR) mass spectrometer. Ketamine was detected and imaged successfully in four hairs taken from a ketamine abuser's scalp.[161] The technique was compared to traditional LC-MS/MS and found to give a higher spatial resolution. Drug-facilitated crimes such as sexual assaults and murders where the victim is under the influence of a hypnotic drug administered to them furtively by the attacker prior to the crime to incapacitate them have become frequent, especially in cultures that drink alcohol, which can magnify the seditive effects of hypnotic drugs such as rohypnol and zolpidem. Often, traces of the drug can be found in the hair of a victim. High resolution single hair analysis of zolpidem in hair by MALDI MSI using an high-resolution FT-ICR instrument (resolution ca. 10^5) has been reported by Shima et al.[162] by monitoring protonated zolpidem at *m/z* 308.1757 in the moustache hair of humans administered with the drug. Zolpidem was found mainly in the hair bulb at the root of the hairs taken at both 20 h and 32 h after administration. Although mass spectral imaging of hair samples is a promising label and chemical-free technique compared to traditional chemical analysis techniques used in criminology, caution is needed in the interpretation of presented results. Variations in growth rate of hairs across a subject's body as well as their position on the body could

lead to false positives. Single hair analysis in particular could potentially suffer from a lack of statistical significance. The different growth rates of hair found in the body could also lead to non-reliable analyses, as analysis of hairs from various parts of the body may give contradictory results.

So-called '*cassette dosing*', where a cocktail of different drugs is administered to a single test subject, has been used in the pharmaceutical industry since the 1990s as a high-throughput method to screen the plasma pharmacokinetics of many different drugs at once *in vivo*. Swales *et al* have demonstrated that MALDI MSI can be used to image the distributions of terfenadine, erlotnib, olanzapine and moxifloxacin in parallel in mice administered with the drugs in a cassette style dosage.[163] The results were compared to liquid-extraction surface analysis (LESA) MS/MS and found to be in good agreement. High spatial resolutions, up to 15 μm, were achieved with the MALDI MSI of lung tissue of orally dosed subjects (Figure 1.14). Care must be taken with the interpretation of cassette pharmacokinetics due to the possibility of drug-drug interactions, especially due to allosteric inhibition by one drug of enzymes that are crucial in clearance pathways of another drug. For this reason, cassette dosing is mainly only used in early-stage blood plasma pharmacokinetic studies.

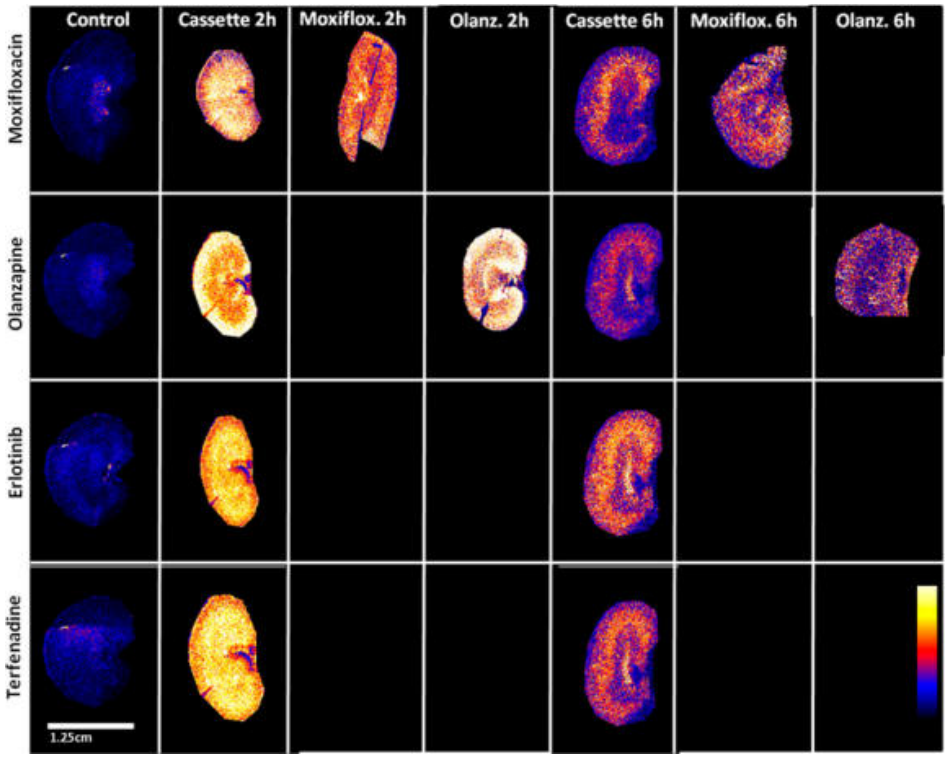

Figure 1.14: MALDI MSI of cassette-dosed excised mouse kidneys after various time points, with full cassette channel overlay and channels for the drugs analysed.[163] Reprinted with permission from Swales *et al*. *Anal*. *Chem.* 2014, 86, 8473. Copyright 2014 American Chemical Society.

The pharmacokinetics of paclitaxel in human patients presenting peritoneal carcinomatosis has been partly assessed by MALDI-MSI from cross-sections of excised peritoneal nodules of patients treated by hyperthermic intraperitoneal chemotherapy (HIPEC). Paclitaxel was only evident in the outermost layers of the nodules, with a deepest penetration of 0.54 mm into the peritoneal tissue observed. MALDI MSI suggests that the drug was taken up in a limited manner by the nodules, and thus care must be taken into the administration of chemotherapeutics, as in this case, other routes of administration with greater proven penetration depth are available.

Improvement of ion counts by changing the matrix deposition solvent has been presented by Barry *et al.*[164] The MALDI MSI of lapatnib-dosed liver tissues was presented. The ion counts of lapatnib versus ambient ions and lipids in total ion chromatograms and solvent extraction gradients of acetonitrile or methanol from *infra red* matrix assisted desorption ionization/electrospray ionisation (IR-MALD/ESI) was assessed. It was found that as the organic component increased, so did the ion counts of lapatnib and lipids, whilst the ion counts for (presumably inorganic) ambient ions decreased (Figure 1.15). It is significant, and indeed typical for MALDI MSI analysis, that the ion counts of the drug are one to ten orders of magnitude lower than for any of the other species at any point in the analysis, highlighting the major difficulty found when analysing drugs in tissues i.e. lack of ion counts when compared to other endogenous species.

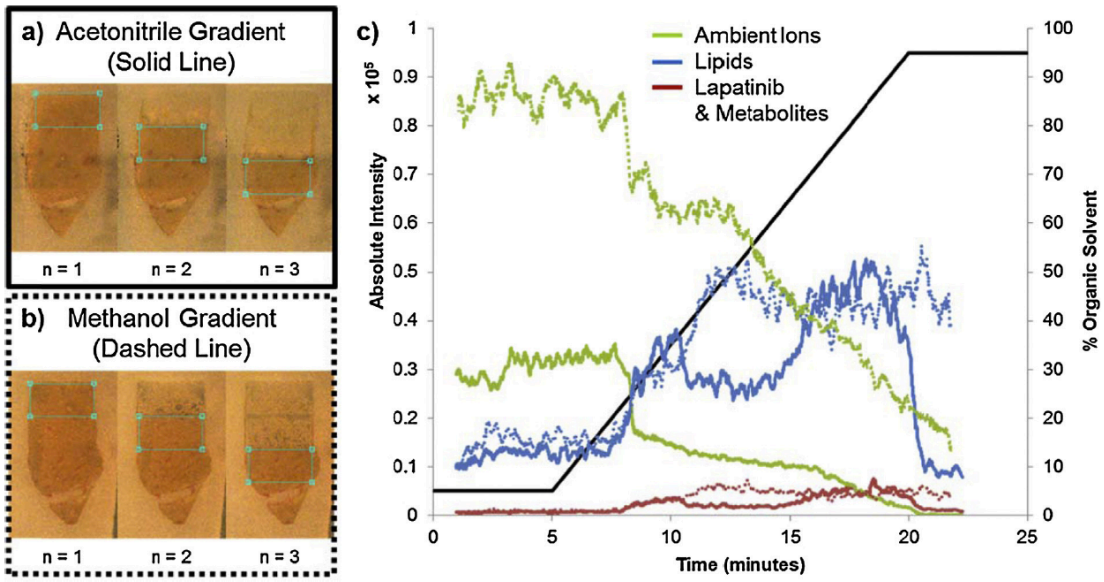

Figure 1.15: Total ion chromatogram for gradient extraction IR-MALDESI imaging of lapitnib-dosed excised liver tissue sections. The total ion counts for the drug increases as the organic extraction component increases in the aqueous-organic solvent mixture. The total ion counts for drugs is generally orders of magnitude lower than those observed for

lipids and ambient ions, succinctly demonstrating one of the major challenges in MALDI MSI of non-polar drug molecules.[164] Reproduced with permission from Elsevier.

Models that predict response to anticancer treatment are needed in cancer therapy to enhance patient survival rates. Mascini *et al* coupled MALDI MSI to the analysis of tissue microarrays, with analysis of the images by Principal Component Linear Discriminant Analysis (PC-LDA) to predict the treatment response of patient-derived xenograft (PDX) models of triple-negative breast cancer.[165] Analysis of two PDX tissue microarrays each containing a treatment responsive and a treatment non-responsive patient can be used for characterisation, using MALDI MSI, mass spectral profiles of the tumours from both patient types, though with varying prediction rates for treatment response (77% and 59% for each of the duplicates). However, this study represents an important development in the use of mass spectrometry imaging in cancer therapy, having great potential for high-throughput analysis of tumour biopsies.

1.15 Approaches to quantification of drugs in tissues by MALDI MSI

Possibly the most challenging aspect of imaging and profiling analysis of complex samples by mass spectrometry for the presence of drugs is the development of quantitative analyses, where the generated ion counts from a sample can be correlated accurately to the amount of the analyte within the sample.[99] The development of quantitative analysis is crucial for the incorporation of MALDI in pre-clinical and indeed clinical diagnostics.[166] The analysis of tissue sections by MALDI MS imaging in particular is an area which has traditionally lacked quantitative capability until quite recently.

Many factors hamper the quantitative use of MALDI on tissue including extraction efficiency, ion suppression from salts, and ensuring homogeneous deposition of matrix, which can often lead to shot to shot inconsistencies and variability in ion counts. This is further compounded by the unaccountable discrepancy in ionisation efficiency between tissue types, a key point which researchers have only recently begun to explore by the use of novel MALDI techniques such as MALDI-MRM-MS (multiple reaction monitoring - mass spectrometry).[167] and the development of novel software by Kallback *et al*. to produce normalised images which take into account the variation in ion counts in a certain tissue with the use of an isotope-labelled internal standard.[104]

There have been various general approaches to address the problem of analytical quantitation, summarized as follows:

- *Isotope labelled internal standards:* another analyte with similar or identical ionisation efficiency is added to the analyte calibration solution to give a ratio of ion counts.[168] ^{2}H or ^{13}C labelled analytes as internal standards are generally considered best and have been used successfully,[100] however structural analogues[168] i.e. molecules similar in structure or chemical properties to each other have also been used. [167]

- *Endogenous species in tissue as internal standards:* biologically ubiquitous molecules such as lipids and steroids can be used in

theory as internal standards as the level should remain consistent in tissues, though in practice this presents significant challenges due to the inhomogenity of ionisation and ion suppression in biological samples.

- *Matrix as internal standard:* as the matrix is generally co-ionised alongside analyte, it is possible to normalise the ion counts versus these peaks if known. This has been done for instance with DHB in the quantitative analysis of raclopride and octreotide in tissue sections.[98, 102]

- *Absolute Quantitation (Calibration standards):* A graph is constructed of ion counts as a function of increasing drug concentration. Recent publications have focused on spotting of drugs onto tissues,[169] though this has the drawback of localized inconsistencies within tissues, and is also dependent on many factors including deposition solvent, matrix and drug. This method of course has the advantage that it is rapid, simple and label free.

- *Comparison with LC-MS/MS*: although LC-MS/MS is not suitable for imaging alone, when used with MALDI MS it can be a potent tool for quantifying ion counts by assay. Many groups have taken advantage of MALDI imaging in combination with LC-MS/MS to achieve quantitative analysis.[98, 102, 133, 167, 170, 171 172, 173]

Propanolol and olanzapine have been imaged and quantified in mouse whole-body sections by Hamm *et al.* using MALDI MS with development of a tissue extinction coefficient, which takes into account ion suppression in tissues.[105] This is simply the ion count intensity ratio of a known concentration of drug on tissue with the same concentration of drug on a standard substrate (usually steel) i.e. I_{tissue} / $I_{standard}$, thus giving a numerical coefficient which represents the extent of ion suppression in any tissue type. The tissue extinction coefficient is unsurprisingly found to be both tissue and drug dependent. Results of the analysis were compared to already established techniques such as LC-MS/MS (olanzapine) and quantitative whole body autoradiography (QWBA) (propanolol) and found to show excellent agreement.

Pirman *et al.* quantitatively determined acetyl carnitine (AC) in piglet brain tissue using a deuterated internal standard (d_3-acetyl carnitine; d_3-AC). This study also attempted to identify *tissue specific* variations in ionisation efficiency. Using a constant concentration and ratio of AC to d_3-AC spotted under thin sections of various tissues, the greatest ion suppression was observed in kidney and liver tissue, with less ion suppression in tissues originating from the heart, brain and testes. The ratio of the ion counts of AC to d_3-AC remained constant throughout, confirming the inherent differences between tissues.[174] Calibration curves were presented in the range 50 – 500 $\mu g\ g^{-1}$. Pirman *et al.* also developed quantitative MALDI QTOF MS/MS imaging of cocaine in human brain tissue using a deuterated internal standard and a wide range MS/MS scan mode followed by scan by scan normalisation to the internal standard.[100]

Calibration plots were presented in the range 0.5 – 500 μg g^{-1} cocaine (Figure 1.16). The results of the quantitation from images in each case were comparable to LC-MS/MS analysis. A similar internal standard approach to quantification in drug-dosed tissues has been used by Bokhart *et al*. to quantitatively image emtricitabine, tenofovir and raltegravir in a cervical tissue model co-coated with corresponding internal standards (lamivudine, acyclovir and prednisolone respectively) using IR-MALD/ESI.[95] Cationisation using NaCl was used to improve the analyte signals. The use of internal standards reduces the shot to shot variability of the analysis in biological tissue. A linear calibration curve for emtricitabine was presented and quantification of emtricitabine over a tissue area of 134 mm^2 was achieved. The analysis presented had a 17.2% ± 1.8 95% confidence interval compared with 28.4% ± 2.8 for the LC-MS/MS analysis.

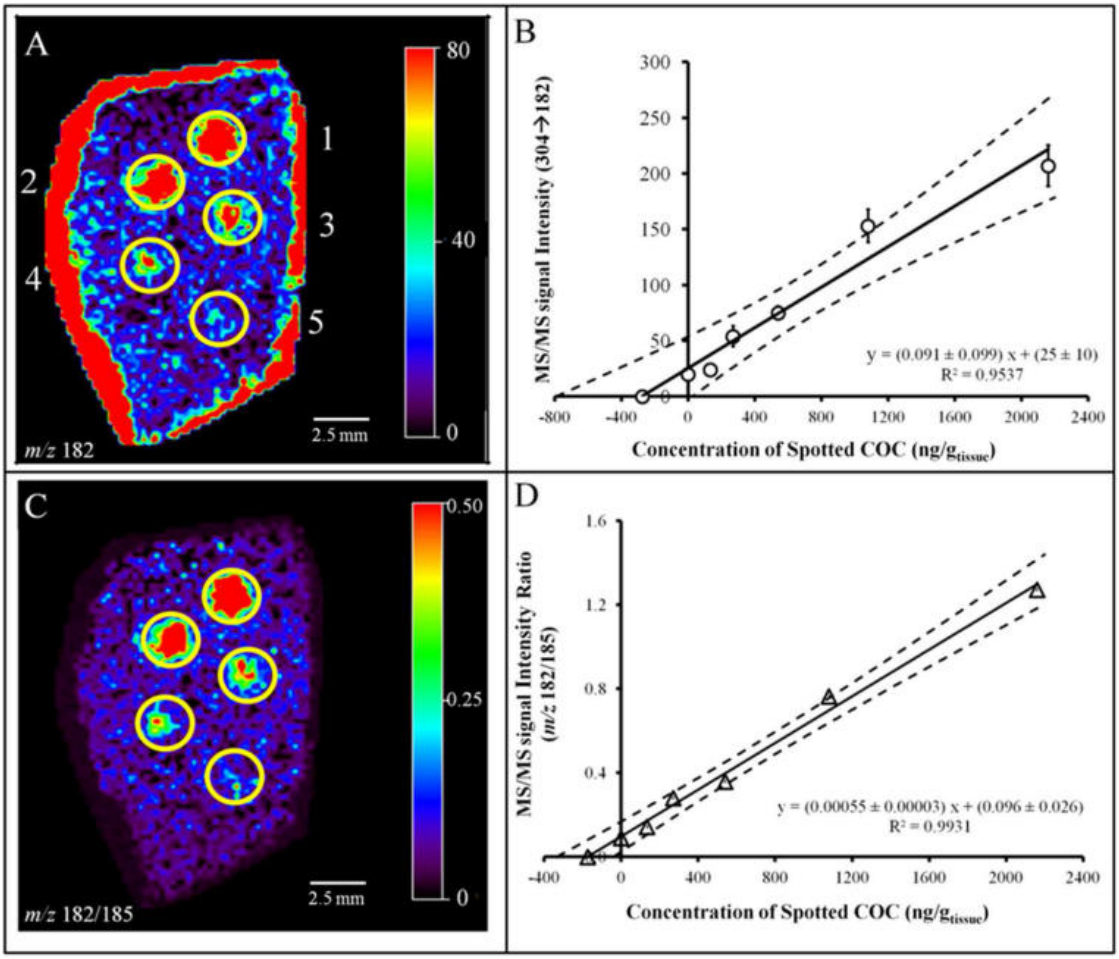

Figure 1.16: Quantitative MS/MS (Q-TOF) determination of cocaine using a deuterated internal standard in brain tissue.[100] (A) Ion intensity of *m/z* 182 and (C) the ratio of *m/z* 182/185 were used to generate MS/MS images. Calibration spots increase in concentration from 200 (spot 5) to 2200 ng/g tissue (spot 1). Corresponding standard addition plots for quantitation with (B) m/z 182 ion intensity and (D) the ratio of m/z 182/185. Normalization to the COC-d3 improved the linearity of the calibration curve leading to improved quantitative estimation of COC in the tissue. Reprinted with permission from by Pirman *et al. Anal. Chem.* 2013, 85, 1081. Copyright 2013 American Chemical Society.

Groseclose *et al* used mimetic tissue models consisting of tissue homogenates spiked with a range of different drug concentrations that are frozen into polymer supports and cross-sectioned. The technique accurately models tissue suppression effects and results for the quantification of nevirapine in rat livers and of lapatnib in canine livers. Xenograft mouse tumours was compared directly to LC-MS analysis and the quantification results were found to be close as-comparing both

techniques, though MALDI MSI tends to underestimate the amount of the drug in all sample types in this case.[175] A similar approach has been used by Takai *et al* using spiked tissue homogenates to quantitatively analyse the concentration of a synthetic cannabinoid in mice.[176] Analyte ionisation efficiency was normalised in the tissues by the use of a structural analogue i.e. an internal standard.

Relative quantification of the tyrosine kinase inhibitor dasatinib, a leukaemia drug, has been reported by Schulz *et al*.[177] They report that the inclusion of the small molecule solvent dimethylsulfoxide (DMSO) in matrix solutions significantly improves the ion intensity of the drug in MALDI MSI of mouse kidney medulla tissues, and relative quantification of the drug in the tissue is possible by comparison to a d_8-dasatnib internal standard. Comparison of the relative quantification to LC-MS was made and found to show the similar variability, with the coefficient of variation found to be lower for MALDI MSI (32%) found to be lower than the LC-MS analysis (38%).

The heterogeneous nature of biological samples across a surface is one of the greatest obstacles in the way of quantitative analysis by MALDI MSI as ion suppression across a tissue section can be variable. Tomlinson *et al* attempted to investigate and evaluate this phenomenon by the use of MALDI MSI and LESA-electrospray in tandem on a single FT-ICR high-resolution mass spectrometry platform.[178] They showed the distribution of GSK1 by MALDI MSI and LESA MS were similar. MALDI MSI signals of lipids from excised lung tissue after dosing with the novel drug GSK1 were shown to vary considerably between lung and adipose tissue, which was mirrored in the LESA analysis. This could be a useful indicator of ion

suppression in tissues as it can be shown that the same drug, under the same conditions, ionises differently in different tissues.

1.16 Summary of Literature Review

It has been shown that a range of mass spectroscopic techniques have desirable properties for the study of biologically relevant molecules such as proteins, drugs and their metabolites. MALDI-MS imaging (MALDI-MSI) is a novel technique for the analysis of drugs and drug metabolites in tissues, and whole animal sections that offers a rapid and sensitive analysis that is complementary to current techniques employed for modeling drug or drug metabolite distributions. The rapid expansion of the field since 1997 has demonstrated the versatility of the MALDI-MSI technique; images of remarkable resolution have been obtained using a range of small-molecule analytes. Hence, MALDI-MSI is an ideal tool for drug discovery and screening of pharmaceutical candidates. Ionisation at ambient pressure is an emerging technique that is allowing the *in situ* analysis of samples. Techniques such as LESA are highly suited to surface sampling and analysis of biological samples under ambient conditions.

Quantitative MSI analyses using various strategies represent the pinnacle of the field so far, and indeed may lead to the widestream adoption of the technology throughout the pharmaceutical industry. However, for the reasons outlined in this introduction, there are a number of factors that make MALDI imaging of drugs extremely challenging and quantitative imaging is currently a much sought-after goal. We have reviewed this area,

and conclude that it is one of the most challenging sub-fields in mass spectrometry in the current era, mainly due to the small molecular weights of the analytes, which can be occluded by matrix peaks combined with the challenge of effective extraction and ionisation and detection.[1] This thesis attempts to make novel steps towards semi-quantitaltive imaging.

1.17. Hypothesis

The overall hypothesis of this thesis is to test and trial a range of new methodologies that may improve the use of MS imaging within laboratories to move towards obtaining quantitative or semi quantitative data from images. As we have seen from the literature review presented, this is a significant challenge, mainly because the conditions found in the analysis of drug molecules in situ in tissues and sections is very much different to those found ex situ, although some approaches are emerging in order to negotiate this. I hypothesize, based upon the literature reviewed and an understanding of the current limits of MS imaging, that this challenge may be approached on a number of fronts simultaneously:

1. Improvement of calibration standards in MALDI imaging.

The use of calibration curves in much of the literature is limited to drug molecules on standard substrates. However, it is known that ionisation on tissues is suppressed by biological entities and ions, and the actual ions generated from a sample may not in fact correspond to the absolute amount of a molecule found within the biological sample i.e. there is often a disparity in ion counts between a grug ionised on tissue as compared to a

drug ionised on steel, which leads to inaccuracy when reading from a calibration curve as the amount of drug would always be underestimated. From the generation of standards based on doped biological tissues or sections, this problem could be eliminated to improve accuracy of MALDI imaging. The use of internal standards in this approach may make it even more accurate and useful for a range of drugs.

2. Improve Sampling to Improve Dug Extraction and Thus Imaging.

Part of the problem with generating images from MALDI MS is to extract the drugs out of the tissues, which can also lead to inaccuracy in data. The use of better, more appropriate sampling by which to extract drugs from tissues in the first place could improve the spectra generated and improve the images and image resolution. The use of liquid extraction using aqueous media from tissue samples could be used to improve the ion counts of drugs found within tissues and could be used to improve the sensitivity of mass spectra generated from tissue samples. This approach when combined with high resolution mass analysers could lead to a step change in image quality.

3. Couple standard MS techniques to industry-standard imaging techniques to develop simple quantitative and semi quantitative standard MS protocols that underpin imaging experiments.

The use of standard MALDI TOF MS has often been overlooked in imaging experiments in favour of more complicated MS/MS imaging experiments that require careful sectioning of subjects followed by a number of sample

prepration steps to produce sections for MS imaging, However, much of this processing could be eliminated if careful excision of organs followed by homogenization is performed, and spectra generated using standard techniques such as MALDI TOF, This could be used in particular for rapid screening of organs to show where a drug has localized before further more detailed analysis using sectioning and MALDI MS MS imaging is considered.

1.18 Aims and Objectives of Thesis

I aim to test the three sub- hypotheses outlined above by fulfilling the following aims and objectives:

In Chapter 2 of this thesis I aim to develop novel calibration standards for MALDI analysis of drug-doped tissue homogenates by MS/MS. Calibration curves are constructed from haloperidol doped at known levels into homogenised porcine liver samples. These calbration curves take into account ion suppression from the tissues and as such should be more accurate than those currently reported. Special attention is paid to optimisation of instrumental and sample prep parameters such as laser type, deposition method, collision energy and matrix deposition solvent. The aim of this chapter is to present a novel methodology by which to prepare a calibration curve that improves the accuracy of MALDI MS imaging experiments.

In Chapter 3 I aim to improve sampling and extraction of drugs from tissue samples using an ambient surface-sampling/ionisation technique (Liquid Extraction Surface Analysis) coupled to an extremely high resolution mass spectrometer based on ESI Orbitrap® mass spectrometery for analysing doped tissue homogenates with two drugs – propanolol and fenclozic acid. The aim of this chapter is to improve the extraction of drugs from tissues and to improve the sensitivity and resolution of what can currently be achieved.

In Chapter 4 I outline a drug distribution study performed at AstraZeneca, Alderley Park using fenclozic acid and propanolol in rats using quantitative whole body autoradiography (QWBA) and liquid scintillation counting (LSC). I show how this can be coupled to qualitative MALDI profiling experiments on homogenised organs excised from the same rats. Profiling barcodes are presented that account for all organs. I show that MALDI is successful at profiling the two drugs and thus we demonstrate its complementarity to existing techniques such as QWBA and LSC currently used ubiquitously in the pharmaceutical industry. The overall aims of this chapter is to couple a standard MS technique to an industry standard imaging technique to improve the capability for rapid screening using mass spectrometry.

Chapter 2: Development of Biological Standards for Analysis and Imaging of Drugs in Tissue by MALDI-MS Imaging.

2.0 Introduction

Imaging the distribution of drugs in single organ and whole animal sections is an important aspect of drug discovery processes in the pharmaceutical industry. MALDI-MS imaging of drugs, which is now a relatively well-established technique, is a qualitative and complementary technique to the current imaging techniques such as quantitative whole body autoradiography (QWBA). Although drugs can be successfully detected and imaged *via* MALDI, reports of the quantitative determination of the concentrations of drugs and drug metabolites in tissue sections combined with imaging are limited to a small number of examples discussed in chapter 1. The determination of the muscarinic antagonist drug tiotropium bromide by dried droplet application of matrix onto sectioned tissue for *in situ* analysis has recently been reported [169]. Linear calibration data on tissue was shown, based on spotting matrix and drug onto tissue sections. This is much more useful than calibration data obtained directly from stainless steel plates as it takes into account the complexity of biological samples. However, the calibration used in this study would not represent the response in a genuine imaging study, where extraction of the perfused drug from tissue is required. In a recent conference, a strategy to section drug doped homogenates using a protein mould was described [179], where the mould was required to achieve good quality sectioned homogenates. Spanton and co-workers recently reported a coupled MALDI-MS imaging – liquid chromatography MS/MS (LC/MS/MS) assay to determine the amount of olanzapine in rat liver tissue [171]. Further development of appropriate drug quantification protocols is

essential if MALDI imaging technique can provide quantitative information in support of other techniques such as whole-body autoradiography [136, 138], to which preliminary results of an analysis can be rapidly validated against. The MALDI technique suffers from drawbacks that have historically limited the use in quantitative determinations on tissue sections. Inhomogeneities in the co-crystallisation of matrix and analyte can lead to poor shot-to-shot reproducibility; the matrix is essential to the laser ionisation of the substrate and any deficiencies of matrix within in the crystal environment around the substrate may lead to reduced ionisation. Likewise, an excess of matrix compared to substrate in any given area can lead to over-ionisation ('sweet spots'). Both of these issues are further compounded by the formation of irregular co-crystal morphologies which may also affect ionisation. As uniformity of samples is a fundamental requirement to a reproducible quantitative determination, conditions for sample and matrix application must be rigorously consistent to ensure homogeneous co-crystallisation. Biological tissues are inherently complex and there are numerous species competing for ionisation, causing ion suppression, reducing output signal and lowering sensitivity. One method to enhance the precision of analysis is the use of internal standards spiked in a sample.[180] The internal standard may be a wholly different analyte which has a known response, or an isotopically modified analogue of an analyte e.g. by deuteration [181, 182]. The latter approach ensures that errors in analysis introduced by chemical differences between the internal standard and analyte are kept to a minimum. Another challenge in MALDI experiments is the choice of an appropriate solvent/matrix

system that maximises the extraction of the usually non-polar drug from the surrounding tissue.

2.0.1 Hypothesis tested in this chapter

The complexity of tissue samples and sections in MALDI imaging presents unique challenges for obtaining quantitative determination of drugs from images. Many studies have used calibration curves based on ex situ ionisation of drugs on standard stainless steel substrates. However, reference standards based on drug-doped tissue homogenates could potentially be useful for optimisation for MALDI imaging, allowing the construction of calibration curves that better simulate this complexity, accounting for effects such as ion suppression found within tissue samples. In this chapter we test the hypothesis that standards that are based on the homogenisation of authentic animal tissue would potentially give a more authentic ionisation process and therefore the calibration curves constructed would be more accurate in reflecting the true amount of drug found in sections.

2.0.2. Aims and Objectives of this chapter

In order to test the above hypothesis we will produce homogenised porcine liver tissue samples spiked with known amounts of an anti-psychotic drug, haloperidol. These will be sectioned and imaged using MALDI MS. The ion counts from these homogenates will be used to produce calibration curves for haloperidol that could potentially be used to for quantitaltive imaging of haloperidol in tissue sections. We will perform some optimisation of ion counts based on solvent selection for drug extraction, laser choice, and a

comparison of two matrix deposition methods so that we may present an optimised protocol for sample preparation and imaging.

2.1 Experimental

General

2,4,6-trihydroxyacetophenone (THAP), sinipinic acid (SA) α-cyano-4-hydroxycinammic acid (CHCA) and 2,5-dihydroxybenzoic acid (DHB), trifluoroacetic acid, haloperidol (4-[4-(4-chlorophenyl)-4-hydroxy-1-piperidyl]-1-(4-fluorophenyl)-butan-1-one) and caffeine were all purchased from Sigma-Aldrich (Poole, UK). HPLC grade solvents methanol, acetonitrile, tetrahydrofuran (THF), 2-methyltetrahydrofuran (2-MeTHF), ethanol, dioxane, ethyl acetate, *n*-butanol and 2-propanol were purchased from Fisher Scientific (Loughborough, UK). Porcine liver was obtained commercially from JS Sainsbury's supermarkets Ltd.

Preparation of spiked homogenates for MALDI imaging: general procedure

Homogenates based on 80%, 90% and 100% porcine liver containing final haloperidol concentrations of 0.5 - 500 μg g^{-1} were prepared automatically using an IKA Ultra-Turrax T25 homogeniser, or manually using a Dounce homogeniser.

Liver tissue was cut into 1 g portions using a surgical scalpel and transferred to plastic test tubes. Water was added as necessary to produce homogenates of 80 – 100% tissue *w/w*. Drug was dissolved in methanol then added to give the final haloperidol concentrations (0.5 – 500 μg g^{-1} *w/w* haloperidol with respect to liver*)*. The samples were homogenised (automatically or manually) before being transferred into either 1) mini-subaseal bungs (1 mL) of 1.1 cm diameter, 2) 1.5 mL Eppendorf tubes of 0.9 cm diameter or 3) 0.5 mL Eppendorf tubes of diameter 0.6 cm. Spiked homogenates were frozen at - 20 ^{o}C. Blank control homogenates were prepared using the same method and omitting the drug addition step. When frozen, the subaseal samples were simply popped out of the rubber mould. For samples in Eppendorf tubes, a scalpel was used to cut the tapered end of the tube followed by removal of the frozen homogenate slug by pushing through the newly-created hole. Homogenates were sliced to a thickness of 12 μm in a cryomicrotome and thaw-mounted onto stainless steel MALDI target plates.

Investigation of drug-matrix combinations for optimised extraction.

CHCA, SA, DHB and THAP matrices were each prepared at 25 mg mL^{-1} in the following solvents: 2-MeTHF, 2-propanol, dioxane, methanol, THF, ethyl acetate, toluene, acetonitrile and ethanol. 0.25 μl of the matrix solution was mixed with haloperidol (50:50 v/v). 0.25 μl of the matrix solution was spotted directly onto 12 μm haloperidol-spiked tissue homogenate (80:20 tissue:water) sections (0.5 μg g^{-1} haloperidol with respect to weight of liver)

mounted onto stainless steel MALDI plates and allowed to crystallise. Ion counts were recorded at 10 discrete locations in the sample images to obtain a mean ion count for each matrix-solvent combination.

Matrix Deposition Techniques for Tissue Analysis

a) Dried droplet deposition

THAP, SA, CHCA or DHB (25 mg mL^{-1}) was dissolved in 80:20 v/v acetonitrile, methanol, tetrahydrofuran (THF), 2-methyltetrahydrofuran (2-MeTHF), ethanol, dioxane, ethyl acetate, *n*-butane or 2-proponal: water with 0.1% trifluoroacetic acid (TFA), was applied by pipette in discrete locations (0.25 μL) on the homogenate sections and allowed to crystallise by slow evaporation.

b) Airspray deposition

CHCA matrix in 80:20 v/v acetonitrile:water with 0.1% TFA was applied onto whole homogenate sections using an artist's airbrush. The solvent was allowed to evaporate. The spray-dry cycle was repeated five times in total, approximating to 5 mL of matrix solution in total.

c) Automated deposition

CHCA matrix in 80:20 v/v acetonitrile:water with 0.1% TFA was applied onto whole homogenate sections on using a Bruker ImagePrep (Bruker Daltonik GmbH, Bremen, Germany) automated matrix deposition system.

Around 5 mL of the matrix solution was applied to the whole plate under a nitrogen atmosphere. The solvent was evaporated within the robot to allow crystallisation of matrix.

Instrumentation

MALDI MS and MS/MS analyses were performed using an Applied Biosystems (Foster City, CA, USA) QSTAR XL (hybrid quadrupole time-of-flight, QqTOF) instrument fitted with an orthogonal UV MALDI ion source (N_2 laser, 337 nm, 20 Hz, 35 μJ or a high repetition Nd:YVO_4 laser 355 nm, 8,000 kHz, 8 μJ). Analyst QS software (Applied Biosystems, Foster City, CA, USA) was used to control the instrumental parameters *via* PC interface. Stainless steel MALDI plates were used in all cases. MALDI images were acquired at a spatial resolution of 200 μm, in either time of flight (TOF) MS mode (*m/z* range 50 – 1000) or in MS/MS studies of drug doped tissues *via* collision induced dissociation (CID) of *m/z* 376 with a collision energy of 35 eV. Resulting ion images of selected *m/z* for lipids of interest or the drug fragment *m/z* 165 in MS/MS studies were prepared using using oMALDI Server or Biomap software with further data processing and spectral examination performed by Analyst QS software.

2.2. Results and Discussion

Haloperidol can be detected by MALDI MS with CHCA as matrix on stainless steel plate, mainly as the protonated species, $[M+H]^+$ with mass-to-charge ratio, *m/z* 376. The $[M-18]^+$ peak observed at *m/z* 358 is due to loss of water. MALDI MS/MS analysis of haloperidol, fragmented by collision-induced dissociation (CID), leads to the observation of the cationic fragments of haloperidol at *m/z* 165 and *m/z* 123 (Figure 1). These latter fragments are also observed in the MALDI MS spectrum. In this case, there is 9.2 x 10^{-13} mol of haloperidol in each spot (5.5 x 10^{11} molecules), which in total garners ca. 7000 total ion counts for the $[M+H]^+$ peak in MS mode,.

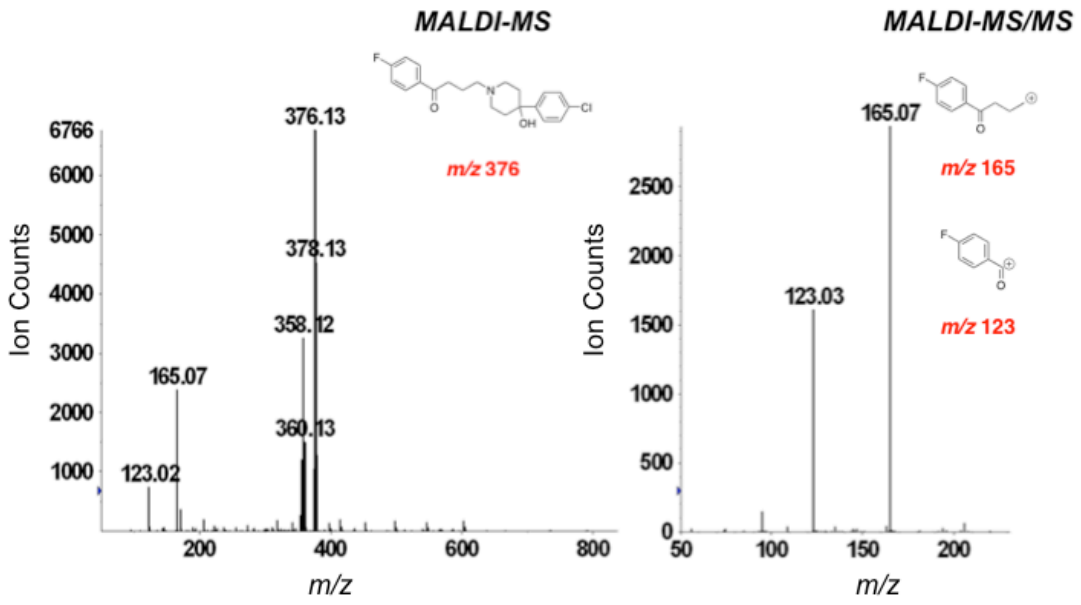

Figure 2.1: MALDI MS spectrum of haloperidol (left) and MALDI MS/MS spectrum after CID of haloperidol selecting the protonated haloperidol molecule $[M+H]^+$ *m/z* 376 (right) on stainless steel. 9.2 x 10^{-13} mol haloperidol on plate. Matrix: CHCA 25 mg mL^{-1} in 80:20 acetonitrile water 0.1% TFA, dried droplet deposition.

Initial research sought to improve various factors associated with the preparation and processing of tissue homogenates, with a view to improving sensitivity and reproducibility. The work detailed herein has concentrated on the following areas: standardisation of homogenates; optimisation of matrix deposition and drug extraction; laser selection and preparation of a MALDI calibration curve for haloperidol in tissue.

Optimisation of collision energy for MS/MS experiments.

Using the QSTAR XL instrument, a stream of gas (N_2 or Ar) is collided in the RF-only collision cell with the ions generated by MALDI which have been accelerated to a high kinetic energy by an applied electric field, and fragmentation (bond breakage) results from the conversion of kinetic energy into internal energy. This process is often described as collision-induced dissociation (CID). Adjustments can be made to the collision energy of the ions and the gas flow, to achieve the optimum fragmentation conditions that give the maximum ion counts for any chosen ion in the MS/MS spectrum. We investigated this for haloperidol on stainless steel plate using the fragmentation product ion observed at *m/z* 165 after selection of the *m/z* 376 precursor. Figure 2 shows the spectra recorded using different collision energies and the expected fragmentation to give m/z=165.

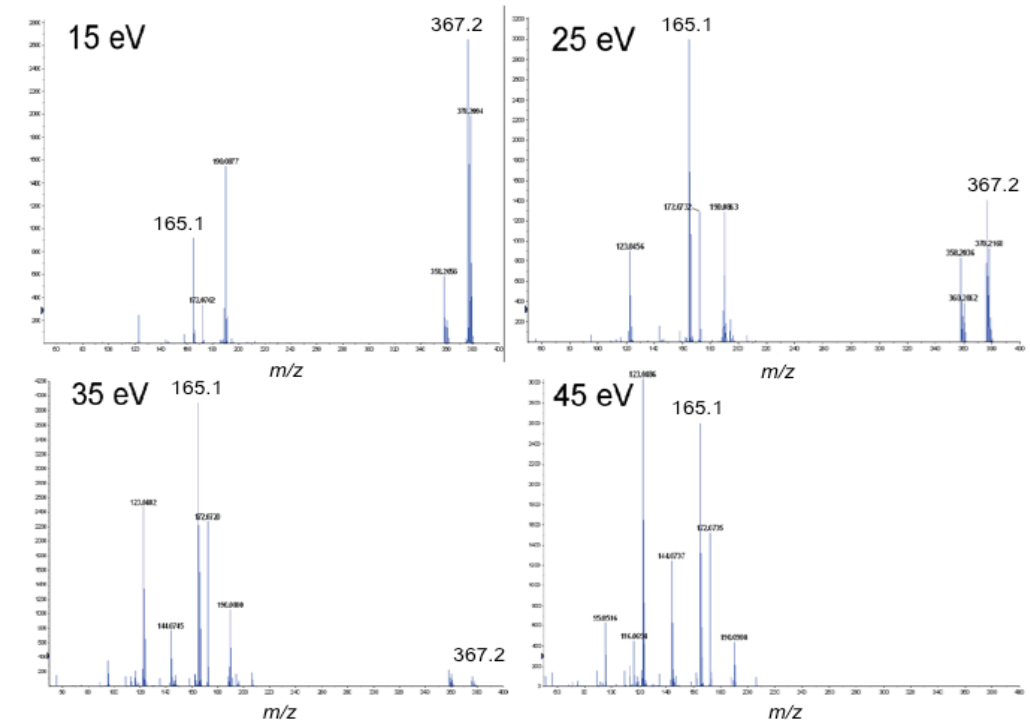

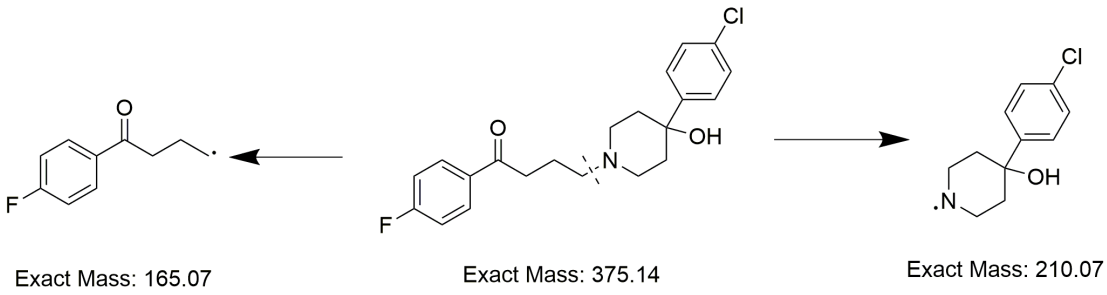

Exact Mass: 165.07 Exact Mass: 375.14 Exact Mass: 210.07

Figure 2.2: MALDI MS/MS spectra generated from CID of the protonated haloperidol molecule, $[M+H]^+$ (*m/z* 376) with collision energies of 15 eV, 25 eV, 35 eV and 45 eV. Below is presented the dealkylation that occurs in the MS/MS to give the major fragment observed at *m/z* 165.

It can be seen that the protonated molecule of haloperidol $[M+H]^+$ at *m/z* 376 is the parent of the product ion observed at *m/z* 165 produced after collision induced dissociation: as collision energy is increased, the protonated haloperidol ion counts at *m/z* 376 decrease, while the ion counts for the product ion observed at *m/z* 165 increase. A graph of ion counts for the *m/z* 165 product ion of haloperidol versus collision energy was produced (Figure

3). At collision energies >35 eV there is a significant decline in the amount of this ion presumably due to more extensive fragmentation at higher collision energies. This curve therefore suggests the optimum collision energy for the production of the ion detected at *m/z* 165 is around 35 eV. A collision energy of 30-35 eV was therefore selected in future MS/MS experiments for imaging applications.

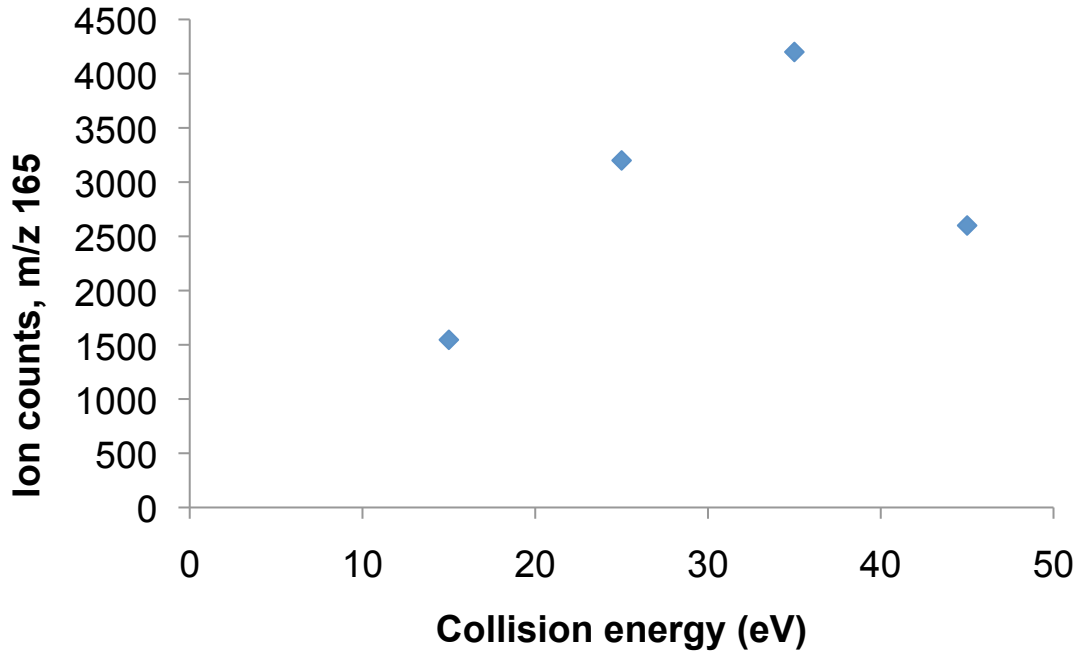

Figure 2.3: Graph showing the trend in ion counts observed at *m/z* 165 corresponding to the fragment of haloperidol *vs.* collision energy used. Optimum collision energy to produce maximum ion counts for the fragment of haloperidol after CID at *m/z* 165 in MALDI MS/MS spectra is around 35 eV, corresponding to the apex in the trend.

Homogenisation of porcine liver tissue

Preliminary experiments involved a manual Dounce homogenization apparatus. In this setup, porcine liver tissue is placed within a test tube along with a known amount of water, and manually ground by the end of a specially shaped glass rod. We found that this technique did not give homogenous material on the basis of a simple visual inspection – larges pieces of liver still remained in the sample after the processing. Conversely, the use of an automated homogenization system (IKA Ultra-Turrax T25 homogeniser) was found to give much better results by visual inspection. The best quality tissue homogenates were found by visual inspection (a homegenous pink mousse) to be produced from a ratio of 80:20 w/w tissue:water, compared to 90:10 and 100:0 ratios. All studies were therefore conducted using 80:20 (80%) homogenates. Mounted sections of homogenates prepared by each method were coated in CHCA matrix by airspray deposition and imaged by MALDI MS. The homogeneity of the porcine liver tissue homogenate, prepared by automated processing, was visualised by images derived from the $[M+H]^+$ ion of the naturally-occurring phosphatidylcholine lipid PC 34:1 at *m/z* 760 (Figure 4). The ion counts were relatively uniform across the sample and used as a measure of homogeneity.

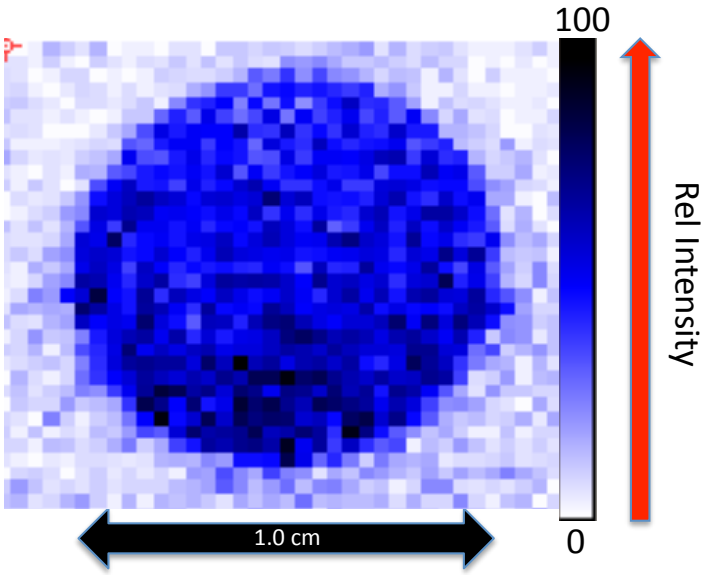

Figure 2.4: MALDI MS image of phosphatidylcholine PC34:1 1 $[M+H]^+$ *m/z* 760 from a porcine liver homogenate section. Matrix: CHCA, 25 mg mL^{-1} in 80:20 MeCN:water, 0.1% TFA. Airspray deposition (artistic airbrush).

The difference in the samples was demonstrated by mounting homogenate sections prepared by both methods on the same plate followed by MALDI imaging of 12 μm, imaging the cationic phosphatidylcholine head group fragment (2-hydroxy-*N,N,N*-trimethylethanaminium ion) at *m/z* 104 (Figure 5). The images for Dounce prepared homogenates displayed inconsistent ion counts across the tissue section, whereas the ion counts for the IKA Turrax homogenates were consistent across the tissue area which demonstrated the successful production of higher quality, more uniform homogenates.

During our studies, it was found that the best quality homogenate sections were obtained from the use of 0.5 mL Eppendorf tubes as the vessel for freezing homogenates in compared to either mini-subaseal moulds (1 mL)

or larger Eppendorf tubes of 1.5 mL. It was found that the homogenates prepared in the smaller Eppendorf tubes (0.6 cm diameter) were easier to section, and in general were more robust towards manipulation than the homogenates prepared in larger Eppendorf tubes or suba-seals. In particular, the sections produced from small-diameter tubes were less prone to physical stress presumably due to their lighter weight. Using smaller diameter vessels, we did not suffer the problems reported recently by Wagner *et al*. [179] which led to the use of a peripheral protein mould to assist tissue sectioning by maintaining sample integrity. Therefore, preparation of small diameter homogenates is a quick and simple method of preparing potential calibration standards.

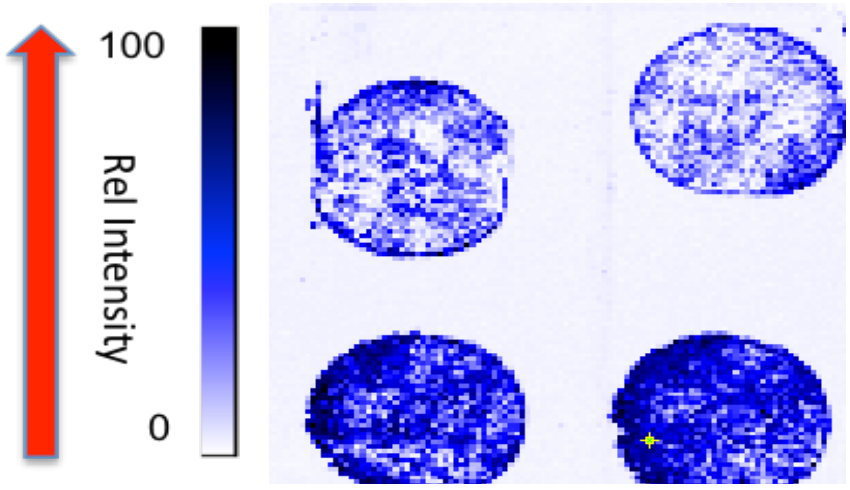

Figure 2.5: MALDI MS/MS ion images of *m/z 104* in porcine liver homogenate sections. Top row: homogenates prepared by Dounce (manual) homogenisation. Bottom row: homogenates prepared by automatic preparation (IKA Turrax). Matrix: CHCA, 25 mg mL^{-1} in 80:20 MeCN:water, 0.1% TFA. Airspray deposition (artistic airbrush). Homogenate sections are ca. 1.0 cm in diameter in all cases.

Justification of Laser choice

Clench and co-workers recently reported the use of a 20 KHz Nd:YVO_4 laser to improve imaging times in MALDI analysis of lipids [52]. Likewise, Spraggins *et al*. reported a 10-fold increase in throughput speed for imaging experiments of lipids in sagittal rat brain tissue using a 5 KHz Nd:YLF laser [183]. In this work, we used both a nitrogen laser (337 nm, 20 Hz, 35 μJ) and Nd:YVO_4 (355 nm, 8,000 kHz, 8 μJ). Comparing the power output of the two lasers, the nitrogen laser delivers approximately 7×10^{-4} W, whilst the Nd:YVO_4 laser delivers 64 W. The use of the Nd:YVO_4 laser resulted therefore in significantly higher ion counts over the same pixel dwell time as the energy delivered is of five orders of magnitude difference which, improves the ion counts, and the sensitivity of detection of haloperidol in tissue homogenates approximately 20-fold using CHCA as matrix by improving the signal to noise ratio of the measurements. Representative images are presented in (Figure 2.6). The Nd:YVO_4 laser was used in all further experiments.

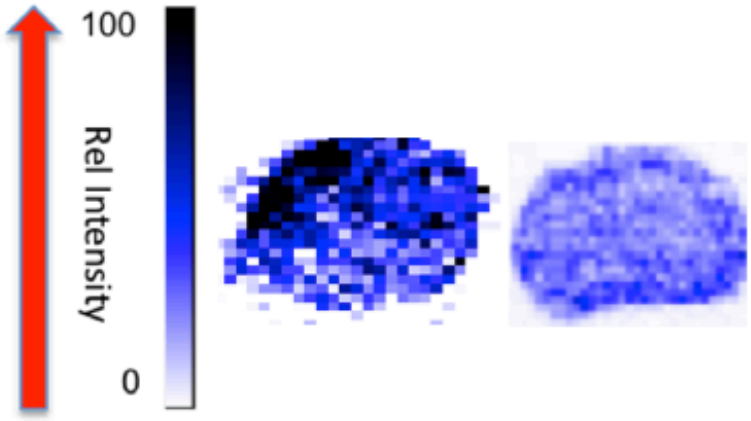

Figure 2.6: MALDI MS/MS ion images of a porcine liver homogenate sections derived from ion counts at *m/z* 165 acquired during CID of protonated haloperidol ion $[M+H]^+$ (*m/z* 376) . Left: 500 μg g^{-1} haloperidol-spiked homogenates ionised using a nitrogen laser ionisation source. Right: 0.5 μg g^{-1} haloperidol-spiked homogenates ionised using the an Nd:YVO_4 laser ionisation source. Matrix: CHCA in 80:20 MeCN:water, 25 mg mL^{-1} , 0.1% TFA, Bruker ImagePrep deposition. Homogenate sections are ca. 1.0 cm in diameter in all cases.

Solvent selection for extraction of haloperidol.

The formation of uniform co-crystals of matrix and drug is critical to successful desorption and ionisation and associated reproducibility during MALDI analysis. As the drug resides within the tissue section to begin with, ionisation of drugs contained in tissues relies heavily on the *extraction* of the drug from the tissue by the solvent in which the matrix has been deposited, so efficient co-crystallisation can occur upon solvent evaporation. A range of solvent-matrix combinations were investigated. Haloperidol was found to be freely soluble in a range of solvents: ethyl acetate, halogenated solvents (e.g. chloroform and DCM), toluene and ethers (e.g. THF and diethyl ether).

It was found that using CHCA as a matrix gave rise to higher ion counts for the *m/z* 165 fragment of haloperidol in MS/MS studies in combination with any of the solvents assessed. THAP, SA or DHB were all found to be less useful for the determination of this drug. Highest ion counts were obtained when CHCA was prepared in toluene, THF, 2-MeTHF, methanol or acetonitrile. As shown in the chart presented in (Figure 2.7).

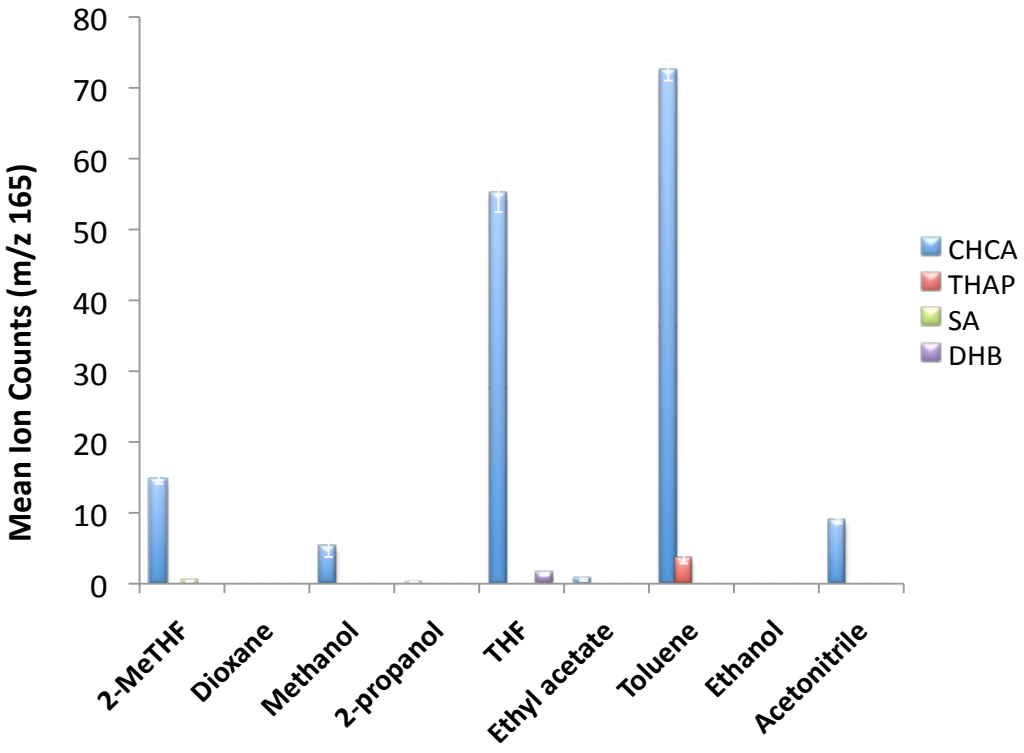

Figure 2.7:MALDI MS/MS analysis of matrix-solvent combinations spiked onto haloperidol (0.5 μg g^{-1}) porcine liver tissue homogenates, acquired from acquired from CID of protonated haloperidol ion $[M+H]^+$ (*m/z* 376) . Matrix 25 mg mL^{-1}, dried droplet deposition.

It is clear from these experiments that choice of solvent will have a significant effect on experimental outcome. Deposition of CHCA matrix in a highly non-polar solvent, toluene, resulted in the highest ion counts compared to other solvents but with ion counts similar to more polar solvents such as THF. The drug itself is non-polar and before these experiments were undertaken it was expected that non-polar solvents would be best for extraction. However, the ion counts recorded with more polar solvents such as acetonitrile and methanol were similar to the relatively non-polar solvent, 2-MeTHF. Thus other effects such as the quality of matrix-drug co-crystallisation and crystal morphology after extraction has occurred may also contribute substantially to the ionisation process on tissue. Knowledge of the solubility of an analyte in a solvent does not, therefore, fully explain suitability for MALDI MS experiments on tissue.

Evaluation of matrix deposition technique.

Deposition of matrix onto tissue homogenates in early experiments was performed by airspray using a commercially obtained artist's airbrush. However, despite the ease of application and suitability distribution analysis, the technique suffers from reproducibility issues. Issues, such as leaching of sample at the edges of the tissue leading to a blurring effect at the tissue boundaries in images, were also observed. This is a particular problem where good boundary definition is needed in imaging organs and tissue compartments or in drug distribution analyses of tissue sections.

During the course of our investigations, it was found that a robotic deposition approach using a Bruker ImagePrep automated system gave superior results compared to airspray deposition. It was not possible to test the full range of solvents from section 3.3 in automated deposition (Bruker ImagePrep robot) due to warranty restrictions – only acetontile and water or mixtures thereof are viable currently with this system. Acetonitrile was used in all automated deposition experiments as the organic component of the matrix solvent. The typical difference observed in image quality between airspray and robotic deposition of matrix is shown in Figure 2.8. The images were constructed using the ion counts recorded at *m/z* 165 (haloperidol fragment) at each pixel. It can be seen that for robotic deposition, there was a much sharper boundary between the stainless steel target plate compared to the tissue section; Conversely, the image from airsprayed tissue section showed evidence of a leaching effect at the boundary between the homogenate and the MALDI plate.

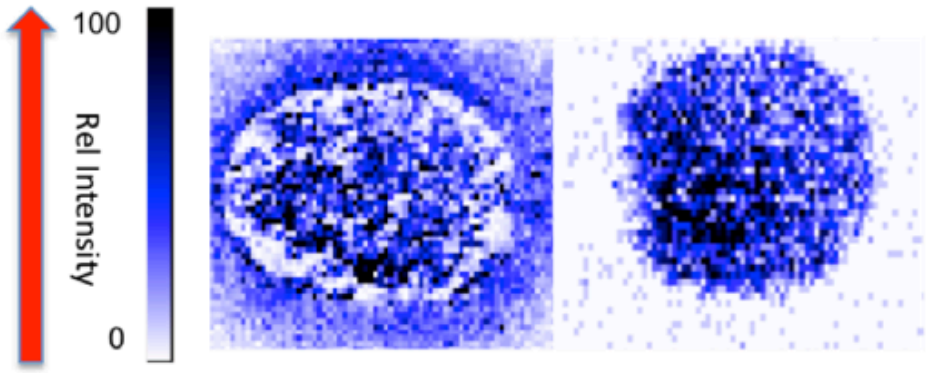

Figure 2.8: MALDI MS/MS image of a porcine liver homogenate section acquired from CID of protonated haloperidol ion $[M+H]^+$ (*m/z* 376). Matrix: CHCA, 25 mg mL^{-1} in 80:20 MeCN:water, 0.1% TFA. Airspray deposition (left) and Bruker ImagePrep automated system (right). Homogenate sections are ca. 1.0 cm in diameter in all cases.

The results agree with the findings of Marko-Varga and co-workers who also used the Bruker ImagePrep system to achieve good resolution in imaging the muscarinic antagonist drug tiotropium bromide in rodent lung tissues.[184] In the same study, it was noted that matrix homogeneity was poor using the ImagePrep system, but in our study we did not find this influenced the results.

It is a reasonable assumption to state that crystallisation occurs differently on different tissue types and there are many other factors aside from this that dictate matrix crystal quality. Tiotropium bromide, however, is possibly an easier analyte to identify compared with haloperidol, as the sensitivity is helped by the fact that it holds a permanent positive charge.

Semi-quantitative determination of haloperidol in tissue homogenates.

Dried droplet deposition of matrix.

A range of haloperidol doped homogenates were analysed to test the feasibility of quantitation. To achieve this, CHCA matrix in acetonitrile was applied to a range of spiked homogenates containing haloperidol concentrations from 0 $\mu g\ g^{-1}$ – 500 $\mu g\ g^{-1}$. In clinical usage, haloperidol and indeed drugs in general are administered typically at mg kg^{-1} (i.e. equivalent to $\mu g\ g^{-1}$) levels in humans, hence the concentration range used was deemed appropriate for the subsequent studies to produce a calibration curve for the semi-quantitative detection of the material.

A calibration curve for the determination of haloperidol in tissue homogenates based on MALDI MS/MS ion counts was prepared by measuring the ion counts from images of spiked homogenates with linearly increasing amounts of haloperidol. An image of these spiked sections along with the associated calibration curve is presented in Figure 2.9. Double log plots of the mean ion counts at *m/z* 165 taken from multiple regions of interest in each homogenate sample versus increasing amounts of haloperidol showed approximate linearity in the region of 0 – 500 $\mu g\ g^{-1}$. This method may be suitable for determining drug concentration at *specific* points in a tissue section i.e. profiling-type experiments; fully quantitative imaging needs further development.

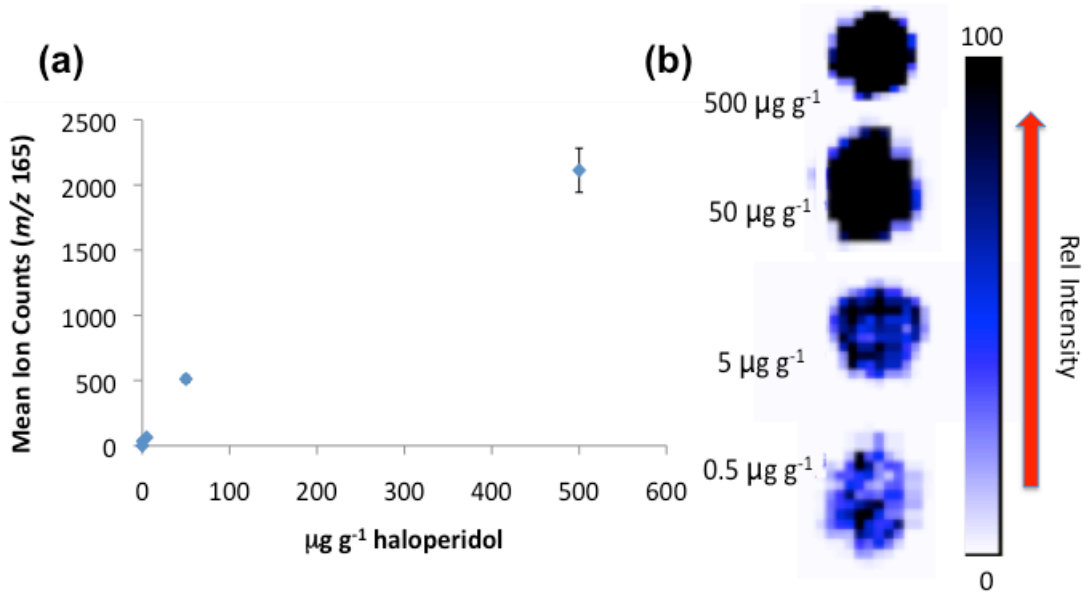

Figure 2.9: Range of concentration of haloperidol doped in porcine liver tissue homogenates by MALDI MS/MS acquired from mean ion counts at *m/z* 165 (*n* = 9 regions of interest, replicate measurements on one sample) after CID of protonated haloperidol ion $[M+H]^+$ (*m/z* 376). (a) Calibration curve for haloperidol-spiked porcine liver tissue homogenates 0 – 500 µg g^{-1}. Error bars represent the standard error of the mean (n = 9). (b) MALDI MS/MS Ion images (*m/z* 165) of spiked porcine liver tissue homogenates acquired from CID of protonated haloperidol ion $[M+H]^+$ (*m/z* 376). Matrix: CHCA, 25 mg mL^{-1} in 80:20 MeCN:water, 0.1% TFA, dried droplet deposition. Homogenate sections are ca. 1.0 cm in diameter in all cases.

Automated deposition of matrix.

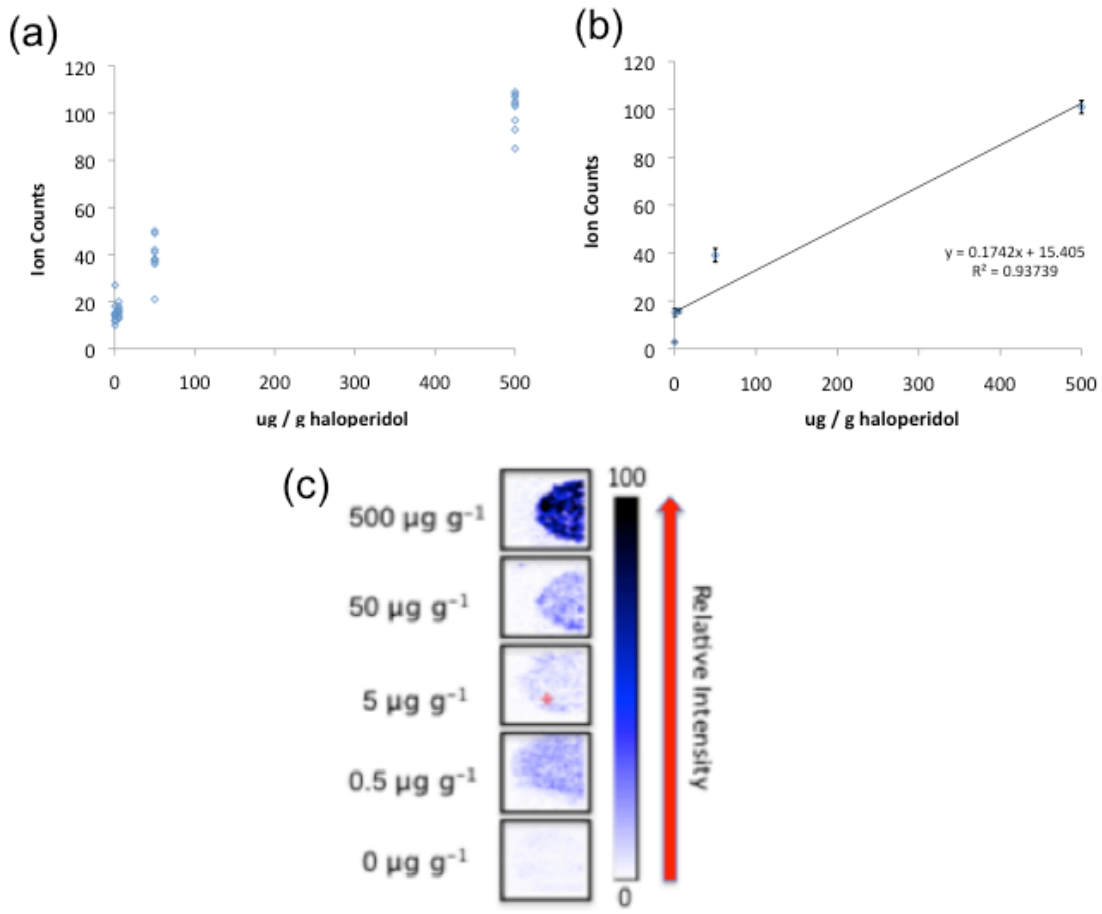

Figure 2.10: Range of concentration of haloperidol doped in porcine liver tissue homogenates by MALDI MS/MS acquired from mean ion counts at *m/z* 165 (*n* = 9 regions of interest) after CID of protonated haloperidol ion $[M+H]^+$ (*m/z* 376). (a) variability in ion counts during measurement at nine different spatial locations on-sample. (b) Calibration curve for haloperidol-spiked porcine liver tissue homogenates 0 – 500 μg g^{-1}. The datapoints represent the mean ion counts from the measurements in (a) (*n* = 9) Error bars represent the standard error of the mean ($\sigma / \sqrt{(n)}$). (c) MALDI MS/MS Ion images (*m/z* 165) of spiked porcine liver tissue homogenates acquired from CID of protonated haloperidol ion $[M+H]^+$ (*m/z* 376). Matrix: CHCA, 25 mg mL^{-1} in 80:20 MeCN:water, 0.1% TFA, Bruker ImagePrep deposition. Homogenate sections are ca. 1.0 cm in diameter in all cases.

As the dried droplet deposition of matrix is generally unsuitable for the analysis of whole tissue sections, a calibration curve from experiments using automated deposition of matrix by the Bruker ImagePrep robot was also

constructed. CHCA matrix in acetonitrile was automatically deposited onto a range of homogenates containing haloperidol concentrations from 0 μg g^{-1} – 50 μg g^{-1}. An image of these sections along with the associated calibration curve is presented in Figure 2.10. Generally, the ion counts at each point are lower compared to when matrix was applied by dried droplet deposition to obtain calibration data, but this is to be expected, as there is overall less matrix per unit area, and less extensive solvent extraction of the drug from tissue; as the matrix provides the major source of ionisation less matrix in a certain area will mean less ion counts. A plot of this data linearises the response of ion counts at *m/z* 165 against increasing drug concentration in the range 0 – 500 μg g^{-1}. Plots of the mean ion counts taken from multiple regions of interest (*n* = 9) in each homogenate sample versus increasing amounts of haloperidol shows concentration-dependent ion counts, A calibration curve using automated deposition is more useful as a reference standard for the determination and imaging of haloperidol in whole tissue sections, or sectioned whole organs from drug-dosed animals, than the corresponding curve for dried droplet deposition of matrix.

To assess the reproducibility of the homogenization technique we prepared fourteen separate homogenates, seven containing 0.5 and seven containing 50 μg g^{-1} haloperidol, which were sectioned and coated with CHCA matrix using the Bruker ImagePrep robot. The ion counts at 9 various points on each homogenate at *m/z* 165 (*n* = 9 regions of interest) after CID of protonated haloperidol ion $[M+H]^+$ (*m/z* 376) were recorded and the results are shown in Figure 2.11.

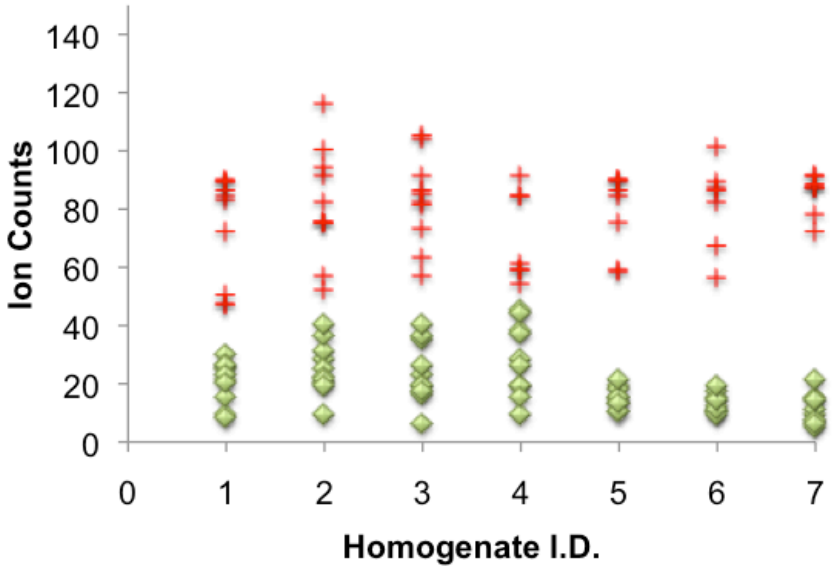

Figure 2.11: Variability in ion counts in drug spiked homogenates. The ion counts at 9 various points on each homogenate at *m/z* 165 (*n* = 9 regions of interest) after CID of protonated haloperidol ion $[M+H]^+$ (*m/z* 376). Red crosses are homogenates with 50 μg g^{-1} haloperidol. Green diamonds are homogenates with 0.5 μg g^{-1} haloperidol.

Calculating Imaging Sensitivity

Table 2.2: Absolute haloperidol amounts in image analysis of separate regions of interest within spiked homogenate sections prepared by optimised experimental procedure (*n* = 9).

μg g^{-1} Haloperidol	Pixel side (mm)	Pixel area (mm^2)	Homogenate depth (mm)	Pixel volume (mm^3)	Haloperidol per pixel (pg)	Mean Ion Counts (DD)	Mean Ion Counts (Robot)
0.5	0.2	0.04	0.012	0.00048	0.24	34.5	15.2
5	0.2	0.04	0.012	0.00048	2.4	63.1	15.7
50	0.2	0.04	0.012	0.00048	24	511	39.1
500	0.2	0.04	0.012	0.00048	240	2112	101

*Refers to the volume of the homogenate doped with haloperidol before cryotome slicing to 0.012 mm depth. Homogenates are assumed to have density of 1 g cm^{-3}.

In this study, the drug was successfully detected in homogenates containing haloperidol 0.5 - 500 μg g^{-1}. This translates to give a working range of 6.3 x 10^{-16} to 6.4 x 10^{-13} mol haloperidol per pixel and highlights a key point in imaging as a whole: detection of the drug is made at a series of sequential points rather than as a response from the homogenate as a whole. The result of the calculation of the amount of haloperidol per pixel is shown in Table 2.2 along with the ion counts revealed in each preparation. The lowest absolute amount of haloperidol we can detect in each pixel from this work is in the order of hundreds of femtograms (10^{-15}). In the case of haloperidol, the sensitivity of the imaging is in the hundreds of attomole (10^{-18}) range per pixel for the lowest haloperidol concentration investigated in this study.

Assessment of Linearity of Calibration Curves

Automated deposition of matrix is generally more reproducible than for dried droplet deposition, demonstrated by lower values for the sample standard deviation (*n* = 9) at equivalent haloperidol concentrations. This may be due to the reproducible conditions of matrix deposition afforded by the Bruker ImagePrep robot, which accurately controls the amount of matrix applied, ruling out any pipetting errors, as well as controlling the conditions for solvent evaporation i.e. temperature and also applies nitrogen in a controlled stream. This ensures that extraction of the drug from the homogenates and co-crystallisation occurs uniformly, leading to similar ion counts between regions of interest, compared to the dried droplet deposition, where solvent application is far less controlled, evaporation is not uniform and may lead to 'sweet spots' within samples, which lowers reproducibility.

Table 2.1: Data from separate regions of interest within spiked homogenate sections prepared by optimised experimental procedure (*n* = 9).

Dried droplet		
μg g^{-1} Haloperidol	**Mean Ion Counts, *m/z* 165**	**Sample Standard Deviation (*s*)**
0	0.33	0.50
0.5	34.5	29.6
5	63.1	25.5
50	511	52.6
500	2112	338
Bruker ImagePrep		
μg g^{-1} Haloperidol	**Mean Ion Counts, *m/z* 165**	**Sample Standard Deviation (*s*)**
0	2.78	3.45
0.5	15.2	4.97
5	15.7	2.33
50	39.1	8.46
500	101	8.01

Mean ion counts and sample standard deviation from each of the points of the calibration curves are presented in Table 2.1. The two calibration lines generated from this data are shown in Figure 2.12.

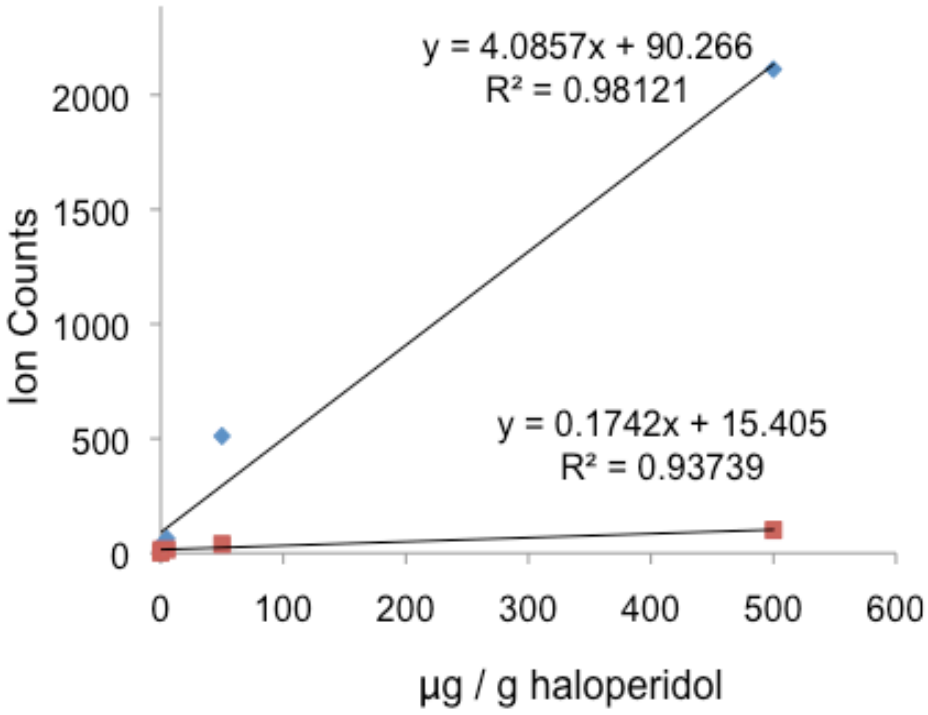

Figure 2.12: Calibration curves generated in this study. Blue diamonds represent the curve generated from dried droplet deposition of matrix, whilst the red squares represent the calibration curve generated from automated deposition by Bruker ImagePrep robot.

We have assessed the suitability of each calibration curve for use according to the quality coefficient for linear calibration curves (*QC%*) which can be used to assess the suitability of a calibration curve for use;[185, 186] mathematically the *QC%* is described by the following equation:

$$QC(\%) = 100\sqrt{\frac{\sum\left(\frac{Y_i - \hat{Y}_i}{\overline{Y}}\right)^2}{n-1}} \qquad (2.1.)$$

Where Y_i is the datapoint measured and $Y\hat{}_I$ is the response predicted by the calibration curve, Y-bar is the average difference between the data and model

and n is the number of points used to construct the calibration curve. The lower this number is, the better the calibration curve, as it reflects the deviation of datapoints away from the trendline. According to literature, the criteria for an extremely accurate calibration curve is that QC < 5.0%.[185, 186] The QC% for the dried droplet calibration curve was calculated to be 115.8%, whilst the same value for the Bruker imageprep robot is 73.4%. Therefore, even though both calibration curves are potentially only semi quantititave at this stage, and will require further optimisation according to the criteria set out above, or the actual response is non-linear. However, it may be concluded that linear calibration curves constructed from data derived for quantitation of haloperidol using the Bruker image prep robot to deposit matrix are more accurate than that produced by using the dried droplet approach under the conditions tested, despite the dried droplet calibration curve having a superior linear regression coefficent (0.98 vs 0.93) for the linear fittings produced from the mean ion count data.

Calculation of a tissue exctinction coefficient for homogenates.

The study by Hamm *et al.,* discussed in chapter 1, introduced the tissue specific extinction coefficient (TEC)[105], a that describes the extent of ion suppression from MALDI in tissues compared with stainless steel, expressed as:

TEC = Ion counts (tissue) / Ion counts (steel)

From our data collected we know that the ion counts for haloperidol MS/MS of the *m/z* 165 fragment on stainless steel is ca. 3000 ion counts for 9.2 x 10^{-13} mol haloperidol (i.e. 3.3 x 10^{15} ions generated per mol) on stainless steel plates (Fig 2.1). From the data in Table 2.2. we know that on tissue homogenates, 6.4 x 10^{-13} mol of haloperidol gives 101 ion counts (i.e. 1.6 x 10^{14} ions generated per mol) if the matrix is deposited by the Bruker ImagePrep robot, whilst for dried droplet deposition this is higher at 2112 ion counts (i.e. 3.3. x 10^{15} ions per mol). Hence the TEC for both techniques can be calculated by dividing these values. For ImagePrep deposition we calculate the TEC to be 0.05. This is consistent with the work of Hamm, who calculated the TEC for liver tissue to be 0.05 for MALDI MS imaging with propanolol using an automated spray deposition of 10 mg ml^{-1} CHCA.[105] However, for dried droplet deposition we find that the TEC is calculated to be 1.0 which suggests that most of the haloperidol is extracted into the CHCA matrix and ionised. However, dried droplet deposition is not suitable for imaging and hence this result suggests that dried droplet be used mainly for quantitative screening of tissues prior to imaging.

Exploring the possibility of internal standards

Generally, the analysis by MALDI of the 12 μm-thickness calibration standards produced in this chapter lead to calibration data that broadly obey linear trends, but further analysis with quality coefficients show that they may not be linear enough to be used as fully quantitative calibration curves. In order to improve the linearity of the calibration curves it is possible to introduce ratiometric measurements that use internal standards – i.e. a co-

spiked molecule that is similar, ideally almost identical, to the analyte. The ion counts of the internal standard can be divided by the ion counts of the analyte (or vice versa) and in theory this should linearise the data as inherent errors are eliminated. Ideally the internal standard will be an isotopically labelled version of the analyte in question – this combination in theory gives the most accurate and precise data. The major advantage of using internal standards that are isotopically labelled is that they will generally behave exactly the same as the analyte; for example ionisation efficiency, extraction by the matrix and distribution should all be relatively similar if not identical. The major disadvantage of using isotopically labelled internal standard is that isotopically labelled chemicals are generally expensive. Often, other drug or bioactive molecules can be employed as internal standards, but this is not ideal due to variations in spatial and tissue distribution and fluctuations in ionisation efficiency between tissue types.

We attempted to linearise MS data from haloperidol using standard addition of caffeine as an internal reference. This was done in an attempt to correct for matrix effects, e.g. differences in ion suppression. Caffeine was chosen because it is inexpensive, readily available without license and is readily ionised due to many basic heteroatoms e.g. nitrogen in its chemical structure. Increasing amounts of haloperidol (0 – 1.2 x 10^{-7} mol) were co-spotted onto stainless steel plates with a constant amount of caffeine (3.3 x 10^{-10} mol) and CHCA matrix. The co-crystallised mixtures were analysed using MALDI MS (Figure 2.13). The mean ion counts for protonated haloperidol (*m/z* 376, *n* = 10) and protonated caffeine (*m/z* 195 *n* = 10) from

the same MALDI spot were taken and the ratio of the counts *m/z* 376 : 196 plotted *vs.* the amount of haloperidol on the MALDI plate. The result was a more linear trend compared with haloperidol on stainless steel with no internal standard (r^2 = 0.9857). Demonstrating that haloperidol ion counts can be linearised with respect to increasing concentration of the drug ,with the use of caffeine as an internal standard, may be useful in future studies of homogenate calibration standards to linearise the data and thus produce more accurate analyses.

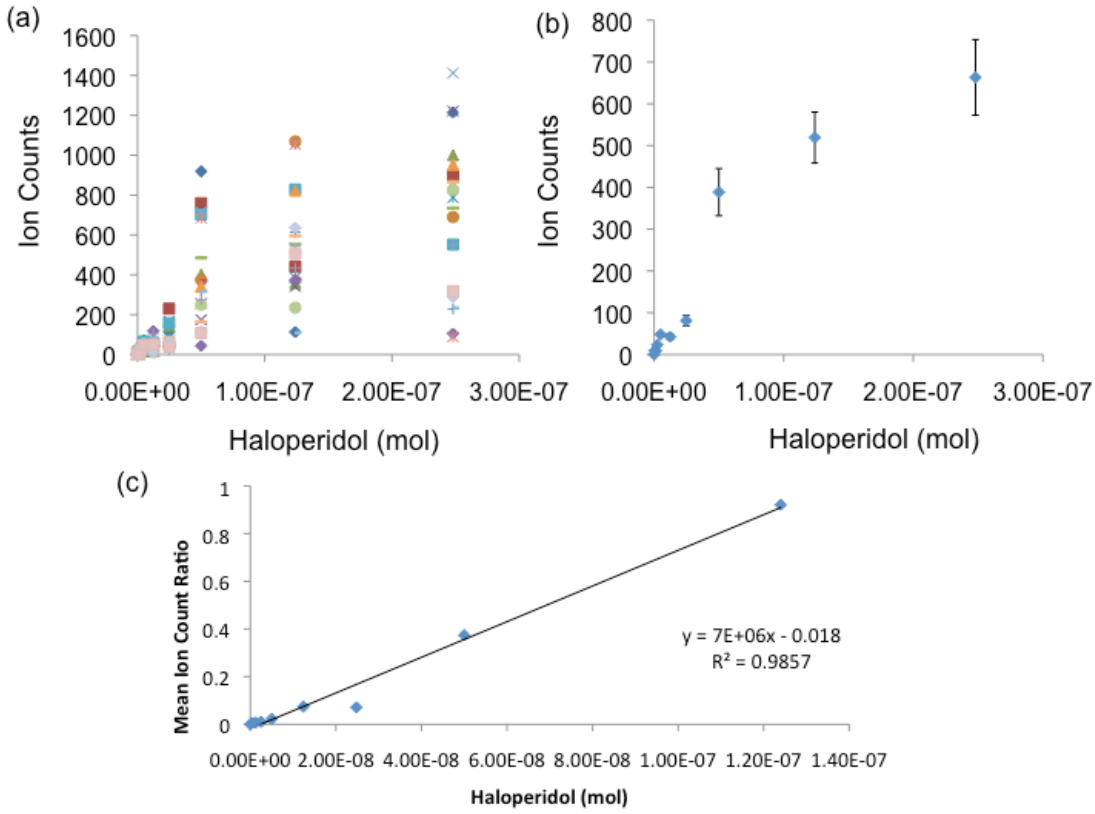

Figure 2.13: Attempted ratiometric MALDI MS quantitation using caffeine as an internal standard. (*n* = 20 per point) of. (a) variability of ion counts for haloperidol (*m/z* 376, *n* = 20) (b) mean ion counts for haloperidol (*m/z* 376). Error bars correspond to the standard error of the mean generated from the data in (a). (c) calibration curve for mean ion counts for haloperidol (*m/z* 376) divided by ion counts

for caffeine (*m/z* 195) as an internal standard (3.32 x 10^{-10} mol). All MALDI MS data was taken on stainless steel plates matrix: 25 mg mL^{-1} CHCA, dried droplet deposition. QSTAR XL instrument, Nd:YVO_4 laser.

The quality coefficient (QC%) of the linear calibration curve generated in Figure 2.13 was also calculated according to equation 2.1. This gave a QC% of 50.6%, which suggests that as presented the calibration curve would not be suitable for accurate quantitative analysis (needs QC of < 5%). However, this is potentially due to the outlier at 2.5 x 10^{-8} mol haloperidol and removal of this could well make the calibration curve suitable. Despite this, the calibration curve generated here may well serve as a good guide for semi-quantitative experimentation.

The use of internal standardization of the MS data vs an endogenous biomarker (choline, m/z 104) as well as vs the dehydrated CHCA matrix peak $[M+H-H_2O]^+$ peak (*m/z* 172) was explored. The plots generated show that linearization of the data is possible with this approach, giving approximately linear curves for ratiometric standardization with either the choline peak (Fig 4.14a) or with the matrix peaks (Fig 4.14b); the quality coefficients of the two curves were calculated to be 232% and 285%, indicating again that despite their apparent linearity according the the R^2 values of the trendlines on each graph that they may only be useful for semi-quantitative analysis as the QC% < 5. These also represent potentially the poorest linear fits in the chapter and as such the internal standard approach using endogenous biomarkers and

matrix peaks may not be a suitable approach toward linearization for spiked liver tissue homogenates.

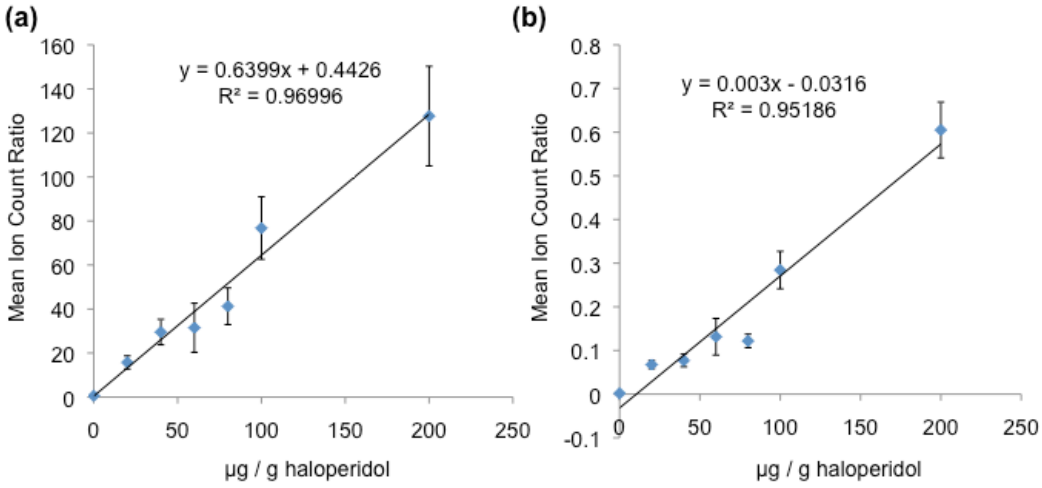

Figure 2.14: Linearization of haloperidol (*m/z* 376) MALDI MS data in liver homogenates by use of internal standards (n = 5). (a) data linearised ratiometrically against the endogenous choline mean ion counts *m/z* 376 : *m/z* 104;, (n = 5) (b) data linearised ratiometrically against the CHCA dehydrate matrix peak mean ion counts *m/z* 376 : *m/z* 104 (n = 5). In all cases the error bars represent the propagated standard error of the mean derived from both measurements.

The effect of homogenate thickness

The effect of homogenate thickness was investigated. Thicker homogenates were cut at 20 and 30 μm, containing haloperidol in the range 0 – 200 μg g^{-1}. CHCA was used as the matrix, which was applied using dried droplet deposition. All instrumental parameters were kept the same as for analysis of the 12 μm homogenates. Plots of haloperidol concentration vs. mean ion counts of the product at *m/z* 165 after CID of protonated haloperidol ($[M+H]^+$, *m/z* 376) are shown in Figure 2.15 for both 20 μm and 30 μm thickness homogenates. This shows that thicker homogenates perform poorly, with a

rapid decline in ion counts that is possibly non-linear with respect to diminishing homogenate thickness – an effect of volume investigated perhaps. These results showed that the 12 μm homogenate thickness was the best choice of those investigated, though thinner sections were not investigated. Thinner homogenates may perform better than 12 μm sections though it is possible that thinner sections may also reach a threshold point where mean ion counts begin to decrease simply due to the lack of analyte within them also as slices get thinner, and additionally errors will potentially become proportionally larger.

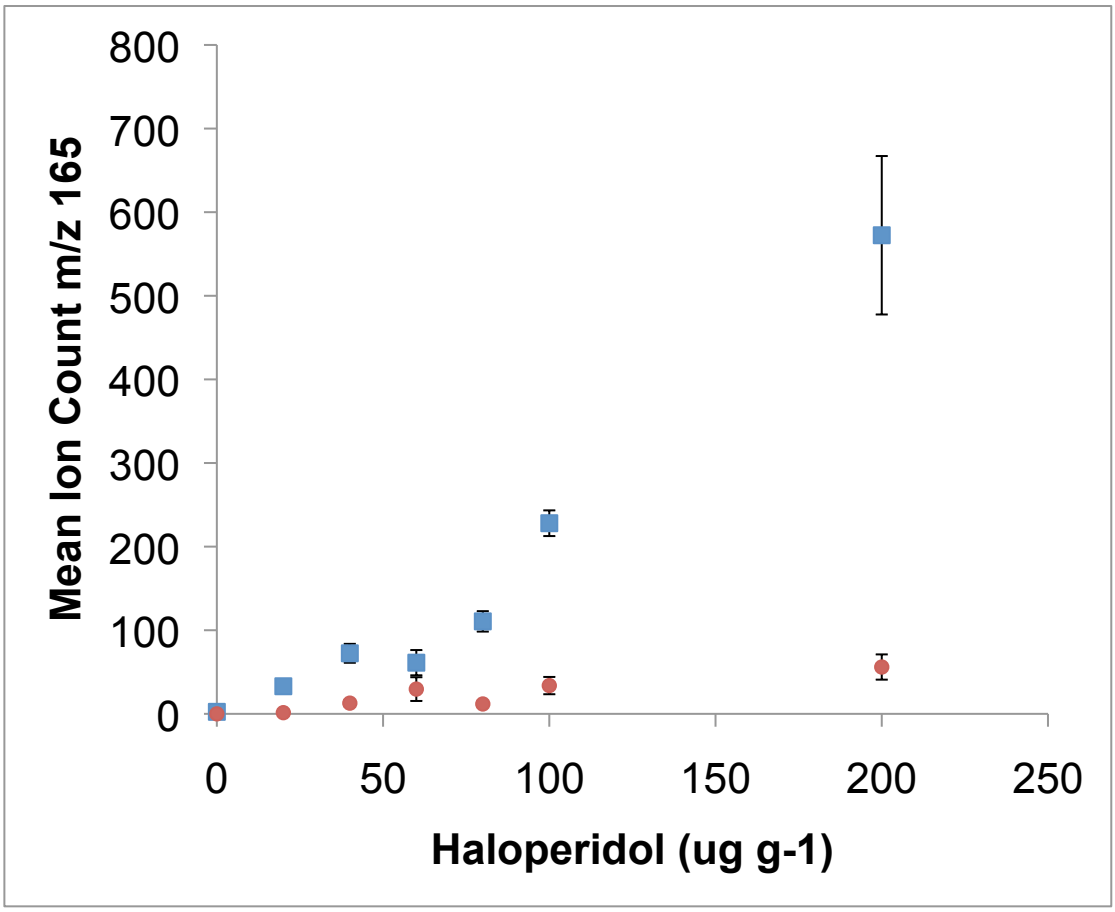

Figure 2.15: Effect of homogenate thickness on mean ion counts (*m/z* 165) in liver tissue homogenates by MALDI MS/MS. (QqTOF) after collision induced dissociation of protonated haloperidol (*m/z* 376) . Matrix: CHCA, 25 mg mL^{-1} in 80:20 MeCN:water, 0.1% TFA, dried droplet deposition. Nd:YVO_4 laser. *n* = 5 for all points. Error bars denote the standard error of the mean in all cases.

2.3 Conclusions

Drug spiked tissue homogenates have been presented as reference standards for use in optimisation and protocols of the quantification of haloperidol in MALDI imaging experiments. Automated homogenisation was found to give superior quality homogenates compared to manually prepared

homogenates for imaging experiments. Introduction of a high repetition rate laser source (Nd:YVO_4 laser) improved sensitivity in imaging homogenates compared to a standard nitrogen laser. Matrices and deposition solvent for matrix coating were found to play a large part in determining resultant ion counts for imaging haloperidol on tissue homogenates, though no trend could be established on the basis of solvent polarity alone. CHCA was found to be the most suitable matrix for imaging haloperidol. Automated deposition of matrix was found to give better resolution of boundaries in an image compared to airspray deposition. Two calibration curves for quantification of haloperidol within tissue homogenates have been presented, the first using dried droplet deposition of matrix (suitable for spot profiling experiments) and the second using automated spraying of matrix (suitable for imaging whole sagittal sections). The sensitivity of detection with the optimised protocol has been determined per pixel and found to be in the attomole range (10^{-18} mol). Further work will now focus on the development of quantitative analysis by the use of internal drug standards; the use of internal biomarkers and matrix peaks did not make the calibration curves better in this case. The use of liquid sampling of these tissue homogenates in particular could be extremely interesting as extraction of the drug can be controlled and thus optimised. Emerging techniques such as liquid extraction surface analysis (LESA) combined with mass spectrometry could provide such an opportunity, which we explore in the next chapter.

Chapter 3: Development of calibration standards using liquid extraction surface analysis mass spectrometry (LESA-MS) for analysis of two drugs in tissues.

3.0. Introduction

The liquid microjunction principle, which is a microscale extraction technique which uses a solvent to extract analytes from and to sample a surface, was first applied by Van Berkel *et al.* to the analysis of spots on thin-layer chromatography plates.[187] A number of organic dye molecules such as fluorescein and rhodamine 6G could be extracted from their spots post-elution on standard reversed-phase plates and detected using positive-ion and negative-ion mode ES-MS, with the limit of dectection in the low nanogram range. Images displayed using mass spectrometric methods showed generally good correlation to the optical images presented. LESA is highly attractive for this kind of analysis as workflow is speeded up considerably, indeed, even in these initial experiments, scanning modes were cited. The advantages, in terms of time saved, are quite obvious though when compared to other traditional TLC analysis techniques, which require 'scratch and elute' type protocols that are hard to reproduce. Notably, one of the other techniques which had success in this field was MALDI, as shown in a significant report from Hercules and co-workers.[188] The proteins bradykinin, angiotensin, and enkephalin were separated by TLC and an absolute detection limit of 2-4 ng was demonstrated. The method also worked for larger peptides and small proteins like bovine insulin chain B, insulin, horse heart cytochrome c, and myoglobin, but TLC separation was poor. Only minor fragmentation was found for all analytes. The method has been used by Hercules for the quantitative analysis of cocaine using a d3-cocaine internal standard.[189] The MALDI TLC method is adaptable to the analysis of a range

of biologically relevant molecules including nucleotides,[190] alkaloids,[191] siderophores,[192] peptides[193, 194] polyethers,[195] and lipids.[196] The technique has more recently been applied to high-quality and direct monitoring of chemical reactions.[197, 198] A comprehensive review of MALDI-TLC has been published by Fuchs et al.[199] Extraction of analytes by LMJ formation is not only limited to TLC plates. Analysis can be performed on a range of substrates; for instance, in one of the reports by Kertesz and Van Berkel,[200] analytes on standard MALDI plates, blood spots on paper, and whole-animal sections were analysed by the technique. Activated carbon has also been used as a substrate[201] as have hybrid substrates in which silica and MALDI layers are placed adjacent to each other on a backing plate.[202]

In addition to the usual advantages from using mass spectrometry to analyse samples e.g. drug and drug metabolites can be analysed with high sensitivity and discerned from each other, no radioactive labeling is required, soft ionisation etc., the LESA technique has inherent advantages compared to traditional vacuum mass spectrometries for a number of reasons, unique to this technique:

I) Eliminates the use of a matrices for MALDI, so organic drug molecules – especially lipophilic molecules – can be easily extracted from tissues. Extraction time can also be tuned according to the method desired.

II) LESA gives true environmental results i.e. the sample is never placed under ultra-high vacuum (UHV) and thus is a true representation of

what is at the surface under ambient conditions; artifacts are essentially eliminated.

III) Sample preparation is eliminated. The chance of chemical alteration of samples is therefore minimised.

IV) Chip-based array electrospray instruments which are often coupled to LESA also offer the ability to sample and analyse many samples in parallel thus rapidly speeding up analysis time.

However, as with all mass spectrometries, there are potential drawbacks to ambient pressure ionisation techniques. As no sample preparation is employed), LESA-MS is expected to be more susceptible to ion suppression; in comparison (especially when coupled to salt-sensitive electrospray ionisation sources), high and medium-vacuum techniques such as MALDI imaging often employ wash steps beforehand to remove excess salts and lipids from the sample surface.[32] But in stating this, it also becomes quite obvious that emerging techniques such as LESA will be complementary to vacuum ionisation techniques in helping researchers understand the effects of ion suppression. The choice of solvent for analysis is often even more crucial than for vacuum techniques as the liquid extraction step requires the extraction solvent to be in contact with the sample for a relatively long time; should the solvent impart chemical modifications or dissolve the sample, the result is potentially very confusing. As the LESA technique is reliant on the formation of the liquid microjunction for a defined period of time, it is this

extraction time that limits the speed of analysis and also the sensitivity of the measurement. For instance, for screening purposes, short extraction times are preferable, but for sensitive imaging techniques, longer extraction times are preferable. However, it should be noted that there are limits on the time that the liquid microjunction can be sustained before collapse; again, this somewhat depends on the choice of solvent and the surface being analysed i.e. polar or non-polar – which can be ascertained approximately by contact angle measurements on the surface / solvent pair. For techniques such as LESA coupled to a chip-based electrospray (as used in this thesis), the amount of analyte sampled at any one point is also dependent on the rate of spraying – typically for an instrument such as the Advion Triversa nanomate this rate is around 0.2 – 0.8 μL min^{-1}. Possibly the major drawback currently for all ambient techniques – for imaging specifically – is their relatively poor resolution, which is often dictated by the surface sampling technique employed. However, it still allows relatively high resolution for areas where obvious boundaries need to be analysed i.e. in organ boundaries in whole animal sections and is highly suited for spot-to-spot analysis in this manner.

LESA has found many applications in biological analysis. For example, LESA has already been employed by a number of groups to profile drugs and drug metabolites. Eikel *et al.* used LESA to study the distribution of terfenedine within mice.[81] It was possible to discern between the drug and its active metabolite, fexofenadine. The results were compared to QWBA, MALDI-MSI and LC-MS/MS and found to give results comparable to each of these standard techniques, thus validating it for use with other drug and drug

metabolites. Resolution of around 1 mm was claimed. Blatherwick *et al.* compared two liquid microjunction techniques, [203] based on LESA, for the analysis of drugs in animal sections. It was found that the LESA technique was complementary to QWBA, allowing profiling of drug and drug metabolites in animal sections with analysis of regions of the subject allowing more rapid analysis compared to traditional MSI workflows, where often a rastering approach is used to analyse the whole section. Edwards *et. al.* used the LESA technique for blood spot analysis to identify haemoglobin variants relevant to diseases such as sickle-cell anaemia.[204] Schadt *et al.*used LESA-MS to study figopitant, a tachykinin neurokinin-1 antagonist and metabolites distribution in the tissues of rats after the intravenous injection of the drug, and was compared to liquid chromatography analysis of tissue extracts. A host of metabolites of figopitant were identified, though the analysis was semiquantitative. Kai *et al*. used LESA combined with a nanoelectrospray ion source and a tandem mass analyser to detect antibiotics produced by actinobacteria.[205] Lanekoff used similar techniques to analyse the fate of nicotine in rat brains.[206] The spatial distribution of exogenous chloroquine and metabolites from tissue sections by LESA sampling analysis coupled with tandem mass spectrometry (LESA-MS/MS) was demonstrated by Van Berkel.[207] The results agreed with analysis by excision of organs followed by extraction and fluorescence analysis of the extracts. The LESA process here presents direct analysis with minimal sample preparation, so it has great potential for challenging the nature of conventional MS workflows. LESA has also found other applications outside of biological analysis. Paine *et al.* investigated the degradation of Polymer-based surface coatings by solar

radiation by using LESA combined with a nanoelectrospray.[208] The work will allow the better understanding of the polymer degradation process and lead to the development of more resistant coatings in the future.

As discussed in the previous chapter, imaging the distribution of drugs in single organ and whole animal sections is an important aspect of drug discovery processes in the pharmaceutical industry. MALDI-MS imaging of drugs, which is now a relatively well-established technique, is a qualitative and complementary technique to the current imaging techniques such as quantitative whole body autoradiography (QWBA). The research presented so far focused on the development of reference standards suitable for use in optimising MALDI-MS imaging protocols.

These samples, based on sectioned tissue homogenates spiked with known amounts of the anti-psychotic drug, haloperidol, were assessed as calibration standards for the quantitative determination of drugs in tissue in MS imaging experiments. The homogenates were used to optimise solvent extraction of the drug in tissue, the matrix deposition method and for a comparison of two lasers in MALDI-MS drug imaging. However, it is extremely important to develop complementary techniques to those that already exist to give further accuracy to the drug discovery process. Currently, imaging by quantitative whole-body autoradiography (QWBA) provides the industry standard, but mass spectrometric techniques can provide superior sensitivity and resolution for imaging analysis. The development of standards in order to achieve quantitation of analytes is still a developing area in ambient ionisation. However, there have been limited reports where internal standards

have been used for the quantification of drugs in tissues – for instance the report by Vishmeh *et al.* which describes the use of loxapine as an internal standard to determine the amount of clozapine in rat brain tissue by DESI.[209]

3.0.1 Hypothesis

MALDI imaging is currently reliant on the efficient extraction of drug molecules from tissue sections and into solution where the matrix is deposited and finally co-crystallisation of the drug with the matrix is required. However, this can be inefficient for biological samples as the drug may not be fully extracted because the matrix is deposited in an organic solvent which may be immiscible with aqueous solution. Efficient extraction may also take time, which cannot really be controlled in a standard deposition of matrix, which is mainly controlled by how fast a solvent evaporates i.e. volatility. This is part of the reason why the TEC in many biological images is so low (typically under 0.10). The use of other sampling techniques by which to extract drugs could improve MS imaging, and LESA is a good candidate to research for this purpose given that extraction can be controlled, and therefore optimised and solvent choice is not dictated by solubility of matrix. In fact, if LESA could be coupled to a mass spectrometric technique with liquid introduction and high resolution mass analysis, it could become an extremely useful tool for mass spectrometry of biological systems.

3.0.2. Aims and Objectives

In this chapter we explore the use of LESA coupled to a high resolution ESI-Orbitrap® mass spectrometer for quantitation of drugs in tissue sections. In order to achieve this two sets of porcine liver tissue homogenates spiked with known amounts of propanolol and fenclozic acid will be produced. LESA combined with high resolution ESI-Orbitrap® MS will then be used to construct calibration curves for each drug. This will demonstrate that reference standards in combination with LESA MS could potentially be a viable approach toward quantitative MS of drugs in biological tissue sections in the future.

3.1. Experimental

Preparation of spiked homogenates for LESA analysis

Homogenates based on porcine liver containing spiked with drugs at various amounts were prepared automatically using an IKA Ultra-Turrax T25 homogeniser as described in chapter 2. The amounts of drugs spiked into the homogenates were in the μg g^{-1} range, (which is in the range of the typical clinical dosages for both drugs) as follows, where the weight of the drug (in μg) is relative to the weight of the tissue (in g) used:

Fenclozic acid: 0 (blank), 8, 10, 20 μg g^{-1}.

Propanolol: 0 (blank) 4, 8, 10, 20, 40 μg g^{-1}.

The homogenates were frozen, sectioned and cut to 12 μm depth using a cryomicrotome, and finally mounted on glass slides for LESA-MS analysis. Sectioned homogenates were stored in a freezer prior to their use.

Surface Sampling by formation of liquid microjunction (LMJ).

The surface of the mounted homogenates was analysed using an Advion TriVersa Nanomate system (Advion, Ithaca, NY, USA) as described previously,[204] with a nanochip electrospray ionization source coupled to a Orbitrap® Velos mass spectrometer (Thermo Scientific, Bremen, Germany), controlled by the advanced user interface (AUI) in the TriVersa NanoMate ChipSoft Manager software. Surface sampling was achieved by a robotic arm containing an automated micropipette equipped with a conductive disposable pipette tip. The pipette is moved over to a solvent reservoir and the tip filled with 2 μL of the electrospray solvent, either methanol (MeOH), acetonitrile (ACN) or 60:40 MeOH:ACN. The loaded pipette was then manoeuvred to a set of pre-entered coordinates (*x, y,* z) over the area to be sampled and the tip was brought into close proximity of the homogenate surface. 1.2 μL of the electrospray solvent was then dispensed to form liquid microjunction (LMJ) between tip and surface at a height of 0.2 mm above the surface. After 10 seconds maintaining LMJ, (which is close to the time limit of collapse of the LMJ) 1 μL of the solution was re-drawn back into the tip. The robotic arm is then withdrawn from the surface, rotated through 90 degrees, and the tip mated with the ESI chip-based array to initiate ionisation of the sample.

Electrospray Mass Spectrometry

In all cases, gas pressures of 0.3 psi were used for sample introduction, with a flow rate of 80 nL min^{-1}. The tip voltage used was 1.8 kV. The capillary temperature was 250 °C. Mass spectra were collected both in full scan mode (*m/z* 0 - 500) and in selected ion mode (SIM) with a resolution of 100 000 at *m/z* 400 in both cases. Collision induced dissociation (CID) took place within the ion trap using helium gas, with detection by an orbitrap® mass analyser at a resolution of 100,000 at *m/z* 400 and 5 co-added microscans. Resulting MS/MS spectra comprised of 10 scans. Data were analysed using XCalibur 2.1. All spectra produced were taken in positive-ion detection mode using an injection time of 15 ms with automatic gain control turned off.

Preparation of theoretical isotope patterns

Theoretical isotope patterns were prepared using the Scientific Instrument Services website: http://www.sisweb.com/mstools/isotope.htm

3.2. Results and Discussion

Fenclozic acid and propanolol are organic drug molecules. Propanolol is commonly used as a beta blocker, while fenclozic acid is an anti-inflammatory with analgesic properties. Both are important drugs which currently find themselves in clinical use. It was decided to investigate the use of both in the developments of reference standards for the LESA-MS technique.

As discussed, the major challenge of MALDI-MS imaging is the extraction of the drug from the tissue into the matrix which is deposited onto the reference standards. A range of factors with sample preparation associated with MALDI-imaging are avoided by the use of LESA-MS. It offers direct extraction from the tissues using a liquid microjuction, which is a droplet bridge that can be deposited onto the tissue and then recovered and re-introduced into a mass spectrometer via an electrospray ionization source. The chip-based electrospray ionisation source, which in theory can massively reduce duty cycle time due to parallel analysis possibilities, is coupled to an Orbitrap® mass analyser.[88] Such a mass analyser provides the opportunity to analyse drugs at very high resolution (up to 150 000, but in this case 100 000 at *m/z* 400) , at high mass accuracy (typically 5 ppm) and in a mass range well above and beyond the needs (*m/z* 0 – 6000) of most drug analyses. Hence the instrument used in this chapter is potentially very suited to spot-to-spot analysis of drugs within tissues, and it was the plan to test its capabilities so.

Therefore, to assess the potential of LESA-MS in creating a quantitative analysis for drugs in tissue samples, spiked tissue homogenates were used as novel calibration standards for label-free analysis and the construction of a calibration curve. Using the protocol established for the production of homogenates developed in chapter 2, we were able to easily produce 12 μm thick tissue homogenates for analysis. The LESA (Advion Nanomate) instrument was set up initially to use a mixture of solvents to form the liquid microjunction (LMJ) on the surface of the homogenate: 60:40 methanol: acetonitrile. Whilst the choice of solvents was heavily influenced by existing knowledge from the solvents investigation in chapter 2, predicted Log P values were also taken into account for both drugs to choose appropriate solvents. For instance, both fenclozic acid and propanolol have predicted log P of 3.1 (www.chemspider.com), where log P is defined as the logarithm of the partition coefficient, P, between the solvents water (fully polar) and octanol (fully non-polar):

$$\text{Log P} = \text{Log} \left([\text{Drug}]_{\text{octanol}} / [\text{Drug}]_{\text{deionised water}} \right)$$

Hence, small values of log P indicate that a drug will be polar, whilst large values of log P suggest that a drug would migrate into octanol and would therefore be non polar. Generally Log P values for pharmaceuticals are around 3 – 4 i.e. relatively non-polar and are 'organic' in nature, and rarely are values higher than 5 observed. Hence the choice of the relatively polar, yet still somewhat organic acetonitrile / methanol mixture seemed quite appropriate for the extraction of *both* drugs. Figure 3.1 shows the mass

spectrum (full scan) after LMJ extraction with 60:40 MeOH:ACN for a homogenate spiked with 40 μg g^{-1} fenclozic acid.

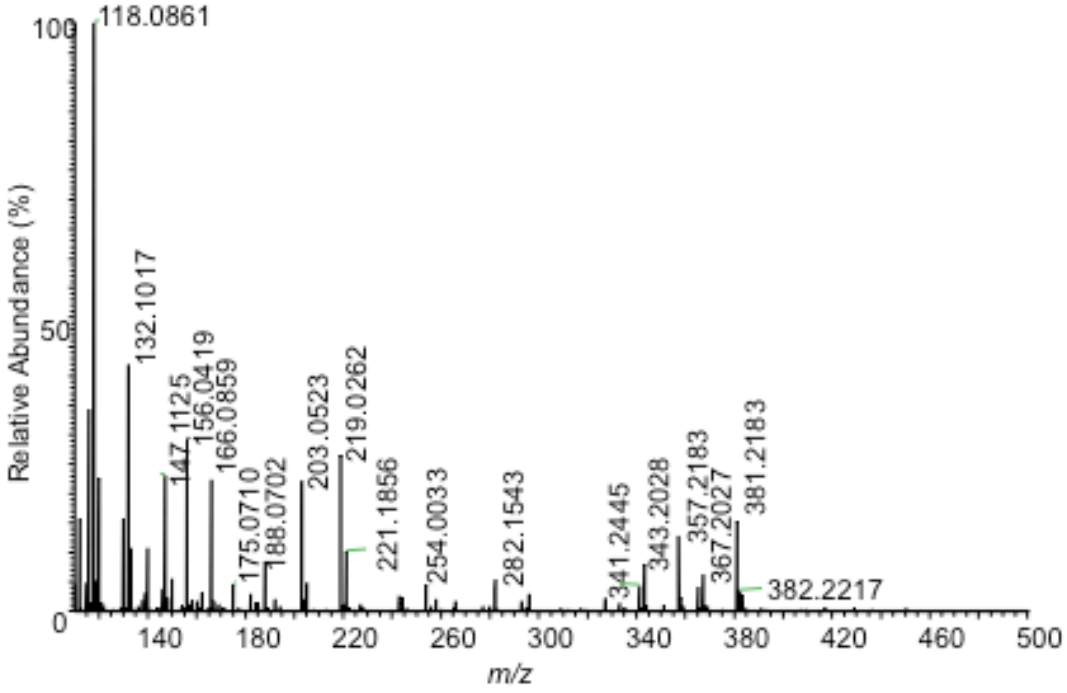

Figure 3.1: Mass spectrum generated by liquid microjunction extraction of a liver tissue homogenate spiked with 40 μg g^{-1} fenclozic acid with 60:40 methanol:acetontrile followed by ESI MS.

The parent ion of fenclozic acid is observed at *m/z* 254.0032 in the spectrum, corresponding to the protonated drug, $[M+H]^+$. The protonation site probably occurs on the nitrogen of the azo-thiophene ring in fenclozic acid, where the lone pair can bond to the proton. As may be expected the peak for fenclozic acid is of low intensity in the spectrum – the ion observed at *m/z* 118.0881 is dominant. This ion could not be assigned at the present time but presumably

arises from the biological substrate. Fragmentation pathways of this drug molecule have been investigated at AstraZeneca (unpublished results, Figure 3.2), and the major product of fragmentation is the result of decarboxylation to leave a cation with *m/z* 207.

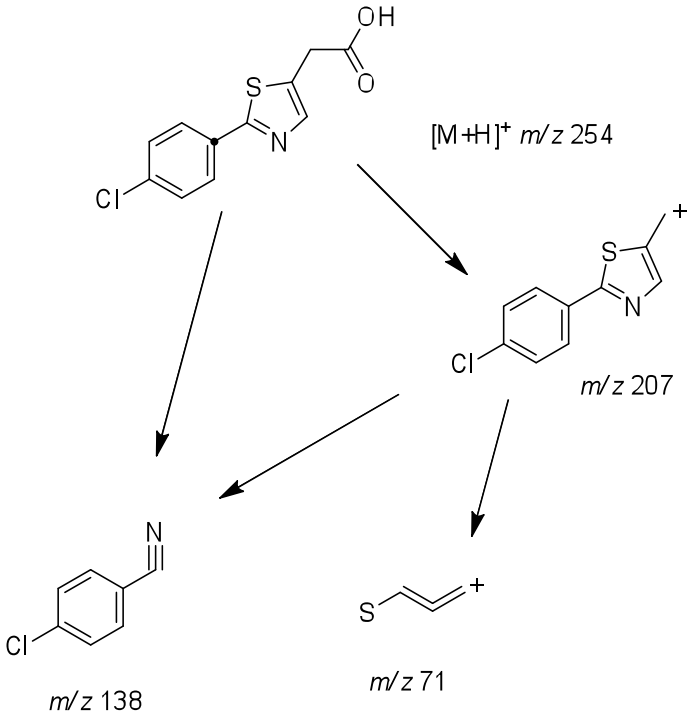

Figure 3.2: Parent ion and fragmentation pathways of fenclozic acid. *m/z* 207 is the major peak observed after CID of *m/z* 254 in the MS/MS spectrum of fenclozic acid in liver tissue homogenates.

An enlargement of the spectral region in the range *m/z* 253 - 255 reveals the presence of the parent ion at *m/z* 254.0032, as shown in Figure 3.3. A theoretical calculated isotope pattern was prepared for the $[M+H]^+$ ion, also shown in Figure 3. The base peak in the theoretical spectrum was generated at *m/z* 254.0043 (c.f. 254.0032 observed experimentally). The theoretical *m/z*

is, therefore, remarkably close to the experimentally observed *m/z* for this ion – within 4 ppm of the theoretical values – and the isotope pattern observed, synonymous with chlorine incorporation is also identical which gave great confidence that this is indeed the ion of interest.

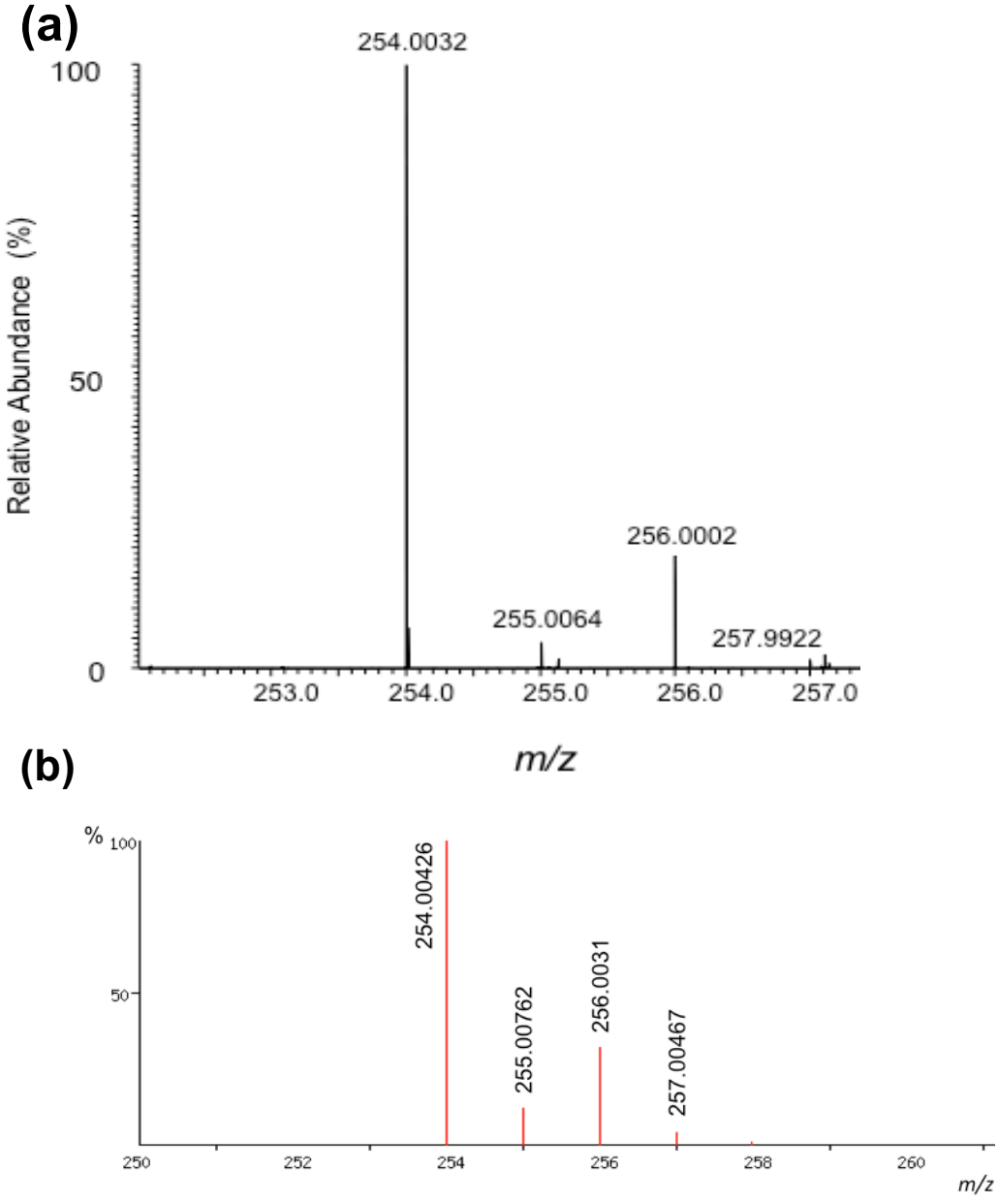

Figure 3.3: (a) Magnification of the protonated fenclozic acid molecule, $[M+H]^+$, in the LESA MS extraction products from the liver tissue homogenate spiked with 40

μm g^{-1} fenclozic acid, after liquid microjunction extraction with 60:40 methanol : acetonitrile. (b) theoretical isotope pattern of fenclozic acid $[M+H]^+$.

Collision induced dissociation was performed on the *m/z* 254.0032 ion to analyse the product ions from fragmentation. The MS/MS spectrum in this case was dominated by a single peak at *m/z* 207.9977 generated from the decarboxylation of the parent ion (Figure 3.4). This was taken as good evidence of the correct peak assignment in the MS spectrum, The neutral product of mass 138 daltons was not observed in the spectrum as it is not charged, hence the spectrum is dominated by the single product ion.

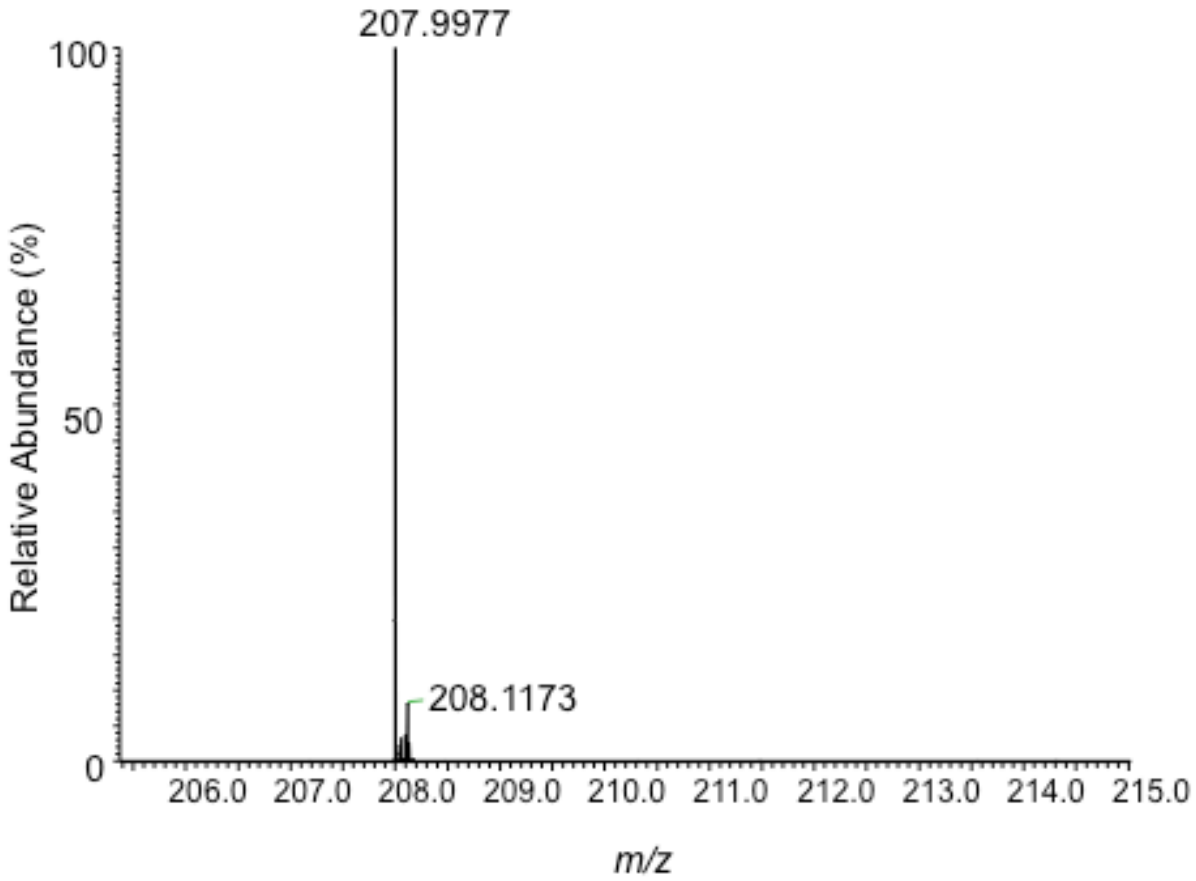

Figure 3.4: MS/MS spectrum, generated by liquid microjunction extraction of a liver tissue homogenate spiked with 40 μg g^{-1} fenclozic acid with 60:40 methanol : acetonitrile and CID of *m/z* 254.0032.

The full mass spectrum for an equivalent 40 μg g^{-1} homogenate spiked with propanolol is shown in Figure 3.5. This spectrum was again produced from direct surface sampling using LESA liquid microjunction with 60:40 MeOH : ACN, with extraction of the drug followed by chip-based nanoelectrospray ionisation and mass analysis.

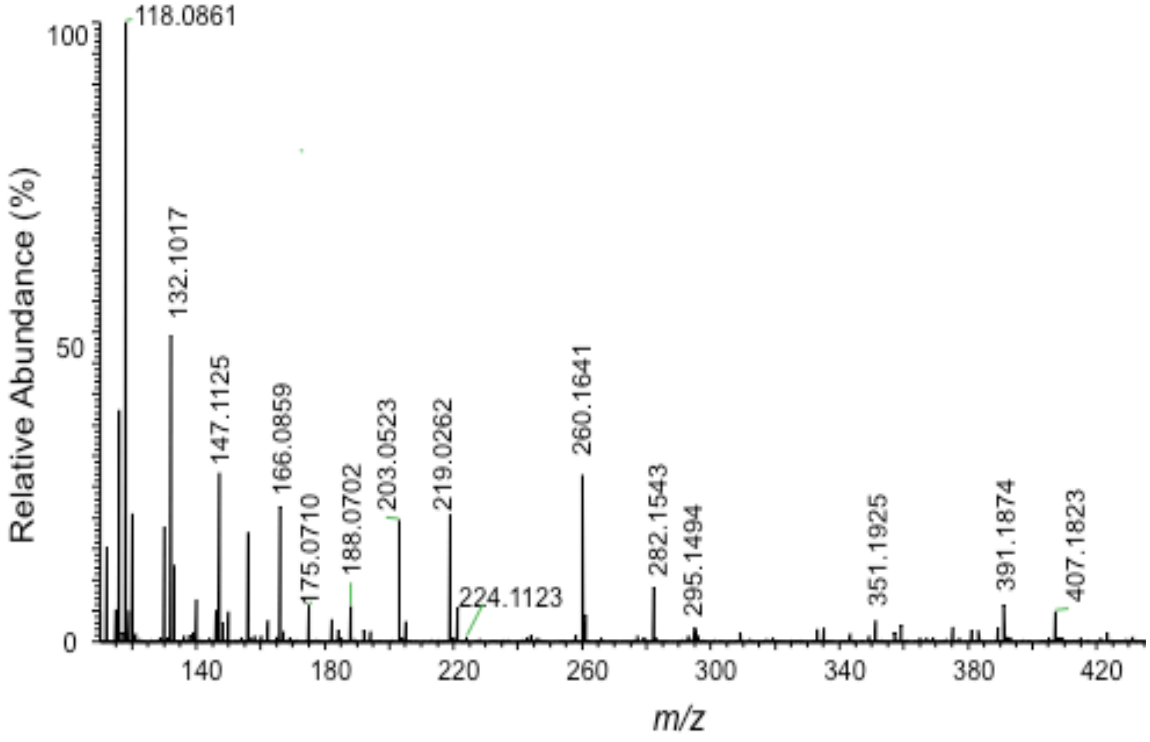

Figure 3.5: Upper: Mass spectrum generated from liquid microjunction extraction of a homogenate spiked with 40 μg g^{-1} propanolol with 60:40 methanol : acetonitrile followed by ESI

The $[M+H]^+$ ion of propanolol was detected at *m/z* 260.1641 within this spectrum, corresponding to the protonated drug according to Figure 3.6. In this diagram, possible fragmentation products are also shown, with pathways for fragmentation including loss of the naphthyl group, and simultaneous loss of hydroxyl and isopropylamine to leave ions with *m/z* 116 and 183 respectively, each arising from direct fragmentation of the parent ion. A calculated theoretical isotope patter for $[M+H]^+$ matched closely with that found experimentally, with the accurate mass generated for the calculation, *m/z* 260.1651 matching to 3 ppm of the experimental value (260.1641) and well within the accuracy of the Orbitrap® mass analyser.

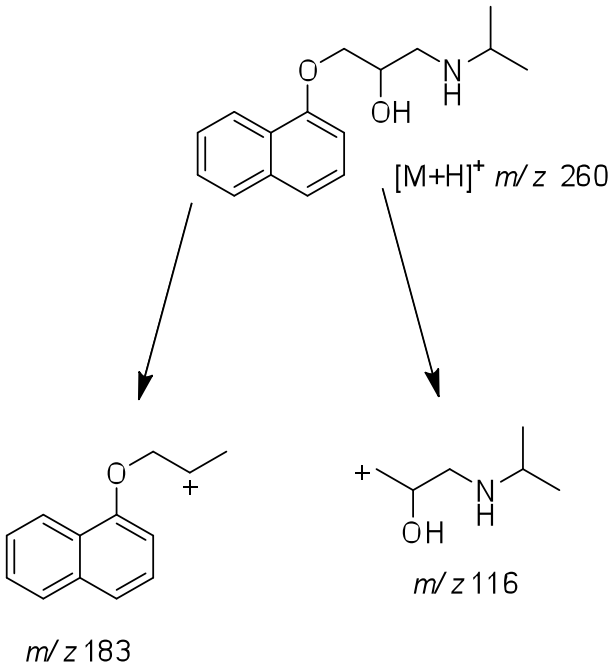

Figure 3.6: Parent ion and possible fragmentation pathways of propanolol.

Again, through the enlargement of the spectrum it was possible to confirm the presence of the ion at *m/z* 260.1638, which corresponds to the protonated

propanolol molecule. The full MS/MS spectrum of fragmentation products of the ion observed at *m/z* 260.1638 after collision induced dissociation (Figure 3.7) suggested that this assignment was indeed correct, with peaks also observed at *m/z* 183.0800 and *m/z* 116.1067, which are tentatively assigned to loss of an isopropyl hydroxylamine species from the parent ion, and loss of hydroxynaphthyl from the parent ion respectively (Figure 3.6).

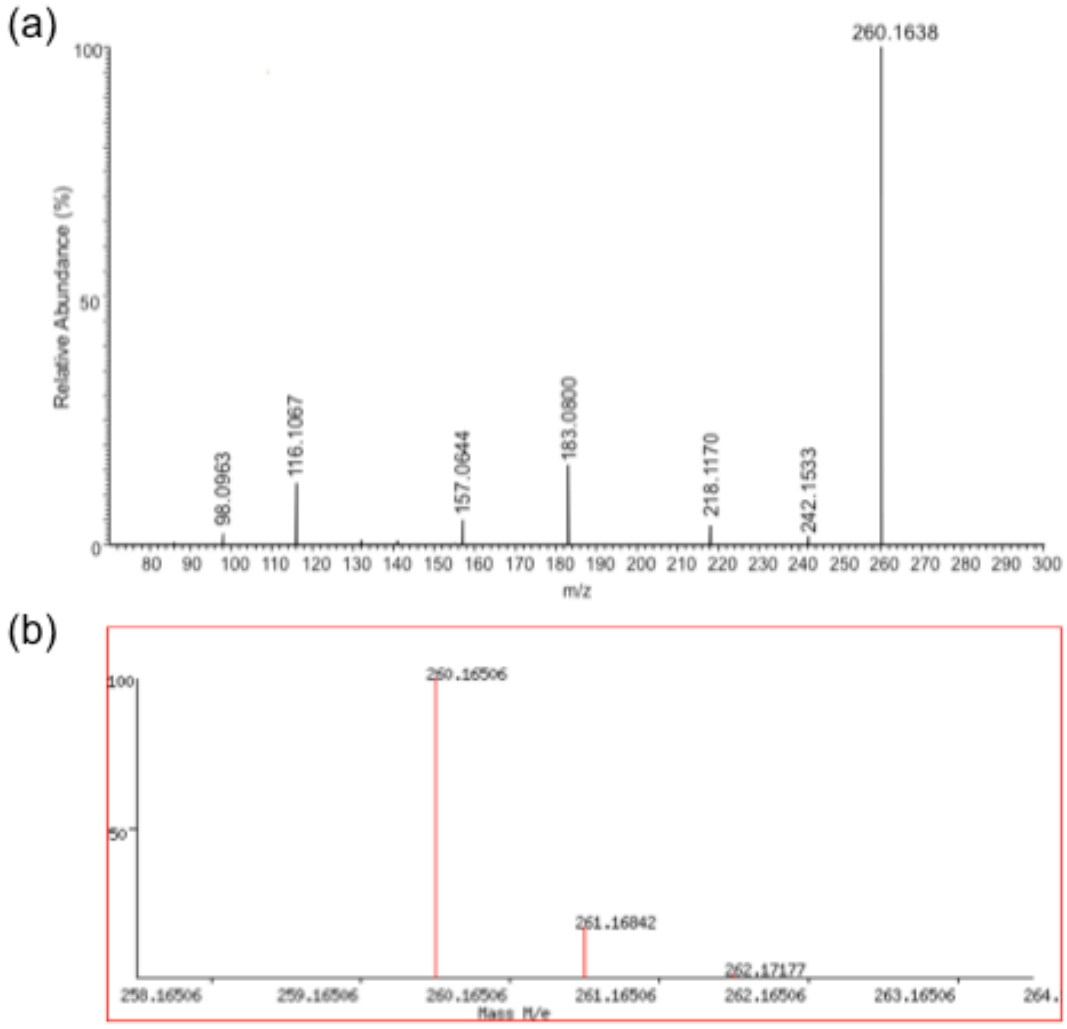

Figure 3.7: (a) MS/MS spectrum generated from liquid microjunction extraction of a liver tissue homogenate spiked with 40 μg g^{-1} propanolol with 60:40 methanol : acetonitrile followed by electrospray ionisation and collision induced dissociation of

the protonated propanolol molecule (*m/z* 260.1638). (b) Theoretical isotope pattern of propanolol $[M+H]^+$.

It was clear that LESA-MS coupled to high resolution mass spectrometry was suitable for the further analysis of the homogenates, with the possibility of developing quantitative drug analyses, based on the homogenate tissue standards. To do this, we made up a range of calibration 'standards' based on these tissue homogenates, and surveyed them using LESA, with the aim of constructing calibration curves for both drugs which in theory could be used to probe tissue samples (homogenized tissues or full animal sections would be suitable) containing unknown amounts of both drugs, and quantify the amounts to a high degree of accuracy. Such calibration standards are useful as they authentically mimic tissue substrates and therefore the inherent error for real analysis is reduced considerably.

Therefore, a series of spiked tissue homogenates were produced which contained a range of concentrations of fenclozic acid in biologically significant amounts: 0, 8, 10 and 20 $\mu g\ g^{-1}$ - where the weight of the drug in μg is measured relative to the weight of the tissue homogenate in g. The 0 $\mu g\ g^{-1}$ fenclozic acid as used as a negative control. In theory, linearly increasing amounts of drugs spiked into tissues should give a linear response of the ion counts associated with the drug in tissue. However, this is not always the case due to the physical and chemical constraints of the drug being extracted efficiently from the tissue, hence the response can be a function of concentration and can often appear non-linear. However, this disadvantage

is offset because the amount of inherent error in quantitative measurements of unknown amounts of the drugs in tissue should in theory be reduced substantially by using calibration standards based on authentic tissue, as known unknown factors such as efficiency of extraction and ionisation suppression from salts (crucial in electrospray) should in theory be eliminated. Non-linearity in the calibration curve itself may also be corrected with the use of internal standards.

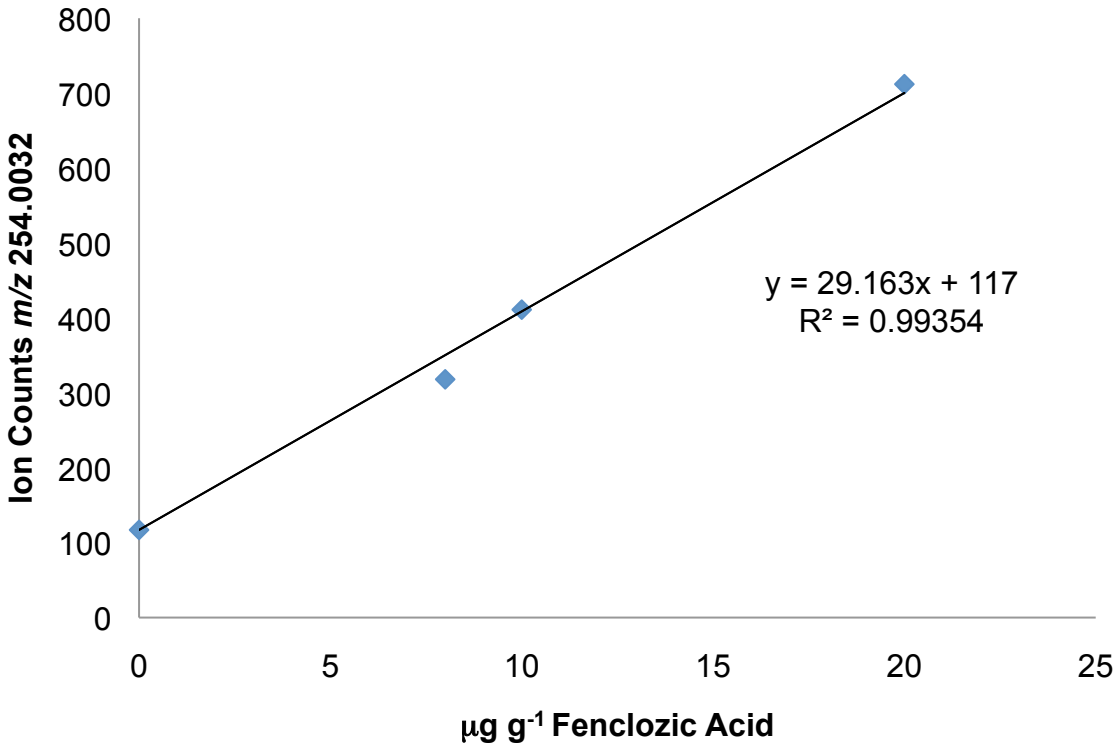

Figure 3.8: Calibration curve for fenclozic acid-spiked tissue homogenates studied by LESA coupled to high-resolution mass spectrometry, showing the trend between ion counts at *m/z* 254.0032 *vs.* the amount of fenclozic acid spiked into tissue homogenates (n = 1 at each point).

It was observed that the ion counts within the range studied showed a strong linear relationship with the amount of fenclozic acid within the tissue

homogenate in the range studied (R^2 = 0.9935, Figure 3.8). It is therefore possible that such a calibration curve could be used effectively to assist in the determination of fenclozic acid in tissues by LESA in the range 0 – 20 μg g^{-1}. However, the blank sample (0 μg g^{-1}) was observed to give around 120 counts at the *m/z* 254.0032. Although this cannot come from the drug, aside from cross-contamination pathways, the point is incorporated in the calibration curve as-presented to eliminate systematic error. This was not seen in blanks for propanolol or indeed in the MALDI analysis of haloperidol. A possibility is that that there could be a conflicting species within the analysis that exists always within the homogenates and simply adds itself to the mean ion counts at *m/z* 254.0032; ion mobility has been used in the past to resolve such problems.[210] The latter experiment involves the seperation of ions by their mobility through a carrier gas using an ion mobility spectrometer, and following this their m/z is determined by a mass analyser. . Alternatively MS/MS product scans could also be used in this case in the future as the MS/MS spectrum of fenclozic acid consists of a single peak at *m/z* 207.977, and thus these spectra act as a signature for the presence of the analyte. However, given the high mass resolution of the Orbitrap® and the difference in mass of 4 ppm between the drug and the contaminating species, it is highly likely that these ion counts arise from cross contamination. Unfortunately as this study was not carried out in replicate it is impossible to confirm this but further replicates could indeed prove or disprove this.

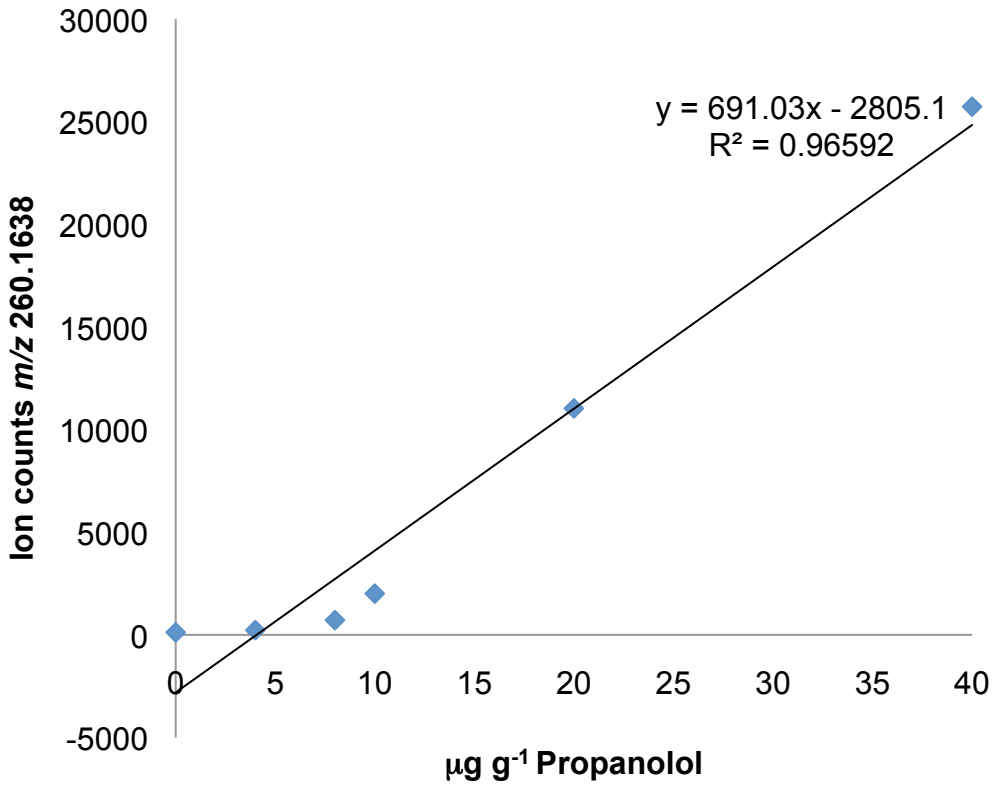

Figure 3.9: Calibration curve for propanolol-spiked liver tissue homogenates studied by LESA coupled to high-resolution mass spectrometry, showing the trend between ion counts at *m/z* 260.1638 *vs.* the amount of propanolol spiked into tissue homogenates. (n = 1 at each point)

.

Similar homogenates spiked with propanolol were set up in the range 0 – 40 μg g^{-1}, and were also studied by LESA to see if a linear calibration curve could be constructed, as for the case of fenclozic acid spiked tissue homogenates (Figure 3.9). The response in ion counts for the propanolol was generally observed to be higher than that for the same amount of fenclozic acid, indicating that either extraction is more efficient for propanolol or ionization is more efficient. It is likely that the latter conclusion applies, based on knowledge of the predicted Log P values for fenclozic acid and propanolol,

because both molecules should have similar solubilities in the given solvent system and hence extraction efficiency should be relatively similar for both compounds, hence the major difference should arise from ionisation efficiency. In spite of lowered counts, it was possible to obtain points for every tissue homogenate studied. The calibration curve demonstrates a linear relationship at higher drug concentrations, though this relationship disappears at lower concentrations; this may be indicative of a threshold effect where extraction below a certain concentration is difficult. By extrapolation of the linear portion of the curve to the x-axis we can get an idea of the quantitation sensitivity of this method for propanolol. In this case it is ca. 7 $\mu g\ g^{-1}$. The test for a useful calibration curve based on the quality coefficent (QC%) described in chapter 2 was applied to both calibration curves generated here. The propanolol curve tested poorly with a QC% of 172.0%; the statistical test for a useable calibration curve for accurate determinations is a QC < 5%.[185, 186] This was not surprising given the great inaccuracy of the curve at lower concentrations of haloperidol. In contrast, the data for fenclozic acid and its associated calibration curve gave a QC% of 4.39% i.e. is potentially a useable calibration curve for quantitiative work. However, it must be noted that this result is based on n = 1 data points for the ion counts and therefore the variability and thus the error on the measurement is unknown. However, saying this it is the best result obtained using LESA with the homogenates and merits further investigation by producing replicates in future work in this area.

Hence, it was concluded that using LESA-nanoelectrospray coupled to high resolution MS may be useful for semi-quantitative purposes for the analysis of

propanolol, with the points acting as ballpark figures for gross determinations and in profiling. The limit of detection in this case is ca. 8 μg g^{-1}. The data could perhaps be linearised if an internal standard was used to produce a ratiometric calibration. Further work using LESA to analyse the organs should definitely be extended to incorporate these ideas, as the results here for propanolol are extremely promising despite their deviation from linearity.

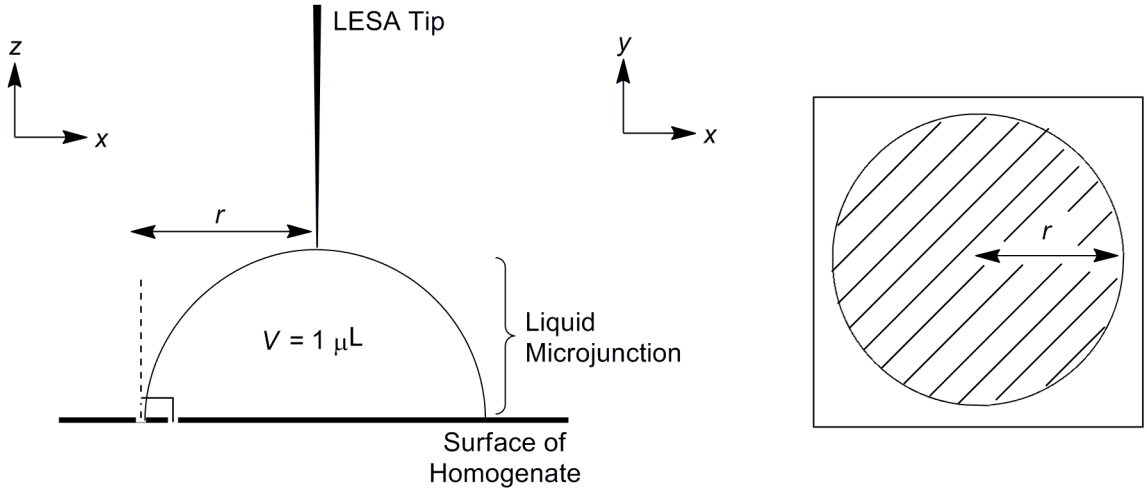

Figure 3.10: Dimensions used to calculate surface sampling area for comparison to MALDI analysis (micropipette tip not to scale). The radius of the half-sphere formed by the liquid microjunction was calculated to be 7.8 x 10^{-4} m or 0.78 mm, which is consistent roughly with a LESA tip width of around 1 mm.

An analysis of the extraction area is useful in comparing the spatial resolution and sensitivity of MALDI vs. direct surface sampling by LESA. The extraction area can also give information on the theoretical maximum amount of analyte that could be extracted in an ideal case. In chapter 2 homogenates probed by MALDI-MS were assessed, and it was calculated that for each pixel

we were sampling an area estimated to be 0.04 mm^2, equating to a side of 0.2 mm per pixel.

To estimate the surface area which the droplet covers on the surface of each homogenate during direct surface sampling by LESA i.e. during liquid microjunction, it was assumed that each roughly 1 μL droplet forms a perfect half-sphere on the surface (i.e. a droplet with contact angle 90 º to surface) and used a volume of 2 μL (2 x 10^{-9} m^3) for the full sphere to calculate the radius of the 1 μL half-sphere (Figure 3.10). The radius of the half-sphere formed by the liquid microjunction therefore was calculated to be 7.8 x 10^{-4} m or 0.78 mm, which is consistent roughly with a LESA tip width of around 1 mm.[81] Conversion of this radius to give the area of a circle gave a surface sampling area of 1.9 mm^2 formed by liquid microjunction with the surface assuming that this area perfectly bisects the sphere of volume 2 μL. By then using the homogenate depth (known from cryomicrotome setup) and the amount of drug spiked into the homogenates per gram of homogenate, it was possible to calculate the amount of drug that in theory may be extracted if the liquid microjunction can extract the entire available drug beneath itself. The results of this analysis alongside the ion counts obtained from each homogenate section is presented in Table 1. This calculation assumes a contact angle of 90º, and hence is an estimate as the real contact angle between the solvent and homogenate was not measured. The contact angle will also change with different solvents and substrates. Hence the results should be interpreted with care in terms of quantitative measurement, but are useful for generating a semi-quantitative measurement.

Table 3.1: Areas of extraction and available drug amounts beneath each liquid microjunction.

μg g^{-1} drug	LMJ radius (mm)	LMJ area (mm^2)	Homogenate depth (mm)	Volume beneath LMJ* (mm^3)	Drug beneath LMJ (pg)	Mean Ion Counts**
FENCLOZIC ACID						
8	0.78	1.9	0.012	0.0228	224	318
10	0.78	1.9	0.012	0.0228	280	411
20	0.78	1.9	0.012	0.0228	560	712
PROPANOL OL						
4	0.78	1.9	0.012	0.0228	112	230
8	0.78	1.9	0.012	0.0228	224	716
10	0.78	1.9	0.012	0.0228	280	2010
20	0.78	1.9	0.012	0.0228	560	11030
40	0.78	1.9	0.012	0.0228	1120	25727

***** Homogenates are assumed to have density of 0.001 g mm^{-3}.

****** From 5 co-added scans.

By calculating the available amount of either fenclozic acid or propanolol beneath each LMJ formed on the surface of the homogenates, it is possible to begin to draw some qualitative conclusions regarding the the LESA technique *vs.* MALDI of homogenates. The first thing of note is that the area sampled by the LESA liquid microjunction is, in theory, a lot larger than that with MALDI (see previous chapter). This results in more drug theoretically available for extraction. However, this is offset by the fact that the sample is diluted into the whole 1 μL during LMJ. Hence, when preparing analyses by LESA it is important to consider flow rate of the electrospray and summing of ES chromatograms in order to balance time of analysis, i.e. duty cycle, with sensitivity. For MALDI this is not a problem as a photon packet generally produces an ion packet and a single spectrum. In this case also, the mass

analyser, the Orbitrap®, is entirely different to the QqTOF used for the analysis of homogenates by MALDI (see introduction) – as the ions are trapped within EM fields one ion can, in theory, be counted more than once with the Orbitrap®. Hence, it may be possible that the limit of detection may be considerably lower if the duty cycle is increased, with a trade-off of time. The extension of the method to ambient surface sampling will perhaps allow the development of analysis of novel surfaces in a quantitative manner, as demonstrate proof-of-principle has been demonstrated here, as well as being complementary to such techniques as MALDI imaging also helping to understand the effects of ion suppression in tissues.

3.4. Conclusions

In this chapter the use of a direct surface sampling extraction technique has been outlined, liquid extraction surface analysis (LESA) coupled to an ambient-pressure electrospray ionisation source and high resolution Orbitrap® mass analyzer, in an attempt to construct calibration standards for the determination of pharmaceutical drug molecules in spiked homogenates. Profiling by LESA presents, in theory, advantageous qualities over MALDI imaging due to its rapidity combined with potentially higher sensitivity due to more efficient extraction of the analyte from the tissue due to the formation of liquid microjunctions (LMJs) during the extraction process, the latter ensuring that the drug has the best chance of being extracted for MS analysis by nanoelectrospray ionization compared with MALDI MS, where the extraction of the drug relies almost solely on how well the matrix extracts the drug after deposition by either airspraying, dried droplet technique or by automated

deposition and additionally, the quality of matrix-drug co-crystals formed after drying *as well as* the efficiency of ionization which is compounded by the complexity of tissues.

It was possible to construct a linear calibration curve for one of the drugs studied, fenclozic acid, despite the blank sample presenting ion counts at the drug *m/z*. We suggest that ion mobility or tandem MS experiments may resolve this issues,in the future. However, the high mass resolution of the Orbitrap® mass analyser used in this study allowed us to confirm accurate mass of the studied peaks in doped samples and gave us confidence that the ions studied corresponded closely (within 5 ppm of theoretical) to the expected mass to charge ratios. A non-linear calibration curve was constructed for propanolol, and although a generally proportional increase of ion counts with drug concentration in the spiked homogenates was observed. However, this does not mean the calibration curve is not useful, because it may well be suited more for experiments where general ballpark figures for the drug are needed in tissues i.e. for semi-quantitative analysis or perhaps semi-quantitative tissue profiling on a spot-to-spot basis i.e. point interrogation. The use of internal standards to produce a ratiometric calibration curve may serve to linearise this data in future studies. IN both cases, more replicates need to be studied to determine the error on the measurements, and the lack of replicates is a major limitation of this study in its current form.

Comparison of the amounts of drug *available* in each technique revealed that although the LESA tends to sample more area and therefore more drug in the homogenate, care must be taken in the interpretation and comparison of the results vs. MALDI. Generally, very sensitive analyses are in theory possible with the use of the technique, at the expense of increased duty cycle time.

As far as is currently known, analysis of drug compounds in tissues by LESA coupled to mass spectrometric methods is *not quantititative* and examination of the available literature reveals few examples of drug analysis perhaps because of this fact. Eikel *et al*. used LESA MS to qualitatively detect the antihistamine terfenadine in various extracted organs from mice, with levels of terfenadine found in the range 0.2 – 550 $\mu g\ g^{-1}$ in the organs by a separate LC-MS/MS assay.[81] Schadt *et al.* qualitatively profiled the distribution of a radiolabelled tachykinin agonist, [14C]-figopitant hydrochloride by LESA-MS in whole rat sections and compared it to quantitative whole body autoradiography (QWBA), where good agreement was found with the *qualitative distribution* (i.e. compound present or not) generated by both methods.[211] The dose of [14C]-figopitant hydrochloride used in this study (5 $mg\ kg^{-1}$) gave concentrations in the organs in the range 0.05 – 25 $\mu g\ g^{-1}$ as found by QWBA. Parson *et al.* analysed chloroquine and its metabolites by LESA MS/MS in a semi-quantitative analysis compared to previous studies in literature, but only relative comparisons could be made.[207]

In all three of these very recent papers there is an implied call to make LESA-MS or MS/MS a quantitative technique due to its great potential for

drug analysis. Indeed, the study by Schadt *et al.* specifically mentions reference standards are needed for this purpose.[211] The paper by Parson *et al.* states "LESA MS/MS…are limited to qualitative or relative quantitation and the development of robust absolute quantitation methods are still in their infancy". [207] The calibration curves produced in this study in this chapter, constructed using from spiked tissue homogenates as reference standards could therefore provide a response to this call and provide a good general way to absolute quantification for LESA-MS analysis for a variety of analyses. Certainly, the calibration curves presented here are in the correct range (i.e. at pharmaceutically relevant levels) required by researchers. The success of the drug analysis using LESA could therefore open new analytical capabilities in the future or indeed fully quantitative imaging using this technique. With the use of internal standards these calibration curves could also be improved.

However, it is acknowledged that there are serious limitations with the current study – the homogenates used to construct the calibration curve were not performed as replicates, and hence the uncertainlty associated with the calibration is currently unknown. The results in this study should therefore be treated with some caution and only represent preliminary, if promising, data towards quantitiation using LESA coupled to MS.

Chapter 4: Mapping the spatial distribution of two radiolabelled drugs in whole animal sections using quantitative whole body autoradiography / phosphor imaging in league with liquid scintillation counting coupled to qualitative MALDI profiling of the drugs in excised organ homogenates by using mass spectral gel views.

4.0. Introduction

Non-human animals such as mice can share remarkable similarity in their DNA sequence to humans.[212] Hence, they possess similar respiratory, cardiovascular and nervous organ systems to humans comprised of similar organs e.g. heart, lungs, liver, brain. 90% of vetinary drugs used are identical to those used in humans. Hence, animals can serve as models for research into the efficacy of drugs in humans to treat disease. For ethical reasons, human subjects cannot be used in initial drug trials e.g. pharmacokinetics, drug distribution, efficacy. Hence animal models are in widespread use as the initial testing point for drugs in clinical trials.

Quantitative whole-body autoradiography (QWBA) is a technique used ubiquitously by the pharmaceutical industry to determine the spatial distribution and amount of radiolabelled compounds within tissue sections, in animals in clinical trials and is the current gold standard for determining spatial distribution of a drug and its metabolites. It was first established as a viable technique for analysis of the distribution of drugs *in vivo* in Sweden in 1954, detailing the imaging of a radiolabelled penicillin in animal subjects.[213]

The technique involves dosing a live subject with a radiolabelled analyte, followed by euthanasia of the subject after a designated distribution time and immediate post-mortem freezing in organic solvent-dry ice baths. The latter freezing step is employed to ensure that the location of the compound is fixated, thus avoiding the leaching of drugs by preparatory procedures used in other histological techniques. The subject is then embedded in a matrix, usually carboxymethyl cellulose from wallpaper paste, and sagittal sectioning is performed using a microtome.

After preparation of sagittal sections is completed, they are mounted on tape and exposed to films that produce the image. Initially, X-ray photography was used for this purpose, but nowadays analytical phosphorimaging has superseded this technique. Imaging plates from these systems contain phosphors (e.g. barium fluorobromide) that emit light when scanned by a laser. Areas that have been exposed to more intense radioactivity emit light more intensely. The digital image is built from detection of the light at a photomultiplier tube, which produces a voltage and so an electronic image containing real intensity information can be built up. Resolution of current instruments is around 10 μm.[214]

Dark areas in the images produced indicate high concentrations of the analyte, whilst lighter areas indicate the parts where the analyte is not found. However, it is important to understand that though radioactivity is detected, it does not necessarily correlate with the intact radiolabelled analyte, but can also be metabolites i.e. anywhere the radioactive nucleus has travelled within the body. Calibration of the dosimeter software with radioactive standards (usually spiked blood[215]) of known activity is performed usually within the same image. The sectioned standards used are usually of the same depth profile as the sagittal sections, and have been encased in the same material for consistency.

A picture can therefore be built up of the fate of the radiolabelled nuclei *in vivo*. Hence, doses for human subjects can be estimated as well as supporting results from other histological and pathological studies of distribution e.g. for toxicity studies. Thus QWBA has become a crucial tool for pharmaceutical research into drug metabolism.

QWBA has several advantages:[214]

- Ability to image drug localisation quantitatively (or qualitatively).

- Determination of an analyte in organs without wasting many animal subjects i.e. always in imaging mode. This is important for ethical considerations.

- Determination of asymmetric distributions within the same organ or tissue.

- Information of unexpected analyte localisation.

- Information regarding areas of major retention.

QWBA has been used to analyse the distribution of a wide range of drugs *in vivo* including the NSAID diclofenac[216], FTY720[217], zolendronic acid[218], and the iron chelation therapeutic deferasirox[219] (Exjade®, Novartis) and is currently widely used in the drug discovery process.[220]

Liquid scintillation counting (LSC) is often combined with QWBA in order to increase its accuracy.[214] Scintillation counting is a standard technique, which is used to estimate the amount of radioactivity in a sample. The radiation released by a radiolabelled molecule is absorbed by an organic

scintillator molecule, which then quantitatively emits a photon of light that can be detected and converted into a voltage by a photomultiplier tube, thus directly and quantitatively measuring the amount of radioactive compound is dissolved in the scintillation liquid allowing the estimation of a drug or drug metabolite within the liquid. Typical liquid organic scintillators include *p*-terphenyl ($C_{18}H_{14}$), PBD ($C_{20}H_{14}N_2O$), butyl PBD ($C_{24}H_{22}N_2O$), PPO ($C_{15}H_{11}NO$), and POPOP ($C_{24}H_{16}N_2O$) dissolved in solvents such as toluene, xylene, benzene, phenyl cyclohexane, triethylbenzene and decalin. Usually ^{14}C is used as the radiolabel in drugs. It is a beta emitter with a half-life of around 6000 years, hence radioactive shelf life is not a problem.

The scintillation process can suffer from certain drawbacks associated with photonic emission. For instance, there may be coloured molecules which can reabsorb the emitted photon in the mixture. Spectral overlap of the scintillator's fluorescence with another molecule's absorption profile is therefore a major problem, that can reduce sensitivity, precision and accuracy. Chemical quenching of the organic scintillator's fluorescent state is also a problem for obvious reasons. Liquid scintillators for analysis are usually degassed and sealed under an inert gas such as nitrogen as quenching of the scintillation signal is possible of oxygen is in the system. Similarly, if species are analysed that undergo chemiluminescence, this may interfere with the scintillation count and make results too high.

To avoid all of these problems samples can be oxidised (in this case meaning burnt in an oxygen rich atmosphere) prior to analysis, before the amount of radiation in them is assessed by scintillation counting.[214] For ^{3}H

and ^{14}C radiolabelled analytes the products of the oxidation are $^{3}H_2O$ and $^{14}CO_2$ respectively which are on the whole optically transparent in the visible region. The former can be analysed directly, whilst the latter is trapped by a solution of amines, where it has high solubility. Both can then be analysed by scintillation counting for an extremely clean and accurate analysis. Comparison of both QWBA and LSC techniques has been made before in rats using the radiolabelled antibiotic [^{14}C]-daptomycin,[221]

However, as touched on, the major disadvantage with radiolabelling studies is that one cannot discern between drug / drug metabolite / impurities. Hence, coupled with label-free mass spectrometric imaging the power, accuracy and precision of the technique could be increased significantly. whilst both QWBA and liquid scintillation counting provide accurate quantitation on the amount of radiolabelled material contained within a certain organ (in the case of LSC and QWBA) as well as the spatial distribution of the drugs within the whole animal section in imaging mode (QWBA), there is absolutely no information given on whether it is drug or drug metabolites being imaged, as both will contain radiolabel. As an example of this, it is widely known that both fenclozic acid and propanolol are metabolized by substitutive hydroxylation on their aromatic rings (M+16).[222, 223] Degradation of the drug *in vivo* is also a problem that is particularly bad for ^{3}H- or ^{125}I-labelled radiotracers where the radioactivity can be lost as $^{125}I_2$ or $^{3}H_2O$ quite easily. The drying of animal sections can also lead to loss of volatile radioactive materials thus producing low results. Costs of QWBA equipment can also be a prohibitive factor for most laboratories' budgets. The natural half-life of

radioactive nuclei impose time constraints on any analysis – sensitivity is exponentially reduced over time. [224]

Mass spectrometric techniques, such as spot to spot profiling of organs and tissues, or indeed mass spectrometric imaging, are complementary techniques to radioluminographic techniques such as QWBA and LSC. Ionisation sources such as MALDI generate monocharged mass ions, usually protonated $[M+H]^+$, and thus the determination of drugs within tissues is possible. Imaging by SIMS offers extremely high resolution. Imaging using ambient sampling techniques coupled to ambient ionisation allows the analysis of specimens without the need for extensive sample preparation. Spectra from MALDI in particular, are simple to interpret and qualitative analysis can be extremely rapid. As a definite *m/z* ratio is determined during analysis, it is possible to discern between drug and metabolites with confidence.

4.0.1 Hypothesis

The fate of drug molecules is of primary concern within pharmacokinetic studies in vivo. The use of standard MALDI TOF MS has often been overlooked in imaging experiments in favour of more complicated MS/MS imaging experiments that require careful sectioning of subjects followed by a number of sample preparation steps to produce whole animal sections. Here we test the hypothesis that through dosing of animal subjects followed by careful excision and homogenization of organs that we may produce a simple screening protocol based on mass spectral interrogation of homogenates that

can test rapidly whether a drug is present within a tissue or organ. We also test whether such an approach is consistent with results from industry-standard radioluminographic techniques.

4.0.2 Aim and Objectives

The overall aim of this chapter is to establish in principle the use of MALDI TOF MS as a rapid screening methodology to aid in drug pharmacokinetic experiments by testing the above hypothesis. In order to achieve this we will fulfil the following objectives: a comparison of the whole-body distribution of the two drugs (propanolol and fenclozic acid) will be made using quantitative whole-body autoradiography (QWBA) and post-oxidisation liquid scintillation counting of excised organs in rats. We then couple these results to MALDI-TOF MS of homogenised organs to qualitatively determine the presence of either fenclozic acid or propanolol. The data produced from profiling experiments will be used to produce mass spectral gels to analyse excised organs rapidly for the presence of drug.

4.1. Experimental

General

[^{14}C]-Fenclozic acid (Astra Zeneca) was administered in isotonic phosphate buffered saline (pH 7.4), which was prepared by dissolving 1 buffer tablet (Sigma Aldrich, Cat. No. P4417) into 200 mL deionised water. [^{14}C]-Propanolol (Astra Zeneca) was administered in 0.9% w/w physiological saline solution prepared by Astra Zeneca laboratory services' scientific preparation team. The stock solution of [^{14}C]-Propanolol was made up at 12.38 mg mL^{-1}, whilst [^{14}C]-fenclozic acid was made up at 11.17 mg mL^{-1}.

Animal Subjects: Justification and Ethics Statement

The animals used in this study were male albino Sprague-Dawley rats aged 2 – 3 months. The justification for using live subjects is that the study cannot compare the use of QWBA/LSC with MALDI as a profiling tool for use in pharmacokinetics without resort to in vivo study. All institutional and national guidelines for the care and use of laboratory animals were followed in this study, which was designed to use minimum animal subjects as possible in-line with the World Medical Association 1989 Helsinki Statement on Animal Use in Biomedical Research, and experiments were not duplicated for these reasons. All animals were euthanised humanely immediately after study.

Preparation of dosed animals for QWBA / LSC

6 male albino rats were orally dosed with [^{14}C]-propranolol or [^{14}C]-fenclozic acid at ca. 25 mg kg^{-1} (see Table 1 for exact values). Three of the animals dosed with either drug were sacrificed by inhalation of fluothane at 2, 6 and 24 hours post dose and snap frozen in a heptane / dry ice to prevent further diffusion of radioactivity.

Carcasses were then embedded in frozen carboxymethylcellulose block (CMC) to ensure specimen structural integrity during the subsequent cryotome steps: a metal mould is placed in a bowl containing hexane / dry ice and allowed to chill, and chilled wallpaper paste (carboxymethylcellulose, 2% aq. v/v) was poured into the mould. The rat carcass, with tail and hind legs removed, was placed partially in the CMC, with either its left or right side uppermost in the mould and held in position until frozen. The mould was then filled with more 2% CMC (aq.) until the whole carcass was covered, with intermittent stroking of fur with a spatula to remove trapped air. When the block is fully frozen, the CMC block was removed from the mould and stored at – 20 °C to be sectioned.

The remaining three animals dosed were sacrificed by inhalation of fluothane at 2, 6 and 24 hours post dose and the following tissues surgically excised: blood, brain, liver, kidney and lungs for liquid scintillation counting. The remainder of the carcass was disposed of.

Sectioning and mounting of encased animals for QWBA

Animals carcasses encased in CMC blocks were sectioned in the sagittal plane using a Leica microcryotome at 30 μm. After sections had dried in the microtome, selected dried sections were mounted on paper cut to 20 × 40 cm. Six sections were chosen as representative of all tissues of interest – blood, brain, kidney, liver and lungs – and were affixed to the paper using magic tape, along with the spiked blood spots for calibration. Sections were labelled using radioactive ink, and finally dusted with talcum powder to prevent sticking to the phosphor imaging plates.

Preparation of radioactive blood standards for QWBA

For the accurate determination of radioactivity content of tissues calibration standards were made up of rodent blood spiked with a known amount of [^{14}C]-glucose.

Typically, 9 μL of [^{14}C]-glucose solution (SSN3356) was weighed into a vial, and to it was added 4 mL of rodent blood. This was followed by a 50% dilution of the first standard with rodent blood to produce the second standard, followed by another 50% dilution to produce the third standard etc.; this dilution series was used until a total of 10 standards had been made. These were used to produce calibration curves for each sacrificed animal undergoing QWBA analysis and provide reference for the phosphor images, where different standards produce different shades of grey on the images, with black

being the most intense signal level. A block to contain blood standards was prepared by drilling 6 mm diameter x 1.3 cm deep holes into CMC blocks.

Calibration curves were produced using AIDA software (Raytest Inc., v4.15). Each calibration curve had an r^2 value of >0.999. AIDA was also used to estimate, using the region determination toolset, the amounts of drugs in organs based on the intensity of the calibration standards. According to Raytest Inc.: the AIDA Image Analyzer software is intended for the evaluation and annotation of images that were obtained by digital optical devices such as CCD cameras, flatbed scanners, fluorescence scanners like FLA scanners, or radioluminography scanners like BAS scanners from Fuji. In addition, the software allows the user to load and evaluate images of other types (e.g. TIF, bitmap). AIDA Image Analyzer can utilize any scanning device that offers a TWAIN compatible driver. The drivers for raytest products are included in the software package. AIDA can use calibration standards to convert the relative intensity integrals to absolute measurements (e.g. μg, nmol). The calibration curve can be reviewed and adapted to fit various functions.

Quantitative Whole Body Autoradiography (QWBA) analysis.

Phosphor imaging plates were erased using a light eraser box (Raytek, U.K.) for approximately 10 mins prior to use. Sagittal sections of sacrificed animals at 2, 6 and 24 h were then exposed to the imaging plate under dark room conditions, stored in the cassette and placed in a shielded safe for 7 days.

After exposure, the imaging plates were placed on an imaging stage which was inserted into a Fuji FLA 5100 QWBA phosphor imaging instrument. The plate was allowed to equilibrate for around 10 mins prior to scanning. The whole plate was then scanned at a resolution of 50 μm.

Selected tissues and organs of interest were defined in the images produced using the region determination tools within the AIDA suite. Using the radioactive content of the blood standards (dpm g^{-1}) and the specific activities of both the [^{14}C]-propanolol and [^{14}C]-fenclozic acid, the concentration of radioactivity in the blood standards was entered into the AIDA software in nmol g^{-1}. Wherever possible, two samples of a tissue were evaluated using AIDA. The limit of reliable measurement was calculated by taking twice the background value in nmol g^{-1}. Data below this limit was not reported.

Oxidation of excised organs, extraction and liquid scintillation counting (LSC)

For each mouse, excised organs were homogenised with a Potter homogeniser to a homogeneous pulp with ca. 1:1 w/w water. Organ homogenates were then extracted with acetonitrile (1:1 v/v). Samples were vortexed then centrifuged at 3000 r.p.m. for 10 min. Supernatants were poured off and kept and the vortex-extraction with acetonitrile was repeated on the pellet. Aliquots of the combined organic extracts were taken and the radioactive content determined by liquid scintillation counting using Ultima Gold™ scintillation cocktail. Remaining residue was weighted onto a combustion cone and and dried. Samples were then oxidised (combusted)

and the radioactive [^{14}C]-carbon dioxide collected using an amine scrubber prior to liquid scintillation counting in Ultima Gold™ scintillation cocktail.

Combination of the solvent extract and combustion analysis gave the final radioactivity amount in the excised organ, and by back-calculation it was possible to quote the amount of drug per unit weight of organ.

Preparation of dosed male albino rats for MALDI – propanolol / fenclozic acid

A male rat of weight 277 g was orally dosed with [^{14}C]-propanolol (556 μL at a concentration of 12.38 mg mL^{-1} in 0.9% w/w physiological saline solution) to give a drug dose of exactly 24.83 mg kg^{-1}. After 6 hours, the animal was sacrificed by inhalation of fluothane, exsanguinated (with blood sample retained) and the following tissues surgically excised: brain, liver, kidney and lungs. A second male rat of weight 257 g was also orally dosed with [^{14}C]-propanolol (514 μL at a concentration of 12.38 mg mL^{-1} in 0.9% w/w physiological saline solution) to give a drug dose of exactly 24.77 mg kg^{-1}. After 2 hours, the animal was sacrificed by inhalation of fluothane, exsanguinated and the liver surgically excised.

A third male rat of weight 255 g was similarly orally dosed with [^{14}C]-fenclozic acid (515 μL at a concentration of 11.17 mg mL^{-1} in isotonic phosphate buffered saline at pH 7.4) to give a drug dose of exactly 22.54 mg kg^{-1}. After 6 hours, the animal was sacrificed by inhalation of fluothane, exsanguinated (with blood sample retained) and the brain, liver, kidney and lungs removed surgically. A fourth male rat of weight 256 g was also orally dosed with [^{14}C]-

fenclozic acid (513 μL at a concentration of 11.17 mg mL^{-1} in isotonic phosphate buffered saline at pH 7.4) to give a drug dose of exactly 22.63 mg kg^{-1}. After 2 hours, the animal was sacrificed by inhalation of fluothane, exsanguinated and the liver surgically excised. The remainder of each carcass was disposed of.

Production of excised organ homogenates for MALDI analysis

Surgically excised organs were weighed and water added to them to a ratio of 1:1 w/w. The organs were then homogenised with a Potter homogeniser until a smooth thin mousse by inspection.

Preparation of homogenates for MALDI Analysis.

Homogenates from each excised organ for rats sacrificed at various timepoints in the study were taken and 0.25 μL of each homogenate spotted onto a stainless steel 384-spot MALDI anchorchip (Bruker Daltonics, Bremen, Germany). The homogenate spot was allowed to dry, and on top of it was spotted directly 0.25 μL of CHCA matrix solution (25 mg mL^{-1} in acetonitrile containing 0.1% TFA).

A rat liver control homogenate (1:1 w/w water) with no drugs doped into it was supplied by AstraZeneca. 0.25 μL of this homogenate was taken and pipetted onto the anchorchip followed by drying. 0.25 μL of CHCA matrix solution (25 mg mL^{-1} in acetonitrile containing 0.1% TFA) was spotted directly on top of the control homogenate prior to analysis.

Preparation of Drug and matrix Standards for MALDI Analysis.

0.25 μL of a solution of propanolol (2.2 x 10^{-5} mol dm^{-3}) in methanol was pipetted onto a stainless steel 384-spot MALDI anchorchip and the solution allowed to dry. 0.25 μL of solution of fenclozic acid (2.2 x 10^{-5} mol dm^{-3}) in methanol was pipetted onto the same MALDI anchorchip at a separate position and the solution allowed to dry. 0.25 μL of CHCA matrix solution (25 mg mL^{-1} in acetonitrile containing 0.1% TFA) was pipetted directly on top of both drug spots and also allowed to dry.

Summary of Samples for MALDI analysis

Table 4.1 gives a full list of samples produced and analysed.

Table 4.1: Homogenate samples studied in MALDI profiling experiments.

Compound	Time Point (h)	Organ
[^{14}C]-propanolol	2	Liver
	6	Liver
	6	Kidney
	6	Brain
	6	Blood
	6	Lung
Propanolol (drug alone, control)	*N/A*	*N/A*
[^{14}C]-fenclozic acid	2	Liver
	6	Liver
	6	Kidney
	6	Brain
	6	Blood
	6	Lung
Fenclozic acid (drug alone, control)	*N/A*	*N/A*
Blank homogenate (control)	*N/A*	*Liver*

MALDI analysis

MALDI MS spectra of homogenates were obtained using a Bruker Ultraflextreme MALDI-TOF/TOF Instrument (Bruker Daltonics, Bremen,

Germany) with a kHz Smartbeam II laser.[225] Positive ion spectra were collected in reflectron mode. Calibration of the instrument was performed using Peptide Calibration Standard II (Bruker Daltonics, Bremen, Germany). The method used the low mass range of the instrument, with a laser frequency of 1000 Hz. 10 000 laser shots were summed to produce each spectrum.

4.2. Results and Discussion

Testing of drug detection in MALDI

MALDI MS was used to investigate all samples. Firstly, drugs alone were analysed. Fenclozic acid was spotted directly onto stainless steel MALDI plates along with CHCA matrix. The full MALDI MS spectrum is shown in Figure 4.1. The spectrum is dominated by the peak for protonated fenclozic acid, $[M+H]^+$ observed at *m/z* 253.984. In the same figure is presented the full mass spectrum of propanolol on stainless steel. In the same way, the major peak in the spectrum is that of protonated $[M+H]^+$ species, observed at *m/z* 260.160. In both spectra, minor peaks are observed which correspond to the CHCA matrix, at *m/z* 379 ($[2CHCA+H]^+$), 228 ($[CHCA+K]^+$), 212 ($[CHCA+Na]^+$). The $[CHCA+H]^+$ ion is absent from both spectra (*m/z* 190).

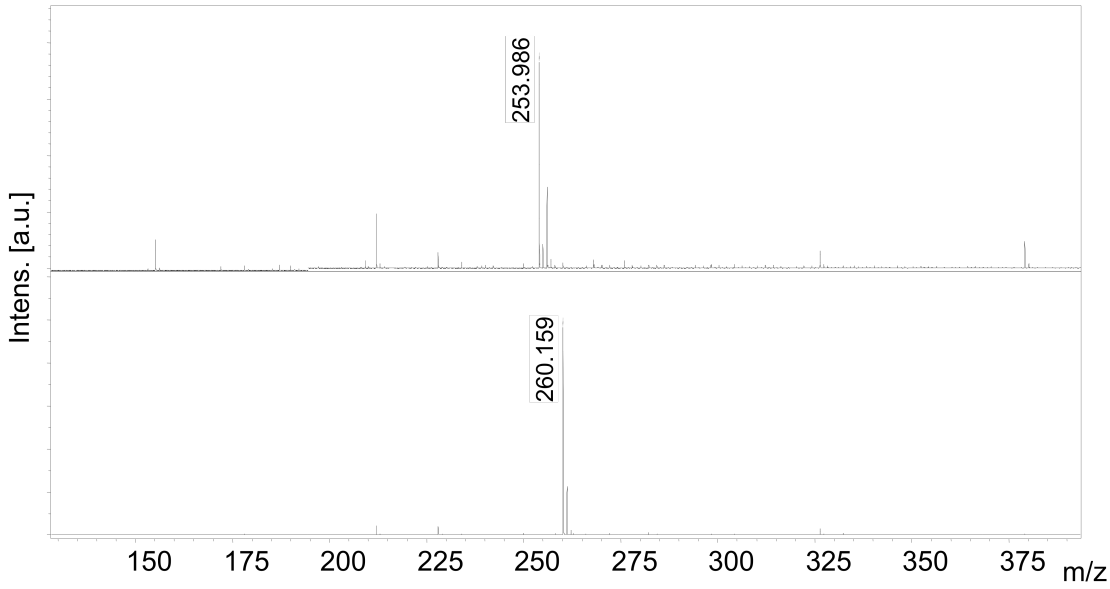

Figure 4.1. MALDI MS spectra of fenclozic acid (upper) and propanolol (lower) (5.5 x 10^{-12} mol) on stainless steel. Matrix: CHCA (25 mg mL^{-1} ACN, 0.1% TFA). Deposition: dried droplet.

Enlargement of the region between *m/z* 250 and *m/z* 264 shows detailed isotope patterns for both drugs. Incorporation of chlorine in the fenclozic acid structure gives it a characteristic 10 : 1 : 3 : 1 isotope pattern (Figure 4.2). Calculation of a theoretical isotope pattern for fenclozic acid agrees well with that observed experimentally.

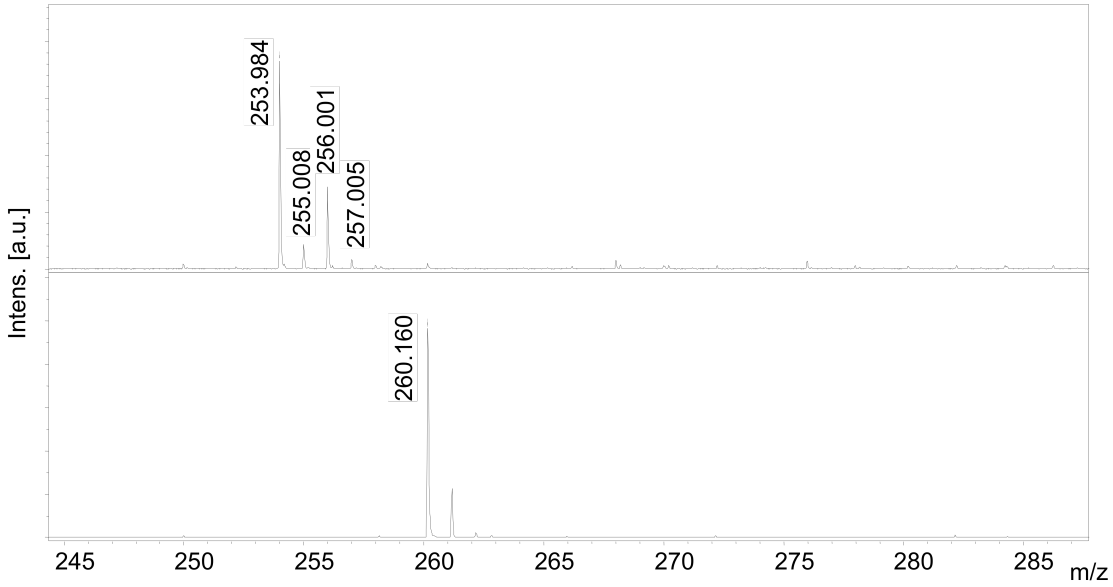

Figure 4.2. Enlargement of MALDI spectra in region *m/z* 250 – 264 for fenclozic acid (upper) and propanolol (middle) respectively on stainless steel.

Dosing of animals for QWBA, LSC and MALDI analysis

Male albino rats were dosed via oral administration in duplicate with either [^{14}C]-propanolol or [^{14}C]-fenclozic acid for time points at 2h, 6h, and 24 h post dose giving 12 animals dosed in total i.e. two sets for each drug at each time point. The animals were dosed at a level of ca. 25 μg g^{-1} of both drugs. Solutions of radiolabelled drugs were made up as stocks at (12.5 mg mL^{-1}) to give a dose volume of ca. 2 mL kg^{-1}. The actual doses received for each animal are shown in Table 4.2. Variations in dose were introduced from variation in syringe to syringe, revealed by accurate weighing of each individual syringe before and after administration. For MALDI analysis, the same dosing was used with unlabelled drugs.

Table 4.2: Details of drug dosing used in the study.

Compound	Time Point (h)	Animal weight (g)	Injection vol. (mL)	Dose (μg g^{-1})
[^{14}C]-propanolol	2	234	0.5470	28.94
	6	273	0.5484	24.87
	24	253	0.5037	24.65
	2	257	0.5142	24.77
	6	277	0.5555	24.83
	24	260	0.5208	24.80
				(mean = 25.50)
[^{14}C]-fenclozic acid	2	257	0.5187	22.53
	6	264	0.5398	22.83
	24	254	0.5085	22.35
	2	256	0.5129	22.63
	6	255	0.5148	22.54
	24	260	0.5317	22.83
				(mean = 22.62)

Preparation of sagitally sectioned rodent subjects for QWBA.

Rats were euthanised 2h, 6h, and 24h post dose using fluothane. This method of euthanasia was chosen over CO_2 inhalation as the latter can cause acidosis in subjects and affect drug distribution *in vivo* and is bad especially for causing disruption to the blood brain barrier, making it more permeable and giving false-positive results. The animals were taken and immediately frozen in a heptane dry ice, encased in carboxymethyl cellulose (CMC). Snap freezing is used to prevent the diffusion of radioactive material throughout the subject post-mortem. Encasement in CMC is required to keep the carcass intact during sectioning and to therefore maintain the integrity of the organs as best possible. Sections were cut to around 30 μm using a cryomicrotome. A visual workflow is presented in Figure 4.3.

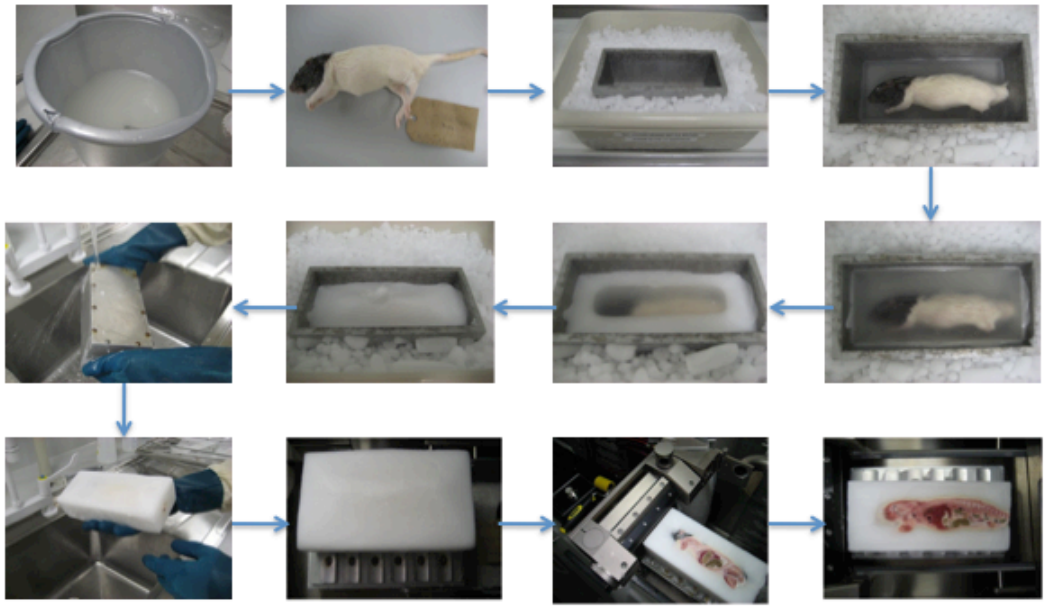

Figure 4.3: Pictorial workflow showing the preparation of rat sagittal sections for quantitative whole body autoradiography (QWBA). The rat is flash frozen, encased in CMC, and sectioned at a thickness of 30 microns in the sagittal plane at midline and +1 cm midline.

Sectioning of animals was entirely successful using this protocol. A digital photograph montage of various sections showing the rat anatomy at various lateral depths (midline, midline + 0.5 cm and midline + 1 cm) is shown in Figure 4.4. Qualitative conclusions on drug distribution from autoradiographic images within the sacrificed rats were made using these images as a guide.

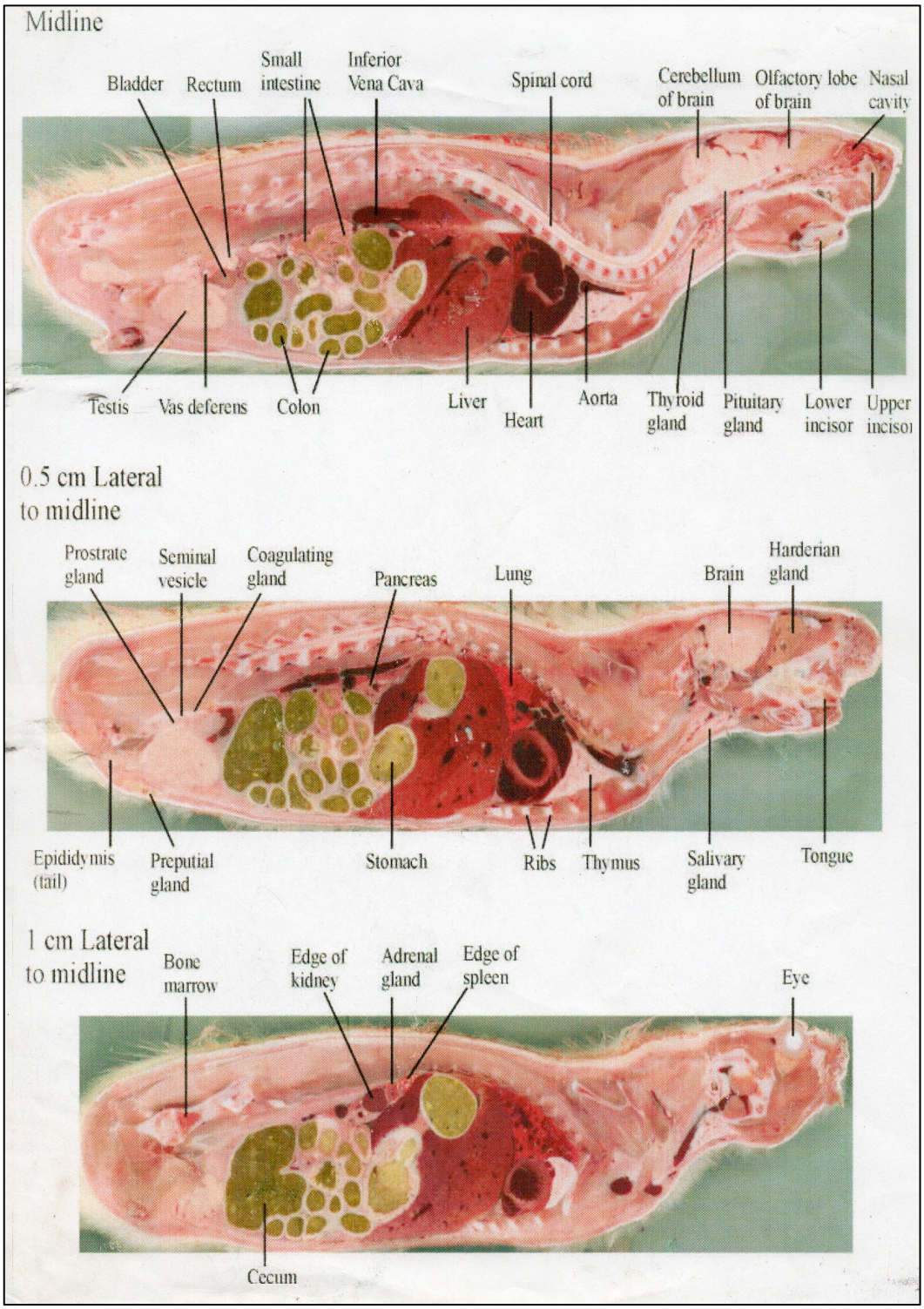

Figure 4.4: Annotated digital photographs of rat anatomy in the sagittal plane (source: AstraZeneca).

QWBA Imaging, LSC and MALDI analysis of [^{14}C] -propanolol dosed rodent subjects.

.

QWBA was used to image and quantify the distribution of the drugs *in vivo* post-mortem for each of the time-points studied. Figure 4.5 shows the grayscale WBA phosphor imaging result summary from the time-course with propanolol. Dark regions represent areas where concentrations of the drug are high. Lighter regions represent areas where the drug is not found. Blood standards with [^{14}C]-glucose of known concentration with specific activity measured in disintegrations per minute (dpm) were made up and are shown in the centre of the image. Representative sagittal sections were chosen for rats sacrificed at 2 h, 4 h and 24 h at two separate lateral depths. The image at 2 hours shows that the majority of the radiolabelled drug or drug metabolites are localized within the stomach and small intestine (black), with an intermediate amount found in the liver (grey), heart (grey) and kidneys (grey) and a smaller amount in the lung (light grey). The location of the radiolabelled material is coherent with the oral route of dosing, i.e. it is mostly found in this early stage in the upper digestive tract. Images taken from animals sacrificed at 6 h show radiolabel is found mostly in the large intestine (black), with smaller amounts found in the liver (grey), heart (grey) and kidney (grey) and smaller amounts in the lung (light grey). Most of the radiolabelled material it seems therefore moved during this time to the lower digestive tract, whilst only a fraction of the dose taken up into organs, suggesting that the bioavailability of propanolol is fairly low and the major route of excretion is through the faeces. Indeed, images taken from animals sacrificed at 24 h

show radiolabelled material has been almost removed from the lower digestive tract which now appears grey rather than black, with drug still in the liver (grey) and kidney (grey) and hardly any left in the lung. The kidney in particular, is extremely interesting, showing almost a radial clearance from the outer-inwards of the radiolabelled drug and metabolites over the time course studied.

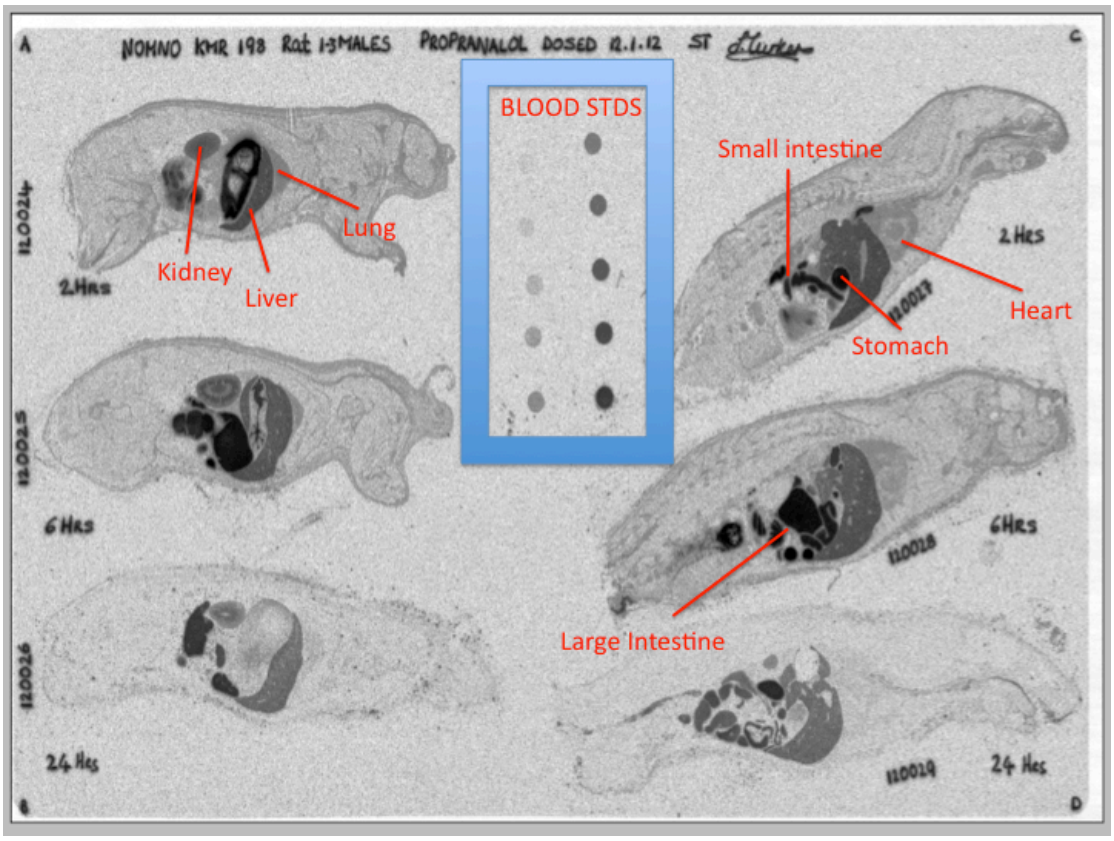

Figure 4.5: QWBA imaging of rats dosed with 25 mg kg^{-1} [^{14}C]-propanolol, sacrificed at 2 (top), 6 (middle) and 24 hours (bottom) post-dose. Samples in duplicate at different lateral section depths (right hand side: midline, left hand side: midline + 1 cm) . Spots inside box at the centre of the image are samples of rodent blood spiked with known amounts of [^{14}C]-glucose. Organs of interest are annotated in red.

AIDA software was used to quantitatively assess the amount of propanolol within selected organs of the sectioned rats. Using the specific activity in dpm

of the [^{14}C]-glucose used to make up the standards, the concentration of the propanolol could be quoted in μg g^{-1} within each organ by using a calibration curve constructed from the blood standards. Figure 4.6 summarizes the data produced for [^{14}C]-propanolol. In every organ studied it was observed that there is a decline in the amount of the drug or metabolites over time. Drug or drug metabolites were mainly found within either the liver or kidney predominantly at any time during the study. There was minimal accumulation of the drug at any point within the blood stream. Some propanolol or its metabolites are found within the lung. There was little propanolol found within the brain of the rats at any time suggesting that this drug is inefficient at crossing the blood brain barrier (BBB). The location of the drug mostly in the liver and kidneys suggests that the drug or metabolites absorbed into the bloodstream is excreted via the liver then the kidneys after travelling directly from the stomach to the liver. The latter observation agrees well with the qualitative conclusions made from the images.

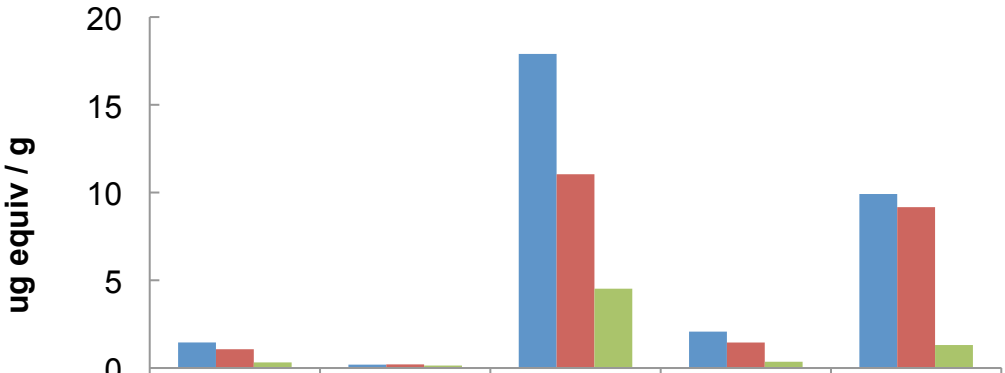

	Blood	Brain	Liver	Lung	Kidney
2 h	1.5	0.2	17.9	2.1	9.9
6 h	1.1	0.2	11.0	1.5	9.2
24 h	0.3	0.1	4.5	0.4	1.3

Figure 4.6: Quantification of [^{14}C]-propanolol in organs by QWBA phosphor imaging. Table below show actual amounts of radiolabel in μg g $^{-1}$ found in each organ for each time point.

To confirm the QWBA results were valid, liquid scintillation counting was used to analyse excised organs. As explained in the introduction to this chapter, this technique relies on the stimulated quantitative emission of photons by radiation in a commercially acquired *scintillation cocktail*. The doses for the second set of rats was almost identical to the first set of rats used for each drug, i.e. 25.47 mg kg^{-1} average for propanolol (n = 6) and 22.62 mg kg^{-1} average for fenclozic acid (n = 6), again the exact doses for the second set of rats can be viewed in Table 4.2. Again, these rats had been sacrificed at identical timepoints to that of the QWBA study, i.e. 2 h, 6 h and 24 h post-dose, to give as close time as possible to the QWBA results for comparative purposes as it is clear from the QWBA results that the distribution of the radiolabelled material in both drugs changed over time.

Organs were excised from the second set of rats produced in this study, weighed and homogenised and finally combusted in an atmosphere of pure oxygen, leading to the production of radioactive carbon dioxide which was captured for scintillation counting. Prior to this the homogenised organs were extracted with acetonitrile and the solution evaporated and added to scintillation cocktail for counting. The combined total dpm counts of the liquid scintillation counting from combusted organs / extraction gave back-calculated amounts of [^{14}C]-propanolol (or [^{14}C]-fenclozic acid, see later section) within

the organs at the time of euthanasia could then be compared to the results produced by QWBA.

The results of the distribution of [^{14}C]-propanolol showed in general a very similar profile to the results produced by QWBA (Figure 4.7). The major site of accumulation is in the liver of the organs studied, with amounts reducing in almost a linear manner over time, matched in relative terms by the profile in the kidneys, again suggesting that the drug is mostly metabolized in the liver and excreted through the kidneys. There is again evidence that some of the drug passes through the lung as for the QWBA study. However, using LSC the drug was not detected in the blood in any significant amount as for the QWBA analysis, which shows that many complementary techniques are often required to build up an accurate picture of the distribution of a drug *in vivo.* We compare both techniques using Bland-Altman analysis later on in this chapter.

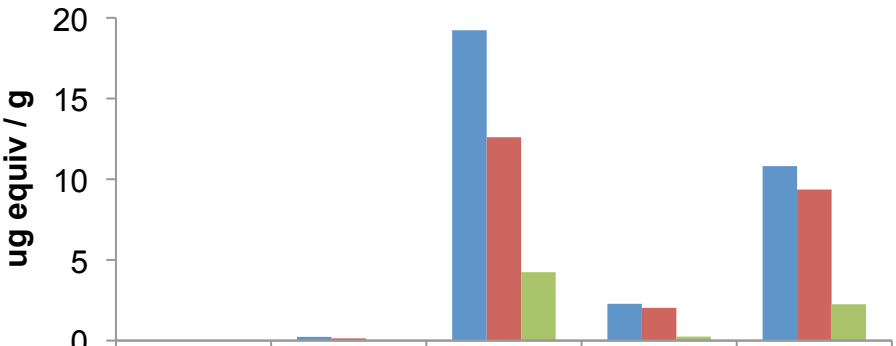

	Blood	Brain	Liver	Lung	Kidney
2 h	0.02	0.23	19.23	2.28	10.81
6 h	0.01	0.14	12.6	2.03	9.36
24 h	0	0.03	4.24	0.25	2.25

Figure 4.7: Quantification of [^{14}C]-propanolol in rat organs by liquid scintillation counting. Table below show actual amounts of radiolabel in μg g $^{-1}$ found in each organ for each time point.

It was possible to detect evidence of propanolol in brain homogenates using MALDI MS. An enlargement of the spectra (Figure 4.8) shows the $[M+H]^+$ peak, which appears at *m/z* 260.19, which we assign to protonated propanolol. The accurate mass matches well with the theoretical for propanolol (260.17). The high intensity peaks at *m/z* 250, 251 and 252 are common to all CHCA coated homogenates, whether they contained drugs or not. It was not possible to assign these peaks with any confidence, however we may potentially conclude that they are not CHCA cluster peaks, as we do not observe any of the masses ascribed to these comprehensively by Smirnov et al.[226] but as they are observed universally we must either conclude that they are matrix fragments or a biologically ubiquitous molecule, ion or ion fragment.

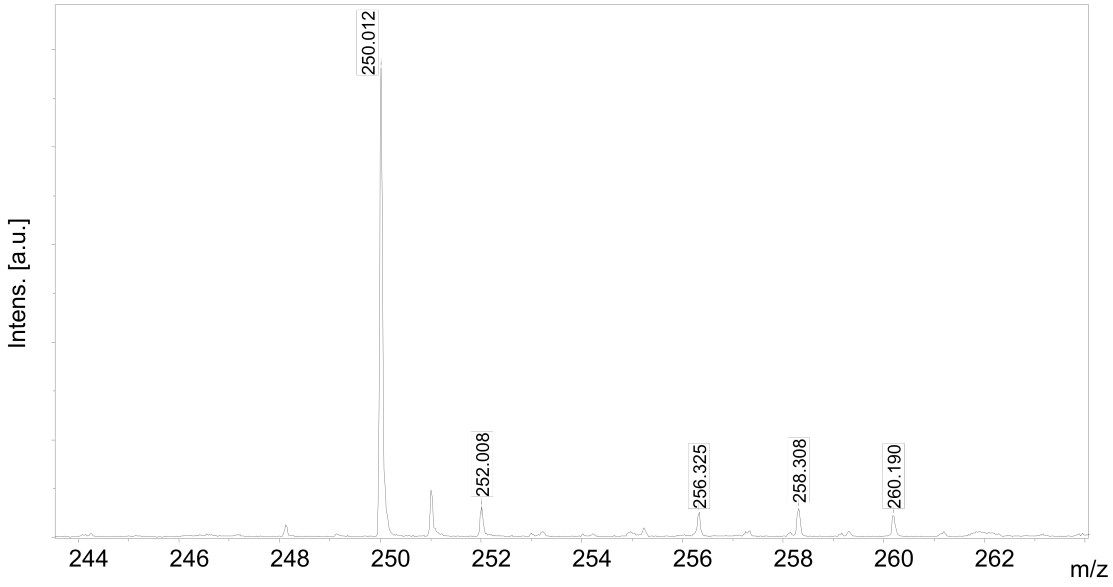

Figure 4.8: Enlargement of MALDI MS spectra of brain homogenate of rats orally

dosed with [^{14}C]-propanolol and sacrificed at 6 h.

Homogenates of lung tissue from rats sacrificed after 6 h post dose with propanolol gave MALDI MS spectra where the $[M+H]^+$ peak for the drug was detected. The peak for propanolol in a lung homogenate is show in Figure 4.9, appearing at *m/z* 260.191. The full spectra is again dominated by CHCA / choline (2-hydroxyethyl trimethylammonium) peaks, the latter which is a fragment from phosphatidyl choline which is a ubiquitous component of cell membranes phospholipid double layer; the choline fragment has a strong signal as it is a positively charged quaternary ammonium ion.

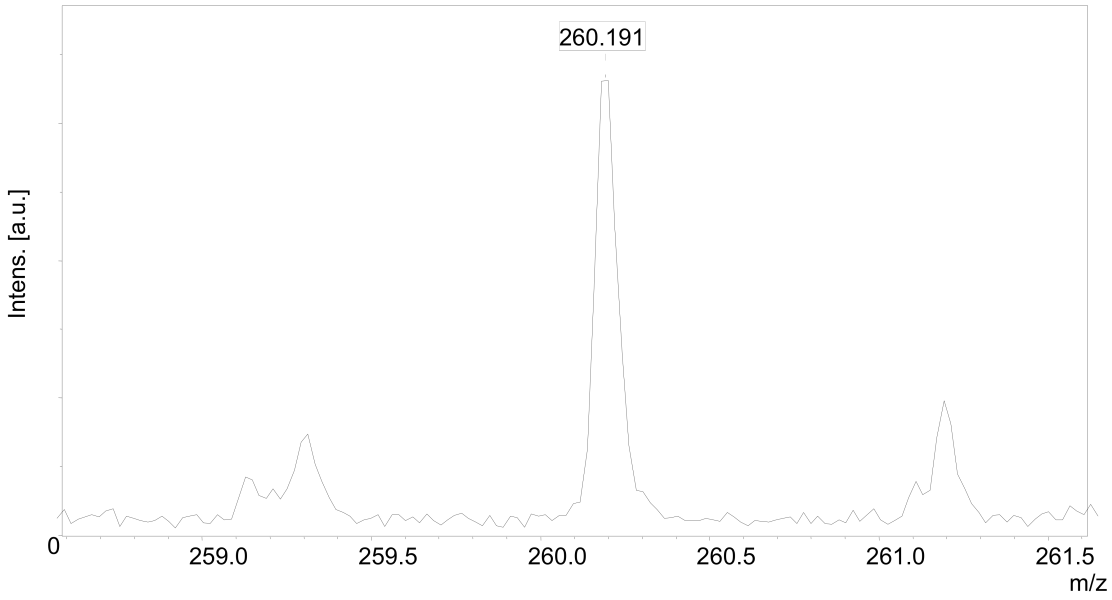

Figure 4.9: Enlargement of MALDI MS spectra of lung homogenates of rats orally dosed with [^{14}C]-propanolol and sacrificed at 6 h. Matrix: CHCA (25 mg mL^{-1} ACN, 0.1% TFA). Deposition: dried droplet

MALDI MS profiling of kidney homogenates was also successful at detecting the presence of propanolol in animals sacrificed after 6 hours (Figure 4.10).

Again, the wider spectra of both homogenates were dominated by peaks attributable to both CHCA and choline as before. Fenclozic acid could not be detected in kidney tissues.

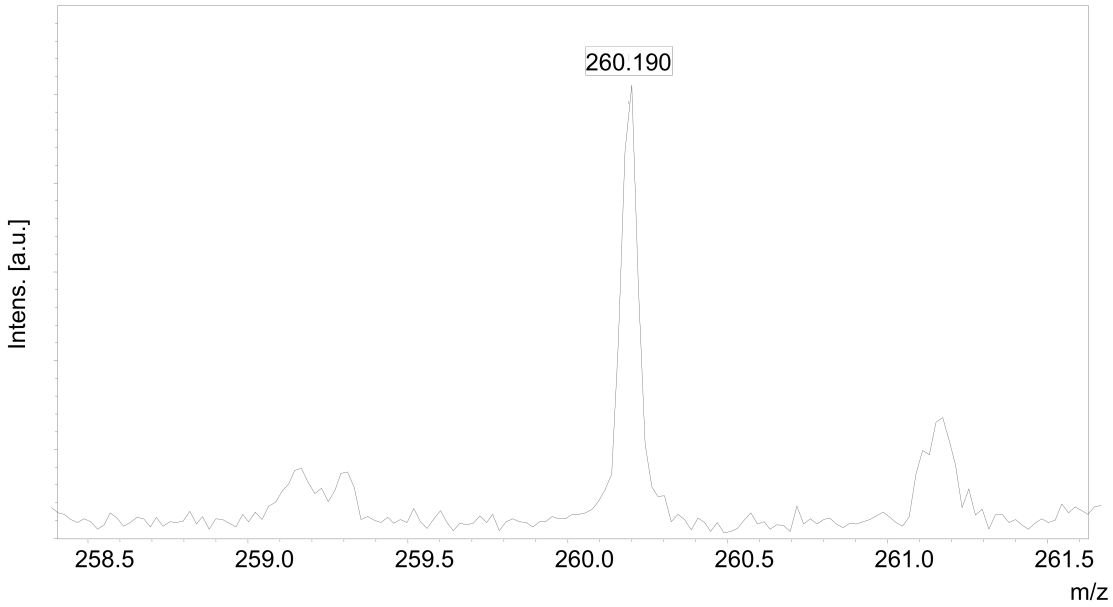

Figure 4.10: Enlargement of MALDI MS spectra of kidney homogenates of rats orally dosed with [^{14}C]-propanolol and sacrificed at 6 h. Matrix: CHCA (25 mg mL^{-1} ACN, 0.1% TFA). Deposition: dried droplet.

MALDI profiling of liver homogenates from animals sacrificed 6 h post oral dose with propanolol also showed evidence of the presence of the drug. For homogenates from excised organs originating from propanolol dosed animals the peak at *m/z* 260 was detected, corresponding to the protonated drug, $[M+H]^+$ (Figure 4.11).

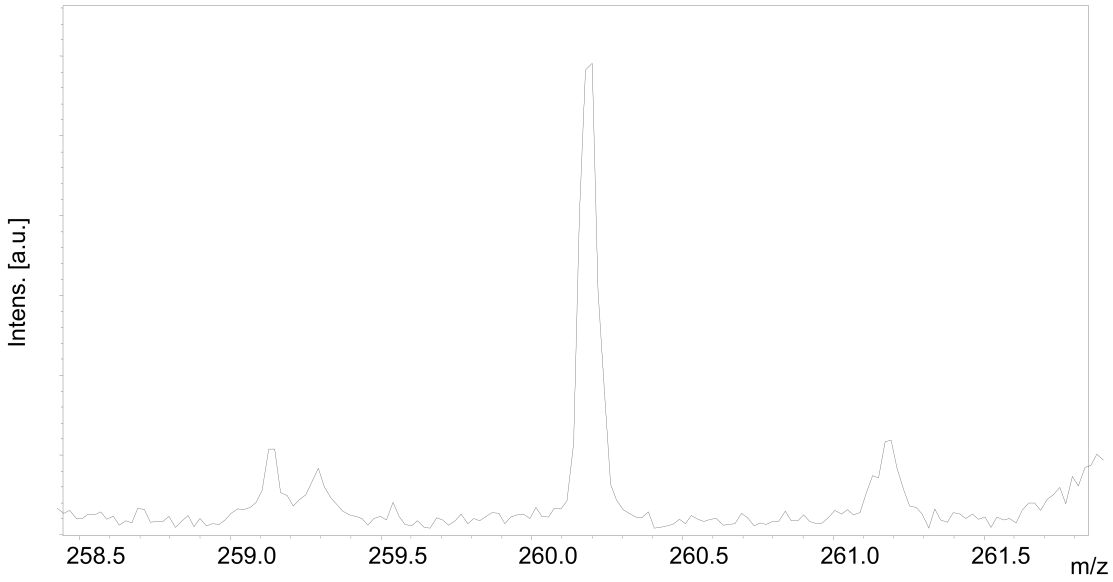

Figure 4.11:. Enlargement of MALDI MS spectra of liver homogenates of rats orally dosed with fenclozic acid (upper, *n* = *4*) and propanolol (lower) and sacrificed at 6 h. Matrix: CHCA (25 mg mL^{-1} ACN, 0.1% TFA). Deposition: dried droplet.

Analysis of blood extracts from animals dosed with propanolol (Figure 4.12) showed strong evidence of the drug, the $[M+H]^+$ peak at *m/z* 260.2 is particularly strong in these samples relative to the other homogenates.

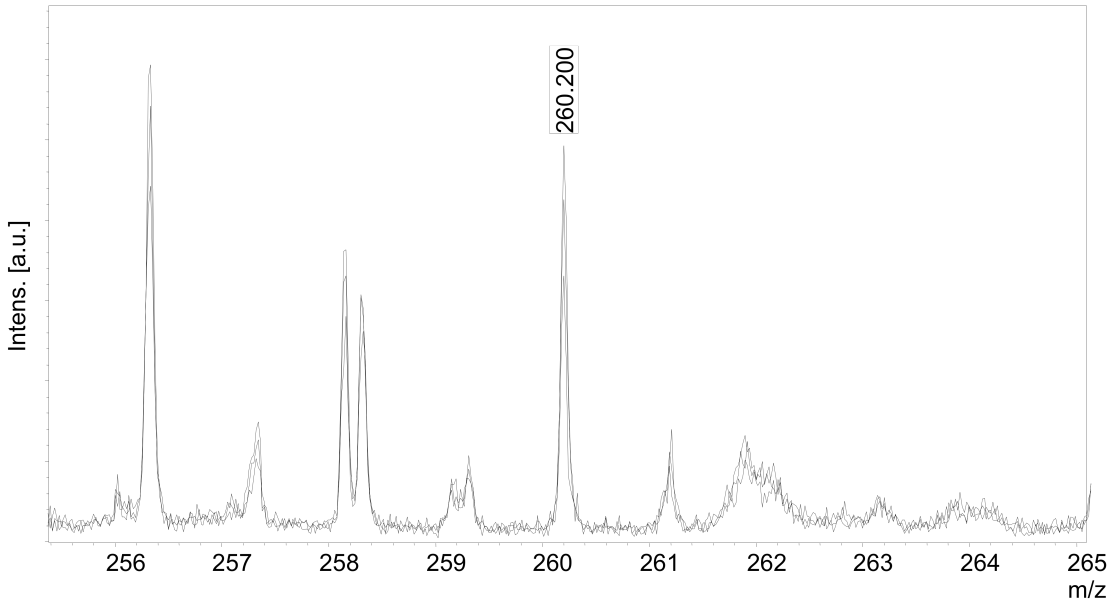

Figure 4.12: Enlargement of MALDI MS spectra of blood extracts of rats orally

dosed with [^{14}C]-propanolol and sacrificed at 6 h (*n* = *4*). Matrix: CHCA (25 mg mL^{-1} ACN, 0.1% TFA). Deposition: dried droplet.

By tiling of the various MALDI MS spectra alongside each other in the regions of interest, a mass spectral gel view for pattern matching analysis could be built up for each organ extract sample (*n* = 5, Figure 4.13). [227] The grayscale in the image has ion intensity information; the more 'black' the bar appears, the more intense the signal for an ion at any *m/z*. The results show that it is possible to detect the $[M+H]^+$ peak for propanolol in every sample apart from a blank homogenate (negative control comprised of a homogenate of liver tissue). Signal intensity from the liver and lung samples are arguably relatively the strongest, but the intensity is generally similar across the board. This perhaps suggests that ionisation of propanolol is generally efficient from all the samples studied, and the low amounts of propanolol found in brain, kidney and blood by QWBA and LSC in the previous are within the limit of detection by MALDI MS profiling using this set of experimental conditions. Peaks assigned to either matrix artefacts or species ionised from the homogenates are observed at *m/z* 259.2, 259.4 and 261.2 in the close vicinity to the drug peaks, ascertained by process of elimination using the control.

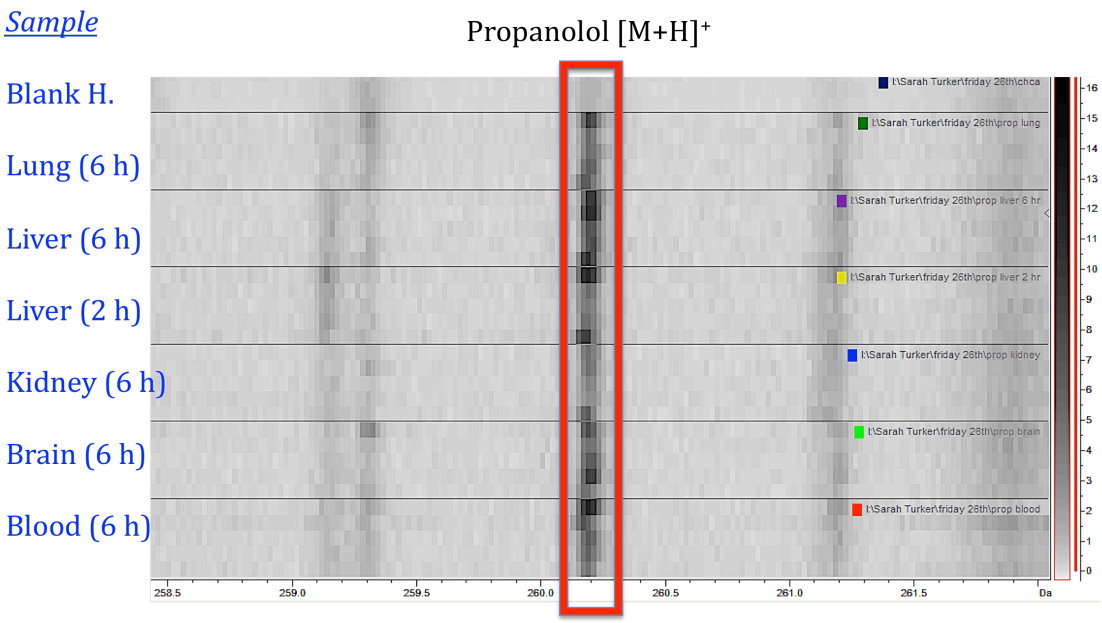

Figure 4.13: Mass spectral gel view data for homogenates produced from [^{14}C]-propanolol dosed rats (*n* = 5), alongside a blank homogenate (*n* = 2). Relative grayscale intensity shown on the right.

QWBA Imaging, LSC and MALDI analysis of [^{14}C] -fenclozic acid dosed rodent subjects.

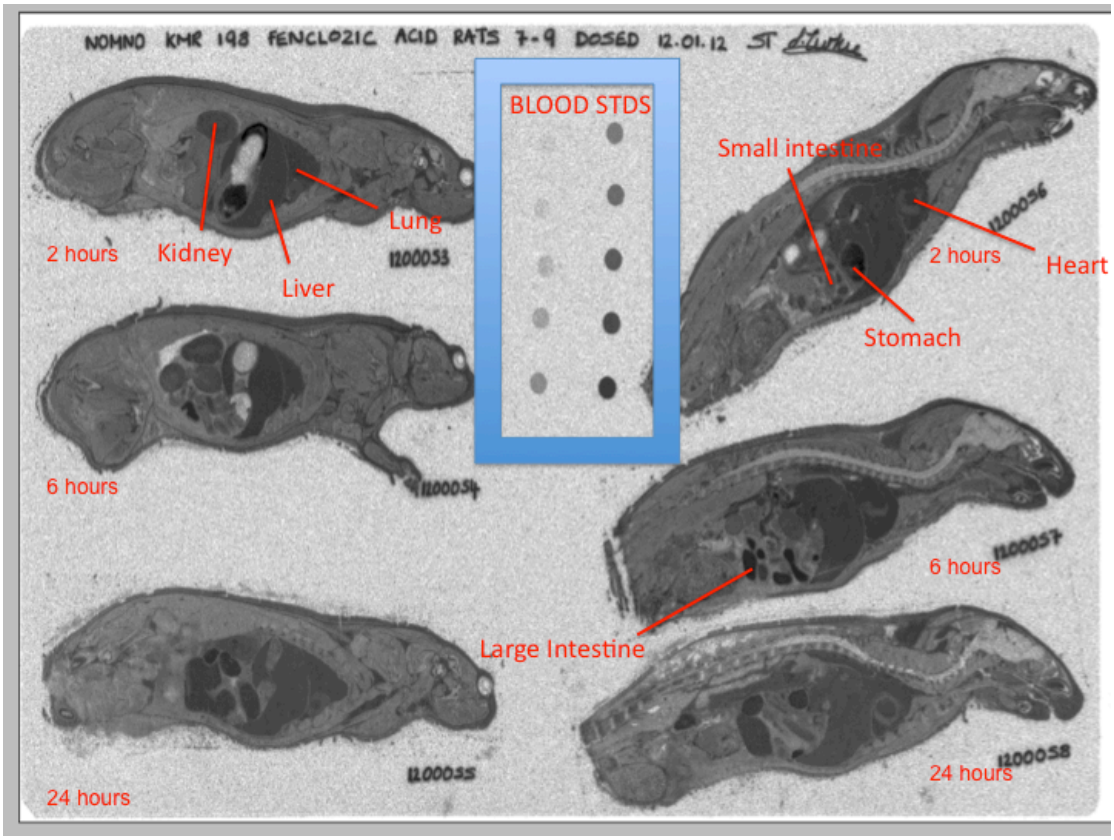

Figure 4.14: QWBA imaging of rats dosed with 25 mg/kg fenclozic acid, sacrificed at 2 (top), 6 (middle) and 24 hours (bottom) post-dose. Samples in duplicate at different lateral depths (right hand side: midline, left hand side: midline + 1 cm). Spots in the box at the centre of the image are samples of rodent blood spiked with known amounts of [^{14}C]-glucose. Organs of interest are annotated in red.

QWBA analysis studying the radiolabel distribution was also performed for rats dosed with [^{14}C]-fenclozic acid and sacrificed at 2h, 6h, and 24 h. Figure 4.14 shows the QWBA phosphor imaging result summary from the time-course with this drug. The image at 2 hours shows that the radiolabelled drug

or drug metabolites are most concentrated within the stomach (black) with significant, but around equal amounts in the lung, liver, kidney and heart, which all appear dark grey. At 6 hours, major locations of drug and drug metabolites include: the large intestine (appears black) and again in the liver, kidney heart and lung. At 24 hours, the drug has been somewhat cleared from the large intestine (now appears grey rather than black) with retention in the liver, kidney heart and lung yet again. The digestive system is the major route of clearance for non-bioavailable drug presumably via faecal matter. The drug seems to be retained in the major organs for a longer amount of time compared with propanolol.

It can be seen from these images that the drug is more widely distributed across the rat at all time periods, signified by the darker tone of the sections throughout. However, this in itself, may not be unsurprising as fenclozic acid is a non-specific anti-inflammatory drug and hence, this mode of distribution is advantageous, possibly even desired. This effect is especially pronounced in the images taken from animals sacrificed at 2h and 6h, where the drug was in circulation. The skin of the animal appears dark grey. By 24 hours, the whole general appearance of the tissue section is slightly less dark (i.e. less radioactive drug / drug metabolites in the blood stream) and it seems that the there is greater localisation within the liver and kidneys, probably as expected as the drug is in the process of being metabolised (liver) and finally excreted (kidneys). The brain and spinal column of the rat stays light throughout the image, suggesting that the drug cannot efficiently penetrate the BBB.

Figure 4.15 shows the quantitative results of the imaging, as analysed by AIDA software *vs.* calibration standards made from rat blood spiked with the drug at known disintegrations per minute (dpm) radioactivity, hence back-calculation of the amount of drug in each tissue is possible from the pixel intensity in each image. These results mirror and confirm the qualitative results by looking at the dark areas of the phosphor image for the organs of interest: there are significant accumulations of the drug in the liver, lung and kidneys in the 2 h, 6 h and 24 h sections. However, the drug is most concentrated within the blood pool of the rats at any time point, reaching a maximum concentration of ca. 68 ug g^{-1} after 6 h, after which time the amount diminishes significantly to 24 h, where over half of the drug has been eliminated from the blood stream. A similar pattern of peak drug concentration at 6 h is observed also in the liver, lung and kidneys. There was minimal accumulation of the drug in the brain at any point, confirming that this is very inefficient at permeating the BBB in rats.

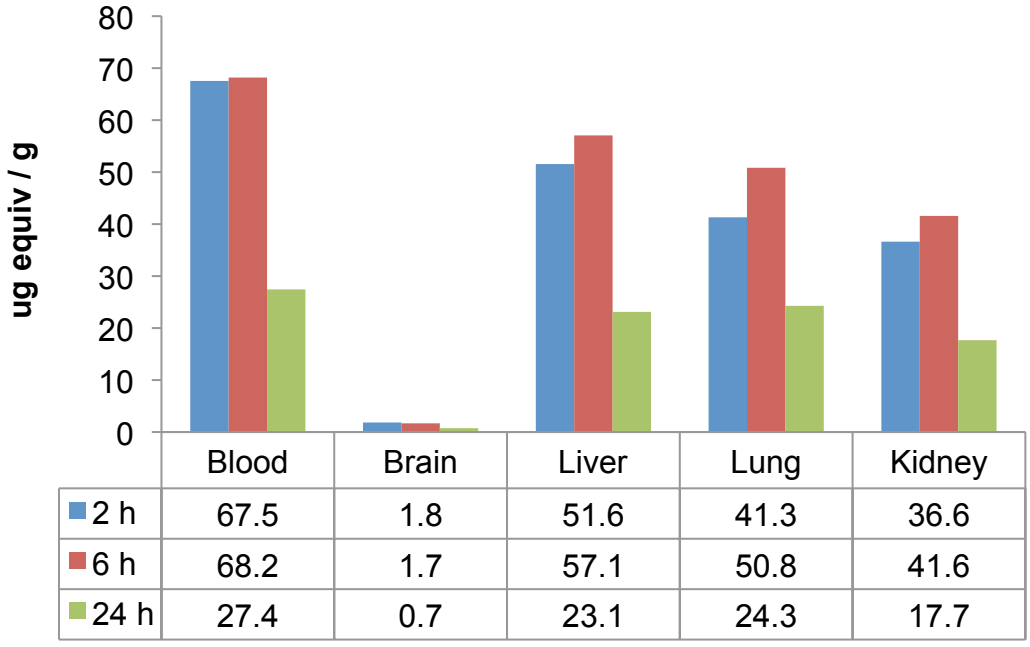

	Blood	Brain	Liver	Lung	Kidney
2 h	67.5	1.8	51.6	41.3	36.6
6 h	68.2	1.7	57.1	50.8	41.6
24 h	27.4	0.7	23.1	24.3	17.7

Figure 4.15. Quantification of [^{14}C]-fenclozic acid in rat organs by QWBA phosphor imaging. Table below show actual amounts of radiolabel in μg g $^{-1}$ found in each organ for each time point.

The distribution of [^{14}C]-fenclozic acid *in vivo* by LSC (Figure 4.16) is also almost identical to that produced by QWBA. Generally, the drug is localized mostly within the blood at any time point, as for the QWBA results, with levels of the drug detected at their highest levels after 6 h in any of the organs tested. The amounts of drug found in the LSC analysis is generally of the same magnitude as found by QWBA for the 2 h and 6 h animals, although there are differences between the 2 h and 6 h levels in the blood compared to the results from QWBA. There are also differences in the levels calculated at 24 h by LSC, with generally more drug detected in blood and kidney, though the results from the lung and liver at 24 h concur with the QWBA results. This

result again shows the value of using two techniques in tandem to analyse the samples. Later in this chapter the results from LSC and QWBA are compared using Bland Altman analysis which shows that the results between the two techniques are comparable within 95% limits of acceptability.

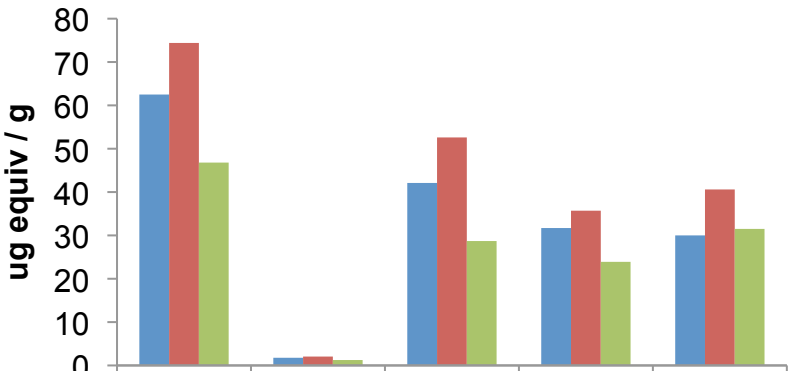

	Blood	Brain	Liver	Lung	Kidney
2 h	62.5	1.77	42.1	31.7	30
6 h	74.4	2.05	52.6	35.7	40.6
24 h	46.8	1.25	28.7	23.9	31.5

Figure 4.16: Quantification of [^{14}C]-fenclozic acid in rat organs by liquid scintillation counting. Table below show actual amounts of radiolabel in μg g $^{-1}$ found in each organ for each time point.

Brain homogenates from rats sacrificed at 6 hours post oral dosing with fenclozic acid were investigated by MALDI MS using CHCA as matrix, by dried droplet deposition. The spectrum is shown in Figure 4.17. The characteristic $[M+H]^+$ peak for fenclozic acid at *m/z* 253.984 was also observed in kidney tissues. In both cases, the signal is weak, but is above the baseline of a blank homogenate. This is consistent with the low amount of radiolabel observed in these organs by to QWBA in comparison to other organs. The phosphatidyl choline head group at *m/z* 104 is prominent in most

spectra, along with the peaks of CHCA.

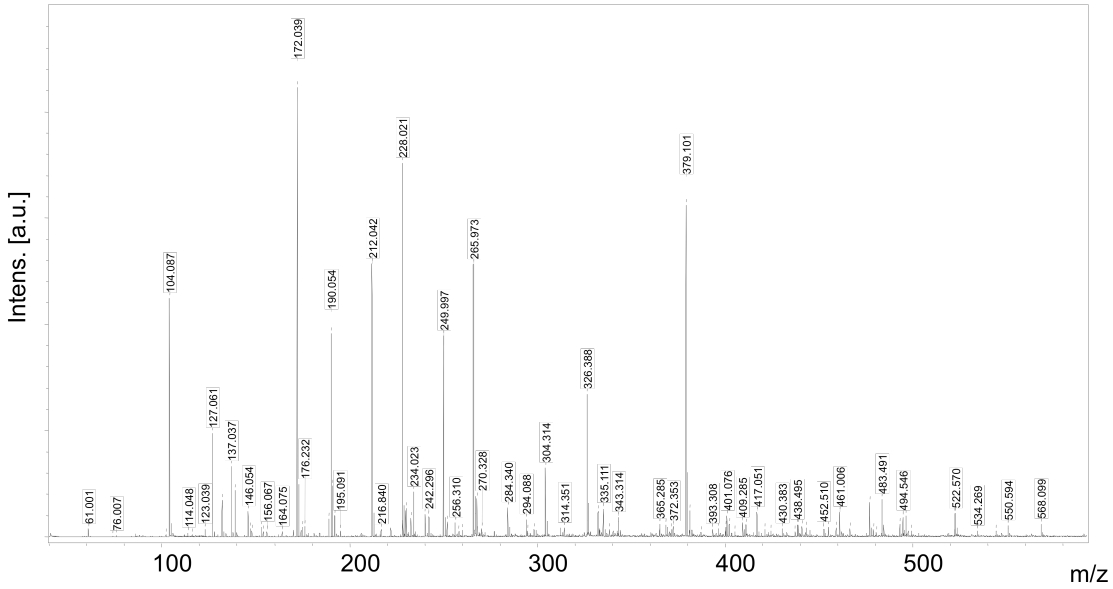

Figure 4.17. MALDI MS spectra for brain homogenates for rats sacrificed 6 h after oral dosing with [^{14}C]-fenclozic acid . Matrix: CHCA (25 mg mL^{-1} ACN, 0.1% TFA). Deposition: dried droplet.

Homogenates of lung tissue from rats sacrificed after 6 h post dose with fenclozic acid gave MALDI MS spectra where the $[M+H]^+$ peak for this drug could be identified; the peak for fenclozic acid at *m/z* 254.025 is accompanied by the correct 10 : 1 : 3 : 1 isotope pattern (Figure 4.18).The spectrum is dominated by CHCA / choline peaks. MALDI profiling of liver homogenates from animals sacrificed 6 h post oral dose with fenclozic acid (Figure 4.19) also showed evidence of the presence of the drug with a peak observed in the spectrum at *m/z* 254.

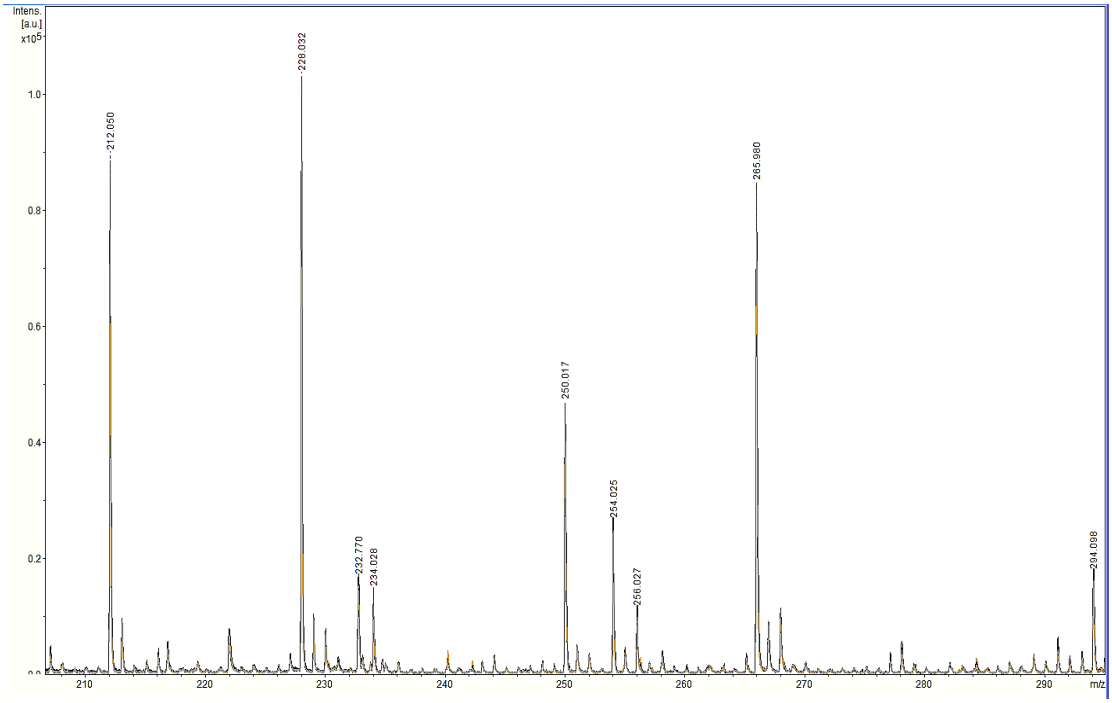

Figure 4.18: MALDI MS spectrum of lung homogenates of rats orally dosed with [^{14}C]-fenclozic acid and sacrificed at 6 h. Matrix: CHCA (25 mg mL^{-1} ACN, 0.1% TFA). Deposition: dried droplet.

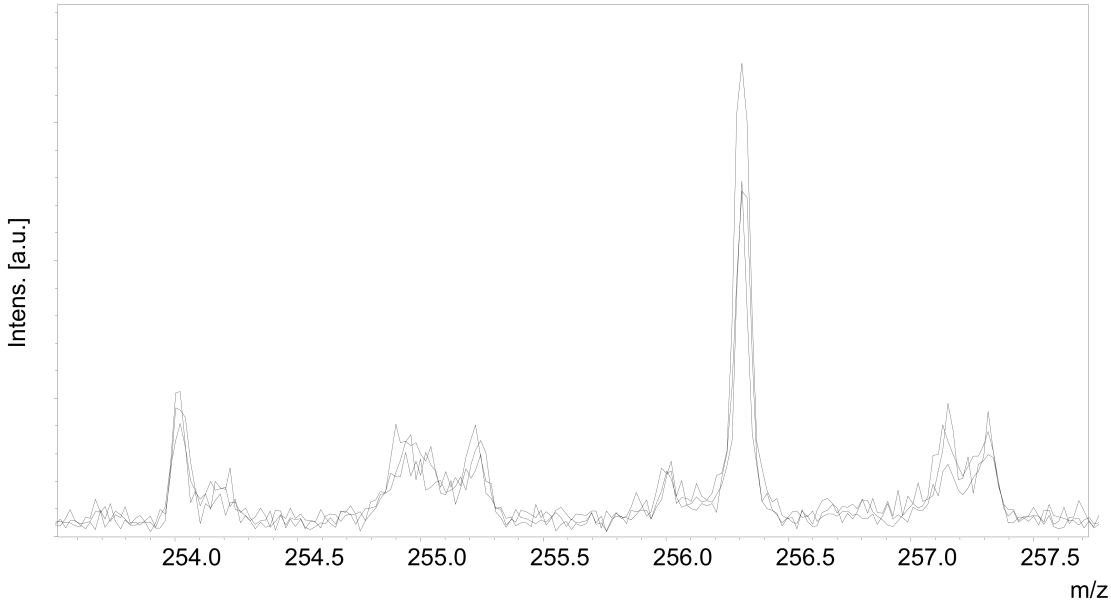

Figure 4.19:. Enlargement of MALDI MS spectra of liver homogenates of rats orally dosed with [^{14}C]-fenclozic acid (*n* = *4*) and sacrificed at 6 h. Matrix: CHCA (25 mg mL^{-1} ACN, 0.1% TFA). Deposition: dried droplet.

.

Analysis of blood extracts from animals dosed with fenclozic acid (Figure 4.20) showed strong evidence of the drug, as expected from QWBA and LSC results (previous chapter), where this drug was detected in relatively high amounts (> 70 μg g^{-1}) ; the $[M+H]^+$ peak at *m/z* 254 is particularly strong in these samples relative to the other homogenates from the fenclozic acid dosed animals. The correct isotope pattern was observed also in this case.

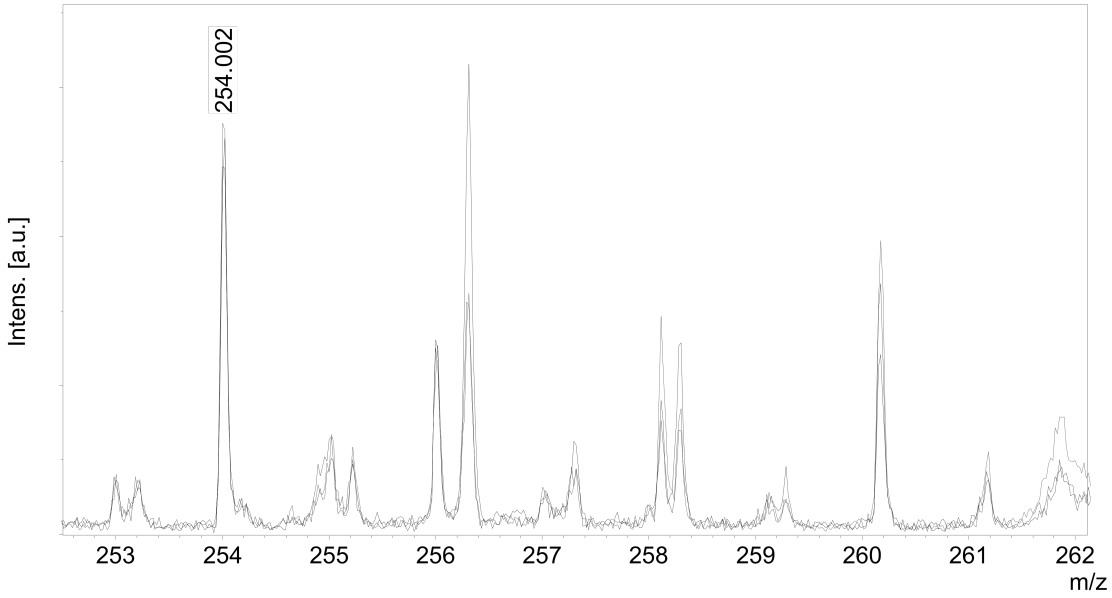

Figure 4.20: Enlargement of MALDI MS spectra of blood extracts of rats orally dosed with [^{14}C]-fenclozic acid and sacrificed at 6 h (*n* = *4*). Matrix: CHCA (25 mg mL^{-1} ACN, 0.1% TFA). Deposition: dried droplet.

All the mass spectra overlayed are shown in Fig 4.21, top. By tiling of the spectra alongside each other in the regions of interest, a mass spectral gel view could be built up for each organ extract sample (*n* = 5). [227] The results for homogenates and blood extracts from fenclozic acid dosed animals are presented in Figure 4.21 bottom. Each line represents the ion counts at

various *m/z* for 5 spectral repeats i.e. 5 separate analysis at different areas on the organ homogenates; dark regions indicate where the ion counts are relatively high at any given *m/z*. Peaks expected for fenclozic acid at *m/z* 254.0 and *m/z* 256.0 – from the expected isotopic pattern of fenclozic acid – are highlighted. It can be seen that these areas are darkest for liver homogenates, lung homogenates and very strong for samples from blood extracts. Samples from brain and kidney show very weak signals, which are quite inconclusive. The blank homogenate does not show any significant dark areas at either *m/z* 254.0 or *m/z* 256.0, confirming that the peaks are genuine. Peaks assigned to either matrix peaks or naturally occuring ionic species are observed at *m/z* 251.0, 252.0, 253.0, 253.1, 255.0, 255.2, 256.3, 257.3 and 258.3 in the immediate area of the drug. These qualitative profiling results generally agree well with the data produced by LSC and QWBA for rats dosed with radiolabelled fenclozic acid in terms of where the drugs should be found; however, the data for the kidney is surprising as there was a significant amount of the detected by QWBA and LSC of the same order of the liver and lungs, yet the signal is very weak for the drug in kidney tissues. Potentially ion suppression in this organ is high for fenclozic acid possibly due to the high salt content of the kidneys, which is used to control water movement by the creation of salt gradients.

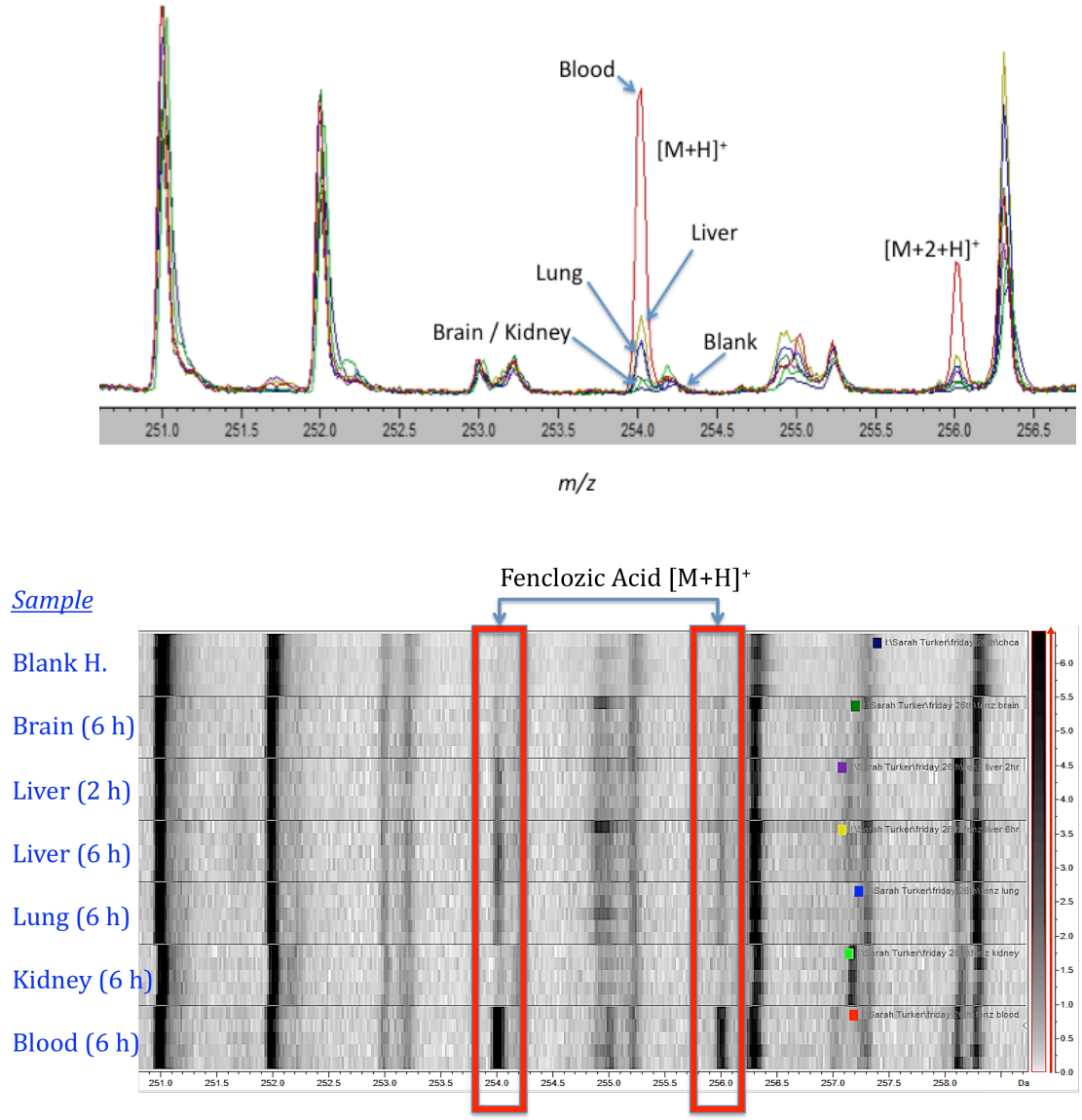

Figure 4.21. Top: overlayed single mass spectra for each homogenate with labeling. Bottom: Gel view of Mass spectral data of homogenates produced from [^{14}C]-fenclozic acid dosed rats (*n* = 5), alongside a blank homogenate (*n* = *5*). Relative ion intensity shown on the scale on the right.

Agreement between QWBA and LSC by Bland Altman Analysis

The QWBA results were compared using Bland Altman analysis which is a method that can be used to compare agreement between techniques and is considered superior to simple correlation plots.[228, 229] In this analysis the mean difference of the results found between two techniques, and allows 95% limits of agreement to be established between the two techniques which allows confidence between the two techniques to be accounted for.[230] Figure 4.22 shows Bland-Altman plots for propanolol and fenclozic acid. From these plots it can be stated that both QWBA and LSC show good agreement between them, and that the majority of the data excluding the one outlier in each plot shows agreement within 95% limits, which is defined as ±1.96 standard deviations of the mean difference. Hence it is possible to confidently use both techniques and compare results between them.

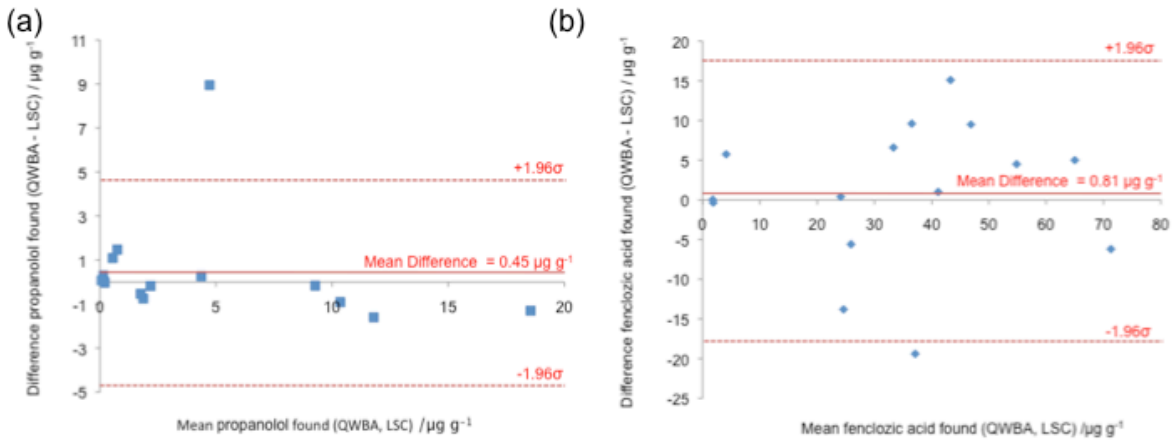

Fig. 4.22: Bland Altman analysis of QWBA vs LSC for the determination of (a) [^{14}C]-propanolol and (b) [^{14}C]-fenclozic acid in rats. The plots show the mean difference between techniques as well as the 95% limits of agreement (±1.96*SD) between the two techniques for comparison.

Comments on distribution; inferences on structure and metabolism

The coupling of MALDI to the more traditional analyses LSC and QWBA allow us to make confident conclusions on the drug distributions and some limited pharmacokinetics as the MALDI analysis allows us to confidently state that the drug is within an organ and furthermore is chemically intact. The results of the distributions through time reflect the chemical nature of the drugs. From the stomach (drugs were orally distributed in this study), drugs are absorbed into the bloodstream, where they are then distributed throughout the animal via the circulatory system if not metabolized and excreted in first-pass by the liver and kidneys.[214] The biodistribution is highly dependent on the structure of the drug; generally those drugs that are acidic (such as fenclozic *acid*) are known to reside mostly in the bloodstream throughout their life in the body, whilst weakly basic drugs (such as propanolol) are able to diffuse into tissues and organs. This is because the pH of the blood is maintained at 7.4 by homeostatic mechanisms and this dictates the ionisation of the drug. pK_a's allow rough prediction of the general distribution characteristics i.e. what form the drug will exist in given any pH. Subtle differences in the pH between tissues and blood plasma, tend to disturb the acid base equilibrium for any drug, and in particular, weakly basic drugs are localized within tissues and kept there due to ionisation. The removal of the basic form from the bloodstream shifts the equilibrium which must then be maintained and more drug enters the tissue irreversibly.[231] The biodistribution observed for fenclozic acid (acidic) and propanolol (weakly basic) in the studies outlined in this chapter are consistent with this premise, with fenclozic

acid mostly localized within the bloodstream, and propanolol localized mainly in tissues.

The picture comparing propanolol with fenclozic acid from all the studies suggests the following:

i) The bioavailability of fenclozic acid is much higher than propanolol i.e. more fenclozic acid reaches general circulation as evidenced from the blood result in both LSC and QWBA for fenclozic acid.

ii) Bioavailable propanolol is absorbed much faster into the bloodstream, as there is no lag time (T_{max}) in reaching peak drug concentration (C_{max}) as for fenclozic acid.

iii) First pass metabolism[214] (i.e. metabolism of the drug directly from the stomach by the liver without entry into the bloodstream) generally removes the large extent of propanolol before it can enter the bloodstream.

iv) Bioavailable fenclozic acid is not removed by first pass metabolism but is excreted slowly by normal hepatic / renal clearance, hence its much longer persistence and relatively high levels in blood plasma.

v) The bioavailability of both drugs is low, which is typical of oral administrative routes, and the majority of the drug is excreted via faeces through the digestive tract.

From the QWBA autoradiography data available, the half-life ($t_{1/2}$) of both drugs was calculated using linear plots of the natural logarithm of the drug concentration found in the organ (in this case the concentration of drug found in the liver) vs. the time (Figure 4.22), where:

$$t_{1/2} = \ln 2 / (\text{slope} \times -2.303)$$

This treatment assumes that the elimination is monophasic i.e. that a single elimination pathway is experienced, which is generally true for both drugs (hepatic-renal clearance either in first pass or later). It is worth noting here that because of the limited time points and replicates that are used in this study that this preliminary result must be treated with caution. To calculate the concentrations of each drug, the density of water 1 g mL^{-1} was used for the liver, so by using the RMM of each drug (propanolol = 259.34 g mol^{-1}, fenclozic acid = 253.70 g mol^{-1}) units of $\mu g\ g^{-1}$ are converted to units of mol dm^{-3}. Data for rats sacrificed at 2 h with fenclozic acid was not used, as C_{max} for the drug was not reached at that point, or indeed in any organ. The half-life of fenclozic acid in rats was calculated as 8.9 h using this method, while for propanolol it was calculated to be 4.6 h. For human subjects with rheumatoid arthritis who were treated with fenclozic acid the effects of the drug were still detected after 35 hours.[232] Unfortunately, in this dataset the third data point is missing for fenclozic acid, and the data for propanol is limited to only 3 time points and therefore this impose limitations on the interpretation of this data, but it was impossible to add further data points to

the curve without resorting to the slaughter of more rodent subjects, which is unethical in such routine studies.

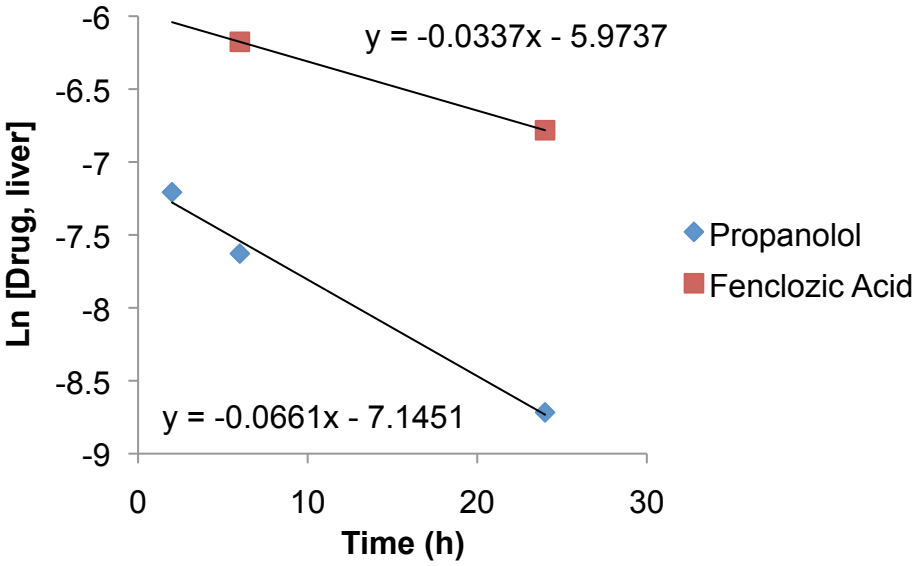

Figure 4.23: Plots used to calculate the half-life of [^{14}C]-fenclozic acid and [^{14}C]-propanolol in rats from the QWBA data generated. To calculate the concentrations of each drug, the density of water 1 g mL^{-1} was used for the liver, so by using the RMM of each drug (propanolol = 259.34 g mol^{-1}, fenclozic acid = 253.70 g mol^{-1}) units of μg g^{-1} are converted to units of mol dm^{-3}. Data for rats sacrificed at 2 h with fenclozic acid was not used, as C_{max} for the drug was not reached at that point, or indeed in any organ. The half-life of fenclozic acid in rats was calculated as 8.9 h using this method, while for propanolol it was calculated to be 4.6 h.

Table 4.3. Summary comparing the techniques in this study for the detection of drugs in whole animal sections and excised homogenates and exsanguinated fluids (6 h sacrifices). Key: + = detected, - = not detected.

Compound	Organ	MALDI, $[M+H]^+$	QWBA ($\mu g\ g^{-1}$)	LSC ($\mu g\ g^{-1}$)
[^{14}C]-propanolol				
	Liver	+	11.0	12.6
	Kidney	+	9.2	9.4
	Brain	+	0.2	0.14
	Blood	+	1.1	0.01
	Lung	+	1.5	2.0
[^{14}C]-fenclozic acid				
	Liver	+	57.1	52.6
	Kidney	+ (weak)	41.6	40.6
	Brain	+ (weak)	1.7	2.1
	Blood	+	68.2	74.4
	Lung	+	50.8	35.7

Table 4.3 summarises the findings in the study. In general, where the drug is detected by either QWBA or LSC we can in general also detect the drug in the homogenates of the excised organ (or exsanguinated fluid in the case of blood). This is true in all cases for [^{14}C]-propanalol. However, for fenclozic acid, there is generally good agreement between techniques, i.e. where significant amounts of radiolabel were found, the drug could be detected by MALDI MS, in all cases apart from that of the kidney tissue, where there is a great discrepancy between the techniques; QWBA and LSC suggest large amounts of fenclozic acid in the kidney, yet the MALDI signal is very weak. This could be due to either (i) the large tissue extinction coefficient found for kidney tissues that suppresses ionisation – for example Hamm et al found that the TEC for kidney tissues was similar for the detection of olanzapine in Brain

(TEC = 0.07), liver (TEC = 0.06) and lung (TEC = 0.08) it was around double for that of kidney tissues (TEC = 0.14) due the large amount of salts in this organ which leads to enhanced ion suppression;[105] or (ii) it could be that the QWBA/LSC techniques only detect radiolabelled material and are detecting metabolites rather than the whole drug,[136] hence why focusing on detection of $[M+H]^+$ may not be the correct approach for this tissue as it would always underestimate the amount of drug within the tissue – this is discussed in the next section.

Discrepancy within Kidney Tissues: Potential Drug Metabolites in MS spectra

As mentioned in the previous section QWBA and LSC only analyses radiolabelled nuclei, which may explain the discrepancy between LSC/QWBA and MALDI MS for the kidney tissues; a radiolabelled metabolite may be being detected by LSC and QWBA, and it would not be detected as $[M+H]^+$ for MALDI. Fenclozic acid is known to be unchanged from the effects of gut metabolism.[233] It is also known that fenclozic acid is metabolized by hydroxylation (M+17) on its aromatic rings.[222, 223] However, the most comprehensive study on metabolites was reported by Clench et al who identified 18 distinct metabolites of fenclozic acid (Table 4.4), which included products from oxidation, hydrolysis, decarboxylation, and conjugation.

Table 4.4. Metabolites of fenclozic acid identified by Clench et al.[234]

Metabolite	Matrix detected	Observed $[M+H]^+$ $[M-H]^-$	Structure/description	New	Key fragment ions observed (positive ion)
Fenclozic acid	Bile /Urine	254.0037 251.9892	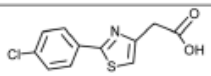		70.9950 138.0105 207.9982
M1	Bile/Urine	269.9986 267.9841	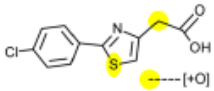 Oxidation (+O)	Yes	86.9905 114.9848 138.0105 154.9722 195.9982 223.9928
M2	Bile/Urine	269.9986 267.9841	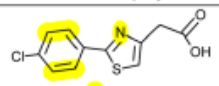 Oxidation (+O)		223.9931 154.0053 70.9950
M3	Bile/ Urine	269.9986 267.9841	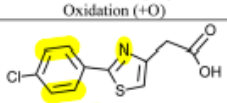 Oxidation (+O)		223.9930 154.0051 70.9949
M4	Urine	269.9986 267.9841	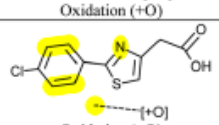 Oxidation (+O)		223.9931 154.0056 70.9950
M5	Urine	269.9986 267.9841	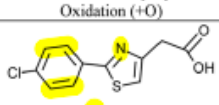 Oxidation (+O)		223.9932 154.0054 70.9950
M6	Bile/Urine	272.0128 ND	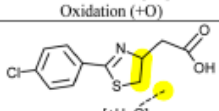 Hydrolysis (+H_2O)	Yes	195.9982 154.9717 138.0105 89.0054
M7	Bile/Urine	272.0128 ND	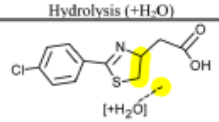 Hydrolysis (+H_2O)	Yes	195.9981 154.9717 138.0108 89.0055
M8	Bile/Urine	239.9877 ND	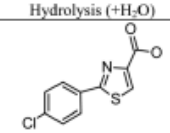 Oxidative decarboxylation	Yes	221.9774 193.9824 150.0103
M9	Bile	297.0095	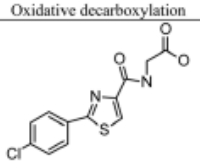 Oxidative decarboxylation + Glycine conjugation	Yes	239.9883 221.9776 193.9828 150.0105
***M10**	Bile/Urine	430.0352 ND	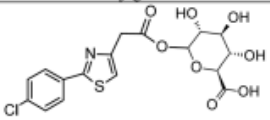 Glucuronidation		207.9987 70.9947
M11	Bile/Urine	397.0979 ND	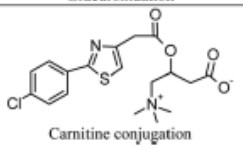 Carnitine conjugation	Yes	338.0246 254.0033 297.9981 144.1015

Metabolite	Matrix detected	Observed $[M+H]^+$ $[M-H]^-$	Structure/description	New	Key fragment ions observed (positive ion)
M12	Bile	382.0621 ND	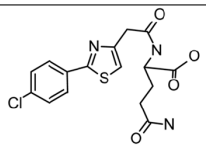 Glutamyl conjugation	Yes	235.9931 207.9882 130.0499 84.0444 70.9950
M13	Bile/Urine	361.0077 ND	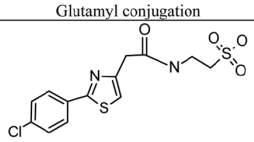 Taurine conjugation		279.0353 235.9939 126.0219
M14	Bile	311.0252 ND	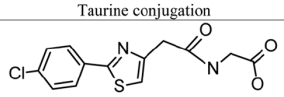 Glycine conjugation		265.0195 235.9932 207.998
***M15**	Bile/Urine	391.0192 389.0035	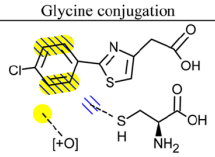 Oxidation (+O) + Cysteine conjugation	Yes	70.9951 154.0056 194.0094 207.9985 222.0045 223.9937 283.9603
***M16**	Bile	448.0398 446.0254	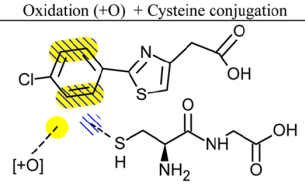 Oxidation (+O) + Cysteineglycine conjugation	Yes	283.9601 223.9935 194.0094 154.0044 70.9950
***M17**	Bile	433.0294 431.0144	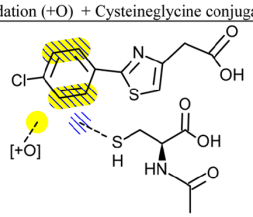 Oxidation (+O) + N-Acetylcysteine conjugation	Yes	415.0190 223.9935 154.0054 70.9950
***M18**	Bile	577.0830 575.0679	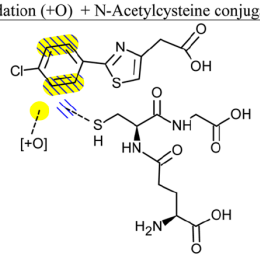 Oxidation (+O) + Glutathione conjugation	Yes	448.0404 373.0083 354.9978 283.9603 177.0335 154.0042 130.0506

It is therefore possible to cross check a peak list from a typical mass spectrum from kidney homogenates generated in this study against these metabolites (Table 4.5), in order to identify if fenclozic acid metabolites are potentially observed in the mass spectra, which would account for the discrepancy between LSC/QWBA and MALDI data.

Table 4.5: List of major peaks observed in typical mass spectra taken from fenclozic acid kidney tissues (6 h sacrifice).[234]

Observed Peak, m/z	Potential Metabolite as-designated by Clench et al. (Table 4.4)	Potential Structure	Potential origins & notes
44.001	N/A	N/A	Not observed in control Could not be assigned
61.001	N/A	N/A	Observed in control (blank+CHCA)
74.062	N/A	N/A	Observed in control
86.068	N/A	N/A	Observed in control
104.087	N/A	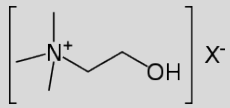	Choline peak Observed in control
118.070	N/A	N/A	Not observed in control Could not be assigned
127.061	N/A	N/A	Observed in control
137.038	N/A	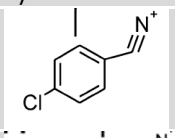	Fenclozic acid aromatic fragment
153.040	M15 fragment	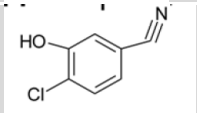	Fragment of M15 (cysteine conjugation)
162.107			
172.039	[CHCA+H]-H_2O	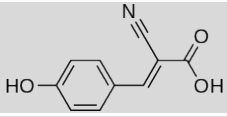	Matrix dehydroxylation Observed in control
184.076	N/A	N/A	Not observed in control Could not be assigned
190.055	$[CHCA+H]^+$	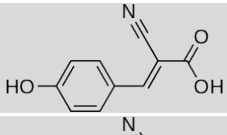	Protonated matrix peak Observed in control
212.042	$[CHCA+Na]^+$	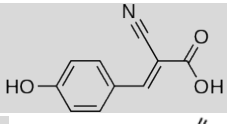	Matrix sodium adduct
222.020	M15 fragment	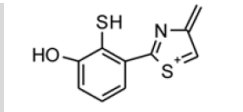	Fragment of M15 (cysteine conjugation)
228.020	N/A	N/A	Observed in control
234.021	N/A	N/A	Observed in control
242.294	N/A	N/A	Observed in control
249.997	N/A	N/A	Observed in control

254.100	Protonated fenclozic acid	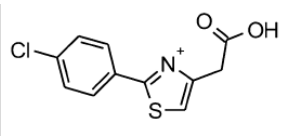	$[M+H]^+$
265.972	N/A	N/A	Observed in control
272.276	M6, M7	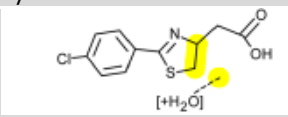 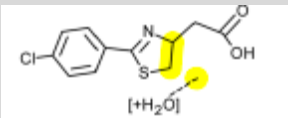	Hydrolysis products
284.341	M15 fragment	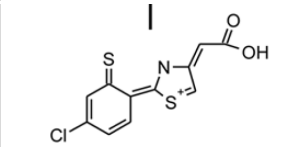	Fragment of M15 (cysteine conjugation)
294.002	N/A	N/A	Observed in control
304.315	N/A	N/A	Observed in control
326.388	N/A	N/A	Observed in control
332.343	N/A	N/A	Observed in control
343.316			
368.422	N/A	N/A	Observed in control
379.101	[2M+H] CHCA Cluster Peak	N/A	Matrix cluster peak (2M) Observed in control
401.083	N/A	N/A	Observed in control
409.284	N/A	N/A	Not observed in control Could not be assigned
417.051	N/A	N/A	Observed in control
438.498	N/A	N/A	Observed in control
452.507	N/A	N/A	Observed in control
461.007	N/A	N/A	Observed in control
476.975			
483.491	N/A	N/A	Observed in control
496.326	N/A	N/A	Observed in control
520.322	N/A	N/A	Observed in control
534.274	N/A	N/A	Not observed in control Could not be assigned
544.318	N/A	N/A	Not observed in control Could not be assigned
550.592	N/A	N/A	Observed in control
558.267	N/A	N/A	Not observed in control Could not be assigned
568.312	[3M+H] CHCA cluster	N/A	Matrix cluster peak (3M) Observed in control
582.258	N/A	N/A	Not observed in control

			Could not be assigned

Indeed it can be shown from the analysis of the MALDI peaks observed in the kidney sample it seems that we potentially see mainly the so-called M15 metabolite, which is the product and potentially we also see fragments from this metabolite within the spectrum. We also see peaks that we may assign potentially to the M6/M7 diastereomeric oxidation product of fenclozic acid. However, the assignment can only be made with limited confidence as it would require further analysis of these ions using MS/MS to look at their fragmentation products, and currently this is a limitation of this study as MS/MS data were not generated. However, it may potentially be concluded that the discrepancy between QWBA/LSC and MALDI for fenclozic acid in kidney tissues can be ascribed potentially to a mixture of factors in play including a large TEC for these tissues as well as the appearance of numerous potential metabolites in the mass spectra indicating that the drug was already broken down / conjugated to cysteine when excretion via the kidneys occurred.

4.3. Conclusions

Quantitative whole body autoradiography has been used to image the distribution of two radiolabelled drugs and their metabolites. QWBA and LSC results generally agree with each other for both radiolabel distributions.

As alluded to in the introduction of the chapter, there are major shortcomings to the QWBA and LSC methods in that it only shows where the ^{14}C isotope

ended up and this could be as either metabolite or the intact drug; the user cannot discern. The shortcomings of QWBA and LSC (and indeed radiolabelling studies in general) are that the user cannot discern between the drugs and metabolites. However, the two drugs have also been profiled by MALDI MS, propanolol and fenclozic acid, in tissue homogenates excised from animals which had been dosed with the drugs and sacrificed after 2 h and 6 h post-dose. MALDI MS can tell the difference between drugs and metabolites and thus when coupled to QWBA and LSC could potentially be a useful tool for rapid analysis. By the use of the three techniques in parallel on the same samples, we then made semi-quantitative conclusions regarding the distribution and pharmocokinetics of the drugs in the animal subjects. The distribution of [^{14}C]-fenclozic acid revealed by both QWBA and LSC and MALDI MS is that the drug or its metabolites are mostly found in the blood, with lesser but significant amounts found in the liver, lung and kidney. Propanolol, in contrast, is mostly found in the liver and kidneys, with smaller amounts found in the lung and minimal amounts in the blood and brain. The half-life of the drugs in rats have been calculated using a linear regression method. The half-life of fenclozic acid in rats was calculated as 8.9 h using this method, while for propanolol it was calculated to be 4.6 h.

Using a 2D layout of spectra from different organs aligned *vs.* a *m/z* scale it was possible to profile homogenates with intensity patterns, in gel view and with relative ion intensity information that show quickly whether the drug is present in the tissue or not, which could be useful for example in deciding which organs merit further interrogation i.e. screening. As the patterns contain relative ion intensity information, it may be possible in future to make these

measurements semi quantitative or quantitative image analysis software such as AIDA or imageJ. However, The major weakness of this study as it stands is that it is not quantitative currently and is therefore of limited use for drug quantitation alongside fully quantitative techniques e.g. QWBA and LSC. The use of internal standards could be a way to quickly achieve this, and merits further investigation in future work. After this is achieved, further Bland Altman analysis could then be used to compare MALDI MS with LSC or QWBA to show if they are comparable for drug quantitation as well as defining the acceptable limits of agreement between MALDI MS and other radioisotope techniques. Another current limitation of the approach was that MS/MS data was not generated – this could have helped unambiguously assign the metabolites from fenclozic acid that is potentially seen in the kidney tissue data, and conclusively prove that the discrepancy between the mass spec and radiolabelling techniques is due to detection of the radiolabelled portions of the metabolite in the latter data – MALDI suggested that the so-called M15 metabolite which arises from conjugation of fenclozic acid to cysteine in vivo and hence it would be interesting in further studies to prove this by MS/MS of the peaks which are potentially associated with the M6/M7 and M15 metabolites.

Chapter 6: Overall conclusions and future work.

Mass spectrometric analysis represents a wonderfully versatile palette of techniques that have the potential to be used routinely in drug distribution analysis. However, the development of universal mass spectrometric techniques and calibration standards so that reliable analysis can be achieved alongside currently used analytical techniques is not yet achieved for all mass spectrometric techniques and is one of the most challenging areas to work in. Certainly, by using mass spectrometry there is the potential for highly accurate, robust analyses to be developed that can fill niches not yet explored in traditional techniques to quantify drug distributions in the pharmaceutical industry currently, such as QWBA and LSC. The major drawback with the latter techniques, which require radiolabelled drugs, is the inability to discern between drug and drug metabolites, something that mass spectrometric techniques can certainly overcome. Mass spectral analysis also sits well ethically, as it does not require the extra slaughter of animals.

The analysis of drugs using mass spectrometric techniques[1] is an emerging technique, relatively recently discovered, and is highly challenging compared to say lipidomics or proteomics. Unlike proteins and lipids, there is never a high concentration of the spiked drug in the tissues, they are not already ionised at pH 7.4 in most cases and often ion suppression from salts makes it challenging to achieve good signal to noise ratio in the case of most measurements. Hence, the development of tissue homogenate calibration standards for drugs, such as our work in chapter 2 with haloperidol represents a very important field of anticipative research for

future efforts – results in solvents for deposition and comparison of deposition methods for imaging are important for the development of reliable imaging protocols that may guide the way for future researchers in this highly challenging field. Results of calibration curves based on MS/MS analysis which have the potential to be linearised vs internal standards can potentially unlock new quantitative analyses for a number of drugs. Likewise, the use of ambient surface sampling-ionisation to construct calibration curves from tissue homogenates described in Chapter 3 may also be important for a number of different analyses in future. Both developed protocols present opportunities to exploit for various applications. With calibration curves for MALDI MS imaging for instance there is the opportunity to spatially profile drug distribution confidently in a quantitative manner, as outlined in the introduction, Chapter 1. With LESA there are many more opportunities to develop instrumental parameters and to optimise the duty cycle time vs. sensitivity. It is expected that these two chapters will be of highest academic impact and are complementary to the studies on quantitative analysis of analytes in tissues by Pirman *et al*,[100, 174] Kallback *et al*.[104] and Hamm *et al*.[105] by MALDI. In all cases, the calibration curves presented by MALDI cover the range 0 – 500 $\mu g\ g^{-1}$, with those presented by LESA in the 0 – 50 $\mu g\ g^{-1}$ range. Thus, they are in the correct range when compared to the reports of quantitative MALDI made by Pirman *et al*. for instance.[174] We have discussed the potential of calibration curves constructed from drug-doped tissue homogenates and using LESA coupled to high resolution mass spectrometry for the absolute quantitation of drugs in tissues, something that is desperately required at the moment to achieve

quantitative analysis by LESA-MS.[81, 207, 211] The calibration standards for propanolol and fenclozic acid as analysed by LESA-MS in chapter 3 generally provide linear or pseudo-linear responses, that with further work, such as correction/normalization to internal standards could present robust calibration standards to achieve quantitation in LESA-MS. This is probably a priority area to explore next because of the great potential of LESA-MS to provide very sensitive surface analysis. In the case of LESA, a major limitation of the data is that the analysis was not completed in replicate which does not allow any analysis of the reproducibility of the technique or indeed any estimation of the error associated with any measurement.

Chapter 4 described a full animal study of drug distribution *in vivo* using a pair of drugs for animals sacrificed at different time points post dose. A range of histological techniques and industry-standard imaging / analysis techniques such as quantitative whole body autoradiography and liquid scintillation counting were used initially to look at potential drug distribution, and combined with mass spectral profiling analysis in the following section, using barcodes built from MALDI data taken from the organs excised, this allowed rapid visual confirmation of the presence of a drug within a specified tissue or organ. Moreover, using the combination of MALDI MS with QWBA and LSC we could estimate half lives of drug molecules and potentially discern this data from that of radiolabelled drug metabolites. However, much more work is required to bring this to fruition as MALDI MS/MS data was not generated in order to confidently and unambiguously assign metabolites. Future work may extend the analysis of

the drug-doped homogenates from excised organs to LESA analysis for comparison with the calibration standards in Chapter 3.

Finally taken as a whole we have shown that mass spectrometry imaging and analysis is a potentially viable technique for the analysis of drugs in tissues, if somewhat challenging in its nature. It is hoped that this work leaves the reader in no doubt regarding the potential usefulness of mass spectrometry for drug analyses.

Bibliography

1. Turker, S. D.; Dunn, W. B.; Wilkie, J., MALDI-MS of drugs: Profiling, imaging, and steps towards quantitative analysis. *Appl. Spectroscopy Rev.* **2016**, 1-27.

2. Burlingame, A. L.; Boyd, R. K.; Gaskell, S. J., Mass spectrometry. *Anal. Chem.* **1998,** 70, (16), 647R-716R.

3. de Hoffmann, E.; Stroobant, V., *Mass Spectrometry: Principles and Applications*. 3rd ed.; John Wiley & Sons Ltd.: Chichester, 2007.

4. Hillenkamp, F.; Karas, M., MALDI, an experience. *Int. J. Mass Spectrom.* **2000,** 200, 71-77.

5. Karas, M.; Bachmann, D.; Hillenkamp, F., Influence of the Wavelength in High-Irradiance Ultraviolet Laser Desorption Mass Spectrometry of Organic Molecules. *Anal. Chem.* **1985,** 57, 2935-2939.

6. Karas, M.; Hillenkamp, F., Laser desorption ionization of proteins with molecular masses exceeding 10000 Daltons. *Anal. Chem.* **1988,** 60, (20), 2299-2301.

7. Tanaka, K.; Waki, H.; Ido, Y.; Akita, S.; Yoshida, Y.; Yoshida, T., Protein and Polymer Analyses up to m/z 100 000 by Laser Ionization Time-of flight Mass Spectrometry. *Rapid Commun. Mass Spectrom.* **1988,** 2, (20), 151-153.

8. Low, W.; Kang, J.; DiGruccio, M.; Kirby, D.; Perrin, M.; Fischer, W. H., MALDI-MS analysis of peptides modified with photolabile arylazido groups. *J. Am. Soc. Mass Spectrom.* **2004,** 15, (8), 1156-1160.

9. Stoeckli, M.; Staab, D.; Schweitzer, A.; Gardiner, J.; Seebach, D., Imaging of a beta-peptide distribution in whole-body mice sections by MALDI mass spectrometry. *J. Am. Soc. Mass Spectrom.* **2007,** 18, (11), 1921-1924.

10. Strupat, K.; Karas, M.; Hillenkamp, F., 2,5-dihydroxybenzoic acid - a new matrix for laser desorption ionization mass-spectrometry. *Int. J. Mass Spectrom. Ion Process.* **1991,** 111, 89-102.

11. Zhu, X.; Papayannopoulos, I. A., Improvement in the detection of low concentration protein digests on a MALDI TOF/TOF workstation by reducing alpha-cyano-4-hydroxycinnamic acid adduct ions. *J. Biomol. Tech.* **2003,** 14, (4), 298-307.

12. Griffin, T. J.; Hall, J. G.; Prudent, J. R.; Smith, L. M., Direct genetic analysis by matrix-assisted laser desorption ionization mass spectrometry. *Proc. Nat. Acad. Sci. U.S.A.* **1999,** 96, (11), 6301-6306.

13. Kirpekar, F.; Nordhoff, E.; Larsen, L. K.; Kristiansen, K.; Roepstorff, P.; Hillenkamp, F., DNA sequence analysis by MALDI mass spectrometry. *Nucleic Acids Res.* **1998,** 26, (11), 2554-2559.

14. Niemeyer, D.; Elssner, T.; Fahr, K.; Peters, D.; Wenzel, T.; Petkovski, E.; Kostrzewa, M., Detection of genetic variation by MALDI-TOF mass spectrometry: rapid SNP genotyping using the GENOLINK system. In *Progress in Forensic Genetics 10*, Doutremepuich, C.; Morling, N., Eds. 2004; Vol. 1261, pp 9-11.

15. Sauer, S.; Kepper, P.; Smyra, A.; Dahl, A.; Ferse, F. T.; Lehrach, H.; Reinhardt, R., Automated solid-phase extraction for purification of single nucleotide polymorphism genotyping products prior to matrix-assisted laser desorption/ionisation time-of-flight mass spectrometric analysis. *J. Chromatogr. A* **2004,** 1049, (1-2), 9-16.

16. Tang, K.; Taranenko, N. I.; Allman, S. L.; Chen, C. H.; Chang, L. Y.; Jacobson, K. B., Picolinic-acid as a matrix for laser mass-spectrometry of nucleic-acids and proteins. *Rapid Commun. Mass Spectrom.* **1994,** 8, (9), 673-677.

17. Tang, W.; Krause, J.; Zhu, L.; Smith, L. M., Factors influencing oligonucleotide stability in matrix-assisted laser desorption/ionization (MALDI) mass spectroscopy. *Int. J. Mass Spectrom.* **1997,** 169, 301-311.

18. Tang, W.; Nelson, C. M.; Zhu, L.; Smith, L. M., Positive ion formation in the ultraviolet matrix-assisted laser desorption/ionization analysis of oligonucleotides by using 2,5-dihydroxybenzoic acid. *J. Am. Soc. Mass Spectrom.* **1997,** 8, (3), 218-224.

19. Zagorevskii, D. V.; Aldersley, M. F.; Ferris, J. P., MALDI analysis of oligonucleotides directly from montmorillonite. *J. Am. Soc. Mass Spectrom.* **2006,** 17, (9), 1265-1270.

20. Zhang, L. K.; Gross, M. L., Location of abasic sites in oligodeoxynucleotides by tandem mass spectrometry and by a chemical cleavage initiated by an unusual reaction of the ODN with MALDI matrix. *J. Am. Soc. Mass Spectrom.* **2002,** 13, (12), 1418-1426.

21. Bunch, J.; Clench, M. R.; Richards, D. S., Determination of pharmaceutical compounds in skin by imaging matrix-assisted laser desorption/ionisation mass spectrometry. *Rapid Commun. Mass Spectrom.* **2004,** 18, (24), 3051-60.

22. Hsieh, Y.; Casale, R.; Fukuda, E.; Chen, J. W.; Knemeyer, I.; Wingate, J.; Morrison, R.; Korfmacher, W., Matrix-assisted laser desorption/ionization imaging mass spectrometry for direct measurement of clozapine in rat brain tissue. *Rapid Commun. Mass Spectrom.* **2006,** 20, (6), 965-972.

23. Hsieh, Y.; Chen, J.; Korfmacher, W. A., Mapping pharmaceuticals in tissues using MALDI imaging mass spectrometry. *J. Pharmacol. Toxicol.* **2007,** 55, (2), 193-200.

24. Cerruti, C. D.; Touboul, D.; Guerineau, V.; Petit, V. W.; Laprevote, O.; Brunelle, A., MALDI imaging mass spectrometry of lipids by adding

lithium salts to the matrix solution. *Anal. Bioanal. Chem.* **2011,** 401, (1), 75-87.

25. Hankin, J. A.; Barkley, R. M.; Murphy, R. C., Sublimation as a method of matrix application for mass spectrometric imaging. *J. Am. Soc. Mass Spectrom.* **2007,** 18, 1646-1652.

26. Hunnam, V.; Harvey, D. J.; Priestman, D. A.; Bateman, R. H.; Bordoli, R. S.; Tyldesley, R., Ionization and fragmentation of neutral and acidic glycosphingolipids with a Q-TOF mass spectrometer fitted with a MALDI ion source. *J. Am. Soc. Mass Spectrom.* **2001,** 12, (11), 1220-1225.

27. Jackson, S. N.; Wang, H. Y. J.; Woods, A. S., Direct profiling of lipid distribution in brain tissue using MALDI-TOFMS. *Anal. Chem.* **2005,** 77, (14), 4523-4527.

28. Jackson, S. N.; Wang, H. Y. J.; Woods, A. S., In situ structural characterization of phosphatidylcholines in brain tissue using MALDI-MS/MS. *J. Am. Soc. Mass Spectrom.* **2005,** 16, (12), 2052-2056.

29. Jackson, S. N.; Woods, A. S., Direct profiling of tissue lipids by MALDI-TOFMS. *J. Chromatography B* **2009,** 877, (26), 2822-2829.

30. Stuebiger, G.; Belgacem, O., Analysis of lipids using 2,4,6-trihydroxyacetophenone as a matrix for MALDI mass spectrometry. *Anal. Chem.* **2007,** 79, (8), 3206-3213.

31. Farah, M. A.; Bose, S.; Lee, J.; Jung, H. C.; Kim, Y., Analysis of glycated insulin by maldi-tof mass spectrometry. *Biochim. Biophys. Acta* **2005,** 3, 269-282.

32. Seeley, E. H.; Oppenheimer, S. R.; Mi, D.; Chaurand, P.; Caprioli, R. M., Enhancement of protein sensitivity for MALDI imaging mass spectrometry after chemical treatment of tissue sections. *J. Am. Soc. Mass Spectrom.* **2008,** 19, (8), 1069-1077.

33. Gyemant, G.; Toth, A.; Bajza, I.; Kandra, L.; Liptak, A., Identification and structural analysis of synthetic oligosaccharides of Shigella sonnei using MALDI-TOF MS. *Carbohydrate Res.* **2001,** 334, (4), 315-322.

34. Sato, Y.; Fukuyama, Y.; Nonami, H.; Erra-Balsells, R.; Stortz, C. A.; Cerezo, A. S.; Matulewicz, M. C., Matrix-assisted ultraviolet laser desorption/ionization time-of-flight (UV-MALDI-TOF) mass spectra of N-acylated and N,O-acylated glycosylamines. *Carbohydrate Res.* **2007,** 342, (17), 2567-2574.

35. Allwood, D. A.; Dreyfus, R. W.; Perera, I. K.; Dyer, P. E., Optical absorption of matrix compounds for laser-induced desorption and ionization (MALDI). *Appl. Surf. Sci.* **1997,** 110, 154-157.

36. Horneffer, V.; Dreisewerd, K.; Ludemann, H. C.; Hillenkamp, F.; Lage, M.; Strupat, K., Is the incorporation of analytes into matrix crystals a prerequisite for matrix-assisted laser desorption/ionization mass

spectrometry? A study of five positional isomers of dihydroxybenzoic acid. *Int . J. Mass Spectrom.* **1999,** 185, 859-870.

37. Steven, R. T.; Race, A. M.; Bunch, J., para-nitroaniline is a promising matrix for maldi-ms imaging on intermediate pressure ms systems. *J. Am. Soc. Mass Spectrom.* **2013,** 24, (5), 801-804.

38. Francese, S.; Bradshaw, R.; Flinders, B.; Mitchell, C.; Bleay, S.; Cicero, L.; Clench, M. R., Curcumin: a multipurpose matrix for maldi mass spectrometry imaging applications. *Anal. Chem.* **2013,** 85, (10), 5240-5248.

39. Bouschen, W.; Spengler, B., Artifacts of MALDI sample preparation investigated by high-resolution scanning microprobe matrix-assisted laser desorption/ionization (SMALDI) imaging mass spectrometry. *Int. J. Mass Spectrom.* **2007,** 266, 129-137.

40. Dai, Y. Q.; Whittal, R. M.; Li, L., Two-layer sample preparation: A method for MALDI-MS analysis of complex peptide and protein mixtures. *Anal. Chem.* **1999,** 71, (5), 1087-1091.

41. Onnerfjord, P.; Ekstrom, S.; Bergquist, J.; Nilsson, J.; Laurell, T.; Marko-Varga, G., Homogeneous sample preparation for automated high throughput analysis with matrix-assisted laser desorption/ionisation time-of-flight mass spectrometry. *Rapid Commun. Mass Spectrom.* **1999,** 13, (5), 315-322.

42. Vorm, O.; Mann, M., Improved mass accuracy in matrix-assisted laser desorption/ionisation time-of-flight mass spectrometry. *J. Am. Soc. Mass Spectrom.* **1994,** 5, 955-958.

43. Jaskolla, T. W.; Karas, M.; Roth, U.; Steinert, K.; Menzel, C.; Reihs, K., Comparison between vacuum sublimed matrices and conventional dried droplet preparation in maldi-tof mass spectrometry. *J. Am. Soc. Mass Spectrom.* **2009,** 20, (6), 1104-1114.

44. Allwood, D. A.; Perera, I. K.; Perkins, J.; Dyer, P. E.; Oldershaw, G. A., Preparation of 'near' homogeneous samples for the analysis of matrix-assisted laser desorption ionisation processes. *Appl. Surf. Sci.* **1996,** 103, (3), 231-244.

45. Aerni, H. R.; Cornett, D. S.; Caprioli, R. M., Automated acoustic matrix deposition for MALDI sample preparation. *Anal. Chem.* **2006,** 78, (3), 827-834.

46. Yamada, Y.; Hidefumi, K.; Shion, H.; Oshikata, M.; Haramaki, Y., Distribution of chloroquine in ocular tissue of pigmented rat using matrix-assisted laser desorption/ionization imaging quadrupole time-of-flight tandem mass spectrometry. *Rapid Commun. Mass Spectrom.* **2011,** 25, (11), 1600-1608.

47. Hensel, R. R.; King, R. C.; Owens, K. G., Electrospray sample preparation for improved quantitation in matrix-assisted laser

desorption/ionization time-of-flight mass spectrometry. *Rapid Commun. Mass Spectrom.* **1997,** 11, (16), 1785-1793.

48. Baluya, D. L.; Garrett, T. J.; Yost, R. A., Automated MALDI matrix deposition method with inkjet printing for imaging mass spectrometry. *Anal. Chem.* **2007,** 79, (17), 6862-6867.

49. Zhu, L.; Parr, G. R.; Fitzgerald, M. C.; Nelson, C. M.; Smith, L. M., Oligodeoxynucleotide fragmentation in maldi/tof mass-spectrometry using 355-nm radiation. *Journal of the American Chemical Society* **1995,** 117, (22), 6048-6056.

50. Holle, A.; Haase, A.; Kayser, M.; Hohndorf, J., Optimizing UV laser focus profiles for improved MALDI performance. *J. Mass Spectrom.* **2006,** 41, (6), 705-716.

51. Qiao, H.; Piyadasa, G.; Spicer, V.; Ens, W., Analyte distributions in MALDI samples using MALDI imaging mass spectrometry. *Int. J. Mass Spectrom.* **2009,** 281, (1-2), 41-51.

52. Trim, P. J.; Djidja, M. C.; Atkinson, S. J.; Oakes, K.; Cole, L. M.; Anderson, D. M. G.; Hart, P. J.; Francese, S.; Clench, M. R., Introduction of a 20 kHz Nd:YVO4 laser into a hybrid quadrupole time-of-flight mass spectrometer for MALDI-MS imaging. *Anal. Bioanal. Chem.* **2010,** 397, (8), 3409-3419.

53. Dreisewerd, K.; Berkenkamp, S.; Leisner, A.; Rohlfing, A.; Menzel, C., Fundamentals of matrix-assisted laser desorption/ionization mass spectrometry with pulsed infrared lasers. *Int. J. Mass Spectrom.* **2003,** 226, (1), 189-209.

54. Feldhaus, D.; Menzel, C.; Berkenkamp, S.; Hillenkamp, F.; Dreisewerd, K., Influence of the laser fluence in infrared matrix-assisted laser desorption/ionization with a 2.94 mu m Er : YAG laser and a flat-top beam profile. *J. Mass Spectrom.* **2000,** 35, (11), 1320-1328.

55. Hess, W. P.; Park, H. K.; Yavas, O.; Haglund, R. F., IR-MALDI of low molecular weight compounds using a free electron laser. *Appl. Surf. Sci.* **1998,** 127, 235-241.

56. Qiao, H.; Spicer, V.; Ens, W., The effect of laser profile, fluence, and spot size on sensitivity in orthogonal-injection matrix-assisted laser desorption/ionization time-of-flight mass spectrometry. *Rapid Commun. Mass Spectrom.* **2008,** 22, (18), 2779-2790.

57. Guenther, S.; Koestler, M.; Schulz, O.; Spengler, B., Laser spot size and laser power dependence of ion formation in high resolution MALDI imaging. *International Journal of Mass Spectrometry* **2010,** 294, (1), 7-15.

58. Koestler, M.; Kirsch, D.; Hester, A.; Leisner, A.; Guenther, S.; Spengler, B., A high-resolution scanning microprobe matrix-assisted laser desorption/ionization ion source for imaging analysis on an ion trap/Fourier

transform ion cyclotron resonance mass spectrometer. *Rapid Commun. Mass Spectrom.* **2008,** 22, (20), 3275-3285.

59. Soltwisch, J.; Dreisewerd, K., An ultraviolet/infrared matrix-assisted laser desorption ionization sample stage integrating scanning knife-edge and slit devices for laser beam analysis. *Rapid Commun. Mass Spectrom.* **2011,** 25, (9), 1266-1270.

60. Steven, R. T.; Palmer, A. D.; Bunch, J., Fluorometric Beam Profiling of UV MALDI Lasers. *J. Am. Soc. Mass Spectrom.* **2013,** 24, (7), 1146-1152.

61. Dreisewerd, K., The desorption process in MALDI. *Chem. Rev.* **2003,** 103, (2), 395-426.

62. Knochenmuss, R., Ion formation mechanisms in UV-MALDI. *Analyst* **2006,** 131, (9), 966-986.

63. Jaskolla, T. W.; Karas, M., Compelling Evidence for Lucky Survivor and Gas Phase Protonation: The Unified MALDI Analyte Protonation Mechanism. *J. Am. Soc. Mass Spectrom.* **2011,** 22, (6), 976-988.

64. Karas, M.; Gluckmann, M.; Schafer, J., Ionization in matrix-assisted laser desorption/ionization: singly charged molecular ions are the lucky survivors. *J. Mass Spectrom.* **2000,** 35, (1), 1-12.

65. Knochenmuss, R., Positive/negative ion ratios and in-plume reaction equilibria in MALDI. *International Journal of Mass Spectrometry* **2008,** 273, (1-2), 84-86.

66. Knochenmuss, R., A quantitative model of ultraviolet matrix-assisted laser desorption/ionization including analyte ion generation. *Anal. Chem.* **2003,** 75, (10), 2199-2207.

67. Knochenmuss, R., A quantitative model of ultraviolet matrix-assisted laser desorption/ionization. *J. Mass Spectrom.* **2002,** 37, (8), 867-877.

68. Knochenmuss, R.; Stortelder, A.; Breuker, K.; Zenobi, R., Secondary ion-molecule reactions in matrix-assisted laser desorption/ionization. *Journal of Mass Spectrometry* **2000,** 35, (11), 1237-1245.

69. Zenobi, R.; Knochenmuss, R., Ion formation in MALDI mass spectrometry. *Mass Spectrom. Rev.* **1998,** 17, (5), 337-366.

70. Fenn, J. B.; Mann, M.; Meng, C. K.; Wong, S. F.; Whitehouse, C. M., Electrospray ionization-principles and practice. *Mass Spec. Rev.* **1990,** 9, (1), 37-70.

71. Fenn, J. B.; Mann, M.; Meng, C. K.; Wong, S. F.; Whitehouse, C. M., Electrospray ionization for mass-spectrometry of large biomolecules. *Science* **1989,** 246, (4926), 64-71.

72. Laiko, V. V.; Baldwin, M. A.; Burlingame, A. L., Atmospheric pressure matrix assisted laser desorption/ionization mass spectrometry. *Anal. Chem.* **2000,** 72, (4), 652-657.

73. Laiko, V. V.; Moyer, S. C.; Cotter, R. J., Atmospheric pressure maldi/ion trap mass spectrometry. *Anal. Chem.* **2000,** 72, (21), 5239-5243.

74. Chen, L. C.; Yoshimura, K.; Yu, Z.; Iwata, R.; Ito, H.; Suzuki, H.; Mori, K.; Ariyada, O.; Takeda, S.; Kubota, T.; Hiraoka, K., Ambient imaging mass spectrometry by electrospray ionization using solid needle as sampling probe. *J. Mass Spectrom.* **2009,** 44, (10), 1469-1477.

75. Takats, Z.; Wiseman, J. M.; Gologan, B.; Cooks, R. G., Mass spectrometry sampling under ambient conditions with desorption electrospray ionization. *Science* **2004,** 306, (5695), 471-473.

76. Cooks, R. G.; Ouyang, Z.; Takats, Z.; Wiseman, J. M., Ambient mass spectrometry. *Science* **2006,** 311, (5767), 1566-1570.

77. Nemes, P.; Vertes, A., Laser ablation electrospray ionization for atmospheric pressure, in vivo, and imaging mass spectrometry. *Anal. Chem.* **2007,** 79, (21), 8098-8106.

78. Laskin, J.; Heath, B. S.; Roach, P. J.; Cazares, L.; Semmes, O. J., Tissue imaging using nanospray desorption electrospray ionization mass spectrometry. *Anal. Chem.* **2012,** 84, (1), 141-148.

79. Roach, P. J.; Laskin, J.; Laskin, A., Nanospray desorption electrospray ionization: an ambient method for liquid-extraction surface sampling in mass spectrometry. *Analyst* **2010,** 135, (9), 2233-2236.

80. Wu, C.; Dill, A. L.; Eberlin, L. S.; Cooks, R. G.; Ifa, D. R., Mass spectrometry imaging under ambient conditions. *Mass Spec. Rev.* **2012**, n/a-n/a.

81. Eikel, D.; Vavrek, M.; Smith, S.; Bason, C.; Yeh, S.; Korfmacher, W. A.; Henion, J. D., Liquid extraction surface analysis mass spectrometry (LESA-MS) as a novel profiling tool for drug distribution and metabolism analysis: the terfenadine example. *Rapid Commun. Mass Spectrom.* **2011,** 25, (23), 3587-3596.

82. Stephens, W. E., A pulsed mass spectrometer with time dispersion. *Physical Review* **1946,** 69, (11-1), 691-691.

83. Wiley, W. C.; McLaren, I. H., TIme-of-flight mass spectrometer with improved resolution. *Review of Scientific Instruments* **1955,** 26, (12), 1150-1157.

84. Mamyrin, B. A., Time-of-flight mass spectrometry (concepts, achievements and prospects). *Int. J. Mass Spectrom.* **2001,** 206, 251-266.

85. Ferguson, R. E.; McCulloh, K. E.; Rosenstom, Observation of products of ionic collision processes and ion decomposition in a linear

pulsed time-of-flight mass spectrometer. *J. Chem. Phys.* **1965,** 42, (1), 100-&.

86. Paul, W.; Steinwedel, H. S., Invention of quadrupole. *Z. Naturforsch* **1953,** 8a, 448.

87. Stafford, G. C.; Kelley, P. E.; Syka, J. E. P.; Reynolds, W. E.; Todd, J. F. J., Recent improvements in and analytical applications of advanced ion trap technology. *Int. J. Mass Spectrom. Ion Process.* **1984,** 60, (SEP), 85-98.

88. Hu, Q. Z.; Noll, R. J.; Li, H. Y.; Makarov, A.; Hardman, M.; Cooks, R. G., The Orbitrap: a new mass spectrometer. *J. Mass Spectrom.* **2005,** 40, (4), 430-443.

89. Cornett, D. S.; Frappier, S. L.; Caprioli, R. M., MALDI-FTICR imaging mass spectrometry of drugs and metabolites in tissue. *Anal. Chem.* **2008,** 80, (14), 5648-5653.

90. Aichler, M.; Walch, A., MALDI Imaging mass spectrometry: current frontiers and perspectives in pathology research and practice. *Laboratory Investigation* **2015,** 95, (4), 422-431.

91. Roempp, A.; Spengler, B., Mass spectrometry imaging with high resolution in mass and space. *Histochemistry and Cell Biology* **2013,** 139, (6), 759-783.

92. Prentice, B. M.; Chumbley, C. W.; Caprioli, R. M., High-speed MALDI MS/MS imaging mass spectrometry using continuous raster sampling. *Journal of Mass Spectrometry* **2015,** 50, (4), 703-710.

93. Nilsson, A.; Goodwin, R. J. A.; Shariatgorji, M.; Vallianatou, T.; Webborn, P. J. H.; Andren, P. E., Mass spectrometry imaging in drug development. *Anal. Chem.* **2015,** 87, (3), 1437-1455.

94. Patel, E.; Cole, L. M.; Bradshaw, R.; Batubara, A.; Mitchell, C. A.; Francese, S.; Clench, M. R., MALDI-MS imaging for the study of tissue pharmacodynamics and toxicodynamics. *Bioanalysis* **2015,** 7, (1), 91-101.

95. Bokhart, M. T.; Rosen, E.; Thompson, C.; Sykes, C.; Kashuba, A. D. M.; Muddiman, D. C., Quantitative mass spectrometry imaging of emtricitabine in cervical tissue model using infrared matrix-assisted laser desorption electrospray ionization. *Analytical and Bioanalytical Chemistry* **2015,** 407, (8), 2073-2084.

96. Nakanishi, T.; Nirasawa, T.; Takubo, T., Quantitative mass barcode-like image of nicotine in single longitudinally sliced hair sections from long-term smokers by matrix-assisted laser desorption time-of-flight mass spectrometry imaging. *Journal of Analytical Toxicology* **2014,** 38, (6), 349-353.

97. McEwen, A. B.; Henson, C. M.; Wood, S. G., Quantitative whole-body autoradiography, LC-MS/MS and MALDI for drug-distribution studies

in biological samples: the ultimate matrix trilogy. *Bioanalysis* **2014,** 6, (3), 377-391.

98. Takai, N.; Tanaka, Y.; Watanabe, A.; Saji, H., Quantitative imaging of a therapeutic peptide in biological tissue sections by MALDI MS. *Bioanalysis* **2013,** 5, (5), 603-612.

99. Sun, N.; Walch, A., Qualitative and quantitative mass spectrometry imaging of drugs and metabolites in tissue at therapeutic levels. *Histochemistry and Cell Biology* **2013,** 140, (2), 93-104.

100. Pirman, D. A.; Reich, R. F.; Kiss, A.; Heeren, R. M. A.; Yost, R. A., Quantitative MALDI tandem mass spectrometric imaging of cocaine from brain tissue with a deuterated internal standard. *Anal. Chem.* **2013,** 85, (2), 1081-1089.

101. Lietz, C. B.; Gemperline, E.; Li, L., Qualitative and quantitative mass spectrometry imaging of drugs and metabolites. *Adv. Drug Deliv. Rev.* **2013,** 65, (8), 1074-1085.

102. Takai, N.; Tanaka, Y.; Inazawa, K.; Saji, H., Quantitative analysis of pharmaceutical drug distribution in multiple organs by imaging mass spectrometry. *Rapid Commun. Mass Spectrom.* **2012,** 26, (13), 1549-1556.

103. Schadt, S.; Kallbach, S.; Almeida, R.; Sandel, J., Investigation of figopitant and its metabolites in rat tissue by combining whole-body

autoradiography with liquid extraction surface analysis mass spectrometry. *Drug Metabolism and Disposition* **2012,** 40, (3), 419-425.

104. Kallback, P.; Shariatgorji, M.; Nilsson, A.; Andren, P. E., Novel mass spectrometry imaging software assisting labeled normalization and quantitation of drugs and neuropeptides directly in tissue sections. *J. Proteomics* **2012,** 75, (16), 4941-4951.

105. Hamm, G.; Bonnel, D.; Legouffe, R.; Pamelard, F.; Delbos, J.-M.; Bouzom, F.; Stauber, J., Quantitative mass spectrometry imaging of propranolol and olanzapine using tissue extinction calculation as normalization factor. *J. Proteom.* **2012,** 75, (16), 4952-4961.

106. van Kampen, J. J. A.; Burgers, P. C.; de Groot, R.; Luider, T. M., Qualitative and quantitative analysis of pharmaceutical compounds by MALDI-TOF mass spectrometry. *Anal. Chem.* **2006,** 78, (15), 5403-5411.

107. Lacey, D.; Hu, X. K.; Loboda, A. V.; Mosey, N. J.; Lipson, R. H., Aspirin revealed: A cationization strategy for detecting acetylsalicylic acid by MALDI mass spectrometry. *Int. J. Mass Spectrom.* **2007,** 261, (2-3), 192-198.

108. Persike, M.; Karas, M., Rapid simultaneous quantitative determination of different small pharmaceutical drugs using a conventional matrix-assisted laser desorption/ionization time-of-flight mass spectrometry system. *Rapid Commun. Mass Spectrom.* **2009,** 23, (22), 3555-3562.

109. Flick, T. G.; Leib, R. D.; Williams, E. R., *Anal. Chem.* **2010,** 82, 1179-1182.

110. Notari, S.; Mancone, C.; Alonzi, T.; Tripodi, M.; Narciso, P.; Ascenzi, P., Determination of HIV inhibitors in human plasma. *J. Chromatography B* **2008,** 863, 249-257.

111. van Kampen, J. J. A.; Burgers, P. C.; Gruters, R. A.; Osterhaus, A. D. M. E.; de Groot, R.; Luider, T. M.; Volmer, D. A., *Anal. Chem.* **2008,** 80, 4969-4975.

112. Wang, H. Y. J.; Jackson, S. N.; McEuen, J.; Woods, A. S., Localization and analyses of small drug molecules in rat brain tissue sections. *Anal. Chem.* **2005,** 77, (20), 6682-6686.

113. Kosanam, H.; Prakash, P. K. S.; Yates, C. R.; Miller, D. D.; Ramagiri, S., Rapid screening of doping agents. *Anal. Chem.* **2007,** 79, 6020-6026.

114. Kovarik, P.; Grivet, C.; Bourgogne, E.; Hopfgartner, G., quantitation of pharmaceuticals in human plasma. *Rapid Commun. Mass Spectrom.* **2007,** 21, 911-919.

115. Kennedy, J. H.; Wiseman, J. M., Analysis of a range drugs *Rapid Commun. Mass Spectrom.* **2010,** 24, 309-314.

116. Earnshaw, C. J.; Carolan, V. A.; Richards, D. S.; Clench, M. R., Direct analysis of pharmaceutical tablet formulations using matrix-assisted

laser desorption/ionisation mass spectrometry imaging. *Rapid Commun. Mass Spectrom.* **2010,** 24, (11), 1665-1672.

117. Meesters, R. J. W.; Cornelissen, R.; van Klaveren, R. J.; de Jonge, R.; den Boer, E.; Lindemans, J.; Luider, T. M., pemetrexed. *Anal. Bioanal. Chem.* **2010,** 398, 2943-2948.

118. Huber, K.; Aichler, M.; Sun, N.; Buck, A.; Li, Z.; Fernandez, I. E.; Hauck, S. M.; Zitzelsberger, H.; Eickelberg, O.; Janssen, K. P.; Keller, U.; Walch, A., A rapid ex vivo tissue model for optimising drug detection and ionisation in MALDI imaging studies. *Histochemistry and Cell Biology* **2014,** 142, (4), 361-371.

119. Rodrigues, L. R.; de Oliveira, D. N.; Ferreira, M. S.; Catharino, R. R., In situ assessment of atorvastatin impurity using MALDI mass spectrometry imaging (MALDI-MSI). *Analytica Chimica Acta* **2014,** 818, 32-38.

120. Gut, Y.; Boiret, M.; Bultel, L.; Renaud, T.; Chetouani, A.; Hafiane, A.; Ginot, Y.-M.; Jennane, R., Application of chemometric algorithms to MALDI mass spectrometry imaging of pharmaceutical tablets. *Journal of Pharmaceutical and Biomedical Analysis* **2015,** 105, 91-100.

121. Cornett, D. S.; Reyzer, M. L.; Chaurand, P.; Caprioli, R. M., MALDI imaging mass spectrometry: molecular snapshots of biochemical systems. *Nature Methods* **2007,** 4, 828-833.

122. McDonnell, L. A.; Heeren, R. M. A., Imaging mass spectrometry. *Mass Spec. Rev.* **2007,** 26, 606-643.

123. Reyzer, M. L.; Caprioli, R. M., MALDI-MS-based imaging of small molecules and proteins in tissues. *Curr. Opin. Chem. Biol.* **2007,** 11, (1), 29-35.

124. Schwartz, S. A.; Reyzer, M. L.; Caprioli, R. M., Direct tissue analysis using matrix-assisted laser desorption/ionization mass spectrometry: practical aspects of sample preparation. *J. Mass Spectrom.* **2003,** 38, (7), 699-708.

125. Sugiura, Y.; Shimma, S.; Setou, M., Thin sectioning improves the peak intensity and signal-to-noise ratio in direct tissue mass spectrometry. *J. Mass Spectrom. Soc. Jpn.* **2006,** 54, (2), 45-48.

126. Prideaux, B.; Atkinson, S. J.; Carolan, V. A.; Morton, J.; Clench, M. R., Sample preparation and data interpretation procedures for the examination of xenobiotic compounds in skin by indirect imaging MALDI-MS. *Int. J. Mass Spectrom.* **2007,** 260, (2-3), 243-251.

127. Sugiura, Y.; Shimma, S.; Setou, M., Two-step matrix application technique to improve ionization efficiency for matrix-assisted laser desorption/ionization in imaging mass spectrometry. *Anal. Chem.* **2006,** 78, (24), 8227-8235.

128. Mainini, V.; Lalowski, M.; Gotsopoulos, A.; Bitsika, V.; Baumann, M.; Magni, F., MALDI-imaging mass spectrometry on tissues. In *Clinical Proteomics: Methods and Protocols, Second Edition*, Vlahou, A.; Makridakis, M., Eds. 2015; Vol. 1243, pp 139-164.

129. Rohner, T. C.; Staab, D.; Stoeckli, M., MALDI mass spectrometric imaging of biological tissue sections. *Mechanisms of Ageing and Development* **2005,** 126, (1), 177-185.

130. Ingendoh, A.; Karas, M.; Killenkamp, F.; Giessmann, U., Factors affecting the resolution in matrix-assisted laser-desorption ionization mass-spectrometry. *Int. J. Mass Spectrom.* **1994,** 131, 345-354.

131. Caprioli, R. M.; Farmer, T. B.; Gile, J., Molecular imaging of biological samples: Localization of peptides and proteins using MALDI-TOF MS. *Anal. Chem.* **1997,** 69, (23), 4751-4760.

132. Chaurand, P.; Stoeckli, M.; Caprioli, R. M., Direct profiling of proteins in biological tissue sections by MALDI mass spectrometry. *Anal. Chem.* **1999,** 71, (23), 5263-5270.

133. Reyzer, M. L.; Hsieh, Y. S.; Ng, K.; Korfmacher, W. A.; Caprioli, R. M., Direct analysis of drug candidates in tissue by matrix-assisted laser desorption/ionization mass spectrometry. *J. Mass Spectrom.* **2003,** 38, (10), 1081-1092.

134. Troendle, F. J.; Reddick, C. D.; Yost, R. A., Detection of Pharmaceutical compounds in tissue by matrix-assisted laser desorption/ ionization and laser desorption/chemical ionization tandem mass spectrometry with a quadrupole ion trap. *J. Am. Soc. Mass Spectrom.* **1999,** 10, 1315-1321.

135. Atkinson, S. J.; Loadman, P. M.; Sutton, C.; Patterson, L. H.; Clench, M. R., Examination of the distribution of the bioreductive drug AQ4N and its active metabolite AQ4 in solid tumours by imaging matrix-assisted laser desorption/ionisation mass spectrometry. *Rapid Commun. Mass Spectrom.* **2007,** 21, (7), 1271-1276.

136. Stoeckli, M.; Staab, D.; Schweitzer, A., Compound and metabolite distribution measured by MALDI mass spectrometric imaging in whole-body tissue sections. *Int. J. Mass Spectrom.* **2007,** 260, (2-3), 195-202.

137. Hopfgartner, G.; Varesio, E.; Stoeckli, M., Matrix-assisted laser desorption/ionization mass spectrometric imaging of complete rat sections using a triple quadrupole linear ion trap. *Rapid Commun. Mass Spectrom.* **2009,** 23, (6), 733-736.

138. Trim, P. J.; Henson, C. M.; Avery, J. L.; McEwen, A.; Snel, M. F.; Claude, E.; Marshall, P. S.; West, A.; Princivalle, A. P.; Clench, M. R., Matrix-assisted laser desorption/ionization-ion mobility separation-mass spectrometry imaging of vinblastine in whole body tissue sections. *Anal. Chem.* **2008,** 80, (22), 8628-8634.

139. Shanta, S. R.; Kim, T. Y.; Hong, J. H.; Lee, J. H.; Shin, C. Y.; Kim, K.-H.; Kim, Y. H.; Kim, S. K.; Kim, K. P., A new combination MALDI matrix for small molecule analysis: application to imaging mass spectrometry for drugs and metabolites. *Analyst* **2012,** 137, (24), 5757-5762.

140. Marko-Varga, G.; Vegvari, A.; Rezeli, M.; Prikk, K.; Ross, P.; Dahlback, M.; Edula, G.; Sepper, R.; Fehniger, T. E., Understanding drug uptake and binding within targeted disease micro-environments in patients: a new tool for translational medicine. *Clin. Translat. Med.* **2012,** 1, (1), 8-8.

141. Liu, X.; Weaver, E. M.; Hummon, A. B., Evaluation of therapeutics in three-dimensional cell culture systems by maldi imaging mass spectrometry. *Anal. Chem.* **2013,** 85, (13), 6295-6302.

142. Kuwayama, K.; Tsujikawa, K.; Miyaguchi, H.; Kanamori, T.; Iwata, Y. T.; Inoue, H., Distribution measurements of 3,4-methylenedioxymethamphetamine and its metabolites in organs by matrix-assisted laser desorption/ionization imaging mass spectrometry using an automatic matrix spraying system with an air brush and a turntable. *Anal. Bioanal. Chem.* **2012,** 404, (6-7), 1823-1830.

143. Kim, Y. H.; Fujimura, Y.; Sasaki, M.; Yang, X.; Yukihira, D.; Miura, D.; Unno, Y.; Ogata, K.; Nakajima, H.; Yamashita, S.; Nakahara, K.; Murata, M.; Lin, I. C.; Wariishi, H.; Yamada, K.; Tachibana, H., In situ label-free visualization of orally dosed strictinin within mouse kidney by MALDI-MS imaging. *Journal of Agricultural and Food Chemistry* **2014,** 62, (38), 9279-9285.

144. Drexler, D. M.; Garrett, T. J.; Cantone, J. L.; Diters, R. W.; Mitroka, J. G.; Conaway, M. C. P.; Adams, S. P.; Yost, R. A.; Sanders, M., Utility of imaging mass spectrometry (IMS) by matrix-assisted laser desorption ionization (MALDI) on an ion trap mass spectrometer in the analysis of drugs and metabolites in biological tissues. *J. Pharmacol. Toxicol.* **2007,** 55, (3), 279-288.

145. Weaver, E. M.; Hummon, A. B., Imaging mass spectrometry: From tissue sections to cell cultures. *Advanced Drug Delivery Reviews* **2013,** 65, (8), 1039-1055.

146. Liu, X.; Weaver, E. M.; Hummon, A. B., Evaluation of therapeutics in three-dimensional cell culture systems by MALDI imaging mass spectrometry. *Analytical Chemistry* **2013,** 85, (13), 6295-6302.

147. Pislyagin, E. A.; Dmitrenok, P. S.; Gorpenchenko, T. Y.; Avilov, S. A.; Silchenko, A. S.; Aminin, D. L., Determination of cucumarioside A(2)-2 in mouse spleen by radiospectroscopy, MALDI-MS and MALDI-IMS. *European Journal of Pharmaceutical Sciences* **2013,** 49, (4), 461-467.

148. Vegvari, A.; Fehniger, T. E.; Rezeli, M.; Laurell, T.; Doeme, B.; Jansson, B.; Welinder, C.; Marko-Varga, G., Experimental models to study drug distributions in tissue using MALDI mass spectrometry imaging. *Journal of Proteome Research* **2013,** 12, (12), 5626-5633.

149. Sugihara, Y.; Vegvari, A.; Welinder, C.; Jonsson, G.; Ingvar, C.; Lundgren, L.; Olsson, H.; Breslin, T.; Wieslander, E.; Laurell, T.; Rezeli, M.;

Jansson, B.; Nishimura, T.; Fehniger, T. E.; Baldetorp, B.; Marko-Varga, G., A new look at drugs targeting malignant melanoma-An application for mass spectrometry imaging. *Proteomics* **2014,** 14, (17-18), 1963-1970.

150. Jones, E. A.; Deininger, S. r.-O.; Hogendoorn, P. C. W.; Deelder, A. M.; McDonnell, L. A., Imaging mass spectrometry statistical analysis. *J. Proteomics* **2012,** 75, (16), 4962-4989.

151. Palmer, A. D.; Bunch, J.; Styles, I. B., The use of random projections for the analysis of mass spectrometry imaging data. *J. Am. Soc. Mass Spectrom.* **2015,** 26, (2), 315-322.

152. Schwartz, M.; Meyer, B.; Wirnitzer, B.; Hopf, C., Standardized processing of MALDI imaging raw data for enhancement of weak analyte signals in mouse models of gastric cancer and Alzheimer's disease. *Anal. Bioanal. Chem.* **2015,** 407, (8), 2255-2264.

153. Race, A. M.; Steven, R. T.; Palmer, A. D.; Styles, I. B.; Bunch, J., Memory efficient principal component analysis for the dimensionality reduction of large mass spectrometry imaging data sets. *Anal. Chem.* **2013,** 85, (6), 3071-3078.

154. Sarkari, S.; Kaddi, C. D.; Bennett, R. V.; Fernandez, F. M.; Wang, M. D., Comparison of clustering pipelines for the analysis of mass spectrometry imaging data. *Ann. Int. Conf. IEEE Eng. Med. Biol. Soc.* **2014,** 2014, 4771-4.

155. Fonville, J. M.; Carter, C. L.; Pizarro, L.; Steven, R. T.; Palmer, A. D.; Griffiths, R. L.; Lalor, P. F.; Lindon, J. C.; Nicholson, J. K.; Holmes, E.; Bunch, J., Hyperspectral Visualization of Mass Spectrometry Imaging Data. *Anal. Chem.* **2013,** 85, (3), 1415-1423.

156. Race, A. M.; Styles, I. B.; Bunch, J., Inclusive sharing of mass spectrometry imaging data requires a converter for all. *J. Proteomics* **2012,** 75, (16), 5111-5112.

157. Huber, K.; Feuchtinger, A.; Borgmann, D. M.; Li, Z.; Aichler, M.; Hauck, S. M.; Zitzelsberger, H.; Schwaiger, M.; Keller, U.; Walch, A., Novel approach of MALDI drug imaging, immunohistochemistry, and digital image analysis for drug distribution studies in tissues. *Analytical Chemistry* **2014,** 86, (21), 10568-10575.

158. Jirasko, R.; Holcapek, M.; Kunes, M.; Svatos, A., Distribution study of atorvastatin and its metabolites in rat tissues using combined information from UHPLC/MS and MALDI-Orbitrap-MS imaging. *Analytical and Bioanalytical Chemistry* **2014,** 406, (19), 4601-4610.

159. Poetzsch, M.; Steuer, A. E.; Roemmelt, A. T.; Baumgartner, M. R.; Kraemer, T., Single hair analysis of small molecules using MALDI-triple quadrupole MS imaging and LC-MS/MS: investigations on opportunities and pitfalls. *Analytical Chemistry* **2014,** 86, (23), 11758-11765.

160. Poetzsch, M.; Baumgartner, M. R.; Steuer, A. E.; Kraemer, T., Segmental hair analysis for differentiation of tilidine intake from external

contamination using LC-ESI-MS/MS and MALDI-MS/MS imaging. *Drug Testing and Analysis* **2015,** 7, (2), 143-149.

161. Shen, M.; Xiang, P.; Shi, Y.; Pu, H.; Yan, H.; Shen, B., Mass imaging of ketamine in a single scalp hair by MALDI-FTMS. *Analytical and Bioanalytical Chemistry* **2014,** 406, (19), 4611-4616.

162. Shima, N.; Sasaki, K.; Kamata, T.; Matsuta, S.; Katagi, M.; Miki, A.; Zaitsu, K.; Sato, T.; Nakanishi, T.; Tsuchihashi, H.; Suzuki, K., Single-hair analysis of zolpidem on the supposition of its single administration in drug-facilitated crimes. *Forensic Toxicology* **2015,** 33, (1), 122-130.

163. Swales, J. G.; Tucker, J. W.; Strittmatter, N.; Nilsson, A.; Cobice, D.; Clench, M. R.; Mackay, C. L.; Andren, P. E.; Takats, Z.; Webborn, P. J. H.; Goodwin, R. J. A., Mass spectrometry imaging of cassette-dosed drugs for higher throughput pharmacokinetic and biodistribution analysis. *Analytical Chemistry* **2014,** 86, (16), 8473-8480.

164. Barry, J. A.; Groseclose, M. R.; Robichaud, G.; Castellino, S.; Muddiman, D. C., Assessing drug and metabolite detection in liver tissue by UV-MALDI and IR-MALDESI mass spectrometry imaging coupled to FT-ICR MS. *International Journal of Mass Spectrometry* **2015,** 377, 448-455.

165. Mascini, N. E.; Eijkel, G. B.; ter Brugge, P.; Jonkers, J.; Wesseling, J.; Heeren, R. M. A., The Use of Mass Spectrometry Imaging to Predict Treatment Response of Patient-Derived Xenograft Models of Triple-

Negative Breast Cancer. *Journal of Proteome Research* **2015,** 14, (2), 1069-1075.

166. Ye, H.; Gemperline, E.; Li, L., A vision for better health: Mass spectrometry imaging for clinical diagnostics. *Clinica Chimica Acta* **2013,** 420, 11-22.

167. Prideaux, B.; Dartois, V.; Staab, D.; Weiner, D. M.; Goh, A.; Via, L. E.; Barry, C. E., III; Stoeckli, M., High-sensitivity MALDI-MRM-MS Imaging of moxifloxacin distribution in tuberculosis-infected rabbit lungs and granulomatous lesions. *Anal. Chem.* **2011,** 83, (6), 2112-2118.

168. Sleno, L.; Volmer, D. A., Assessing the properties of internal standards for quantitative matrix-assisted laser desorption/ionization mass spectrometry of small molecules. *Rapid Commun. Mass Spectrom.* **2006,** 20, (10), 1517-1524.

169. Nilsson, A.; Fehniger, T. E.; Gustavsson, L.; Andersson, M.; Kenne, K.; Marko-Varga, G.; Andren, P. E., Fine mapping the spatial distribution and concentration of unlabeled drugs within tissue micro-compartments using imaging mass spectrometry. *PLoS One* **2010,** 5, (7).

170. Goodwin, R. J. A.; Pitt, A. R., Mass spectrometry imaging of pharmacological compounds in tissue sections. *Bioanalysis* **2010,** 2, (2), 279-293.

171. Koeniger, S. L.; Talaty, N.; Luo, Y.; Ready, D.; Voorbach, M.; Seifert, T.; Cepa, S.; Fagerland, J. A.; Bouska, J.; Buck, W.; Johnson, R. W.; Spanton, S., A quantitation method for mass spectrometry imaging. *Rapid Commun. Mass Spectrom.* **2011,** 25, (4), 503-510.

172. Castellino, S.; Groseclose, M. R.; Sigafoos, J.; Wagner, D.; de Serres, M.; Polli, J. W.; Romach, E.; Myer, J.; Hamilton, B., Central nervous system disposition and metabolism of fosdevirine (GSK2248761), a non-nucleoside reverse transcriptase inhibitor: an LC-MS and matrix-assisted laser desorption/ionization imaging ms investigation into central nervous system toxicity. *Chem. Res. Toxicol.* **2013,** 26, (2), 241-251.

173. Goodwin, R. J. A.; Scullion, P.; MacIntyre, L.; Watson, D. G.; Pitt, A. R., Use of a solvent-free dry matrix coating for quantitative matrix-assisted laser desorption ionization imaging of 4-bromophenyl-1,4-diazabicyclo(3.2.2)nonane-4-carboxylate in rat brain and quantitative analysis of the drug from laser microdissected tissue regions. *Anal. Chem.* **2010,** 82, (9), 3868-3873.

174. Pirman, D. A.; Kiss, A. s.; Heeren, R. M. A.; Yost, R. A., Identifying tissue-specific signal variation in MALDI mass spectrometric imaging by use of an internal standard. *Anal. Chem.* **2012,** 85, (2), 1090-1096.

175. Groseclose, M. R.; Castellino, S., A Mimetic Tissue Model for the Quantification of drug distributions by MALDI imaging mass spectrometry. *Analytical Chemistry* **2013,** 85, (21), 10099-10106.

176. Takai, N.; Tanaka, Y.; Saji, H., Quantification of small molecule drugs in biological tissue sections by imaging mass spectrometry using surrogate tissue-based calibration standards. *Mass spectrometry (Tokyo, Japan)* **2014,** 3, (1), A0025-A0025.

177. Schulz, S.; Gerhardt, D.; Meyer, B.; Seegel, M.; Schubach, B.; Hopf, C.; Matheis, K., DMSO-enhanced MALDI MS imaging with normalization against a deuterated standard for relative quantification of dasatinib in serial mouse pharmacology studies. *Analytical and Bioanalytical Chemistry* **2013,** 405, (29), 9467-9476.

178. Tomlinson, L.; Fuchser, J.; Fuetterer, A.; Baumert, M.; Hassall, D. G.; West, A.; Marshall, P. S., Using a single, high mass resolution mass spectrometry platform to investigate ion suppression effects observed during tissue imaging. *Rapid Communications in Mass Spectrometry* **2014,** 28, (9), 995-1003.

179. Wagner, D. S.; Gloseclose, M. R.; Richards-Peterson, L.; Gorycki, P.; Castellino, S. In *Integration of imaging mass spectrometry into drug development and the importance of distribution and quantitation*, ASMS 59th Conference on Mass Spectrometry and Allied Topics, Denver, U.S.A., 2011; Springer: Denver, U.S.A., 2011; p 36.

180. Duncan, M. W.; Roder, H.; Hunsucker, S. W., Quantitative MALDI MS. *Brief. Func. Genom. Proteom.* **2008,** 7, (5), 355-370.

181. Sogawa, K.; Kodera, Y.; Noda, K.; Ishizuka, Y.; Yamada, M.; Umemura, H.; Maruyama, K.; Tomonaga, T.; Yokosuka, O.; Nomura, F., The measurement of a fibrinogen alpha C-chain 5.9 kDa fragment (FIC 5.9) using MALDI-TOF MS and a stable isotope-labeled peptide standard dilution. *Clin. Chim. Acta* **2011,** 412, (11-12), 1094-1099.

182. Reich, R. F.; Cudzilo, K.; Levisky, J. A.; Yost, R. A., Analysis of cocaine - COC d3 deuterated internal standard. *J. Am. Soc. Mass Spectrom.* **2010,** 21, 564-571.

183. Spraggins, J. M.; Caprioli, R., High-Speed MALDI-TOF Imaging Mass spectrometry: rapid ion image acquisition and considerations for next generation instrumentation. *J. Am. Soc. Mass Spectr.* **2011,** 22, (6), 1022-1031.

184. Vegvari, A.; Fehninger, T.; Gustavsson, L.; Nilsson, A.; Andren, P. E.; Kenne, K.; Nilsson, A.; Laurell, T.; Marko-Varga, G., Essential tactics of tissue preparation and matrix nano-spotting for successful compound imaging mass spectrometry. *J. Proteomics* **2010,** 73, 1270-1278.

185. Moosavi, S. M.; Ghassabian, S., Linearity of calibration curves for analytical methods: a review of criteria for assessment of method reliability. In *Calibration and Validation of Analytical Methods - A Sampling of Current Approaches*, IntechOpen: 2018.

186. Loco, J. V.; Elskens, M.; Croux, C.; Beernaert, H., Linearity of calibration curves: use and misuse of the correlation coefficient. *Accred. Qual. Assur.* **2002,** 7, 281-285.

187. Van Berkel, G. J.; Sanchez, A. D.; Quirke, J. M. E., Thin-layer chromatography and electrospray mass spectrometry coupled using a surface sampling probe. *Anal. Chem.* **2002,** 74, (24), 6216-6223.

188. Gusev, A. I.; Proctor, A.; Rabinovich, Y. I.; Hercules, D. M., Thin-layer chromatography combined with matrix-assisted laser-desorption ionization mass-spectrometry. *Anal. Chem.* **1995,** 67, (11), 1805-1814.

189. Nicola, A. J.; Gusev, A. I.; Hercules, D. M., Direct quantitative analysis from thin-layer chromatography plates using matrix-assisted laser desorption/ionization mass spectrometry. *Appl. Spectrosc.* **1996,** 50, (12), 1479-1482.

190. Isbell, D. T.; Gusev, A. I.; Taranenko, N. I.; Chen, C. H.; Hercules, D. M., Analysis of nucleotides directly from TLC plates using MALDI-MS detection. *Fresenius J. Anal. Chem.* **1999,** 365, (7), 625-630.

191. Santos, L. S.; Haddad, R.; Hoehr, N. F.; Pilli, R. A.; Eberlin, M. N., Fast screening of low molecular weight compounds by thin-layer chromatography and "on-spot" MALDI-TOF mass spectrometry. *Anal. Chem.* **2004,** 76, (7), 2144-2147.

192. Hayen, H.; Volmer, D. A., Rapid identification of siderophores by combined thin-layer chromatography/matrix-assisted laser desorption/ionization mass spectrometry. *Rapid Commun. Mass Spectrom.* **2005,** 19, (5), 711-720.

193. Salo, P. K.; Salomies, H.; Harju, K.; Ketola, R. A.; Kotiaho, T.; Yli-Kauhaluoma, J.; Kostiainen, R., Analysis of small molecules by ultra thin-layer chromatography-atmospheric pressure matrix-assisted laser desorption/ionization mass spectrometry. *J. Am. Soc. Mass Spectrom.* **2005,** 16, (6), 906-915.

194. Bakry, R.; Bonn, G. K.; Mair, D.; Svec, F., Monolithic porous polymer layer for the separation of peptides and proteins using thin-layer chromatography coupled with MALDI-TOF-MS. *Anal. Chem.* **2007,** 79, (2), 486-493.

195. Watanabe, T.; Kawasaki, H.; Kimoto, T.; Arakawa, R., Characterization of polyether mixtures using thin-layer chromatography and matrix-assisted laser desorption/ionization mass spectrometry. *Rapid Commun. Mass Spectrom.* **2007,** 21, (5), 787-791.

196. Paglia, G.; Ifa, D. R.; Wu, C. P.; Corso, G.; Cooks, R. G., Desorption electrospray ionization mass spectrometry analysis of lipids after two-dimensional high-performance thin-layer chromatography partial separation. *Anal. Chem.* **2010,** 82, (5), 1744-1750.

197. Chen, C. C.; Yang, Y. L.; Ou, C. L.; Chou, C. H.; Liaw, C. C.; Lin, P. C., Direct monitoring of chemical transformations by combining thin layer chromatography with nanoparticle-assisted laser desorption/ionization mass spectrometry. *Analyst* **2013,** 138, (5), 1379-1385.

198. Leriche, E. D.; Hubert-Roux, M.; Grossel, M. C.; Lange, C. M.; Afonso, C.; Loutelier-Bourhis, C., Direct TLC/MALDI-MS coupling for modified polyamidoamine dendrimers analyses. *Anal. Chim. Acta* **2014,** 808, 144-150.

199. Fuchs, B.; Suss, R.; Nimptsch, A.; Schiller, J., MALDI-TOF-MS directly combined with tlc: a review of the current state. *Chromatographia* **2009,** 69, S95-S105.

200. Kertesz, V.; Van Berkel, G. J., Fully automated liquid extraction-based surface sampling and ionization using a chip-based robotic nanoelectrospray platform. *J. Mass Spectrom.* **2010,** 45, (3), 252-260.

201. Chen, Y. C.; Shiea, J.; Sunner, J., Thin-layer chromatography mass spectrometry using activated carbon, surface-assisted laser desorption/ionization. *J. Chromatograph. A* **1998,** 826, (1), 77-86.

202. Mehl, J. T.; Hercules, D. M., Direct TLC-MALDI coupling using a hybrid plate. *Anal. Chem.* **2000,** 72, (1), 68-73.

203. Blatherwick, E. Q.; Van Berkel, G. J.; Pickup, K.; Maria, M. K.; Beaudoin, M.-E.; Cole, R. O.; Day, J. M.; Iverson, S.; Wilson, I. D.;

Scrivens, J. H.; Weston, D. J., Utility of spatially-resolved atmospheric pressure surface sampling and ionization techniques as alternatives to mass spectrometric imaging (MSI) in drug metabolism. *Xenobiotica* **2011,** 41, (8), 720-734.

204. Edwards, R. L.; Creese, A. J.; Baumert, M.; Griffiths, P.; Bunch, J.; Cooper, H. J., Hemoglobin variant analysis via direct surface sampling of dried blood spots coupled with high-resolution mass spectrometry. *Anal. Chem.* **2011,** 83, (6), 2265-2270.

205. Kai, M.; González, I.; Genilloud, O.; Singh, S. B.; Svatoš, A., Direct mass spectrometric screening of antibiotics from bacterial surfaces using liquid extraction surface analysis. *Rapid Commun. Mass Spectrom.* **2012,** 26, (20), 2477-2482.

206. Lanekoff, I.; Thomas, M.; Carson, J. P.; Smith, J. N.; Timchalk, C.; Laskin, J., Imaging nicotine in rat brain tissue by use of nanospray desorption electrospray ionization mass spectrometry. *Anal. Chem.* **2013,** 85, (2), 882-889.

207. Parson, W. B.; Koeniger, S. L.; Johnson, R. W.; Erickson, J.; Tian, Y.; Stedman, C.; Schwartz, A.; Tarcsa, E.; Cole, R.; Van Berkel, G. J., Analysis of chloroquine and metabolites directly from whole-body animal tissue sections by liquid extraction surface analysis (LESA) and tandem mass spectrometry. *J. Mass Spectrom.* **2012,** 47, (11), 1420-1428.

208. Paine, M. R. L.; Barker, P. J.; Maclauglin, S. A.; Mitchell, T. W.; Blanksby, S. J., Direct detection of additives and degradation products from polymers by liquid extraction surface analysis employing chip-based nanospray mass spectrometry. *Rapid Commun. Mass Spectrom.* **2012,** 26, (4), 412-418.

209. Vishmeh, R.; Waldon, D. J.; Teffera, Y.; Zhao, Z., *Anal. Chem.* **2012,** 84, 5439-5445.

210. Blatherwick, E. Q.; Svensson, C. I.; Freguelli, B. G.; Scrivens, J. H., Localisation of adenine nucleotides in heat-stabilised mouse brains using ion mobility enabled MALDI imaging. *Int. J. Mass Spectrom.* **2013,** 345, 19-27.

211. Schadt, S.; Kallbach, S.; Almeida, R.; Sandel, J., Investigation of figopitant and its metabolites in rat tissue by combining whole-body autoradiography with liquid extraction surface analysis mass spectrometry. *Drug Metabol. Disp.* **2012,** 40, (3), 419-425.

212. Chinwalla, A. T., Initial sequencing and comparative analysis of the mouse genome. *Nature* **2002,** 420, (6915), 520-562.

213. Ullberg, S., Studies on the distribution and fate of 35S-labelled benzyl penicillin in the body *Acta Radiol. Suppl.* **1954,** 118, 1-118.

214. Lappin, G.; Temple, P., *Radiotracers in drug development* CRC Press: Boca Raton, 2006.

215. Schweitzer, A.; Fahr, A.; Niederberger, W., A simple method for quantitation of 14C whole body autoradiograms. *Appl. Radiat. Isotopes* **1975,** 33, 329-333.

216. Schweitzer, A.; Hasler-Nguyen, N.; Zijlstra, J., Preferential uptake of the non-setroidal antiinflammatory drug diclofenac into inflamed tissues after a single oral dose in rats. *BMC Pharmacol.* **2009,** 9, 5.

217. Foster, C.; Howard, L.; Schweitzer, A.; Persohn, E.; Hiestand, P., *JPET* **2007,** 323, 469-476.

218. Weiss, H.; Pfaar, U.; Schweitzer, A.; Wiegand, H.; Skerjanec, A.; Schran, H., Biodistribution and plasma protein binding of zoledronic acid. *Drug Metab. Dispos.* **2008,** 36, 2043-2049.

219. Bruin, G.; Faller, T.; Wiegand, H.; Schweitzer, A.; Nick, H.; Schneider, J., Pharmacokinetics, distribution metabolism and excretion of deferasirox and its iron complex in rats. *Drug Metab. Dispos.* **2008,** 36, 2523-2538.

220. Solon, E. G.; Balani, S. K.; F.W., L., Whole-body autoradiography in drug discovery. *Curr. Drug Metab.* **2002**.

221. Chay, S. H.; Pohland, R. C., Comparison of quantitative whole-body autoradiographic and tissue dissection techniques in the evaluation of the tissue distribution of c-14 daptomycin in rats. *J. Pharm. Sci.* **1994,** 83, (9), 1294-1299.

222. Fitzgerald, J. D.; O'Donnell, S. R.; Austin, M., Pharmacology o f4-hydroxypropranolol, a metabolite of propranolol. *Brit. J. Pharmac.* **1971,** 43, 222-235.

223. Howe, R.; Moore, R. H.; Rao, B. S.; Wood, A. H., Metabolism of 2-(4-chlorophenyl)thiazol-4-ylacetic acid (fenclozic acid) and related compounds by microorganisms. *J. Med. Chem.* **1972,** 15, (10), 1040-1045.

224. Solon, E. G.; Schweitzer, A.; Stoeckli, M.; Prideaux, B., Autoradiography, MALDI-MS, and SIMS-MS imaging in pharmaceutical discovery and development. *Aaps J.* **2010,** 12, (1), 11-26.

225. Suckau, D.; Resemann, A.; Schurenberg, M.; Hufnagel, P.; Franzen, J.; Holle, A., A novel MALDI LIFT-TOF/TOF mass spectrometer for proteomics. *Anal. Bioanal. Chem.* **2003,** 376, 952-965.

226. Smirnov, I. P.; Zhu, X.; Taylor, T.; Huang, Y.; Ross, P.; Papayanopoulos, I. A.; Martin, S. A.; Pappin, D. J., Suppression of alpha-Cyano-4-hydroxycinnamic Acid Matrix Clusters and Reduction of Chemical Noise in MALDI-TOF Mass Spectrometry. *Anal. Chem.* **2004,** 76, (10), 2958-2965.

227. Singhal, R.; Carrigan, J. B.; Wei, W.; Taniere, P.; Hejmadi, R. K.; Forde, C.; Ludwig, C.; Bunch, J.; Griffiths, R. L.; Johnson, P. J.; O., T.; Alderson, D.; Gunther, U. L.; Ward, D. G., MALDI profiles of proteins and lipids for the rapid characterisation of upper GI-tract cancers. *J. Proteomics* **2013,** 80, 207-215.

228. Bland, J. M.; Altman, D. G., Measurement in medicine: the analysis of method comparison studies. *J. Roy. Stat. Soc. Series D (The Statistician)* **1983,** 32, 307-317.

229. Bland, J. M.; Altman, D. G., Statistical methods for assessing agreement between two methods of clinical measurement. *Lancet* **1986,** 327, 307-310.

230. Giavarina, D., Understanding Bland Altman analysis. *Biochem. Med.* **2015,** 25, (2), 141-151.

231. Evans, G., *A Handbook of Bioanalysis and Drug Metabolism* CRC Press: Boca Raton, 2004.

232. Chalmers, T. M.; Kellgren, J. H.; Platt, D. S., Evaluation in man of fenclozic acid (i.c.i.54,450: myalex), a new anti-inflamator agent ii. clinical trial in patients with rheumatoid arthritis. *Ann. Rheum. Dis.* **1969,** 28, 595-601.

233. Curtis, C. G.; Powell, G. M.; Bradbury, A.; Rhodes, C., The fate of fenclozic acid in the gut and its effect on some aspects of gut metabolism. *Xenobiotica* **1983,** 13, 483-496.

234. Martin, S.; Lenz, E. M.; Keene, W.; Clench, M. R., Identification of the reactive metabolites of fenclozic acid in bile duct cannulated rats. *Anal. Chem.* **2014,** 86, 11281-11289.